Bioprocess Development for the Syntheses of Selected Phosphorylated Metabolites

Vom Promotionsausschuss der
Technischen Universität Hamburg-Harburg
zur Erlangung des akademischen Grades
Doktor der Naturwissenschaften (Dr. rer. nat.)
genehmigte Dissertation.

von
Getachew Shibabaw Molla

aus
Debark (Ethiopia)

2016

1. Gutachter: Prof. Dr. rer. nat. Andreas Liese
2. Gutachter: Prof. Dr. rer. nat. Wolfgang Streit

Vorsitzender des Prüfungsausschusses: Prof. Dr. rer. nat. An-Ping Zeng

Tag der mündlichen Prüfung: 26.07.2016

Acknowledgment

I would like to thank my PhD supervisor Prof. Dr. Andreas Liese for his invaluable scientific guidance in the entire of this study; moreover, for his managerial skill that I have informally learned much.

Thanks to Dr. Roland Wohlgemuth for organizing the project in cooperation with Sigma-Aldrich and for invaluable discussion throughout the course of this thesis. Thanks to Prof. Dr. Wolfgang Streit, Dr. Jennifer Chow and Birhanu M. Kinfu for the nice cooperation. Thanks to Monika Müller from DSM for sending DNA samples used for an *in situ* ATP regeneration project and discussion during our telephone conference.

I would like to thank my second examiner Prof. Dr. Wolfgang Streit from the University of Hamburg for critically reviewing this thesis.

I am thankful to the Federal Ministry of Education and Research of Germany (BMBF) for the financial support of this thesis under project "P28" in the cluster of "Biocatalysis2021" (project number: 0316055).

Thanks to Dr. Alexander Himmelspach, Lorenzo Pesci and Miriam Assman for the fruitful discussion that we had in our sub-group meeting at the Institute of Technical Biocatalysis. Thanks to Sileshi G. Wubshet (PhD) and Nils Torsson Nyberg (PhD) at the University of Copenhagen and Dr. Erhard Haupt at Hamburg University for the offer and support to perform NMR measurements. I want moreover to thank Dr. Erhard T.K. Haupt and Dr. Alexander Himmelspach for their time to discuss about NMR data analysis. I would like to thank Maren Breuer for her contribution in the fermentation experiments.

I would like to thank Lorenzo Pesci, Birhanu M. Kinfu, Dr. Alexander Himmelspach, Dr. Selin Kara and Bastian Kannengiesser for their time to critically review part of this thesis.

Thanks to Sandesh Deshpande, Venkatesh P. Jayaraman, Sisi Yang, Malte Barkowski for the contribution during their own thesis and project work as well as Patrick John Simmons and Aleksandra Sani Tomic for the contribution during their apprenticeship.

Thanks to both the former and the current members of Institute of Technical Biocatalysis (ITB)-Technical University of Hamburg-Harburg (TUHH) for the pleasant working atmosphere. It was fun as well as a very teaching experience to be a coworker with all of you.

Certainly, my deepest gratitude goes to my parents for their limitless moral and material support to pursue my academic interest.

Publications

▪ Getachew S. Molla, R. Wohlgemuth, Andreas Liese "One-pot enzymatic reaction sequence for the syntheses of D-glyceraldehyde 3-phosphate and L-glycerol 3-phosphate*", J. Mol. Catal. B: Enzym.*124 (2016) 77-82 DOI: 10.1016/j.molcatb.2015.12.004

▪ Getachew S. Molla, P. J. Venkatesh, Andreas Liese "Single-pot enzymatic reaction sequence for the synthesis of D-glyceraldehyde-3-phosphate" *Chem. Ing. Tech.* 86 (9) (2014) 1424-1425 DOI: 10.1002/cite.201450599

▪ Getachew S. Molla, R. Wohlgemuth, Wolfgang Streit, Birhanu M. Kinfu, Jennifer Chow, Andreas Liese "Bioreaction engineering leading to efficient synthesis of L-glyceraldehyde-3-phosphate", *Biotechnol. J.* (2016). DOI: 10.1002/biot.201600625

Publications (submitted)

Getachew S. Molla, Alexaneder Himmelspach, Roland Wohlgemuth, Erhard T.K. Haupt, Andreas Liese "Mechanistic and kinetics elucidation of Mg^{2+} / ATP ratio effect on glycerol kinase", *J. Mol. Catal. B: Enzym* (2017)

Patent (ready to be submitted)

▪ Getachew S. Molla, Daniel Sellin, Hoc Khiem Trieu, Andreas Liese "IR-transparent microtiter plate for reaction screening in aqueous or organic liquid phase", *TuTech Innovation GmbH* (2016)

Lecture

▪ Getachew S. Molla "Bioprocess development for the syntheses of enantiopure phosphorylated metabolites", Integrated Biotechnology and Process Engineering, Hamburg, Germany, 2014

Book chapter

▪ Dominik Gauss, Bernhard Schönenberger, Getachew S. Molla, Birhanu M. Kinfu, Jennifer Chow, Andreas Liese, Wolfgang Streit, Roland Wohlgemuth "Biocatalytic phosphorylation of metabolites" in Applied Biocatalysis: From Fundamental Science to Industrial Applications; Wiley-VCH(2016) (ISBN: 9783527336692) DOI: http://dx.doi.org/10.1002/9783527677122.ch8

Poster presentations

▪ Getachew S. Molla, R. Wohlgemuth, Wolfgang Streit, Andreas Liese "Bioprocess development for the synthesis of optically pure D- and L-glyceraldehyde-3-phosphate", Biomaterials Made From Bioreactors, Dresden, Germany, 2014

▪ Getachew S. Molla, R. Wohlgemuth, Wolfgang Streit, Andreas Liese, "Bioprocess development for the syntheses of enantiopure phosphorylated metabolites", Integrated Biotechnology and Process Engineering, Hamburg, Germany, 2014

▪ Getachew S. Molla, Sandesh, D., R. Wohlgemuth, Wolfgang Streit, Chow, J., B.M. Kinfu, Andreas Liese "Biocatalytic production of enantiomerically pure phosphorylated metabolites", Integrated Biotechnology and Process Technique, Hamburg, Germany, 2013

▪ Getachew S. Molla, Sandesh, D., Chow, J., B.M. Kinfu, Venkatsh, R. Wohlgemuth, Wolfgang Streit, Andreas Liese "Enzymatic synthesis of enantiomerically pure D- and L-glyceraldehyde-3-phosphate", Northern Industrial Biotechnology Association (IBN), Hamburg, Germany, 2013

▪ Getachew S. Molla, Daniel Sellin, Bastian Kannengiesser, Janosch Fagaschewski, Lutz Hilterhaus, Sven Bohne, Jörg Müller, Andreas Liese "IR microtiter assay for screening of enzyme-catalyzed reactions in liquid phase", The 6th International Congress on Biocatalysis, Hamburg, Germany, 2012

▪ Getachew S. Molla, R. Wohlgemuth, Wolfgang Streit, Andreas Liese "New biocatalytic routes for the production of phosphrylated metabolites", Integrated Biotechnology and Process Technique, Hamburg, Germany, 2011.

Abstract

An *in vitro* synthesis of optically pure phosphorylated metabolites is useful in various natural biological and synthetic processes. The aim of this thesis was to develop bioprocesses for the syntheses of *sn*-glycerol-3-phosphate (*sn*-G3P), L-glyceraldehyde-3-phosphate (L-GAP) and D-glyceraldehyde-3-phosphate (D-GAP).

Asymmetric phosphorylation of glycerol catalyzed by glycerol kinase from *Cellulomonas* sp. (EC 2.7.1.30) utilizing ATP as a phosphoryl donor and Mg^{2+} as an essential activator was used for the synthesis of *sn*-G3P. This enzyme exhibits maximum activity at the optimum Mg^{2+} to ATP molar ratio of [0.12 to 0.3]. The enzyme shows Michaelis-Menten kinetics with respect to glycerol as well as ATP maintaining constant Mg^{2+} to ATP molar ratio and two-step kinetics with respect to ATP at a fixed concentration of Mg^{2+}. Detailed kinetics and mechanistic analyses were performed applying ^{31}P and ^{1}H NMR. The two-step kinetics with respect to ATP at the fixed Mg^{2+} concentration is due to the formation of multiple Mg-ATP complexes. The active site of glycerol kinase exhibits different catalytic property with respect to different Mg-ATP complex species. Validation of reaction kinetics models shows 96.8% and 98.8% 2-D correlation of experimental and numerically simulated data matrices.

Glycerol kinase from *Cellulomonas* sp. catalyzed phosphorylation of L-glyceraldehyde by ATP was developed for the synthesis of L-GAP. L-GAP decomposes at the reaction of pH 8 and shows a half-life of 6.86 h. The enzyme exhibits maximum activity at the optimum Mg^{2+} to ATP molar ratio of 0.7. Validation of reaction kinetics model shows 99.9% 2-D correlation of experimental and numerically simulated data matrices. Experimental and numerical evaluations of different reactor types reveal that batch-wise operation is the most convenient process for the synthesis of L-GAP.

A one-pot enzymatic reaction sequence was designed for the synthesis of D-GAP using fructose-1,6-bisphosphate aldolase from rabbit muscle (RAMA) (EC 4.1.2.13), *sn*-glycerol-3-phosphate dehydrogenase (*sn*-G3PDH) from rabbit muscle (EC 1.1.1.8) and formate dehydrogenase from *Candida boidinii* (FDH) (EC 1.2.1.2). The reaction sequence circumvents the thermodynamic limitation of aldol cleavage of D-fructose-1,6-bisphosphate (D-F16BP) that leads to 100% conversion of D-F16BP. A reaction kinetics model defining the entire reaction cascade was developed and validation of the model shows 98.5% 2-D correlation

of experimental and numerically simulated data matrices. The evaluation of different reactor types was performed. Batch-wise operation in STR is the most convenient procedure for the one-pot enzymatic synthesis of D-GAP.

Zusammenfassung

Die Synthese von enantiomerenreinen phosphorylierten Metaboliten *in vitro* ist von großem Nutzen für diverse natürliche biologische und synthetische Prozesse. Das Ziel der vorliegenden Arbeit war die Entwicklung eines Bioprozesses zur Synthese von *sn*-Glycerin-3-phosphat (*sn*-G3P), L-Glyceraldehyd-3-phosphat (L-GAP) und D-Glyceraldehyd-3-phosphat (D-GAP).

Die asymmetrische Phosphorylierung von Glycerin katalysiert durch *Cellulomonas* sp. Glycerinkinase (EC 2.7.1.30) unter Verwendung von ATP als Phosphorylquelle und Mg^{2+} als essentiellen Aktivator wurde zur Synthese von *sn*-G3P genutzt. Das Enzym zeigt die maximale Aktivität bei einem optimalen Verhältnis Mg^{2+} zu ATP von 0.12 – 0.3. Für das Enzym wurde sowohl in Bezug auf Glycerin als auch ATP eine Michaelis-Menten-Kinetik bei konstantem Mg^{2+} zu ATP Verhältnis und eine zweistufige Kinetik in Bezug auf ATP bei festgelegter Mg^{2+}-Konzentration gefunden. Unterstützt durch ^{31}P- und ^{1}H-NMR spektroskopische Untersuchungen wurden detaillierte kinetische und mechanistische Analysen durchgeführt. Die zweistufige Kinetik in Bezug auf ATP bei konstanter Mg^{2+}-Konzentration basiert auf der Bildung von mehreren Mg-ATP-Komplexen. Das aktive Zentrum der Glycerinkinase zeigt unterschiedliche katalytische Eigenschaften gegenüber den verschiedenartigen Mg-ATP-Komplexen. Die Validierung der Reaktionskinetikmodelle zeigt eine 96.8%-ige und eine 98.8%-ige 2-D-Korrelation zwischen den experimentellen und nummerisch simulierten Daten.

Die durch Glycerinkinase aus *Cellulomonas* sp. katalysierte Phosphorylierung von L-Glyceraldehyd mit ATP wurde zur Synthese von L-GAP entwickelt. Beim pH-Wert der Reaktion von 8 wird das L-GAP mit einer Halbwertszeit von 6.86 Stunden zersetzt. Das Enzym zeigt seine maximale Aktivität bei einem optimalen Mg^{2+} zu ATP Verhältnis von 0.7. Die Validierung des Reaktionskinetikmodells zeigt eine 99.9%-ige 2-D-Korrelation zwischen den experimentellen und nummerisch simulierten Daten. Die effizienteste Prozessführung zur Synthese von L-GAP kann nach experimentellen und numerischen Evaluierungen im Satz-Betrieb erzielt werden.

Zur Synthese von D-GAP wurde ein einstufiges, enzymatisches Verfahren entwickelt unter Benutzung von Fructose-1,6-biphosphataldolase (EC 4.1.2.13) und *sn*-Glycerin-3-phosphatdehydrogenase (EC 1.1.1.8) beide aus Kaninchenmuskel und *Candida boidinii* Formiatdehydrogenase (EC 1.2.1.2). Die Reaktionssequenz umgeht die thermodynamische

Limitierung der Aldolspaltung des D-Fructose-1,6-biphosphats (D-F16BP), was zum 100%-igen Umsatz bezogen auf D-F16BP führt. Ein Kinetikmodell zur Beschreibung der gesamten Reaktionskaskade wurde entwickelt und validiert unter 98.5%-iger Übereinstimmung der experimentellen und numerischen Daten. Die Evaluierung unterschiedlicher Reaktortypen wurde durchgeführt. Als vielversprechendste Prozessführung stellte sich ein einstufiger Rührkesselreaktor zur enzymatischen Synthese von D-GAP heraus.

Contents

1. Introduction

Throughout years of experience, chemical phosphorylation synthetic methodologies have shown enormous progress in the application of various phosphorylating reagents to prepare phosphorylated compounds. A broad spectrum of chemical phosphorylation methodologies has been developed, ranging from the use of phosphoric acid at elevated temperatures of 100°C to 150°C in a single step [1, 2] to the design of multi-step synthetic routes using various functional group protecting reagents, subsequent phosphorylation and deprotection in order to achieve selective phosphorylation [3–11]. Most often, multi-step chemical phosphorylation synthetic routes are however lengthy and use toxic reagents; for example, up to 10 steps using $HgCl_2$ and HgO for preparation of D-glyceraldehyde-3-phosphate (D-GAP) [8, 9]. The scope of using phosphorylating reagents such as phosphorochloridate or *p*-nitrophenyl phosphate has been modified in order to achieve chemo-selective phosphorylation without functional group protection by combining with metallo-organic bases (e.g. *tert*-butylmagnesium chloride) [12]. Preparation of phosphorylated compounds has been achieved by isolation from natural sources using acid or alkaline hydrolysis [4, 13–15] as well as by oxidative treatment using $Pb(OAc)_4$ which is extremely toxic [10, 11]. Figure 1.1 shows a reaction scheme of oxidative cleavage of D-fructose-6-phosphate (D-F6P) by $Pb(OAc)_4$ for the synthesis of D-GAP [10].

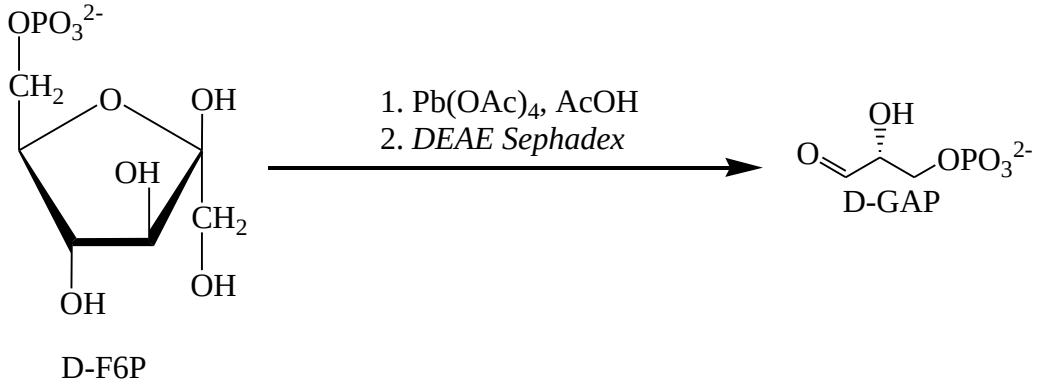

Figure 1.1: Reaction scheme for the synthesis of D-glyceraldehyde-3-phosphate (D-GAP) by the oxidative cleavage of D-fructose-6-phosphate (D-F6P) using $Pb(OAc)_4$

Despite significant progress, the application of chemical phosphorylation synthetic procedures often lack of chemo-, regio- and stereoselectivity generating side-products [2, 16, 17]. Chemical phosphorylation therefore requires additional reaction steps including functional group

protection and deprotection as well as challenging downstream processing (DSP) for the separation of closely related side-products such as isomers. Employing functional group protection chemistry improves selectivity. However, the most often used acid or alkaline treatment to split-off the protective residue causes intramolecular rearrangement reactions like isomerization and racemization yielding a mixture of isomeric products [2, 18, 18, 19]. Aiming to prepare optically pure phosphorylated compounds using acid or alkaline mediated isolation from optically pure natural sources usually fails to yield only the desired product due to intramolecular rearrangement reactions occurring in the process of isolation (as shown in Figure 4.1) [2, 4, 15, 18, 19]. The lack of selectivity in chemical phosphorylation methodologies therefore signifies basic limitations in order to prepare optically pure phosphorylated compounds; for example, intermediary phosphorylated metabolites that are the focus of this thesis.

Due to the different biological activity of enantiomers, an *in vitro* preparation of optically pure phosphorylated metabolites is useful in various applications including pharmaceuticals, nutrition and reagents for biomedical research as well as for metabolic engineering to analyze enzyme functions in metabolic pathways [20–24]. For example, it has been described that L-glyceraldehyde-3-phosphate (L-GAP) shows bactericidal effect on *Escherichia coli* (*E. coli*) while D-GAP, a central metabolite in glycolysis, does not show similar effect on *E. coli* [25]. In synthetic applications to prepare novel products, phosphorylated metabolites are useful to design one-pot *in vitro* biocatalytic reaction sequences using aldolases, transketolases or transferases [10, 20, 26–36]. Few phosphorylated metabolites have moreover been used as cosubstrates for cofactor regenerations of nicotinamide adenine dinucleotide phosphate dependent biooxidation reactions [22]. The use of biocatalysts has been established in research, development and production environments of a number of industries [22–24, 37, 38]; albeit very limited application of biocatalytic phosphorylation in synthetic application compare to their ubiquitous use in nature [39, 40].

The high inherent chemo-, regio- and stereoselectivity of biocatalysts avoid unwanted side reactions; therefore, enhance productivity as well as simplifies DSP. On the other hand, the high stereoselectivity of biocatalysts can be a limitation in case of using racemic starting materials and requirement of general synthetic procedure to convert both enantiomers. While better performance of biocatalysts at physiological pH and temperature is advantageous, stagnant

narrow range of these conditions can be challenging if the stability and solubility of other reaction species do not fit to these conditions. For instance, triosephosphate metabolites are stable at acidic pH bellow 4 while most phosphotransferases show no activity at this pH region [41–46]. The stability of biocatalysts and requirement of expensive cofactors are of among the major concerns for their application in industry. Remarkable progresses have been shown on immobilization technologies and advancement of membrane technologies in order to improve stability and reusability of enzymes as well as development of cofactor regeneration [22–24, 47, 48].

2. Biocatalytic Phosphorylation of Metabolites

Biocatalytic phosphorylation is an ubiquitous reaction occurring in metabolism that cellular life depends much on it [39, 40]. This reaction class relies on the free energy due to cleavage of phospho-anhydride linkage in phosphoryl donor compounds such as ATP as one of crucial factors driving thermodynamics uphill. Therefore, enzyme classes involved in phosphorylation reactions, common phosphoryl donors and issues of biocatalytic phosphorylation reaction engineering as well as limitations for the purpose of practical scale synthesis will be discussed.

2.1. Enzyme Classes Catalyzing Phosphorylation Reactions

Different enzymes classes are involved in phosphorylation reactions. Table 2.1 shows the enzyme classes, their natural role and examples.

Table 2.1: Enzyme classes catalyzing phosphorylation reactions, their natural roles and examples

Enzyme class	Natural role	Example
Transferase (EC 2)	Transfer of phosphoryl group from a phosphoryl donor to acceptors except water	Glycerol kinase (EC 2.7.1.30)
Hydrolase (EC 3)	Hydrolysis of phosphate group	Alkaline phosphatase (EC 3.1.3.1)
Isomerase (EC 5)	Intramolecular rearrangement of phosphoryl group	Phosphoglucomutase (EC 5.4.2.2)

Mechanistically, in contrast to the formation of phosphoenzyme intermediate as in the case of alkaline phosphatases and phosphoglucomutase, the transfer of phosphoryl group in the case of phosphotransferases/kinases occurs directly between phosphoryl donor and acceptor substrates in a ternary complex within the enzyme's active site [39]. Phosphotransferases/kinases are the focus of this section due to their broad use in synthetic applications. Moreover, the discussion will be extended to the other enzyme classes as well. The enzyme sub-class phosphotransferase/kinase (EC 2.7.) is further categorized into a number of branches based on

acceptor functional group type and transferred phosphoryl moiety as well as other specific types of phosphoryl acceptors. Table B.1 in appendix B shows a list of the categories of phosphotransferases/kinases [49]. Figure 2.1 shows a generic reaction scheme of phosphotransferases\kinases catalyzed alcohol phosphorylation utilizing ATP as a phosphoryl donor.

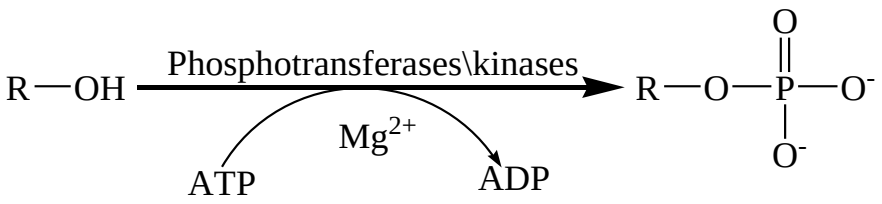

Figure 2.1: A reaction scheme illustrating phosphotransferases\kinases catalyzed phosphorylation of alcohol utilizing ATP as a phosphoryl donor

2.2. Phosphoryl Donors

For various *in vivo* and *in vitro* biocatalytic phosphorylation reactions, ATP serves as the most often utilized phosphoryl donor. Several other high energy phosphoryl donors have been described for both *in vivo* and *in vitro* biocatalytic phosphorylation reactions; nevertheless, with high specificity in comparison to ATP. Most of the phosphoryl donors described for *in vitro* phosphorylation reactions are nucleotide triphosphates (NTPs) [50–53], pyrophosphate [54, 55], triphosphate (PP_i3) [56], acetyl phosphate [57],[22, 58, 59], carbamoyl phosphate [22, 59], methoxycarbonyl phosphate [22, 59], phosphoenolpyruvate [22, 41, 59, 60] and inorganic polyphosphate (PP_in) [61–66]. PP_in has been used as a phosphoryl donor for an industrial production of $NADP^+$ using PP_in/ATP dependent NAD kinase (NADK) [67]. Successful enzymatic phosphorylation of hexose has been described using phosphoramidate as phosphorylating agent [68, 69]. Inorganic triphosphate (PP_i3) has been described as a potential phosphate source for nucleoside kinases from human and *Drosophila melanogaster* [56].

2.3. Reaction Engineering for Biocatalytic Phosphorylation of Metabolites

In the last three decades several biocatalytic preparations of phosphorylated metabolites have been described [54, 57, 61, 70–74]. Scaleup has however been challenging mainly due to technical and economy issues. Bioprocess engineering therefore bridges the gap that allows

designing of technically optimized and economically viable biocatalytic phosphorylation processes.

Efficient and upscalable biocatalytic phosphorylation process can be designed by investigating properties of reaction species including biocatalyst, substrate, product, cofactor and reaction kinetics as well as thermodynamics. Biocatalyst properties include activity, stability and selectivity. The most important properties of other reaction species include stability and solubility in a reaction medium, which is favorable for the biocatalyst. Several factors need to be considered to study the aforementioned properties such as pH, temperature, ionic strength, redox potential (oxygen sensitivity), heavy metal ions, divalent metal ions and reaction buffer type as well as their interactive effect.

The synthetic potential of phosphatases for the preparation of phosphorylated compounds in a reverse condensation reaction has been utilized by adjusting the optimal pH and substrates concentration [22, 75–77] for the reaction thermodynamics. Figure 2.2 shows a reaction scheme of phosphatases catalyzed reversible phosphorylation of organic compounds with –OH functional group.

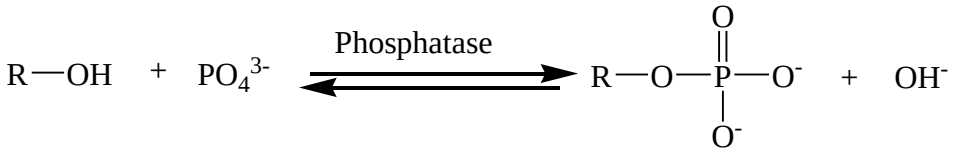

Figure 2.2: Reaction scheme illustrating phosphatase catalyzed reversible phosphorylation for the preparation of phosphorylated compounds utilizing inorganic orthophosphate (P_i) as a phosphorylating agent

Optimization of reaction condition with respect to the influence of pH is crucial for phosphatases catalyzed reverse condensation reaction thermodynamics. It has been described that the concentration of D-glucose-6-phosphate prepared by alkaline phosphatase catalyzed phosphorylation of glucose showed 3-fold increase by shifting pH from 5 to 4 [76]. The equilibrium conversion of alkaline phosphatase catalyzed phosphorylation of glycerol, using P_i as phosphoryl donor, has been described to be shifted by increasing the concentration of glycerol and P_i [75]. Figure 2.3 shows the synthetic potential of different phosphatases utilizing their respective individual optimal pH and influence of substrates concentration on the equilibrium of reversible phosphorylation reactions [22, 75–77].

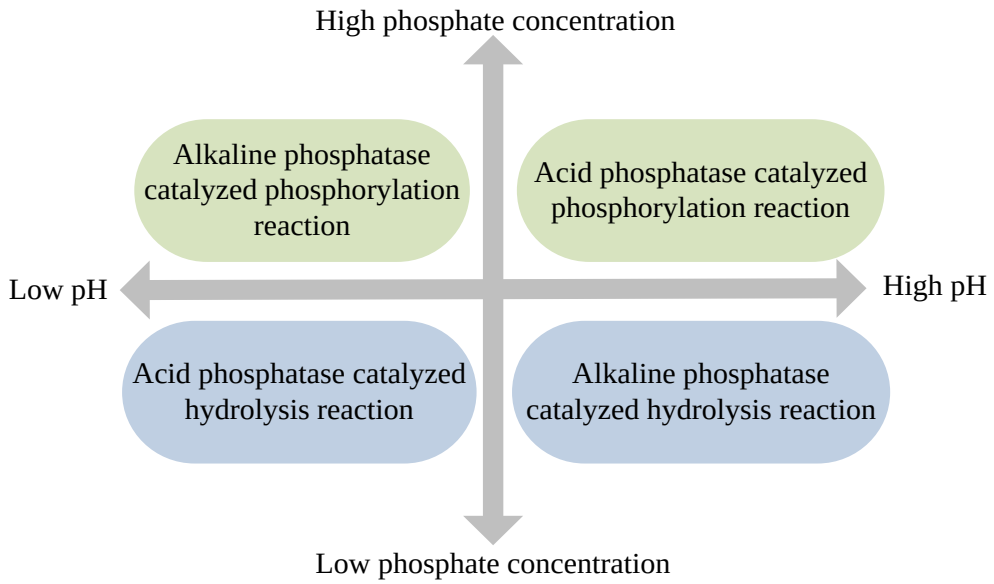

Figure 2.3: Utility of different optimal pH and phosphate concentration levels for acid phosphatase and alkaline phosphatase catalyzed hydrolysis and reverse phosphorylation reactions

Most often enzymes show reciprocal activity and stability responses as a function of temperature; moreover, such a property relates to the enzyme source. In addition to the effect on the biocatalyst, temperature is a crucial factor for the stability of chemically labile phosphorylated metabolites and cofactors. Therefore, an optimal temperature with respect to the activity and stability of an enzyme as well as the stability of phosphorylated metabolites and cofactors must be determined. Phosphotransferases/kinases containing cysteine residues (e.g., glycerol kinase) are oxygen sensitive, and their stability can be enhanced by the addition of reducing agents such as dithiothreitol (DTT) or 2-mercaptoethanol [51, 70, 78–81]. Those reagents stabilize the enzymes by reducing the inermolecular or intramolecular disulfide bonds formed between the cysteine residues.

The requirement to immobilize soluble enzymes on heterogeneous supports is often considered to enhance stability and ease of reusability. Besides stability enhancement, the success of immobilized phosphorylating enzymes has been mentioned to suppress inhibition [70, 75, 76, 82, 83]. An immobilized alkaline phosphatase on corn grits showed 25% inhibition at 150 mM phosphate while the free enzyme showed 50% inhibition at 1 mM phosphate [75]. The application of two immobilized phosphotransferases in a batch operation has been mentioned for reaction systems coupled with cofactor regeneration [70, 79]; however, such an operation often

shows low efficiency due to mass transport limitations. Hence, due to an interactive and in some cases reciprocal influence of several chemical and physical factors on properties of biocatalytic phosphorylation reactions, detailed characterization as well as optimization is indispensable for the successful development of biocatalytic phosphorylation processes [187]. Figure 2.4 shows a schematic diagram illustrating the basic procedures in order to define the optimum reaction conditions.

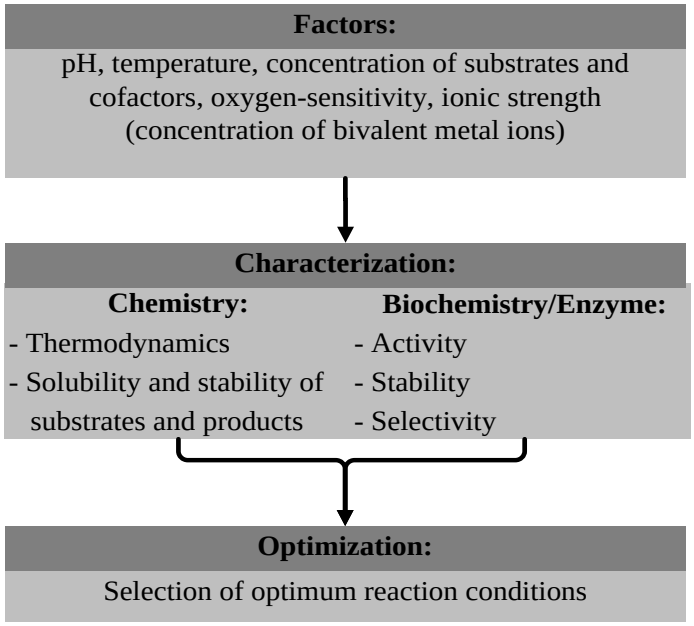

Figure 2.4: A schematic diagram illustrating biocatalytic phosphorylation reaction conditions optimization in order to select optimum reaction conditions

Nearly all phosphotransferases/kinases essentially require a divalent metal ion, preferably Mg^{2+}, for their activity [39] albeit few described kinase activity without the addition of Mg^{2+} [51, 84]. The enzyme kinetics with respect to Mg^{2+} must be investigated in detail for the choice of an appropriate Mg^{2+} concentration. Other divalent metal ions such as Co^{2+} and Ca^{2+} are mentioned to be inhibitors of phosphotransferases/kinases [51, 85, 86]. The effect of divalent metal ions on the activity of phosphotransferases/kinases is crucial in order to choose a phosphoryl donor substrate with non-influencing counter cation or to perform an appropriate pretreatment. For instance, the Ca^{2+} salt of ATP is not an appropriate substrate for glycerol kinase; therefore, Ca^{2+} must be removed by a pretreatment using an ion exchange method.

The activity of various phosphotransferases/kinases as well as phosphatases depends on Mg^{2+} to anionic phosphoryl donor molar ratio that enzymes show maximum activity at an optimum molar

ratio [85, 87–90]. The optimum molar ratio of Mg^{2+} to guanosine 5'-triphosphate (GTP) for guanosine 5'-diphosphate pyrophosphorylase and Mg^{2+} to PP_i^{4-} for non-specific alkaline phosphatases has been mentioned to be 1:1 [85, 88]. Those enzyme classes moreover exhibit different kinetic responses as a function of Mg^{2+} or anionic phosphoryl donor concentration depending on the magnitude of Mg^{2+} to anionic phosphoryl donor molar ratio [77, 85, 87, 89, 90]. Non-specific alkaline phosphatases show inhibition by PP_i^{4-} and Mg^{2+} if the concentration of one is larger than the other [85]. Few phosphotransferases/kinases exhibit a sigmoidal activity response as a function of anionic phosphoryl donor concentration at a fixed Mg^{2+} concentration while Michaelis-Menten kinetics maintaining a constant Mg^{2+} to anionic cofactor molar ratio [85, 89, 90]. Detailed characterization must therefore be performed for the kinetics and mechanistic elucidation of phosphotransferases/kinases with respect to Mg^{2+} and the anionic phosphoryl donor. These include:

1. The enzyme activity as a function of Mg^{2+} to anionic phosphoryl donor molar ratio and determination of an optimum molar ratio at which the enzyme shows maximum activity,
2. The effect of Mg^{2+} in modifying the physical and chemical features of anionic phosphoryl donor and how this effect depends on Mg^{2+} to anionic phosphoryl donor molar ratio,
3. Correlation of interaction behavior of Mg^{2+} to anionic phosphoryl donor with the enzyme activity profile as a function of Mg^{2+} to anionic phosphoryl donor molar ratio
4. The effect of Mg^{2+} on the enzyme activity due to non-specific interaction that can be elucidated by performing sets of activity assays using different enzyme concentrations.

Investigation of reaction kinetics is crucial in order to choose an appropriate specific reactor mode of operation along with other factors such as stability and solubility of reaction components, technical suitability and economic viability to scaleup a process. A process kinetics model can be developed using the knowledge of reaction kinetics and mass balances of a reactor. Hence, by using process input variables such as the concentrations of substrate, cofactor and biocatalyst, numerical simulation of the process performance can be performed. Moreover, using state and control variables of the process, multi-objective optimization with the scope of process intensification can as well be performed (e.g. minimizing biocatalyst consumption, maximizing space-time yield (STY), specific productivity (SP) and total turnover number (ttn)) [187]. Figure 2.5 shows a schematic diagram of comprehensive flowchart for bioprocess development.

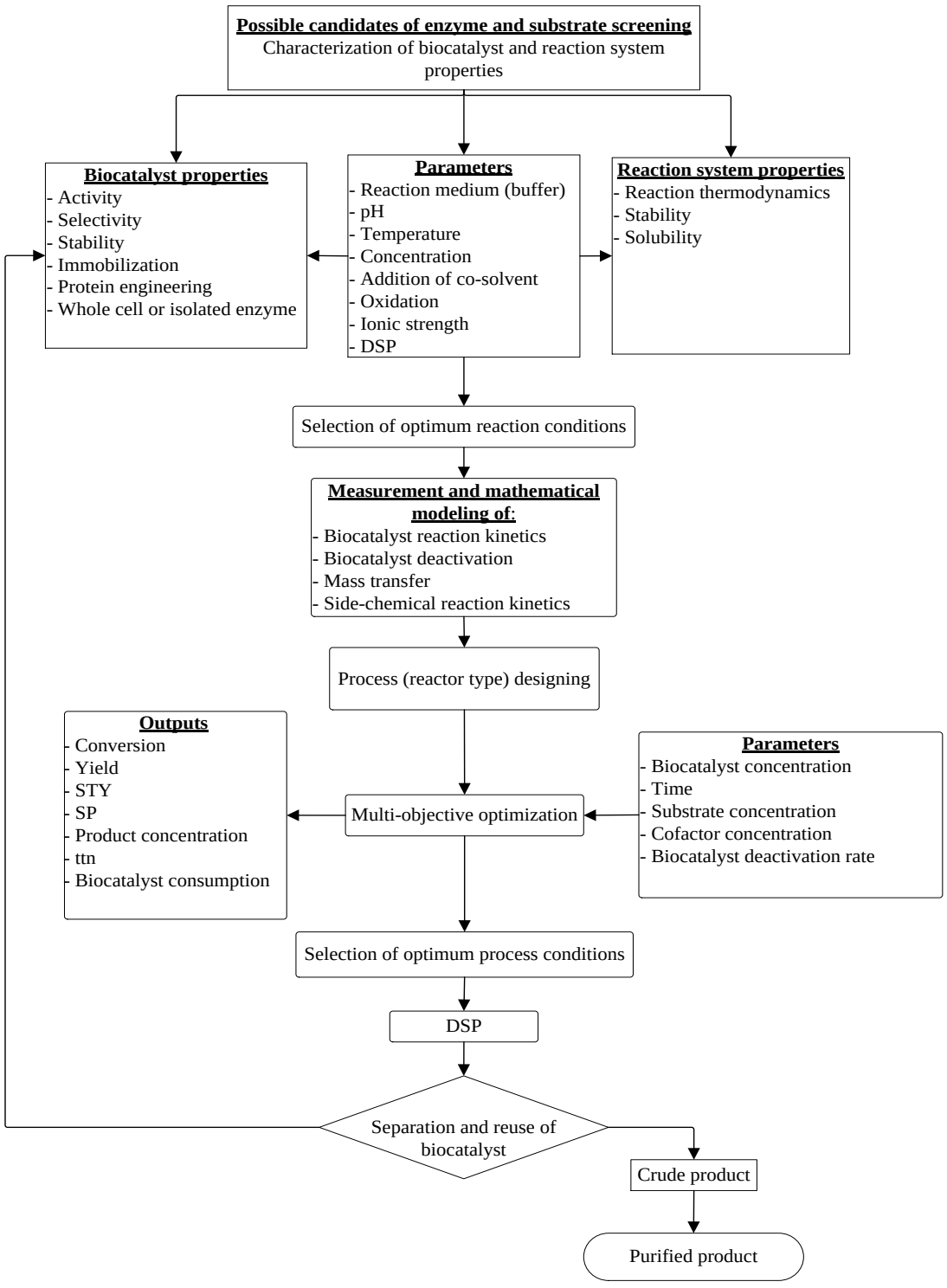

Figure 2.5: Schematic diagram illustrating a comprehensive flowchart for bioprocess development; STY = space-time yield, SP = specific productivity and ttn = total turnover number

The application of homogeneous and heterogeneous enzymes has been described using different reactor types for preparative scale syntheses of phosphorylated compounds [58, 75, 76, 79, 88].

Performance comparison of two reactor types for the synthesis of *sn*-glycerol-1(3)-phosphate catalyzed by immobilized alkaline phosphatase showed 2.3-fold larger yield in a fixed-bed recirculation reactor than in a batch reactor, may be due to controlled substrate and product feeding as well as reduced substrate and product inhibition [75]. The feasibility of a continuous packed-bed reactor using immobilized acid phosphatase for the syntheses of several phosphorylated compounds has recently been demonstrated [76]. A continuous mode of operation is particularly attractive for the syntheses of labile phosphorylated products irrespective of reaction kinetics type because the product residence time at reaction conditions can be minimized. Moreover, conditions including pH and temperature of efflux, which is already separated from the enzyme, can be adjusted to stabilize the product without considering their effect on the enzyme. Comprehensive studies including 1) reaction system optimization for the selection of appropriate enzyme, substrate and reaction conditions, 2) reaction kinetics model development to characterize the concentration effect of substrate and product on enzyme activity and 3) reactor kinetics model development by combining reaction kinetics and mass balance a reactor type to optimize with the focus of process intensification are therefore crucial to rationally design an economic viable bioprocess.

2.4. Limitations of Biocatalytic Phosphorylation of Metabolites

The stoichiometric requirement of expensive high energy phosphoryl donors such as NTPs, most often ATP, by phosphotransferases\kinases limits large scale synthetic applications of these enzymes. The development of inexpensive *in situ* ATP regeneration systems could therefore potentiate the industrial applications of phosphotransferases\kinases. Moreover, an *in situ* ATP regeneration improves the process efficiency by factors such as driving thermodynamically limited reaction forward, *in situ* removal of inhibitory side-product (i.e. ADP) and simplifies DSP. Few *in situ* ATP regeneration reaction systems have been described including pyruvate kinase/phosphoenolpyruvate [22, 41, 59, 60], acetate kinase/acetyl phosphate [22, 57–59], carbamate kinase/carbamoyl phosphate and acetate kinase/methoxycarbonyl phosphate [22, 59]. Nevertheless, several factors limit their application. In all cases, the cosubstrates are more expensive than ATP according to the current Sigma-Aldrich price catalogue (for details see in chapter 8). Chemical lability of cosubstrates at reaction pH, e.g. half-life of acetyl phosphate at pH 7.5, 25°C of 21 h [59] and half-life of methoxycarbonyl phosphate at pH 7.5, 25°C of 0.3 h

[59]. Stability of regenerating enzymes, e.g. half-life of acetate kinase at pH 8.5 and 37°C has been described to be 90 min [58]. Inhibition of regenerating enzymes by coproduct, e.g. inhibition of pyruvate kinase by pyruvate [22] and acetate kinase by acetate [91]. Figure 2.6 shows a generic reaction scheme of phosphotransferases\kinases1 catalyzed alcohol phosphorylation reaction coupled with an *in situ* ATP regeneration catalyzed by phosphotransferases\kinases2.

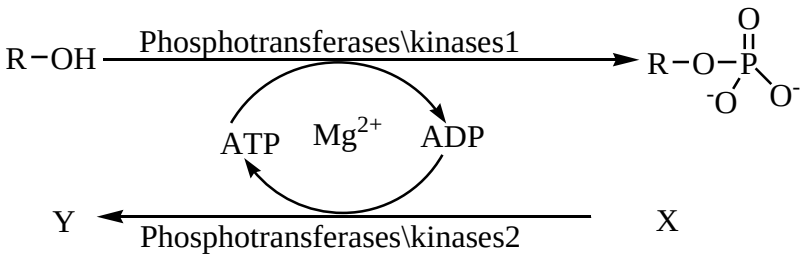

Figure 2.6: A generic reaction scheme illustrating depletion of ATP for the phosphorylation of alcohol catalyzed by phosphotransferases/kinases1 coupled with an *in situ* ATP regeneration using high energy phosphoryl donor cosubstrate X catalyzed by phosphotransferases/kinases2 yielding dephosphorylated coproduct Y

The other main limitation in the application of phosphotransferases\kinases for the synthesis of phosphorylated metabolites is incompatible properties of these enzymes with the stability of few phosphorylated metabolites as a function of pH. Most phosphotransferases/kinases are active and stable at neutral pH region and they essentially require Mg-ATP complex as a substrate. Mg-ATP complex formation depends on pH, moreover, disrupts at pH below 4 [92]. On the other hand, few essential phosphorylated metabolites such as DL-glyceraldehyde-3-phosphate (DL-GAP) and dihydroxyacetone phosphate (DHAP) are stable in acidic pH below 4. Figure 2.7 shows stabilities of various phosphorylated compounds as a function of pH in aqueous solution.

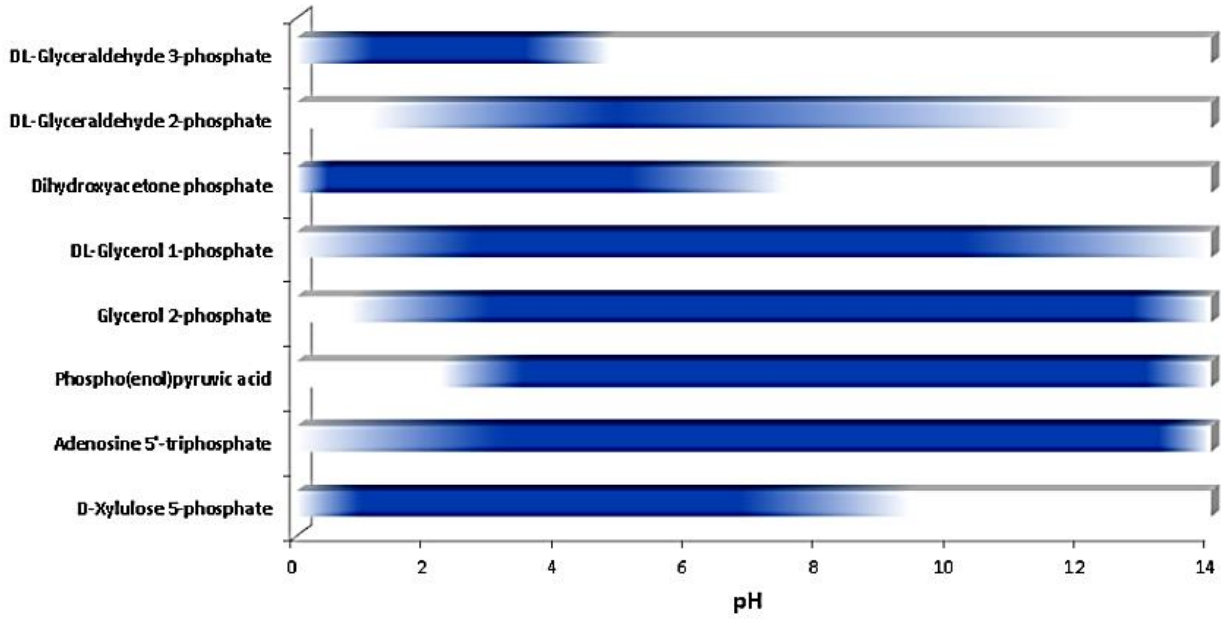

Figure 2.7: Stabilities of few phosphorylated compounds as a function of pH in aqueous solution; the blue colored part of the bars indicate the pH regions where the compounds are stable (the plot was generated by Dominik Gauss at Sigma-Aldrich GmbH Buchs, Switzerland).

3. Aims of the Thesis

The use of optically pure phosphorylated metabolites in various applications and the basic limitations of chemical phosphorylation methodologies to prepare these compounds have already been described in chapter 1. In addition to safety, health and environmental requirements, the need for straightforward and highly chemo-, regio- and stereoselective phosphorylation reactions have guided the development of biocatalytic phosphorylation processes. In consequence, this thesis has been carried out with the focus of twofold general objectives. Those are:

1. To developed enzymatic reaction sequences for the syntheses of the following selected phosphorylated metabolites:
    - *sn*-Glycerol-3-phosphate
    - L-Glyceraldehyde-3-phosphate
    - D-Glyceraldehyde-3-phosphate
2. To establish practical scale enzymatic synthesis to be implemented in cooperation with project partners: Sigma-Aldrich GmbH (Buchs, Switzerland) and working group of Prof. Dr. Wolfgang Streit at the University of Hamburg

The thesis has moreover defined several specific reaction engineering as well as process engineering issues for the enzymatic syntheses of those target-phosphorylated metabolites. These include:

- Enzyme screening for the syntheses of *sn*-glycerol-3-phosphate and L-glyceraldehyde-3-phosphate
- Substrate screening for the synthesis of L-glyceraldehyde-3-phosphate
- Reaction system development for an *in situ* cofactors (i.e. ATP and NADH) regenerations
- Design of one-pot enzymatic reaction sequence for the synthesis of D-glyceraldehyde-3-phosphate
- Comprehensive reaction engineering study comprising of:
    - Activity, stability and selectivity of all enzymes applied
    - Stability of cofactors and the target products
    - Evaluation of reaction thermodynamics and method development to circumvent thermodynamic limitations
    - Reaction kinetics model development

- Development of reactor concept by numerical simulation as well as performance evaluation of different reactor types
- Development of DSP methods

➢ Application of multinuclear NMR technology for mechanistic elucidation of the effect of polydentate anionic (i.e. ATP) and divalent cation (i.e. Mg^{2+}) cofactors complexation on the glycerol kinase kinetics

4. Synthesis of *sn*-Glycerol-3-Phosphate

The therapeutic effect of calcium glycerol phosphate has recently been described for preserving and/or treating of intestinal integrity in ischemia [93, 94]. The mechanism of calcium glycerol phosphate therapeutic action may be due to the inhibition of alkaline phosphatase that catalyzes the hydrolysis of sphingosine-1-phosphate; therefore, the availability and durability of sphingosine-1-phosphate preserves gut epithelial integrity [93, 94]. The addition of therapeutically effective amount of calcium glycerol phosphate in chewing gum can eliminate cariogenic effect and improves dental health [95]. Calcium glycerol phosphate is useful for freshening and reducing acidity of mouth as well as throat of human [96]. Calcium glycerol phosphate can be used as an additive in sublingual aspirin tablet [97]. It has been discovered that calcium glycerol phosphate is capable of mitigating abdominal-area physical problems such as irritable bowel syndrome [98, 99]. The dermatological application of calcium glycerol phosphate has been described, which is beneficial in cellular reparation [100, 101]. The addition of calcium glycerol phosphate in acidic foods and beverages can reduce heartburn as well as gastrointestinal distress [102–107]. *sn*-Glycerol-3-phosphate is a key building block of phospholipids in bacteria and eucarya. It is therefore useful for an *in vitro* preparation of optically pure α-glycerophospholipids that can be tailored with a desired fatty acid chain length and acyl-number as well as position using enzymes such as *sn*-glycerol-3-phosphate O-acyltransferase (EC 2.3.1.15) [33, 34, 108–112].

Glycerol phosphate was synthetically prepared for the first time by mixing glycerol with phosphoric acid at 100°C [1]. The first isolation of glycerol phosphate from egg lecithin was achieved by acid hydrolysis [13]. The barium salt of glycerol phosphate was obtained by boiling brain cephalin with baryta-water [14]. The treatment of glycerol by phosphoric acid in order to prepare glycerol phosphate however yields a mixture of several phosphate esters including but not limited to α- or β-monoester, diester and triester in which their composition depends on the ratio of reactants, temperature and pressure [2, 16, 17]. Several modifications of chemical phosphorylation methodologies and applications of various phosphorylating reagents have been developed in order to obtain pure α- or β-glycerol phosphate [17, 113, 114]. An attempt to prepare optically pure *sn*-glycerol-3-phosphate has been described by isolation from various optically active natural sources or chemical phosphorylation of optically active D-acetone

glycerol [3–7]. For the phosphorylation of D-acetone glycerol, phosphorous oxychloride or phenylphosphoryl dichloride as phosphorylating reagents in the presence of quinolone has been applied with subsequent acid hydrolysis to split-off the acetone residue [5–7]. The application of similar procedure using L-acetone glycerol as a starting material yields *sn*-glycerol-1-phosphate [5, 6, 115]. Even though the glycerol phosphate residue in various natural sources possesses optical purity, retaining its optical purity is challenging due to racemization and isomerization in the process of isolation [2, 18, 19]. The acid or alkaline hydrolysis of various components of brain cephalin and lecithin produce a mixture of α- and β-glycerol phosphate that the α-isomer as a major product in case of acid hydrolysis and the β-isomer as major product in case alkaline hydrolysis [4, 15]. The treatment of pure α- and β-glycerol phosphate in the conditions of acid hydrolysis employed for the isolation of glycerol phosphate from natural sources has been described to yield a mixture of 73% α-isomer and 27% β-isomer, irrespective of which isomer was used as starting material [15]. The acid hydrolysis of pure L-α-glycerylphosphorylcholine yields 88% *sn*-glycerol-1(3)-phosphate and 12% β-glycerol phosphate [18]. It has been described that in acidic pH *sn*-glycerol-3-phosphate undergoes intramolecular rearrangement generating an equilibrium mixture of *sn*-glycerol-1(3)-phosphate and β-glycerol phosphate; moreover, the reaction mechanism shown in Figure 4.1 has been proposed [18].

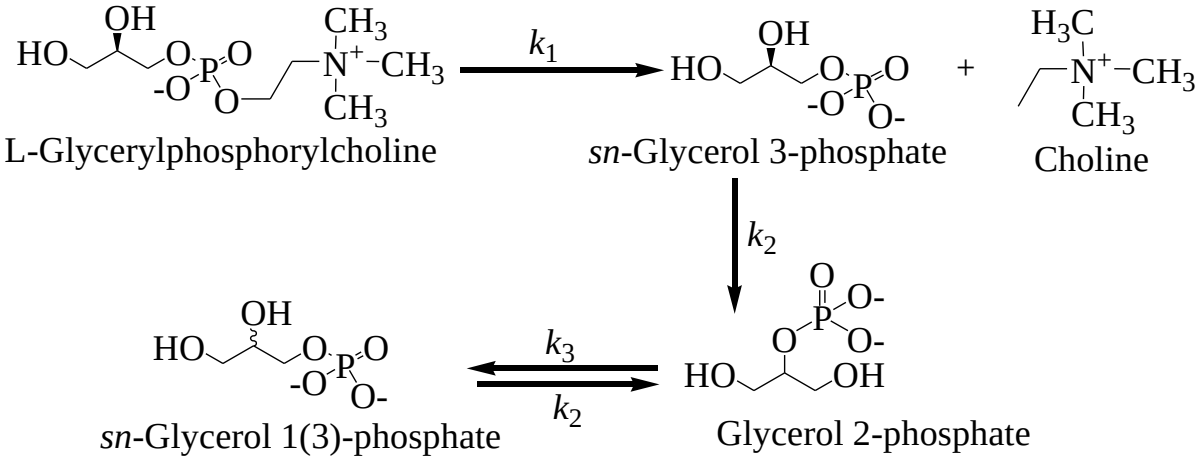

Figure 4.1: Schematic reaction mechanism illustrating acid hydrolysis of L-α-glycerylphosphorylcholine and an intramolecular rearrangement of *sn*-glycerol-3-phosphate to β-glycerol phosphate (glycerol 2-phosphate) as well as the further rearrangement of β-glycerol phosphate to racemic *sn*-glycerol-1(3)-phosphate [18]

The process of removing functional group protective residue in the case of the preparation of *sn*-glycerol-3-phosphate using protected glycerol as a starting material usually causes isomerization

and racemization reactions yielding a mixture of isomeric product. Despite progresses, results signify a basic limitation for the synthesis of optically pure *sn*-glycerol-3-phosphate both by isolation from natural source and chemical phosphorylation of protected glycerol.

4.1. Biocatalytic Asymmetric Phosphorylation of Glycerol

The appearance of *sn*-glycerol-3-phosphate as an alcoholic fermentation and glycolysis intermediate metabolite and its biological utility was discovered in pioneering works of Meyerhof and coworkers [5, 116]. As biological fates, *sn*-glycerol-3-phosphate enters into glycolysis or gluconeogenesis metabolic pathway through oxidation to DHAP catalyzed by cytosolic *sn*-glycerol-3-phosphate dehydrogenase (*sn*-G3PDH) (EC 1.1.1.8) or mitochondrial *sn*-glycerol-3-phosphate dehydrogenase (*sn*-G3PDH) (EC 1.1.5.3) or provides a backbone for the biosynthesis of phospholipid catalyzed by *sn*-glycerol-3-phosphate O-acyltransferase (EC 2.3.1.15). An *in vitro* asymmetric phosphorylation of glycerol has been discovered catalyzed by cat kidney extracts. The barium salt of the phosphorylated product was isolated and identified as an acid resistant *sn*-glycerol-3-phosphate [117, 118]. By studying the distribution of ^{14}C-labelled glycerol tracer in glycogen, glycerol has been described to be utilized by rat tissue in an asymmetrical manner [119, 120]. It has moreover been mentioned that glycerol is asymmetrically phosphorylated by kinase that yields *sn*-glycerol-3-phosphate [119, 121]. This kinase was isolated from rat liver and purified as well as called as glycerol kinase (EC 2.7.1.30) [51]. Figure 4.2 shows the reaction scheme for the asymmetric phosphorylation of glycerol catalyzed by glycerol kinase (EC 2.7.1.30) yielding *sn*-glycerol-3-phosphate. The enzyme utilizes ATP as a phosphoryl donor and requires the cofactor Mg^{2+}. The phosphorylated product has been described to be solely *sn*-glycerol-3-phosphate [51, 72, 73, 122]. Figure 4.3 shows the reaction progress curve for glycerol kinase (EC 2.7.1.30) catalyzed asymmetric phosphorylation of glycerol that depicts the depletion of ATP and formation of ADP.

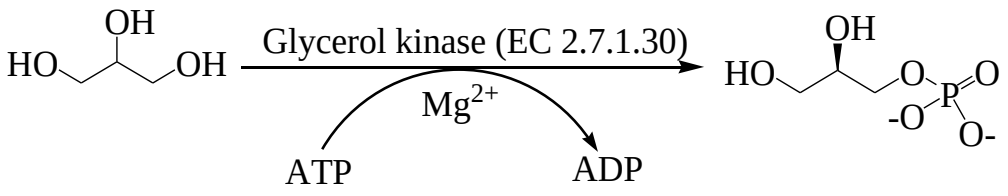

Figure 4.2: Reaction scheme of asymmetric phosphorylation of a prochiral glycerol catalyzed by glycerol kinase (EC 2.7.1.30) yielding *sn*-glycerol-3-phosphate utilizing ATP as a phosphoryl donor and cofactor Mg^{2+}

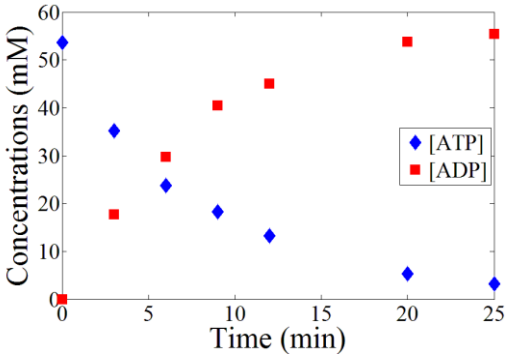

Figure 4.3: Reaction progress of the asymmetric phosphorylation of glycerol catalyzed by glycerol kinase (EC 2.7.1.30); reaction conditions: 50 mM ATP, 50 mM glycerol, 10.5 mM Mg^{2+}, 0.06 mg/mL glycerol kinase from *Cellulomonas* sp. in 100 mM Tris-HCl buffer, pH 8.5, and 30°C

4.2. Optimization of Reaction Condition

Issues concerning with substrate and enzyme screening as well as selection of optimum reaction conditions are crucial early stage research for bioprocess development. Sub-chapter 4.2.1 describes the influences of several factors including oxygen sensitivity, pH, buffer type, temperature and substrates concentration as well as the interactive effect of pH and temperature on the activity and stability of glycerol kinase from various microbial sources. Sub-chapter 4.2.2 describes a broader scope of reaction system optimization considering the effect of pH, ionic strength and concentration of reaction species on the reaction thermodynamics. Hence, the most convenient glycerol kinase among different microbial sources such as *Bacillus stearothermophilus*, *Cellulomonas* sp., *E. coli* and *Streptomyces canus* as well as optimum reaction conditions can be selected.

4.2.1. Enzyme Screening and Effect of Temperature and pH

A model has been developed illustrating the substrate specificity of glycerol kinase that three carbons as backbone and the presence of at least two hydroxyl groups are essential requirements [122, 123]. A broad examination on the substrate spectrum of glycerol kinase has been described elsewhere [70]. Amino acid analysis of glycerol kinase from *E. coli* has revealed that it contains 20 cysteine residues and all exist as free sulfhydryl functional groups [80, 81]. Due to the sulfhydryl group residue, glycerol kinase has been described to be oxygen sensitive, hence losing its activity by shaking in the air that requires reducing agents as stabilizer [51, 70]. Few synthetic applications of glycerol kinase from various microbial sources, in both free and immobilized form, have been described using deoxygenated reaction solution containing reducing agent DTT as well as performing reactions under argon [59, 70, 79]. Two sets of experiments were carried out, in one set using deoxygenated reaction solution containing 50 mM DTT under nitrogen

while in the other set reaction solution without deoxygenating and no addition of DTT was used. Results showed no significant enzyme activity difference in both sets of experiments. Figure 4.4 shows the activity of commercially available glycerol kinase from *Bacillus stearothermophilus*, *Cellulomonas* sp., *E. coli* and *Streptomyces canus* assayed for the asymmetric phosphorylation of glycerol. Moreover, the activity of glycerol kinase at the given temperature in Figure 4.4 relates to the enzyme sources. However, the temperature range of activity assay is limited not only due to the activity and stability of glycerol kinase but also because temperature is a crucial factor for the stability of chemically labile phosphorylated metabolites and cofactors.

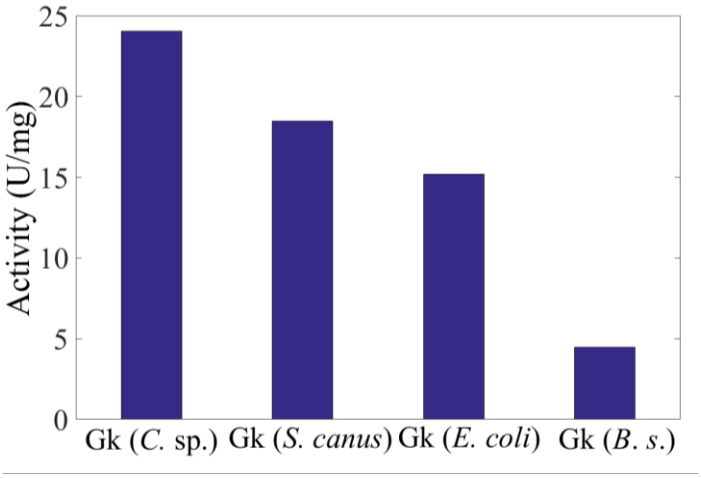

Figure 4.4: Activity of commercially available glycerol kinases (Gk) (EC 2.7.1.30) from *Cellulomonas* sp. (*C.* sp., 0.046 mg/mL), *Streptomyces canus* (*S. canus*, 0.045 mg/mL), *E. coli* (0.045 mg/mL) and *Bacillus stearothermophilus* (*B. s.*, 0.073 mg/mL) for the asymmetric phosphorylation of glycerol yielding *sn*-glycerol-3-phosphate; reaction conditions: 50 mM ATP, 50 mM glycerol, 100 mM Mg^{2+}, in 100 mM Tris-HCl buffer, pH 8.5, and 25°C

The activity and operational stability of glycerol kinase from *Cellulomonas* sp., *E. coli* and *Streptomyces canus* were investigated as a function of temperature and pH as well as their interactive effect. The operational stabilities of these glycerol kinases were examined by measuring the remaining activity after incubation in reaction buffer containing 100 mM ATP or 100 mM glycerol and 100 mM Mg^{2+} at different pH and temperature levels. The enzymes were incubated in two sets of incubation solutions containing 100 mM ATP or 100 mM glycerol in order to examine the effect of substrates e.g. stabilization effect of glycerol as described in literature [51, 81].

A homotetrameric glycerol kinase from *E. coli* [80] or homodimeric in which each subunit composed of two major domains acting as pseudo-tetrameric structure [124] was discovered by Hayashi, et al. (1967). Figure 4.5 and Figure 4.6 show the activity and stability of glycerol kinase from *E. coli* as a function of pH, respectively, analyzed in this study. Half-life of the enzyme is defined as the time that the enzyme lots half of its activity. Results show that glycerol kinase from *E. coli* exhibits nearly constant activity from pH 7.5 to pH 9.5 and is most stable in neutral pH region with decreasing stability as pH increases.

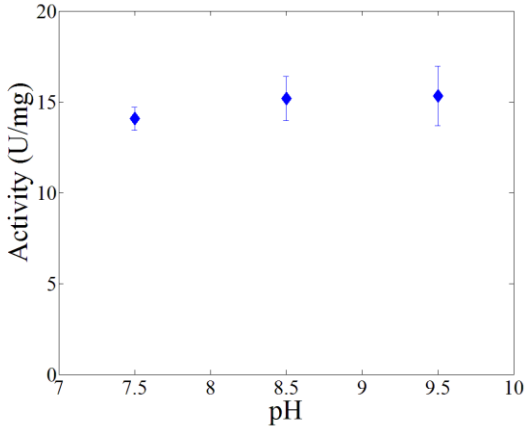

Figure 4.5: Activity of glycerol kinase from *E. coli* as a function of pH; reaction condition: 50 mM ATP, 50 mM glycerol, 100 mM Mg^{2+}, 0.045 mg/mL glycerol kinase from *E. coli* in 100 mM Tris-HCl buffer at 25°C

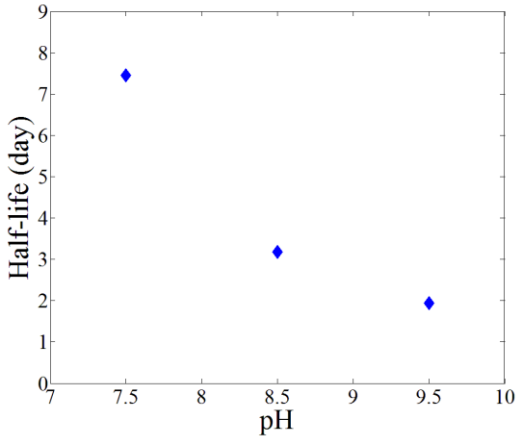

Figure 4.6: Half-life time of glycerol kinase form *E. coli* as a function of pH; incubation conditions: 100 mM ATP or 100 mM glycerol, 100 mM Mg^{2+} in 100 mM Tris-HCl buffer at 25°C and remaining activities were measured using conditions for the activity assay in Figure 4.5

Glycerol kinase from *Cellulomonas* sp., MW of 55 kDa by SDS-PAGE as shown in Figure B.12 appendix B was discovered by Sogabe, et al. (2009). Figure 4.7 and Figure 4.8 show the activity and stability of glycerol kinase from *Cellulomonas* sp. as a function of pH as well as temperature, respectively. The activity of glycerol kinase from *Cellulomonas* sp. increases with increasing temperature from 25°C to 45°C and pH from 7.5 to 9.5; in contrast to the reported nearly constant activity in this pH region [125]. No significant loss of the enzyme activity was shown from pH 7.5 to pH 9.5 at 25°C and 30°C in a month of incubation period. The stability of this enzyme drastically drops at 45°C and exhibits the maximum stability at pH 8.5 and 45°C. Moreover, the enzyme showed complete loss of activity at pH below 4.

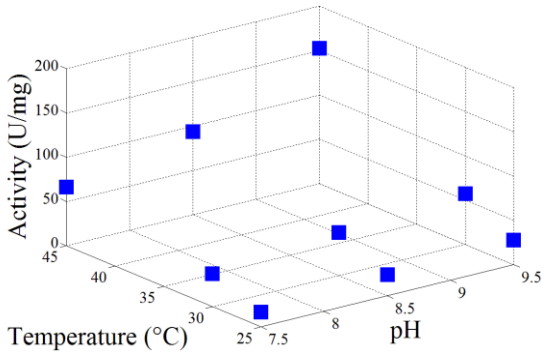

Figure 4.7: Activity of glycerol kinase from *Cellulomonas* sp. as a function of pH and temperature; reaction condition: 50 mM ATP, 50 mM glycerol, 100 mM Mg^{2+}, 0.046 mg/mL glycerol kinase from *Cellulomonas* sp. in 100 mM Tris-HCl buffer

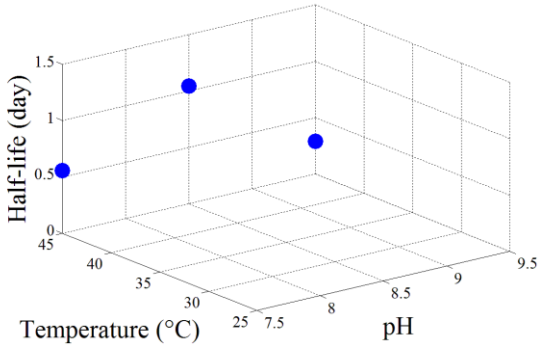

Figure 4.8: Half-life of glycerol kinase from *Cellulomons* sp. as a function of pH and temperature; incubation conditions: 100 mM ATP or 100 mM glycerol, 100 mM Mg^{2+} in 100 mM Tris-HCl buffer and remaining activities were measured using conditions for the activity assay in Figure 4.27

A monomeric glycerol kinase from *Streptomyces canus* (MW of 70 kDa) was discovered by Imamura, et al. (1982). The activity of this enzyme increases with increasing temperature but remains nearly constant activity from pH 7.5 to pH 9.5. The stability of glycerol kinase from *Streptomyces canus* decreases with increasing temperature and most stable at pH 8.5. Figure 4.9 and Figure 4.10 show the activity and stability of glycerol kinase from *Streptomyces canus*, respectively.

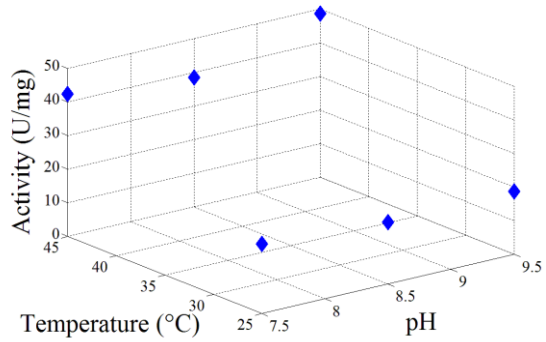

Figure 4.9: Activity of glycerol kinase from *Streptomyces canus* as a function of pH and temperature; reaction condition: 50 mM ATP, 50 mM glycerol, 100 mM Mg^{2+}, 0.0453mg/mL glycerol kinase from *Streptomyces canus* in 100 mM Tris-HCl buffer

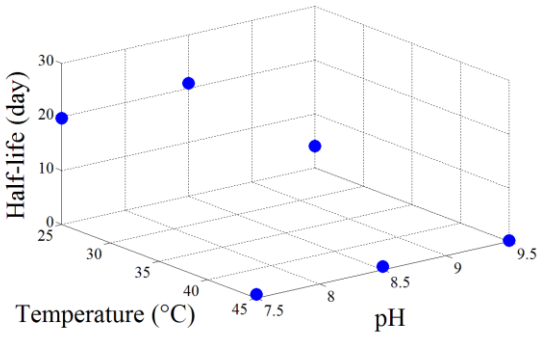

Figure 4.10: Half-life of glycerol kinase from *Streptomyces canus* as a function of pH and temperature; incubation conditions: 100 mM ATP or 100 mM glycerol, 100 mM Mg^{2+} in 100 mM Tris-HCl buffer and remaining activities were measured using conditions for the activity assay in Figure 4.9

The activity and stability of an enzyme relate to the enzyme source; moreover, the glycerol kinases studied above show similar activity profiles compared to glycerol kinases from other sources with respect to pH as shown in Table 4.1. Neutral to slightly alkaline pH is therefore an optimal pH region for the activity of glycerol kinase.

Table 4.1: Optimum pH for the activity of glycerol kinase from various sources

Enzyme sources	**Optimal pH**
***Cellulomonas* sp.**	pH 9.5 (this study)
E. coli	pH 7.5 to 9.5 (this study)
Streptomyces canus	pH 7.5 to 9.5 (this study)
Human liver *and fiberoblasts*	pH 8.5 to 9.5 [126]
Calf liver	pH 9 to 9.5 [127],
Acetobacter xylinum	pH 8.4 to 9.2 [71]
Pediococcus pentosaceus	pH 7.5 [128]
Bacillus stearothermophilus	pH 9 [128]

Moreover, in order to select favorable reaction conditions, attention must be paid to other relevant factors such as interaction of buffer with reaction species, interaction of buffer with the enzyme and simplicity of DSP etc. Figure 4.11 shows the activity of glycerol kinase from *Cellulomonas* sp. and *Streptomyces canus* in Tris-HCl and TEA buffer. Both enzymes show higher activity in Tris-HCl than in TEA buffer.

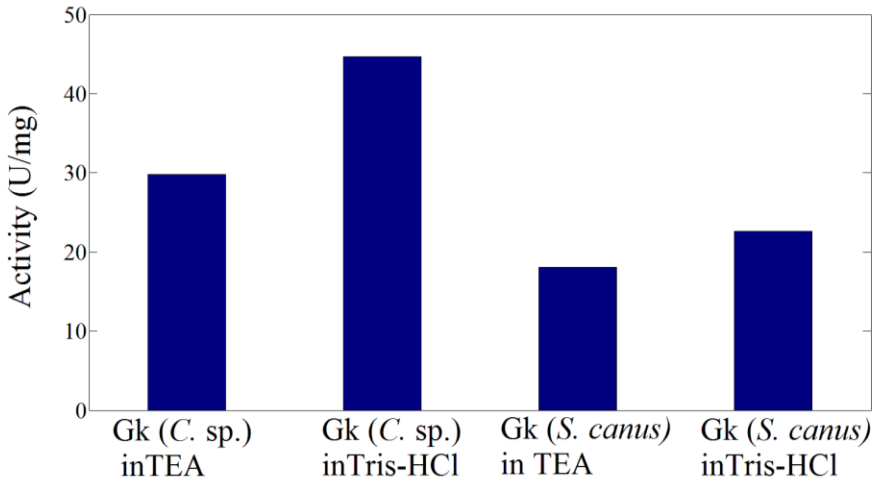

Figure 4.11: Activity of glycerol kinase from *Cellulomonas* sp. and *Streptomyces canus* in different buffer media; reaction conditions: 50 mM ATP, 50 mM glycerol, 100 mM Mg^{2+}, 0.24 mg/mL glycerol kinase from *Cellulomonas* sp. and 0.36 mg/mL glycerol kinase from *Streptomyces canus* at pH 8.5 and 30°C

Screening among glycerol kinases from *Bacillus stearothermophilus*, *Cellulomonas* sp., *E. coli* and *Streptomyces canus* have shown that glycerol kinase from *Cellulomonas* sp. exhibited the highest activity and is the most stable one. It therefore leads to select glycerol kinase from *Cellulomonas* sp. for the synthesis of *sn*-glycerol-3-phosphate.

4.2.2. Reaction Thermodynamics

Despite unfavorable change in reaction Gibbs free energy ($\Delta_r G$) in the reverse direction, several studies have treated glycerol kinase catalyzed asymmetric phosphorylation of glycerol by ATP as reversible [129–136]. It has been described that glycerol kinase from *Trypanosoma brucei* catalyzes phosphorylation of ADP by *sn*-glycerol-3-phosphate and could be used for ATP regeneration [131]. On the other hand, the same reaction has been treated as an irreversible in several other studies [51, 87, 137].

Therefore, the effects of factors including pH, ionic strength and mass action on the reaction thermodynamics were determined. The thermodynamic properties of the reaction system as a function of these parameters was determined in this study using a biochemical thermodynamics calculator called eQuilibrator$^{2.0}$ [138]. Figure 4.12 and Figure 4.13 show $\Delta_r G$ and K_{eq} as a function of pH, respectively. Figure 4.14 and Figure 4.15 show $\Delta_r G$ and K_{eq} as a function of ionic strength, respectively. Calculations were performed by varying substrate and product

concentrations between 1 nM and 10 mM and results showed no concentration effects on the reaction equilibrium position.

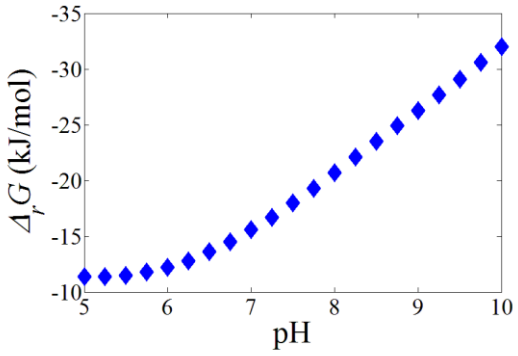

Figure 4.12: Change in reaction Gibbs free energy ($\Delta_r G$) of asymmetric phosphorylation of glycerol by ATP as a function of pH; calculation conditions: 10 mM ATP, 10 mM glycerol, 1 nM ADP, 1 nM *sn*-glycerol-3-phosphate, ionic strength of 0.1 M and 25°C

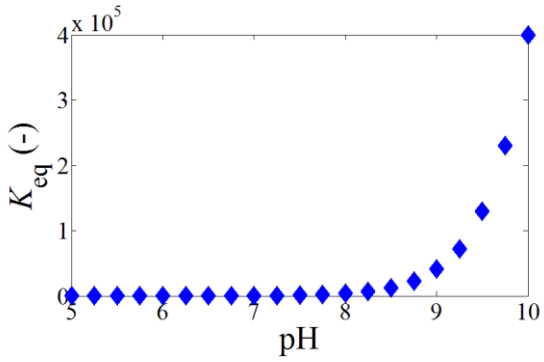

Figure 4.13: Reaction equilibrium constant (K_{eq}) of the asymmetric phosphorylation of glycerol by ATP as a function of pH; calculation conditions: 10 mM ATP, 10 mM glycerol, 1 nM ADP, 1 nM *sn*-glycerol-3-phosphate, ionic strength of 0.1 M and 25°C

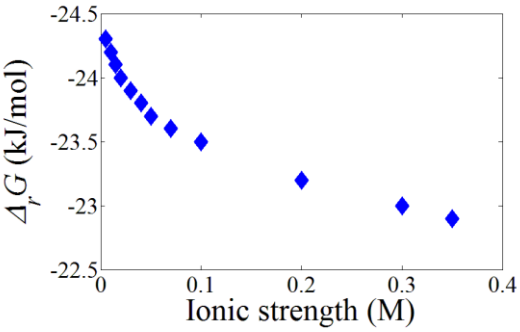

Figure 4.14: Change in reaction Gibbs free energy ($\Delta_r G$) of the asymmetric phosphorylation of glycerol by ATP as a function of ionic strength; calculation conditions: 10 mM ATP, 10 mM glycerol, 1 nM ADP, 1 nM *sn*-glycerol-3-phosphate, pH 8.5 and 25°C

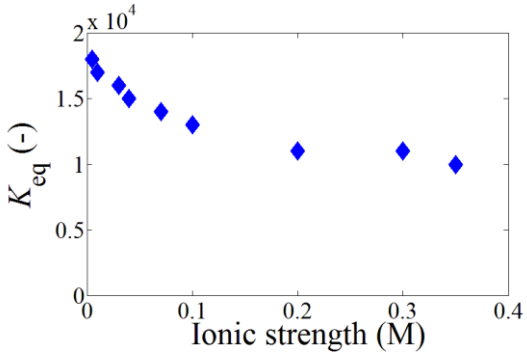

Figure 4.15: Reaction equilibrium constant (K_{eq}) of the asymmetric phosphorylation of glycerol by ATP as a function of ionic strength; calculation conditions: 10 mM ATP, 10 mM glycerol, 1 nM ADP, 1 nM *sn*-glycerol-3-phosphate, pH 8.5 and 25°C

Hence, the reaction favors forward at the tested reasonable pH and ionic strength values for the glycerol kinase catalyzed asymmetric phosphorylation of glycerol by ATP. Figure 4.16 moreover shows the reaction progress curve of a batch reaction using stoichiometric amounts of ATP and glycerol achieving complete conversion. Thus, the asymmetric phosphorylation of glycerol by

ATP catalyzed by glycerol kinase will be treated as irreversible for further investigation of reaction kinetics and process development.

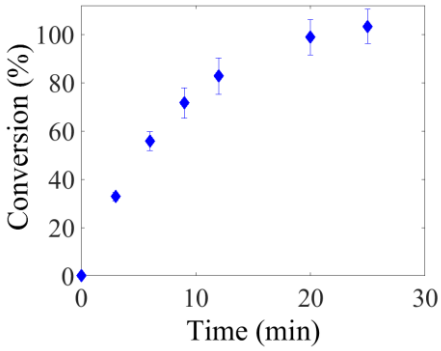

Figure 4.16: Substrate conversion plot for a batch reaction of the asymmetric phosphorylation of glycerol catalyzed by glycerol kinase; reaction conditions: 50 mM ATP, 50 mM glycerol, 10.5 mM Mg^{2+}, 0.06 mg/mL glycerol kinase from *Cellulomonas* sp. in 100 mM Tris-HCl buffer, pH 8.5, and 30°C

4.3. Reaction Kinetics of Asymmetric Phosphorylation of Glycerol

An investigation of biocatalytic reaction kinetics serves as a major tool to understand the reaction mechanism. Detailed analysis of reaction kinetics including kinetic parameter identification, parameter determination and an appropriate reaction kinetic model development serves to rationally design a bioprocess that utilizes the maximum possible enzyme activity. A consecutive enzymatic reaction sequence as shown in Figure 4.17 was used to assay the activity of glycerol kinase as a function glycerol concentration [51, 72].

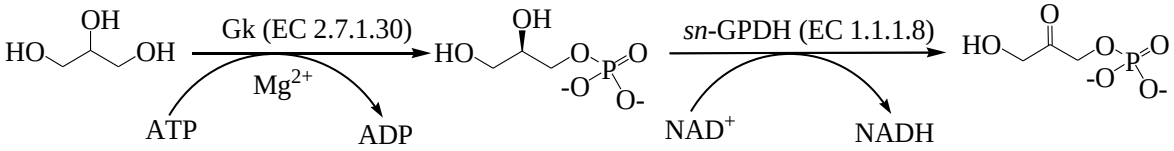

Figure 4.17: Reaction scheme used for the activity assay of glycerol kinase as a function of glycerol concentration; the asymmetric phosphorylation of glycerol catalyzed by glycerol kinase (Gk) (EC 2.7.1.30) yielding *sn*-glycerol-3-phosphate and the product undergoes subsequent oxidation catalyzed by *sn*-glycerol-3-phosphate dehydrogenase (*sn*-G3PDH) (EC 1.1.1.8) that generates stoichiometric amount of NADH

Glycerol must be phosphorylated in the first step of the reaction sequence to form *sn*-glycerol-3-phosphate so that the second reaction step generates stoichiometric amounts NADH. The NADH formation was monitored via UV spectrophotometer at 340 nm. The most important factor to be considered in this assay is that the first step of the reaction sequence must always be rate limiting. For that purpose: 1) the ratio of the two enzymes was chosen in such a way where

activity linearly increases with increasing amount of glycerol kinase while constant with addition of *sn*-G3PDH (results shown in Figure 4.18) and 2) 10-fold excess concentration of NAD^+ relative to glycerol concentration was applied. The applied concentration of NAD^+ was 14-fold larger than the K_m of *sn*-G3PDH (0.7 mM) for NAD^+ [72]. Moreover, as can be seen in Figure 4.19, NAD^+ has no effect on the activity of glycerol kinase.

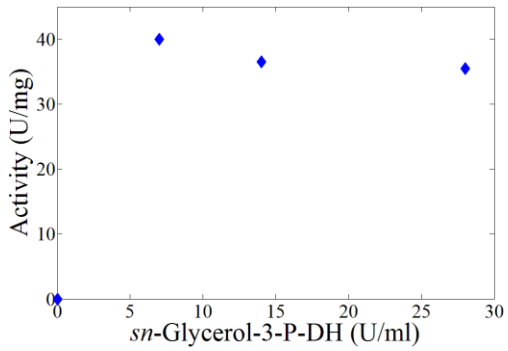

Figure 4.18: Activity of glycerol kinase for glycerol phosphorylation monitored by using enzymatic assay shown in Figure 4.17 as a function *sn*-G3PDH amount added into the reaction mixture, reaction conditions: 30 mM ATP, 5 mM glycerol, 30 mM Mg^{2+}, 15 mM NAD^+, 0.002 mg/mL glycerol kinase from *Cellulomonas* sp. in 100 mM Tris-HCl buffer, pH 8.5, and 25°C

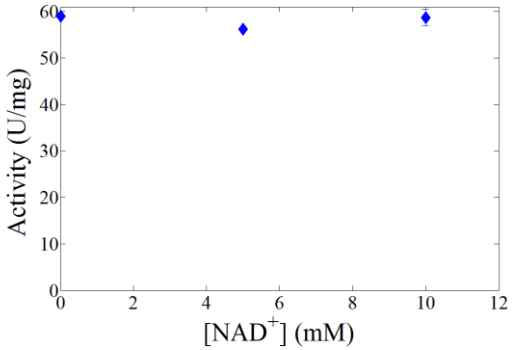

Figure 4.19: Activity of glycerol kinase as a function of NAD^+ concentration; reaction conditions: 50 mM ATP, 50 mM glycerol, 10 mM Mg^{2+}, 0.06 mg/mL glycerol kinase from *Cellulomonas* sp. in 100 mM Tris-HCl buffer, pH 8.5, and 25°C

Figure 4.20 shows the hyperbolic activity response of glycerol kinase from *Cellulomonas* sp. as a function of glycerol concentration. The enzyme displays Michealis-Menten kinetic behavior with respect to glycerol and a linear plot shown in Figure 4.21 was applied to determine v_{max} and K_m. These kinetic constants including values from literature for comparison are listed in Table 4.2.

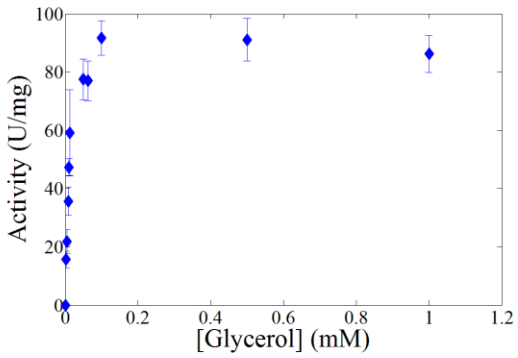

Figure 4.20: Activity of glycerol kinase from *Cellulomonas* sp. as a function glycerol concentration; reaction conditions, 30 mM ATP, 6 mM Mg^{2+}, 10 mM NAD^{+}, 0.0001 mg/mL glycerol kinase from *Cellulomonas* sp., 7 U/mL *sn*-glycerol-3-phoisphate dehydrogenase in 100 mM Tris-HCl buffer, pH 8.5, and 25°C

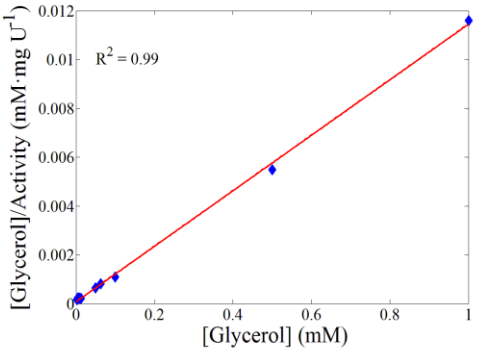

Figure 4.21: Linearization of hyperbolic activity response of glycerol kinase from *Cellulomonas* sp. as a function of glycerol concentration; reaction conditions, 30 mM ATP, 6 mM Mg^{2+}, 10 mM NAD^{+}, 0.0001 mg/mL glycerol kinase from *Cellulomonas* sp., 7 U/mL *sn*-glycerol-3-phoisphate dehydrogenase in 100 mM Tris-HCl buffer, pH 8.5, and 25°C

Table 4.2: The K_m values of glycerol kinase from *Cellulomonas* sp. and various sources with respect to glycerol

Microbial sources	*Cellulomonas* sp.	*E. coli*	*Candida mycoderma*	*Plasmodium falciparum*	*Streptomyces canus*
$K_{m,Glycerol}$	12 µM ± 2 µM (this study), 6.9 µM [125]	1.3 µM [73] 10 µM [81]	15 µM [130] 55 µM [87]	18 µM [139]	48 µM [86]

It has been described that hepatic glycerol kinase from rat displays inhibition by high concentration of glycerol [137]. The effect of glycerol concentrations larger than 1 mM on the enzyme activity was investigated in this study and the results shown in Figure 4.22 depict that the enzyme exhibits no substrate surplus inhibition by glycerol. It has been mentioned that glycerol kinases from rat liver [140], *Pediococcus pentosaceus* [128], *Cucumis sativus* [53], *Trypanosoma brucei* [129], muscles of vertebrates and invertebrates [141], *Candida mycoderma* [130]and rat hepatic [137] display inhibition by the product *sn*-glycerol-3-phosphate. On the other hand, glycerol kinases from *E. coli* [73, 81], rat liver, beef liver, human liver and *Candida*

mycoderma [87] as well as *T. brucei* [129] show no inhibition by *sn*-glycerol-3-phosphate. The inhibition of glycerol kinase by *sn*-glycerol-3-phosphate was investigated using the calcium salt of glycerol phosphate. Results of the enzyme activity as a function of calcium glycerol phosphate and calcium chloride concentrations shown in Figure 4.23 prove that the decrease of enzyme activity is due to the counter cation (Ca^{2+}). Therefore, glycerol kinase from *Cellulomonas* sp. shows no inhibition by *sn*-glycerol-3-phosphate. In most of those studies, the counter cation of *sn*-glycerol-1(3)-phosphate salt used to examine the inhibition was not mentioned; therefore, the discrepancy of results may ascribe to the effect of different counter cations. It has been described that the addition of Ca^{2+} potentiated glycerol kinase inhibition by ADP [137]; however, this could be explained that the addition of Ca^{2+} suppresses the enzyme activity due to the formation of enzymatically inactive Ca-ATP complexes. The inhibition result of glycerol kinase from *Cellulomonas* sp. by Ca^{2+} in this study agrees with similar property of glycerol kinase from various sources [51, 86]; in contrast, the addition of Ca^{2+} has been mentioned to activate glycerol kinase from *Pediococcus pentosaceus* [128]. The influence of Ca^{2+} on the reaction equilibrium was moreover examined and results showed that Ca^{2+} affects only the reaction kinetics.

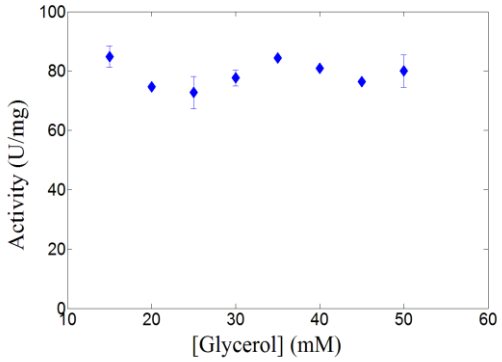

Figure 4.22: Examination of glycerol kinase from *Cellulomonas* sp. inhibition by glycerol; reaction conditions: 50 mM ATP, 5 mM Mg^{2+}, 0.015 mg/mL glycerol kinase from *Cellulomonas* sp. in 100 mM Tris-HCl buffer, pH 8.5, and 25°C

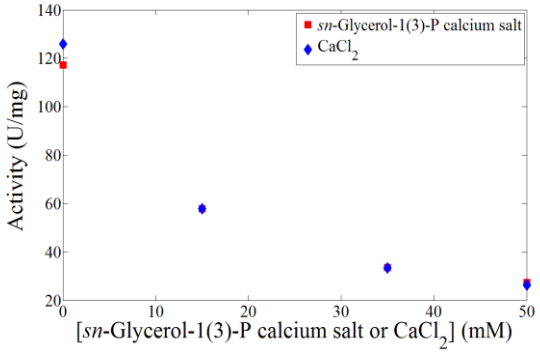

Figure 4.23: Inhibition test of glycerol kinase from *Cellulomonas* sp. by *sn*-glycerol-1(3)-phosphate and Ca^{2+}; reaction conditions: 50 mM ATP, 50 mM glycerol, 10.5 mM Mg^{2+}, 0.06 mg/mL glycerol kinase from *Cellulomonas* sp. in 100 mM Tris-HCl buffer, pH 8.5, and 30°C

4.3.1. The Effect of Mg^{2+} to ATP Molar Ratio on the Enzyme Activity

Glycerol kinase from *Cellulomonas* sp. essentially requires cofactors ATP as phosphoryl donor and divalent metal ion, preferably Mg^{2+}. Mg^{2+} is not consumed by the action of the enzyme , it rather forms various complexes with ATP. The interaction of Mg^{2+} and ATP produces Mg-ATP complexes with various physical and chemical features depending on the Mg^{2+} to ATP molar ratio among other factors such as pH, temperature, concentration of other polyvalent chelating anions as well as cations [142]. Various Mg-ATP complexes with dynamic configurations and intermolecular exchange equilibria form at different Mg^{2+} to ATP molar ratio [142]. It has been described that about 80% of ATP exist as a $[MgATP]^{-2}$ complex configuration when the concentration of Mg^{2+} is higher than that of ATP by 1 to 20 mM [143] while at Mg^{2+} to ATP molar ratio of 0.5 the major complex configuration is $[Mg(ATP)_2]^{-6}$ [142]. The formation of Mg-ATP complexes with various physical and chemical features affects the catalytic properties of glycerol kinase including the apparent affinity constant ($K_{m,app}$) and catalytic constant (k_{cat}).

Most often, for the kinetic characterization and synthetic application of glycerol kinase, stoichiometric or excess moles of Mg^{2+} relative to the moles of ATP have been applied [79, 144–148]. It has been suggested that $[MgATP]^{2-}$ complex acts as a "true" substrate for glycerol kinase [11, 57, 127, 149]. Only few investigations on the activity of glycerol kinase with respect to Mg^{2+} concentration have been mentioned; nevertheless, no interpretation of results as a function of Mg^{2+} to ATP molar ratio [11, 57, 121]. It has been described that free ATP acts as a positive modifier and free Mg^{2+} inhibits glycerol kinase [11]; whereas, both free ATP and free Mg^{2+} inhibit glycerol kinase [57]. Therefore, in this study detailed kinetics analyses of glycerol kinase from *Cellulomonas* sp. with respect to Mg^{2+} to ATP molar ratio, determining the optimum molar ratio where the enzyme shows maximum activity and the kinetic responses of the enzyme as a function of ATP concentration at a fixed Mg^{2+} concentration as well as a constant Mg^{2+} to ATP molar ratio were performed.

Three sets of activity measurements of glycerol kinase from *Cellulomonas* sp. as a function of Mg^{2+} concentration were carried out at 5 mM, 50 mM and 70 mM ATP. Figure 4.24 and Figure 4.25 show the activity of glycerol kinase from *Cellulomonas* sp. as a function of Mg^{2+} concentration and Mg^{2+} to ATP molar ratio, respectively. In all sets of the activity assays, glycerol kinase from *Cellulomonas* sp. shows no activity without the addition of Mg^{2+}. This

reveals Mg^{2+} as an essential requirement for the enzyme activity. The addition of Mg^{2+} enhances the enzyme activity in all sets of activity assays; however, surpassing a maximum the resulting activity is decreased again with subsequent addition of Mg^{2+}. The maxima occur at different concentration levels of Mg^{2+}, depending on the concentration of ATP (as shown in Figure 4.24). As shown in Figure 4.25, the maxima occur at the same molar ratio of Mg^{2+} to ATP.

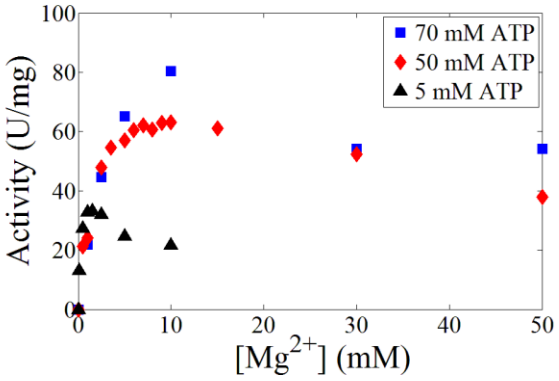

Figure 4.24: Activity of glycerol kinase from *Cellulomonas* sp. as a function Mg^{2+} concentration at different fixed ATP concentrations; reaction conditions: [5 mM; 50 mM; 70 mM] ATP, 50 mM glycerol, various amounts of glycerol kinase from *Cellulomonas* sp. in 100 mM Tris-HCl buffer, pH 8.5, and 25°C

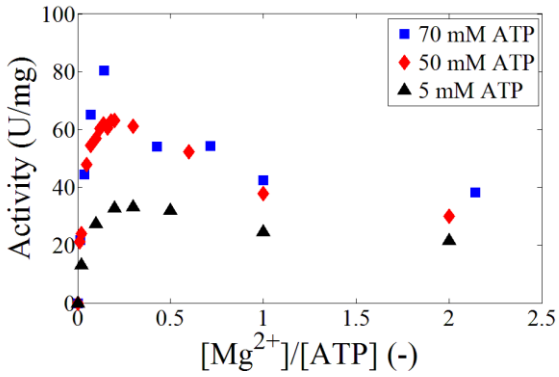

Figure 4.25: Activity of glycerol kinase as a function of Mg^{2+} to ATP molar ratio at different fixed ATP concentrations; reaction conditions: [5 mM; 50 mM; 70 mM] ATP, 50 mM glycerol, various amounts of glycerol kinase from *Cellulomonas* sp. in 100 mM Tris-HCl buffer, pH 8.5, and 25°C

An estimation of the optimum Mg^{2+} to ATP molar ratio where the enzyme shows maximum activity and the effect of Mg^{2+} at large Mg^{2+} to ATP molar ratio of up to 10 were performed experimentally. As results shown in Figure 4.26, the optimum Mg^{2+} to ATP molar ratio appears to be in the interval of [0.12 to 0.3]. Subsequent increase of Mg^{2+} to ATP molar ratio larger than the values in the optimum region suppresses the enzyme activity to a non-zero asymptotic value.

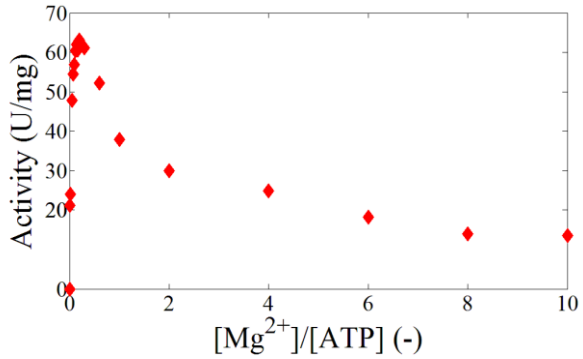

Figure 4.26: Activity of glycerol kinase as a function of Mg^{2+} to ATP molar ratio; reaction conditions: 50 mM ATP, 50 mM glycerol, [0 - 500 mM] Mg^{2+}, various amounts of glycerol kinase from *Cellulomonas* sp. in 100 mM Tris-HCl buffer, pH 8.5, and 25°C

Optimal Mg^{2+} concentration of about 3 mM has been described for glycerol kinase from various sources at 6 mM ATP; however, nearly similar activities for 1 mM and 3 mM Mg^{2+} [51]. Therefore, interpreting these results with respect to Mg^{2+} to ATP molar ratio would generate optimal Mg^{2+} to ATP molar ratio of about [0.16 to 0.5] that shows similar but not identical activity profile with the results acquired in this study. Assuming $[MgATP]^{2-}$ as a "true" substrate, it has been described that excess ATP than the concentration required to generate 1:1 Mg^{2+} to ATP molar ratio acts as a positive modifier inhibitor [87]. Whereas, at low concentration of $[MgATP]^{2-}$ the excess ATP acts as inhibitor and excess Mg^{2+} always acts as inhibitor [87]. The description is merely due to quantitative reason that equal concentrations of ATP have different effects on shifting the magnitude of Mg^{2+} to ATP molar ratio depending on the concentration of $[MgATP]^{2-}$. At a high concentration of $[MgATP]^{2-}$, a large amount of ATP is required to shift the molar ratio to the optimum level that shows ATP as a pseudoactivator. At low concentrations of $[MgATP]^{2-}$ the same amount of ATP shifts the Mg^{2+} to ATP molar ratio below the optimum level that shows ATP as a pseudoinhibitor.

The effects of factors such as glycerol concentration, pH, buffer type and amount of glycerol kinase on the activity profile of the enzyme as a function of Mg^{2+} to ATP molar ratio were investigated. Figure 4.27 shows the effects of pH and reaction buffer type on the activity profile of glycerol kinase as a function of Mg^{2+} to ATP molar ratio. Figure 5.10 in chapter 5 shows the effect of glycerol kinase concertation. All results showed no influence of these factors on the activity pattern of glycerol kinase as a function of Mg^{2+} to ATP molar ratio. Similar kinetics behavior has been described for other enzymes involved in phosphoryl transfer reaction that require divalent Mg^{2+} and polyvalent phosphoryl donor [77, 85, 87–90]. Moreover, Mg^{2+} does not influence the reaction thermodynamics as complete conversion was achieved by performing a batch reaction at 33-fold larger Mg^{2+} to ATP molar ratio than the optimum molar ratio.

However, the enzyme retained 22.5% of its initial activity relative to its activity at the optimum molar ratio.

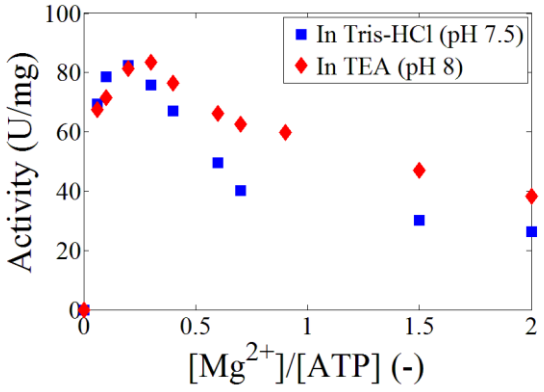

Figure 4.27: The effect of reaction buffer type and pH on the activity profile of glycerol kinase from *Cellulomonas* sp. as a function of Mg^{2+} to ATP molar ratio; reaction conditions: 50 mM ATP, 50 mM glycerol, [0 - 100 mM] Mg^{2+} various amounts of glycerol kinase from *Cellulomonas* sp. in 100 mM Tris-HCl buffer, pH 7.5, or in 100 mM TEA buffer, pH 8, and 30°C

4.3.2. Two-step Kinetics Property of Glycerol Kinase

Sets of initial rate measurements of glycerol kinase from *Cellulomonas* sp. as a function of ATP concentration were performed either maintaining constant Mg^{2+} to ATP molar ratio or at a fixed Mg^{2+} concentration. It has been described that glycerol kinases from *E. coli* and *Candida mycoderma* show glycerol independent activity of ATP hydrolysis yielding ADP and P_i [132, 150]. Non-specific glycerol kinase catalyzed depletion of ATP without the addition of glycerol was investigated and the result shown in Figure 4.28 depicts that the enzyme shows no ATPase activity without the addition of glycerol nor ATP is unstable in the reaction conditions.

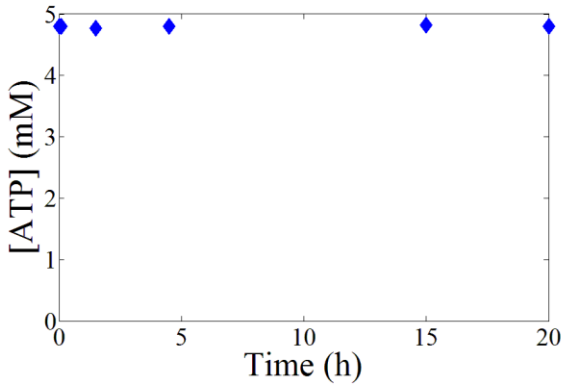

Figure 4.28: Non-specific glycerol kinase catalyzed glycerol independent hydrolysis of ATP; reaction conditions: 5 mM ATP, 5 mM Mg^{2+}, 0.03 mg/mL glycerol kinase from *Cellulomonas* sp. in 100 mM Tris-HCl buffer, pH 8.5, and 25°C

Figure 4.29 shows the hyperbolic activity response of glycerol kinase from *Cellulomonas* sp. as a function of ATP concentration maintaining Mg^{2+} to ATP molar ratio of 0.3. The enzyme exhibits

a Michaelis-Menten kinetic pattern. The kinetic constants, v_{max} and K_m of 72.62 U/mg ± 4.93 U/mg and 2.061 mM ± 0.083 mM, respectively, were determined using double reciprocal linearization method as shown in Figure 4.30.

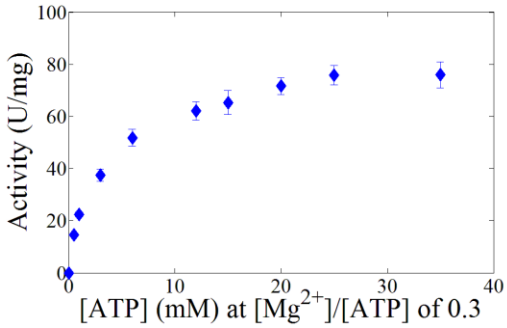

Figure 4.29: The activity of glycerol kinase from *Cellulomonas* sp. as a function ATP concentration maintaining constant Mg^{2+} to ATP molar ratio of 0.3; reaction conditions: 50 mM glycerol, [0 - 35 mM] ATP, corresponding amounts of Mg^{2+} that establish Mg^{2+} to ATP molar ratio of 0.3, various amounts of glycerol kinase from *Cellulomonas* sp. in 100 mM Tris-HCl buffer, pH 8.5, and 30°C

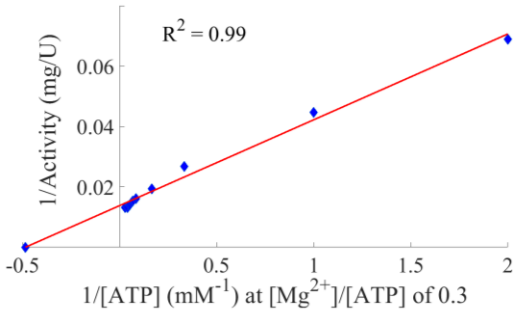

Figure 4.30: Linearization of hyperbolic activity response of glycerol kinase from *Cellulomonas* sp. as a function ATP concentration maintaining constant Mg^{2+} to ATP molar ratio of 0.3 using double reciprocal linearization method; reaction conditions: 50 mM glycerol, [0 - 35 mM] ATP, various amounts of glycerol kinase from *Cellulomonas* sp. in 100 mM Tris-HCl buffer, pH 8.5, and 30°C

A kinetic model developed using the kinetics knowledge of glycerol kinase with respect to ATP maintaining constant Mg^{2+} to ATP molar ratio is not capable of simulating reaction progress. This is because, as shown in Figure 4.31, the decrease of reaction velocity with increasing conversion can be affected by variables including formation of an inhibitor ADP, depletion of ATP and glycerol; moreover, the depletion of ATP means the increase of Mg^{2+} to ATP molar ratio. The increase of Mg^{2+} to ATP molar ratio with reaction progress means the shift of Mg^{2+} to ATP molar ratio larger than the starting optimum value that creates pseudo-ATP surplus inhibition. An attempt to simulate the progress of a batch reaction using a competitive inhibition constant for ADP determined numerically by non-linear progress curve fitness (i.e. $K_{ic,ADP}$ of 0.012 mM) always yields the simulated reaction progress faster than the experimental reaction progress as shown in Figure 4.32. For the simulation the reaction kinetic equation shown in Eqn(4.1) in and the differential equations shown in Eqn(4.2) and Eqn(4.3) were applied.

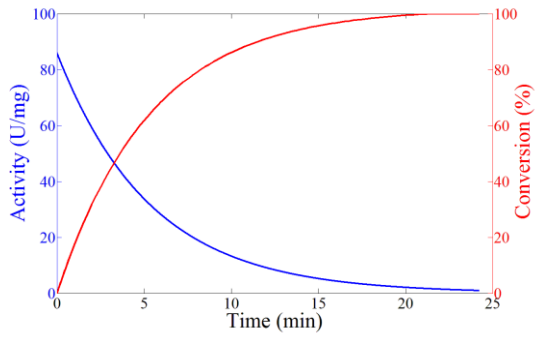

Figure 4.31: The decrease of glycerol kinase activity and the increase of conversion vs. reaction time; conversion data were numerically calculated from a batch reaction by using non-linear least regression (RMSE = 1.5%); reaction conditions: 25 mM ATP, 50 mM glycerol, 7.5 mM Mg^{2+}, 0.06 mg/mL glycerol kinase from *Cellulomonas* sp. in 100 mM Tris-HCl buffer, pH 8.5, and 30°C

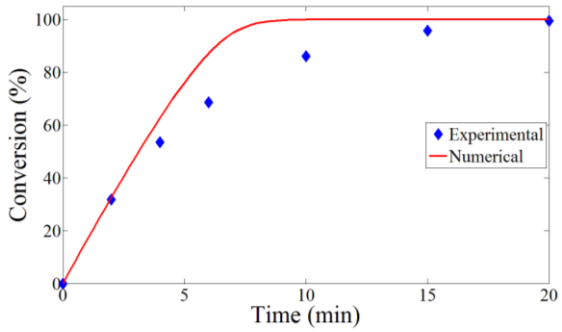

Figure 4.32: Experimentally determined conversion and numerically computed conversion vs. reaction time; reaction conditions: 25 mM ATP, 50 mM glycerol, 7.5 mM Mg^{2+}, 0.06 mg/mL glycerol kinase from *Cellulomonas* sp. in 100 mM Tris-HCl buffer, pH 8.5, and 30°C

Initial rate measurements of glycerol kinase from *Cellulomonas* sp. as a function of ATP concentration were performed at fixed 10.5 mM Mg^{2+} and 35 mM of ATP, establishing a Mg^{2+} to ATP molar ratio of 0.3. Figure 4.33 shows two-step kinetics of glycerol kinase as a function of ATP concentration. The enzyme exhibits pseudo-ATP activation after about 6 mM of ATP. Figure 4.34 shows the lower-step enzyme kinetics under magnification up to 6 mM ATP. When measuring the initial rate of glycerol kinase as a function of ATP concentration at a fixed Mg^{2+} concentration two major factors affect the enzyme activity. These are the increase of enzyme activity due to increasing Mg-ATP complex concentration and the shift of Mg^{2+} to ATP molar ratio that affects the K_m and k_{cat} of the enzyme. In the lower-step, the increase of reaction rate up to 6 mM ATP is dominated by the increase of substrate concentration. Here the enzyme exhibits a Michaelis-Menten kinetics pattern with large affinity and less catalytic activity. This is because as depicted in Figure 4.26, the increase of activity is minimal due to the change in Mg^{2+} to ATP molar ratio in the region of higher Mg^{2+} to ATP molar ratio. Surpassing the concentration 6 mM ATP the enzyme activity starts to reflect the increase of activity not only due to increase of substrate concentration but also the shift of Mg^{2+} to ATP molar ratio to the optimal level.

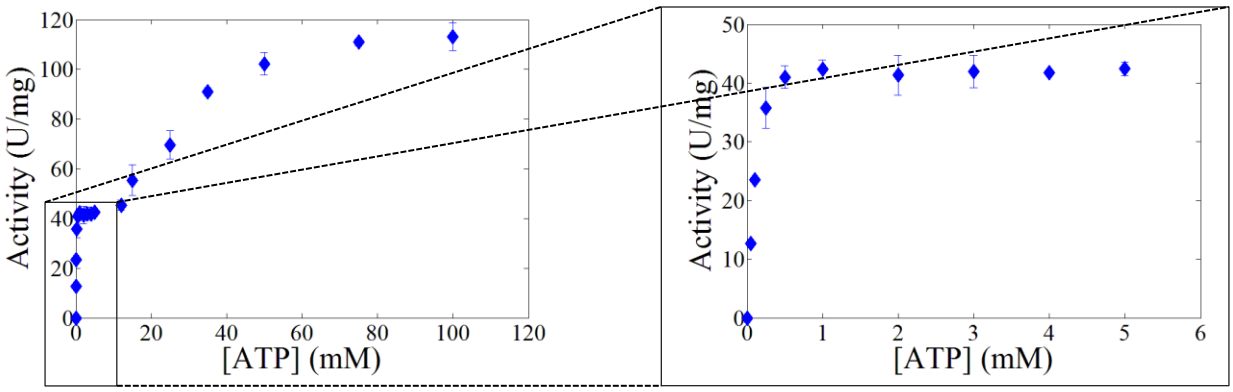

Figure 4.33: Activity of glycerol kinase as a function of ATP concentration at a fixed 10.5 mM of Mg^{2+}; reaction conditions: 50 mM glycerol, 10.5 mM Mg^{2+}, various amounts of glycerol kinase from *Cellulomonas* sp. in 100 mM Tris-HCl buffer, pH 8.5, and 30°C

Figure 4.34: Magnification of activity of glycerol kinase as a function of ATP concentration up to 6 mM ATP at a fixed 10.5 mM of Mg^{2+}; reaction conditions: 50 mM glycerol, 10.5 mM Mg^{2+}, various amounts of glycerol kinase from *Cellulomonas* sp. in 100 mM Tris-HCl buffer, pH 8.5, and 30°C

Moreover, other sets of initial rate measurements as a function of ATP concentration were carried out at 1.5 mM and 21 mM Mg^{2+}. Figure 4.35 and Figure 4.36 show the activity results of the whole concentration range and the magnification up to 6 mM ATP, respectively. As anticipated, the lower-step kinetics at 21 mM Mg^{2+} shows similar Michaelis-Menten kinetic pattern as of at 10.5 mM Mg^{2+} while at 1.5 mM Mg^{2+} the enzyme exhibits less affinity and larger catalytic activity than at 10.5 mM Mg^{2+}. In the upper-step kinetics, the enzyme activity at 21 mM Mg^{2+} increases up to 100 mM ATP without saturation while saturated in cases of 10.5 mM Mg^{2+} (shown in Figure 4.33). The enzyme kinetics at 1.5 mM Mg^{2+} displays pseudo-ATP surplus inhibition. The decrease of enzyme activity at 1.5 mM Mg^{2+} after about 20 mM ATP is due to the shift of Mg^{2+} to ATP molar ratio below the optimum molar ratio interval.

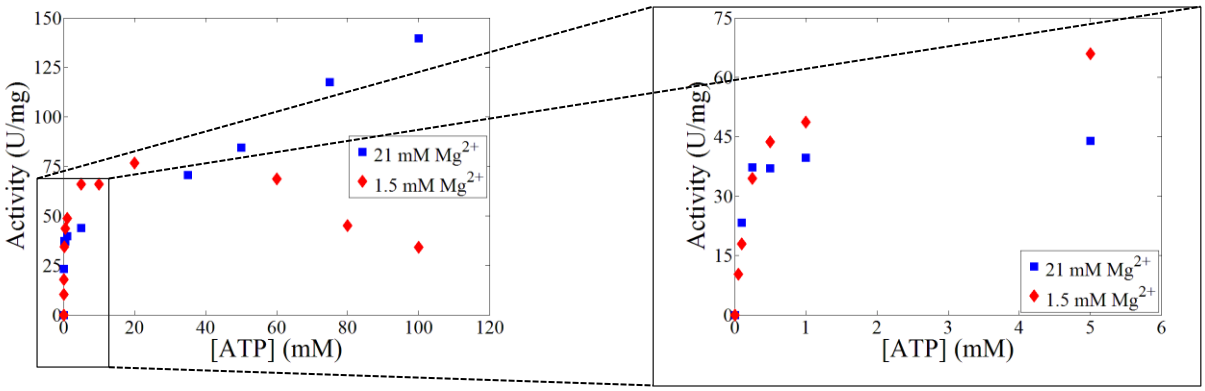

Figure 4.35: Activity of glycerol kinase as a function of ATP concentration at fixed 1.5 mM and 21 mM Mg^{2+}; reaction conditions: 50 mM glycerol, 1.5 mM and 21 mM Mg^{2+}, various amounts of glycerol kinase from *Cellulomonas* sp. in 100 mM Tris-HCl buffer, pH 8.5, and 30°C

Figure 4.36: Magnification of activity of glycerol kinase as a function of ATP concentration up to 6 mM ATP at fixed 1.5 mM and 21 mM Mg^{2+}; reaction conditions: 50 mM glycerol, 1.5 mM and 21 mM Mg^{2+}, various amounts of glycerol kinase from *Cellulomonas* sp. in 100 mM Tris-HCl buffer, pH 8.5, and 30°C

It has been described that glycerol kinase from *E. coli* shows two apparent K_m values with respect to ATP [81] as well as two apparent K_m and v_{max} values for glycerol kinase from *E. coli* and *Haemophilus influenza* [151]. Several attempts have been described to explain the two-step kinetics behavior of glycerol kinase with respect to ATP. Most of them based the following presumptions:

1) Heterogeneity of the enzyme preparation i.e. the presence of glycerol kinase isozyme [81]
2) Existence of several or at least two independent active sites onto a glycerol kinase molecule with different affinity constants (K_m) and catalytic constants (k_{cat}) [81, 132, 151]
3) Non-ordered bi-substrate mechanism that substrates combines with more than one form of an enzyme molecule [81],
4) Presence of ATPase activity [78] and
5) The allosteric regulatory kinetic behavior of glycerol kinase by its own substrate (i.e. homotropic effect) due to the existence of regulatory site where ATP binds separate from the active site [132].

Few have furthermore developed reaction kinetics models using parameters determined by non-linear square fitness of experimental data for user-defined reaction mechanism based on the

assumed existence of two independent active sites with two apparent K_m and v_{max} values in respect to ATP [132, 151]. However, those presumptions to explain the two-step kinetics pattern can be excluded because glycerol kinase exhibits Michealis-Menten kinetic pattern with respect to glycerol (as shown in Figure 4.20) and ATP maintaining constant Mg^{2+} to ATP molar ratio (as shown in Figure 4.29) as well as no ATPase activity (as shown in Figure 4.28). The two-step kinetics behavior of glycerol kinase as a function of ATP at a fixed Mg^{2+} concentration can rather be explained due to the multiple and dynamic Mg-ATP complex formations at different Mg^{2+} to ATP molar ratios. Therefore, the same active site of glycerol kinase exhibits different K_m and k_{cat} in respect to Mg-ATP complexes of different physical and chemical features. Detailed elucidation of physical and chemical modification of ATP by Mg^{2+} using ^{31}P and ^{1}H NMR as well as mechanistic explanation and correlation with the enzyme activity profile as a function of Mg^{2+} to ATP molar ratio will be discussed in chapter 6.

The inhibition of glycerol kinase from various sources by ADP and AMP has been described; however, in few cases acquired data have been misinterpreted [58, 71, 81, 87, 128, 137, 140, 141, 152]. It has been mentioned that in the activity assay containing 1 mM ATP, 1 mM ADP suppresses 26% of the enzyme activity at 0.2 mM Mg^{2+} and 83% at 20 mM Mg^{2+} and 0.2 mM AMP suppresses 30% of the enzyme activity at 2 mM Mg^{2+} and 70% at 10 mM Mg^{2+} [140]. In the case of ADP the Mg^{2+} to ATP molar ratio increased from 0.2 to 20 and in the case of AMP the Mg^{2+} to ATP molar ratio increased from 0.5 to 10; therefore, the decrease of activity could be ascribed due to the increase of Mg^{2+} to ATP molar ratio and not because Mg^{2+} potentiates the enzyme inhibition by ADP and AMP. Grunnet, et al. (1967) has described that the addition of high concentration of ATP counteracted the inhibition of glycerol kinase from various sources by AMP produced at 2 mM ATP and 4 mM Mg^{2+} (i.e. $[Mg^{2+}]/[ATP] = 2$) while the addition of high concentration of Mg^{2+} in the given assay condition increased the extent of inhibition by AMP. At the given Mg^{2+} to ATP molar ratio of 2, the effects of ATP and Mg^{2+} on the activity of glycerol kinase most ascribe due to the adjustment of Mg^{2+} to ATP ratio to or larger than the optimum interval.

The inhibition of glycerol kinase by ADP is of a major interest for practical synthetic purpose as the formation of AMP at the reaction condition is negligible. ATP and ADP are polydentate ligands with various electron donating sites including negatively charged oxygen atoms of

phosphate chain at the reaction pH, hydroxyl groups of the ribose sugar and nitrogen atoms of the purine base. Therefore, ADP binds with Mg^{2+} in similar chemistries as ATP does but with less affinity [153]. The mechanism in which ADP inhibits glycerol kinase can be by competition with ATP for binding with the enzyme active site, by complexation with Mg^{2+} that shifts the Mg^{2+} to ATP molar ratio or both. Thus, inhibition of glycerol kinase by ADP was examined by performing sets of activity measurements as a function of ADP concentration at different Mg^{2+} to ATP molar ratio. Figure 4.37 and Figure 4.38 show the activity of glycerol kinase measured experimentally and relative inhibition as a function of ADP concentration at different Mg^{2+} to ATP molar ratio, respectively. The decrease of glycerol kinase activity as a function of ADP concentration is irrespective of Mg^{2+} to ATP molar ratio that nearly similar percent of inhibition imposed by ADP at different Mg^{2+} to ATP molar ratio.

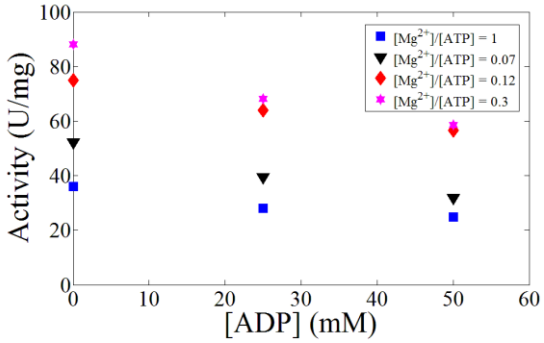

Figure 4.37: Activity of glycerol kinase from *Cellulomonas* sp. as a function of ADP concentration at different Mg^{2+} to ATP molar ratio; reaction conditions: 50 mM ATP, 50 mM glycerol, [3.5 mM, 6 mM, 15 mM, 50 mM] Mg^{2+}, various amounts of glycerol kinase from *Cellulomonas* sp. in 100 mM Tris-HCl buffer, pH 8.5, and 30°C

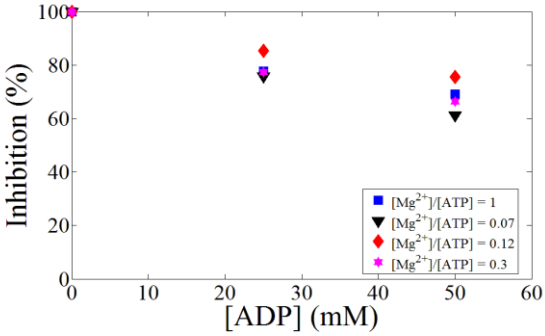

Figure 4.38: Relative inhibition of glycerol kinase from *Cellulomonas* sp. as a function of ADP concentration at different Mg^{2+} to ATP molar ratio; reaction conditions: 50 mM ATP, 50 mM glycerol, [3.5 mM, 6 mM, 15 mM, 50 mM] Mg^{2+}, various amounts of glycerol kinase from *Cellulomonas* sp. in 100 mM Tris-HCl buffer, pH 8.5, and 30°C

The inhibition of glycerol kinase by ADP is thus due to the competition with ATP for binding with the enzyme's active site. Figure 4.39 shows results of two sets of activity measurements as function of ATP concentration at a fixed 10.5 mM Mg^{2+} without and with the addition of 1 mM ADP in order to examine inhibition type and to determine inhibition constant. As can be seen in Figure 4.39 ADP affects the affinity constant (K_m) of the enzyme, not the v_{max}.

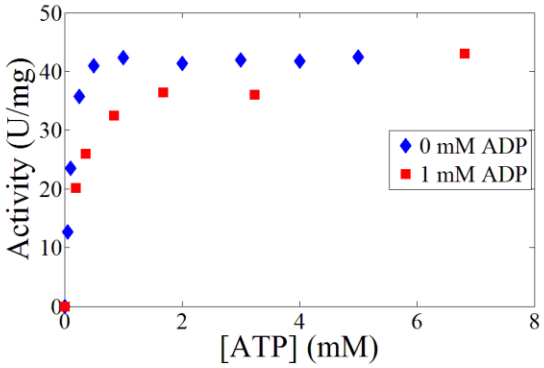

Figure 4.39: The influence of ADP on the kinetic of glycerol kinase from *Cellulomonas* sp. with respect to ATP at a fixed 10.5 mM Mg^{2+}; reaction conditions: [0 - 6.8 mM] ATP, 50 mM glycerol, 10.5 mM Mg^{2+}, 1 mM ADP, various amounts of glycerol kinase from *Cellulomonas* sp. in 100 mM Tris-HCl buffer, pH 8.5, and 30°C

As a strategy to apply polyphosphate kinase (PPK)/PP_in mediated *in situ* ATP regeneration for glycerol kinase asymmetric phosphorylation of glycerol (shown in Figure 4.40), the effect of PP_in on the activity of glycerol kinase was investigated. The potential application of PPK from various sources to regenerate ATP was investigated. Preliminary results are provided in chapter 8. The knowledge of glycerol kinase from *Cellulomonas* sp. activity with respect to PP_in concentration is crucial for further analysis reaction coupling efficiency.

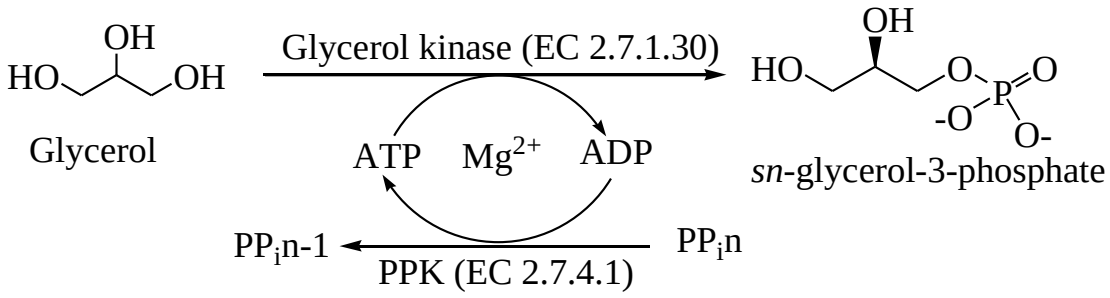

Figure 4.40: A reaction scheme illustrating the asymmetric phosphorylation of glycerol catalyzed by glycerol kinase (EC 2.7.1.30) yielding *sn*-glycerol-3-phosphate coupled with the phosphorylation of ADP to *in situ* regenerate ATP using polyphosphate kinase (PPK) (EC 2.7.4.1) that utilizes PP_in as a phosphoryl donor

Since PP_in forms complexes with Mg^{2+} in similar not identical chemistry as ATP does, the effect of PP_in on the activity of glycerol kinase from *Cellulomonas* sp. was examined at three rationally set Mg^{2+} to ATP molar ratio levels: At Mg^{2+} to ATP molar ratio larger than the values in the optimum interval, at the upper and lower limits of the optimum ratio interval. Figure 4.41 shows that the effect of PP_in on the activity of glycerol kinase depends on the level of Mg^{2+} to ATP molar ratio. If the Mg^{2+} to ATP molar ratio is set to be the lower limit of the optimum ratio interval or below, PP_in suppresses the enzyme activity. If the Mg^{2+} to ATP molar ratio is set to be the upper limit of optimum interval, PP_in shows no effect on the enzyme activity; however, up to a concentration level of PP_in where non-effective Mg^{2+} is fully titrated by PP_in. Further

addition of PP_in leads to suppressed enzyme activity. On the other hand, at the Mg^{2+} to ATP molar ratio of 2, the addition of PP_in enhances the enzyme activity. The PP_in induced increase of enzyme activity however stays up to a concentration of PP_in high enough to titrate the excess amount of Mg^{2+} than the amount required establishing the lower limit of Mg^{2+} to ATP optimum molar ratio. The inhibition and activation of glycerol kinase by PP_in at different Mg^{2+} to ATP molar ratios can be explained by the complexation of PP_in with Mg^{2+} that shifts the Mg^{2+} to ATP molar ratio below or to the optimum level, respectively.

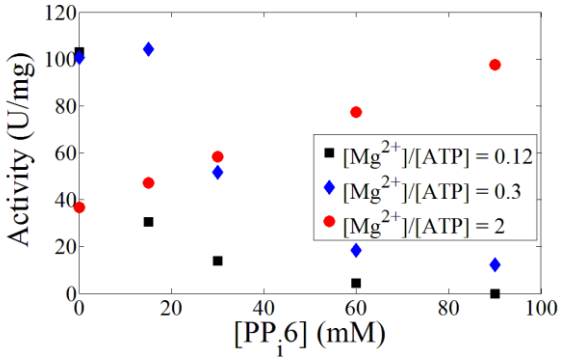

Figure 4.41: Activity of glycerol kinase from *Cellulomonas* sp. as a function of sodium hexametaphosphate (PP_i6) concentrations at different Mg^{2+} to ATP ratio; reaction conditions: 50 mM glycerol, 50 mM ATP, 5 mM, 15 mM and 100 mM Mg^{2+}, 0.08 mg/mL glycerol kinase from *Cellulomonas* sp. in 100 mM Tris-HCl buffer, pH 8.5, and 30°C

Table 4.3 shows the kinetics parameters of glycerol kinase from *Cellulomonas* sp. with respect to ATP, maintaining a constant Mg^{2+} to ATP molar ratio and at different fixed Mg^{2+} concentrations as well as inhibition constant by ADP.

Table 4.3: Kinetic constants and their magnitude of glycerol kinase from *Cellulomonas* sp. with respect to ATP at different fixed concentrations of Mg^{2+} and maintained Mg^{2+} to ATP molar ratio of 0.3 as well as inhibition constant by ADP

Kinetic parameters	Magnitude	Standard deviation
$K_{m,\ ATP\ at\ [Mg^{2+}]/[ATP]\ =\ 0.3}$	2.061 mM	0.083 mM
$K_{m,\ ATP\ at\ 10.5\ mM\ Mg^{2+}}$	0.12 mM	0.006 mM
$K_{m,\ ATP\ \ at\ 21\ mM\ Mg^{2+}}$	0.09 mM	0.0139 mM
$K_{m,\ ATP\ at\ 1.5\ mM\ Mg^{2+}}$	0.28 mM	0.004 mM
$K_{ic,\ ADP\ at\ 10.5\ mM\ Mg^{2+}}$	1.7 mM	Not determined
$K_{ic,\ ADP\ at\ 21\ mM\ Mg^{2+}}$	1.7 mM	Not determined
$v_{max\ at\ [Mg^{2+}]/[ATP]\ =\ 0.3}$	72.62 U/mg	4.93 U/mg
$v_{max\ lower\text{-}step\ at\ 10.5\ mM\ Mg^{2+}}$	44.96 U/mg	2.29 U/mg
$v_{max\ lower\text{-}step\ at\ 21\ mM\ Mg^{2+}}$	45.15 U/mg	1.41 U/mg
$v_{max\ at\ 1.5\ mM\ Mg^{2+}}$	68.17 U/mg	4.50 U/mg

Eqn(4.1) shows the double substrate Michaelis-Menten reaction kinetics equation developed for the glycerol kinase from *Cellulomonas* sp. catalyzed asymmetric phosphorylation of glycerol by ATP composed of competitive product inhibition by ADP.

$$v_1 = v_{max} \times \frac{[ATP]}{K_{m,ATP} \times \left(1 + \frac{[ADP]}{K_{ic,ADP}}\right) + [ATP]} \times \frac{[Glycerol]}{K_{m,Glycerol} + [Glycerol]} \qquad \text{Eqn(4.1)}$$

4.3.3. Validation of Reaction Kinetics Model

The reaction kinetics model shown in Eqn(4.1) was validated by simulating time-courses of reactions with different starting substrate and enzyme concentrations. The model validation was performed by integrating the differential reaction kinetics equation over time using ode45 solver

of Matlab®2014b computational software. The Matlab® script developed for the computation is provided as supplementary information in appendix B. Eqn(4.2) and Eqn(4.3) show differential equations for simulation of substrate and product concentrations for a batch mode of operation, respectively. Eqn(4.4) and Eqn(4.5) composed of convection and reaction terms show steady-state differential equations for simulation of substrate and product concentrations for a continuous mode of operation, respectively. $[S]_0$ and $[S]$ are influx and efflux of substrate concentration, respectively. $[P]_0$ and $[P]$ are influx, which is negligible, and efflux product concentration, respectively.

$$\frac{\partial[ATP]}{\partial t} = \frac{\partial[Glycerol]}{\partial t} = [Glycerol\ kinase](-v_1) \qquad \text{Eqn(4.2)}$$

$$\frac{\partial[ADP]}{\partial t} = \frac{\partial[Glycerol-3-phosphate]}{\partial t} = ([Glycerol\ kinase])(v_1) \qquad \text{Eqn(4.3)}$$

$$\frac{\partial[ATP]}{\partial t} = \frac{\partial[Glycerol]}{\partial t} = \frac{([S]o-[S])}{\tau} - [Glycerol\ kinase](v_1) \qquad \text{Eqn(4.4)}$$

$$\frac{\partial[ADP]}{\partial t} = \frac{\partial[Glycerol-3-phosphate]}{\partial t} = \frac{([P]-[P]o)}{\tau} + [Glycerol\ kinase](v_1) \qquad \text{Eqn(4.5)}$$

Batch reactions were carried out at 10.5 mM and 21 mM Mg^{2+} that the corresponding kinetic constants were used for simulations and model validation. Experimental conversion and numerically simulated conversion matrices at different starting substrate concentrations using 10.5 mM Mg^{2+} and 21 mM Mg^{2+} showed 2-D correlation of 96.8% and 98.8%, respectively. Figure 4.42 and Figure 4.43 show graphical fitness between experimentally monitored by HPLC and numerically simulated product as well as substrate concentrations using kinetic constants at 10.5 mM and 21 mM Mg^{2+}, respectively.

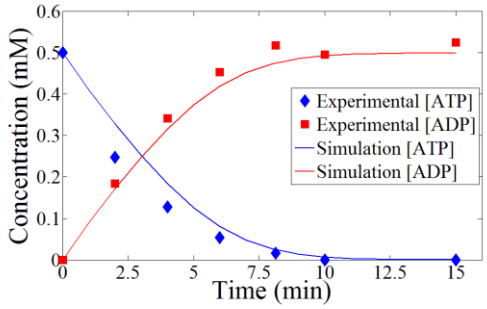

Figure 4.42: Graphical fitness of experimentally measured and numerically simulated ATP and ADP concentrations for a batch reaction; reaction conditions: 0.5 mM ATP, 50 mM glycerol, 10.5 mM Mg^{2+}, 0.0025 mg/mL glycerol kinase from *Cellulomonas* sp. in 100 mM Tris-HCl buffer, pH 8.5, and 30°C

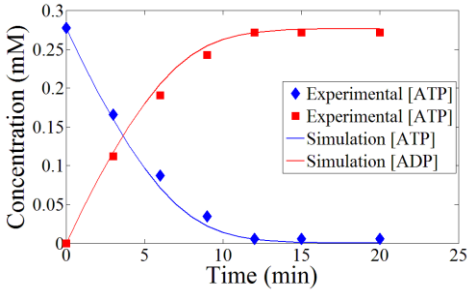

Figure 4.43: Graphical fitness of experimentally measured and numerically simulated ATP and ADP concentrations for a batch reaction; reaction conditions: 0.25 mM ATP, 50 mM glycerol, 21 mM Mg^{2+}, 0.00125 mg/mL glycerol kinase from *Cellulomonas* sp. in 100 mM Tris-HCl buffer, pH 8.5, and 30°C

4.4. Process Simulation and Evaluation

The performances of batch-wise operation using a stirred tank reactor (STR) and continuous operation using a continuously operated stirred tank reactor (CSTR) were simulated and evaluated for the reaction system presented in Figure 4.2. Figure 4.44 shows performance simulation and evaluation as well as comparison between STR and CSTR based on conversion. Conversion is defined as the number of converted substrate molecules per starting molecules of substrate. The better performance with respect to conversion is defined the reactor that offers larger conversion in a short time at the same enzyme concentration. Glycerol kinase from *Cellulomonas* sp. exhibits inhibition by the coproduct ADP. The batch-wise operation via STR is therefore advantageous due to the gradually increase of ADP while CSTR is disadvantageous because ADP leads to low steady-state reaction rate. Hence, CSTR requires 55-fold more enzyme concentration in order to achieve 99.8% conversion at the same time. In other words, if equal amount of enzyme would be loaded in both reactor types, CSTR must be operated for 55-fold longer residence time than the reaction time required in STR to achieve the same 99.8% conversion. The low performance of CSTR can be circumvented by using cascade configuration of CSTRs (e.g. as shown in Figure 5.28) because of the approximated characteristics of cascade CSTRs to plug flow reactor (PFR). However, this requires additional process costs such as energy consumption and hardware or in the case of PFR to immobilize the enzyme.

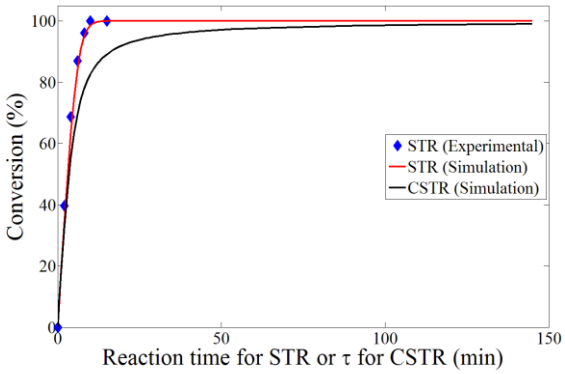

Figure 4.44: Performance evaluation of stirred tank reactor (STR), continuously operated stirred reactor (CSTR) based on conversion; reaction conditions: 0.5 mM ATP, 50 mM glycerol, 10.5 mM Mg^{2+}, 0.0025 mg/mL glycerol kinase from *Cellulomonas* sp. in 100 mM Tris-HCl buffer pH 8.5 and 30°C

4.5. Interim Summary

Results of glycerol kinase screening among various microbial sources have led to select the most active and stable glycerol kinase from *Cellulomonas* sp.. Glycerol kinase from *Cellulomonas* sp. essentially requires a divalent metal ion (i.e. Mg^{2+}) for its activity. The interaction of Mg^{2+} and ATP yields Mg-ATP complexes of different chemical and physical features depending on Mg^{2+} to ATP molar ratio. Results of activity assays as a function of Mg^{2+} to ATP molar ratio have revealed that the enzyme shows maximum activity in the optimum Mg^{2+} to ATP molar ratio of [0.12 to 0.3]. The enzyme exhibits Michaelis-Menten kinetics with respect to glycerol as well as ATP maintaining constant Mg^{2+} to ATP molar ratio. Moreover, the enzyme shows two-step kinetics with respect to ATP when assayed at 10.5 mM and 21 mM Mg^{2+}. The enzyme exhibits pseudo-ATP surplus inhibition and pseudo-ATP activation depending on Mg^{2+} to ATP molar ratio. The enzyme shows inhibition by ADP, AMP and Ca^{2+} but not by *sn*-G3P and P_i. The inhibition by AMP and ADP is of a competitive type with ATP while the inhibition by Ca^{2+} is due to the formation of enzymatically inactive Ca-ATP complexes. The enzyme shows inhibition or activation by PP_in depending on the magnitude of Mg^{2+} to ATP molar ratio. This is due to the complexation of PP_in with Mg^{2+} that shifts the Mg^{2+} to ATP molar ratio below or to the optimum level. Experimental conversion and numerically simulated conversion matrices at different starting substrate concentrations at 10.5 mM Mg^{2+} and 21 mM Mg^{2+} show 2-D correlation of 96.8% and 98.8%, respectively. Simulation and performance evaluation of different reactor types lead to select batch-wise operation via STR as the most efficient reactor type for the synthesis of *sn*-glycerol-3-phosphate.

5. Synthesis of L-Glyceraldehyde-3-Phosphate

Triosephosphate metabolites such as L-glyceraldehyde-3-phosphate (L-GAP) are synthetically useful to design *in vitro* single-pot cascade biocatalytic reaction sequences using enzymes such as aldolases or transketolases [26–28, 28, 29]. Though L-GAP does not frequently occur in the central metabolic pathways as its enantiomer D-glyceraldehyde-3-phosphate (D-GAP), it is one of synthetically useful phosphorylated metabolites. L-GAP has been described to be biologically non-utilizable [5] and to have a bactericidal effect on *E. coli* while D-GAP does not have the same effect [25]. The mechanism how *E. coli* loses its viability in the presence of L-GAP has not yet been elucidated. In aqueous solution, L-GAP exists as a mixture of its hydrated and free aldehyde form in a molar ratio of 29:1[154]. Kalyananda, et al. (1987) has described that the mechanism in which *E. coli* losses viability in the presence of L-GAP may be due to a potential interference caused by the hydrated form of L-GAP as an analog of *sn*-glycerol-3-phosphate in enzymes involved in *sn*-glycerol-3-phosphate metabolism. Other mechanism could be that the accumulation of L-GAP in *E. coli* at physiological pH decomposes to inorganic phosphate and methylglyoxal, which is a potential toxic metabolites to various cell types [156–159]. On the other hand, *E. coli* (YghZ) enantioselectively transforms L-GAP to *sn*-glycerol-3-phosphate using an NADPH dependent aldose reductase as a complement of triose phosphate isomerase (TIM) deficiency that enters into gluconeogenesis metabolic pathway [45, 160]. Despite not yet known *in vivo* biosynthetic pathway for the formation of L-GAP, the existence of an enzymatic pathway for the formation of L-GAP has been postulated to facilitate gluconeogenesis in the TIM-deficient strain of *E. coli* [45]. The L-GAP:NADPH dependent aldose reductase from *E. coli* shows high affinity for L-GAP (i.e. K_m of 28 µM) and large specificity that shows no activity for structural analogues of L-GAP including D-GAP and DHAP [155]. It is thus arguable that L-GAP:NADPH dependent aldose reductase by *E. coli* possess such high affinity and specificity for non-naturally occurring metabolite L-GAP.

Thus, the development of practical synthetic methodology for the preparation of optically pure L-GAP is of a major advantage for metabolic elucidation purposes. Few biocatalytic reaction systems for the synthesis of L-GAP have been described and they are based on kinetic resolution of DL-glyceraldehyde (DL-GA) or phosphorylation of L-glyceraldehyde (L-GA) (as shown in Figure 5.1) catalyzed by glycerol kinase (EC 2.7.1.30) [41, 71, 73, 121, 161]. On the other hand,

it has been described that glycerol kinase from *Acetobactur xylinum* shows no activity for the phosphorylation of D- and L-glyceraldehyde but for DHA and glycerol [71]. Additionally, dihydroxyacetone kinase from rat brain cytosol fraction has been described to catalyze the phosphorylation of glycerol, dihydroxyacetone, D- and L-glyceraldehyde [127].

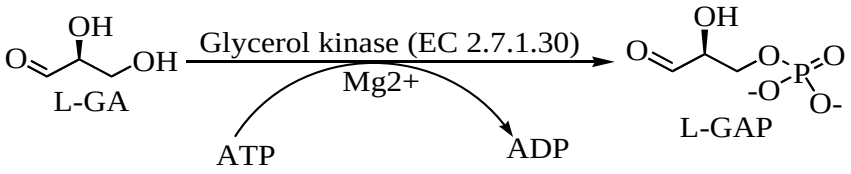

Figure 5.1: Reaction scheme illustrating glycerol kinase (EC 2.7.1.30) catalyzed phosphorylation of L-glyceraldehyde (L-GA) by ATP yielding L-glyceraldehyde-3-phosphate (L-GAP) and ADP

This section describes results of a comprehensive reaction engineering study in order to design an efficient biocatalytic process for the synthesis of L-GAP. Reaction engineering investigations including substrate and enzyme screening, stability of L-GAP under conditions of the reaction, development of a reaction kinetics model, numerical simulation as well as performance evaluation of different reactor types for optimized glycerol kinase catalyzed synthesis of L-GAP and DSP will be described.

5.1. Substrate and Enzyme Screening

Glycerol kinase catalyzes enantioselective phosphorylation of L-glyceraldehyde; therefore, L-GAP can be synthesized either by kinetic resolution using racemic DL-glyceraldehyde or by phosphorylation of using enantiopure L-glyceraldehyde starting materials. Figure 5.2 shows the selectivity of glycerol kinase from *Cellulomonas* sp. using D-glyceraldehyde and L-glyceraldehyde as starting material. Complete conversion was achieved in the case of L-glyceraldehyde while no conversion occurred in the case of D-glyceraldehyde.

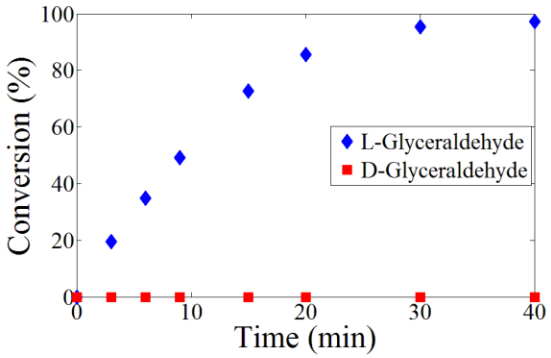

Figure 5.2: Phosphorylation of D- and L-glyceraldehyde catalyzed by glycerol kinase from *Cellulomonas* sp.; reaction conditions: 50 mM ATP, 30 mM D- and L-glyceraldehyde, 35 mM Mg^{2+} and 0.02 mg/mL glycerol kinase from *Cellulomonas* sp. in 100 mM TEA buffer, pH 8, and 25°C

Even though DL-glyceraldehyde (40.4 €/g; Sigma-Aldrich price catalog 2015) is cheaper than L-glyceraldehyde (800 €/g; Sigma-Aldrich price catalog 2015), the use of DL-glyceraldehyde as a starting material has a drawback. The drawback is that D-glyceraldehyde induces ATPase activity of glycerol kinase that catalyzes non-effective hydrolysis of ATP to ADP and P_i [73, 123, 130]. It has been described in sub-chapter 4.3.2 (Figure 4.28) that glycerol kinase from *Cellulomonas* sp. exhibits no ATPase activity without the addition of other partner substrates nor ATP is unstable under reaction conditions. In an aqueous solution, the carbonyl functional group of D-glyceraldehyde exists in a reversible hydrated geminal-diol form [162]. Therefore, in binding with the active site of glycerol kinase instead of the terminal –OH group as in the case of L-glyceraldehyde, one of the geminal-diols acts as phosphoryl group acceptor that produces hemiacetal phosphate. Thus, the hemiacetal phosphate is labile and undergoes splitting-off the phosphate moiety either at the active site of the enzyme or after release into the reaction solution [73, 123, 130]. Figure 5.3 shows the requirement of nearly a 10-fold molar excess of ATP with respect to L-glyceraldehyde in DL-glyceraldehyde to achieve full conversion of L-glyceraldehyde when the starting material is DL-glyceraldehyde. Attention must be paid to this metric depending on the starting concentrations of reaction species. The formation of P_i in the use of DL-glyceraldehyde as a starting material can afterwards interfere in DSP. Hence, the phosphorylation of enantiopure L-glyceraldehyde has been selected for process development to prepare L-GAP. As described in sub-chapter 4.2.1 with respect to enzyme screening, glycerol kinase from *Cellulomonas* sp. was selected for the synthesis of L-GAP.

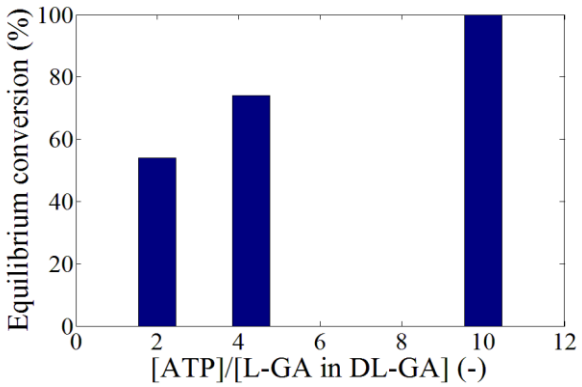

Figure 5.3: Final conversion of L-glyceraldehyde (L-GA) as a function of molar ratio of ATP to L-glyceraldehyde in DL-glyceraldehyde (DL-GA) for the kinetic resolution of DL-glyceraldehyde; reaction conditions: 15 mM ATP, 15 mM Mg^{2+} and [3 mM, 7 mM and 15 mM] DL-glyceraldehyde, 0.0453 mg/mL glycerol kinase from *Cellulomonas* sp. in 100 mM TEA buffer, pH 8, and 25°C

5.2. Product Stability

Triosephosphate metabolites such as DHAP, D- and L-GAP are unstable at neutral and alkaline pH conditions [41–46]. A reaction mechanism of DL-GAP decomposition at neutral pH conditions via an enediolate phosphate intermediate yielding methylglyoxal and P_i has been described elsewhere [43, 46]. In alkaline pH conditions the decomposition yields lactic acid instead of methylglyoxal [41, 163]. The stabilities of D- and L-GAP at neutral and alkaline pH conditions depend very much on the molecular structure, e.g. whether the glyceraldehyde is phosphorylated in the 2- or 3-position, temperature and the medium composition. Figure 5.4 shows a reaction scheme of DL-GAP decomposition pathways under neutral and alkaline pH conditions.

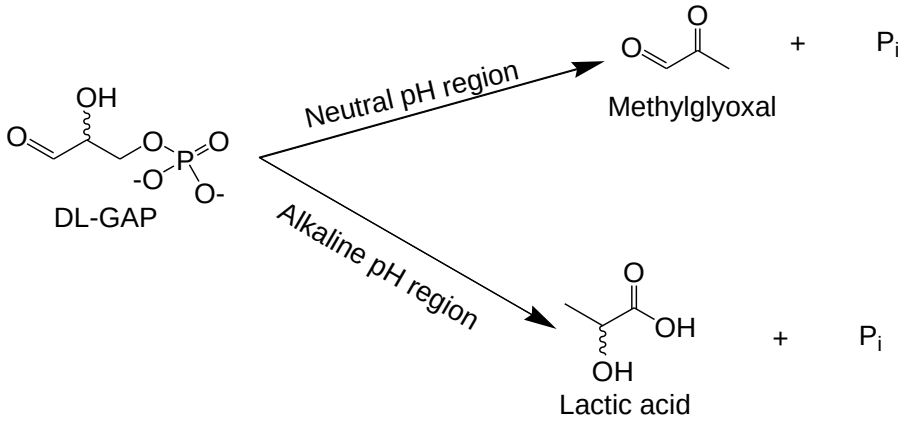

Figure 5.4: Schematic reaction illustrating DL-GAP decomposition in neutral and alkaline pH conditions

The instability of L-GAP at neutral pH conditions is a critical factor for the development of a biocatalytic process using glycerol kinase from *Cellulomonas* sp., because the enzyme shows no activity at a pH below 4, while L-GAP is stable at pH below 4. Figure 5.5 and Figure 5.6 show

graphically the depletion of DL-GAP incubated in 100 mM TEA buffer, pH 8, at 30°C and 60°C, respectively. The rate of DL-GAP depletion in 100 mM TEA buffer, pH 8, and at different temperatures can be defined by first order kinetics. Table 5.1 shows rate constants and half-lives of DL-GAP at different temperature levels.

Table 5.1: The rate constants of DL-GAP depletion and half-lives in 100 mM TEA buffer, pH 8, and at different temperatures levels

Temperature (°C)	**Rate constant (s^{-1})**	**Half-life (h)**
25	2.3×10^{-5}	8.35
30	2.8×10^{-5}	6.86
60	1.2×10^{-3}	0.15

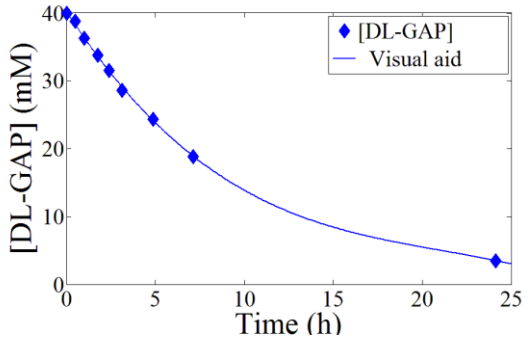

Figure 5.5: The depletion of 40 mM DL-glyceraldehyde-3-phosphate (DL-GAP) incubated in 100 mM TEA buffer, pH 8, at 30°C

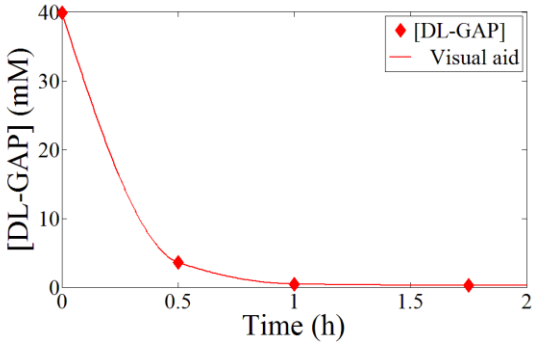

Figure 5.6: The depletion of 40 mM DL-glyceraldehyde-3-phosphate (DL-GAP) incubated in 100 mM TEA buffer, pH 8, at 60°C

The decomposition of DL-GAP was investigated in different buffer media since it has been described that tertiary amine buffer catalyzes the phosphate elimination reaction and the rate of elimination increases with increasing buffer concentration [46]. Results showed that DL-GAP decomposed in similar rates when incubated in media including non-buffered aqueous medium pH 8, 100 mM TEA buffer, pH 8, 50 mM TEA buffer, pH 8, and 100 mM potassium phosphate buffer (PPB), pH 8, while 100 mM Tris-HCl buffer, pH 8, stabilizes DL-GAP. Figure 5.7 shows the decomposition of DL-GAP in different buffer media. The stability of DL-GAP incubated in

100 mM Tris-HCl buffer, pH 8, has enhanced with half-life of 33 h compare to its stability in 100 mM TEA buffer, pH 8, with half-life of 8.35 h. The stabilization of DL-GAP by Tris-HCl buffer may be due to interactions of DL-GAP with the Tris-HCl buffer [164]; however, Tris-HCl buffer cannot be used as the reaction medium as it affects the activity of glycerol kinase due to the condensation of L-glyceraldehyde.

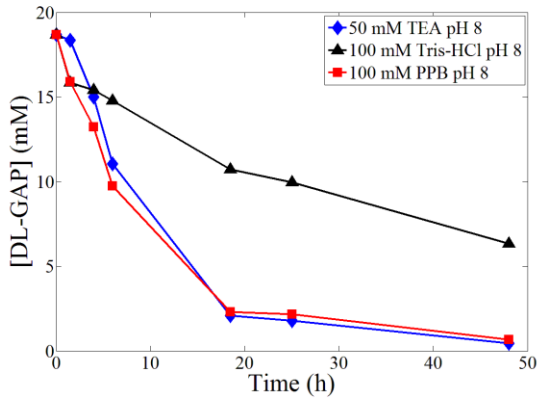

Figure 5.7: The depletion of 20 mM DL-glyceraldehyde-3-phosphate (DL-GAP) incubated in 50 mM TEA buffer, pH 8, 100 mM Tris-HCl buffer, pH 8, and 100 mM potassium phosphate buffer (PPB), pH 8, at 25°C

5.3. Reaction Kinetics of L-Glyceraldehyde Phosphorylation

As described in the chapter 4 glycerol kinase from *Cellulomonas* sp. essentially requires the cofactors ATP as phosphoryl donor and Mg^{2+}. The interaction of Mg^{2+} and ATP forms various complexes of different physical and chemical features depending on Mg^{2+} to ATP molar ratio among other factors [142]. The effect of Mg^{2+} to ATP molar ratio on the kinetics and thermodynamics of glycerol kinase catalyzed phosphorylation of L-glyceraldehyde will therefore be described in sub-chapter 5.3.1 below.

5.3.1. The Effect of the Mg^{2+} to ATP Molar Ratio on Enzyme Activity

Two sets of activity assays of glycerol kinase catalyzed phosphorylation of L-glyceraldehyde as a function of Mg^{2+} concentration were carried out at 30 mM and 70 mM ATP. The results shown in Figure 5.8 demonstrate that the enzyme shows no activity without the addition of Mg^{2+} and maximum activity at different concentration levels of Mg^{2+} in both sets of activity assays. Figure 5.9 shows the activity results of both sets of measurements plotted as a function of the Mg^{2+} to ATP molar ratio generating an optimum Mg^{2+} to ATP molar ratio of 0.7 where the enzyme

exhibits maximum activity. A subsequent increase of the Mg^{2+} to ATP molar ratio higher than the optimum value suppresses the enzyme activity to a non-zero asymptotic value.

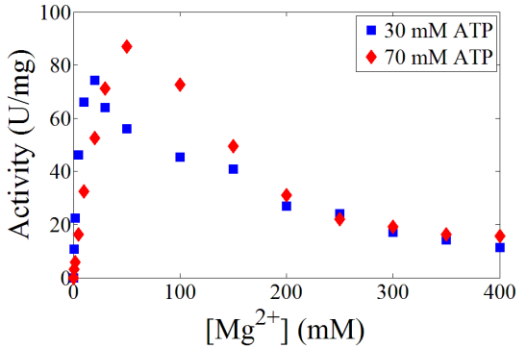

Figure 5.8: Activity of glycerol kinase as a function of Mg^{2+} concentration at different concentrations of ATP; reaction conditions: [30 mM, 70 mM] ATP, 30 mM L-glyceraldehyde, 0.02 mg/mL glycerol kinase from *Cellulomonas* sp. in 100 mM TEA buffer, pH 8, and 25°C

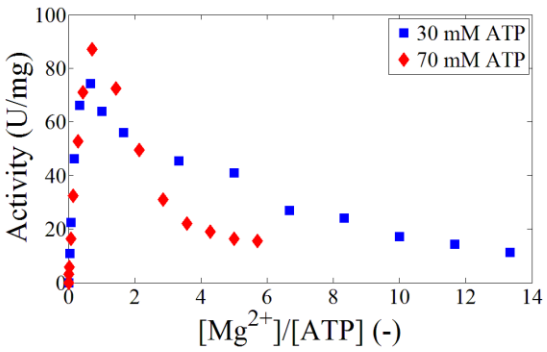

Figure 5.9: Activity of glycerol kinase as a function of Mg^{2+} to ATP molar ratio; reaction conditions: [30 mM, 70 mM] ATP, 30 mM L-glyceraldehyde, [0 - 400 mM] Mg^{2+}, 0.02 mg/mL glycerol kinase from *Cellulomonas* sp. in 100 mM TEA buffer, pH 8, and 25°C

Other sets of activity assays were carried out using different amounts of glycerol kinase in order to examine the effect of enzyme concentration on the activity profile of the enzyme as a function of the Mg^{2+} to ATP molar ratio. The results shown in Figure 5.10 demonstrate that the enzyme activity profile as a function of the Mg^{2+} to ATP molar ratio as well as the optimum Mg^{2+} to ATP molar ratio are not affected by glycerol kinase concentration.

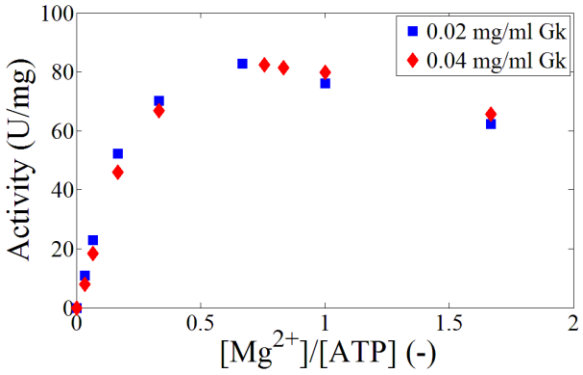

Figure 5.10: Influence of glycerol kinase (Gk) concentration on its activity as a function of Mg^{2+} to ATP molar ratio; reaction conditions: 30 mM ATP, 30 mM L-glyceraldehyde, [0 - 50 mM] Mg^{2+}, [0.02 mg/mL and 0.04 mg/mL] glycerol kinase from *Cellulomonasp* sp. in 100 mM TEA buffer, pH 8, and 25°C

It has been described in sub-chapter 4.3.1, Figure 4.26, that glycerol kinase from *Cellulomonas* sp. exhibits maximum activity in the optimum Mg^{2+} to ATP molar ratio interval of [0.12 to 0.3] for the asymmetric phosphorylation of glycerol. The same enzyme exhibits maximum activity at

the optimum Mg^{2+} to ATP molar ratio of 0.7 for the phosphorylation of L-glyceraldehyde. It has been shown moreover in Figure 4.27 that the optimum Mg^{2+} to ATP molar ratio interval for the asymmetric phosphorylation of glycerol remains unaffected by changing the buffer type to TEA pH 8, which is used for the phosphorylation of L-glyceraldehyde. It therefore appears that the different optimum Mg^{2+} to ATP molar ratios for the two systems may raise due to the functional group difference between glycerol and L-glyceraldehyde. In order to investigate the influence of the structural difference between glycerol and L-glyceraldehyde, the activity of glycerol kinase as a function of the Mg^{2+} to ATP molar ratio was examined using dihydroxyacetone as a substrate, which is a structural isomer of L-glyceraldehyde. The result shown in Figure 5.11 depicts that the enzyme exhibits a similar activity profile and optimum Mg^{2+} to ATP molar ratio in the case of dihydroxyacetone phosphorylation as of L-glyceraldehyde phosphorylation. Moreover, no effect was detected in the examination of the effect of dihydroxyacetone concentration relative to ATP concentration on the activity of glycerol kinase as a function of the Mg^{2+} to ATP molar ratio.

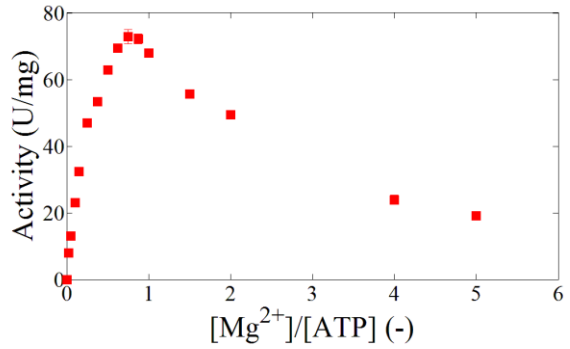

Figure 5.11: Activity of glycerol kinase as a function of Mg^{2+} to ATP molar ratio for the phosphorylation of dihydroxyacetone; reaction conditions: 40 mM ATP, 20 mM dihydroxyacetone, [0 - 200 mM] Mg^{2+}, 0.05 mg/mL glycerol kinase from *Cellulomonas* sp. in 100 mM TEA buffer, pH 8, and 30°C

Therefore, the fact that glycerol kinase from *Cellulomonas* sp. shows different optimum Mg^{2+} to ATP molar ratios in the case of glycerol and L-glyceraldehyde may raise due to the structural difference between them. This happens when the enzyme undergoes unsymmetrical conformational modifications upon binding these substrates and exhibits different catalytic properties. By reacting glycerol kinase with 5,5'-dithiobis(nitro-2-benzoic acid) in order to detect the number of reactive sulfhydryl groups per enzyme molecule, Thorner et al. (1973) has described the conformational change of the enzyme induced by binding glycerol. Substrate induced conformational modification of glycerol kinase from various microbial sources has moreover been mentioned elsewhere [165, 166].

Despite thermodynamically favorable with $\Delta_r G$ of -16.6 kJ/mol at pH 8 and ionic strength of 0.6 M as determined by eQuilibrator$^{2.0}$ [138], the effect of Mg^{2+} concentration on the reaction equilibrium for the phosphorylation of L-glyceraldehyde was examined. The examination was performed by establishing a 23.7-fold higher Mg^{2+} to ATP molar ratio than the optimum Mg^{2+} to ATP molar ratio. The purpose of this examination was to elucidate if there is an irreversible formation of enzymatically non-utilizable Mg-ATP complex at a very high Mg^{2+} to ATP molar ratio. The results shown in Figure 5.12 depict that a high concentration of Mg^{2+} does not affect the equilibrium conversion; however, the enzyme activity is suppressed by a factor of 22 relative to its activity at the optimum Mg^{2+} to ATP molar ratio. The final conversion of 94% ascribes to the thermodynamic activity of ATP in the reaction mixture.

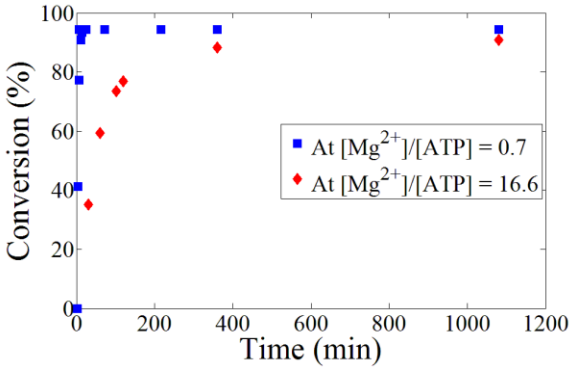

Figure 5.12: The influence of Mg^{2+} concentration on the equilibrium conversion of glycerol kinase catalyzed phosphorylation of L-glyceraldehyde by ATP; reaction conditions: 30 mM ATP, 30 mM L-glyceraldehyde, [21 mM and 500 mM] Mg^{2+}, 0.02 mg/mL glycerol kinase from *Cellulomonas* sp. in 100 mM TEA buffer, pH 8, and 30°C

5.3.2. Development of Reaction Kinetics Model and Validation

Initial rate measurements as a function of concentration of L-glyceraldehyde and ATP were carried out in order to perform reaction kinetics analyses and to develop kinetics model. The initial rate measurements as a function of ATP were carried out at fixed 21 mM and 50 mM Mg^{2+}, establishing the optimum Mg^{2+} to ATP molar ratio of 0.7 at 30 mM and 71.43 mM ATP, respectively. Figure 5.13 and Figure 5.14 show the enzyme activity as a function of L-glyceraldehyde concentration and the linear plot using double reciprocal linearization method, respectively, that the enzyme exhibits Michaelis-Menten kinetics pattern.

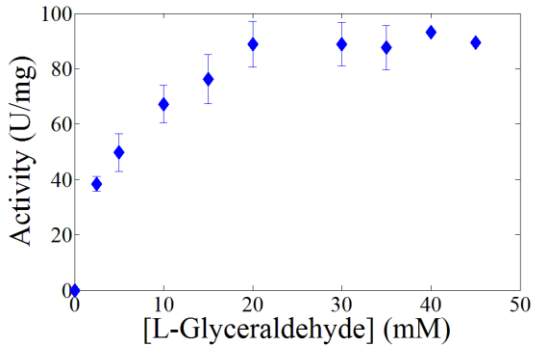

Figure 5.13: Activity of glycerol kinase from *Cellulomonas* sp. as a function of L-glyceraldehyde concentration; reaction conditions: 50 mM ATP, [0 - 45 mM] L-glyceraldehyde, 35 mM Mg^{2+}, various amounts of glycerol kinase from *Cellulomonas* sp. in TEA buffer, pH 8, and 25°C

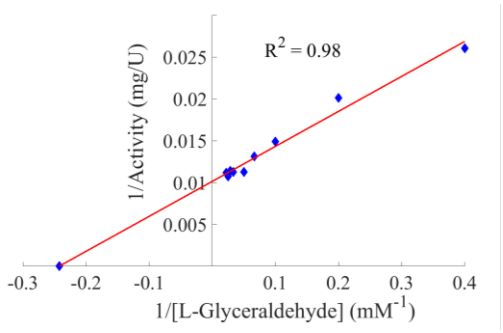

Figure 5.14: Linearization of hyperbolic activity response of glycerol kinase from *Cellulomonas* sp. as a function of L-glyceraldehyde concentration using double reciprocal plot; reaction conditions: 50 mM ATP, [0 - 45 mM] L-glyceraldehyde, 35 mM Mg^{2+}, various amounts of glycerol kinase from *Cellulomonas* sp. in TEA buffer, pH 8, and 25°C

Glycerol kinase inhibition by L-GAP was investigated using commercially available DL-GAP. Slight inhibition was detected in assaying the enzyme activity as a function of DL-GAP concentration due to the presence of methylglyoxal as a decomposition product of DL-GAP. This was confirmed because DL-GAP exerted larger degree of inhibition after preliminary incubation at the reaction pH 8 before the start of the reaction. 25 mM DL-GAP exerted 23.6% and 39.4% inhibition when reactions were started after 20 min and 1 h preparation of DL-GAP containing reaction mixture at pH 8, respectively. Therefore, the results indicate the inhibition of glycerol kinase by the decomposed products of DL-GAP at pH 8 these are methylglyoxal and P_i. Figure 5.15 shows the inhibition of glycerol kinase by methylglyoxal while Figure 5.20 shows P_i does not inhibit the enzyme. The inhibition of glycerol kinase by methylglyoxal was however not included in the reaction kinetics model development due to the aim to run L-GAP synthesis process in a short reaction time that negligible formation of methylglyoxal and enhances yield. Process development performing the synthesis of L-GAP in a short reaction time has therefore not only advantageous of enhancing the selectivity but also avoiding enzyme inhibition by the side-product methylglyoxal.

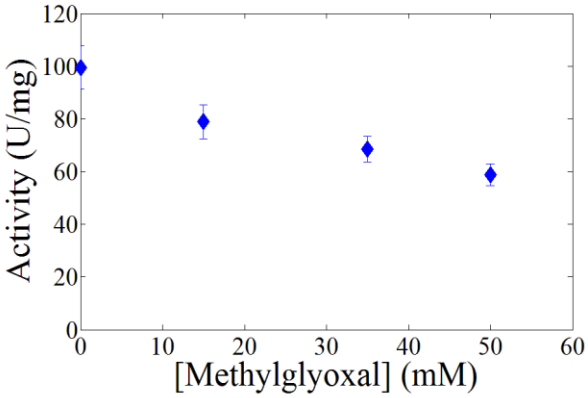

Figure 5.15: Inhibition of glycerol kinase from *Cellulomonas* sp. by DL-glyceraldehyde-3-phosphate decomposition side-product, methylglyoxal; reaction conditions: 50 mM ATP, 50 mM L-glyceraldehyde, 35 mM Mg^{2+}, [0 - 50 mM] methylglyoxal, 0.08 mg/mL glycerol kinase from *Cellulomonas* sp. in 100 mM TEA buffe, pH 8, and 30°C

Figure 5.16 and Figure 5.17 show hyperbolic activity of glycerol kinase as a function of ATP concentration at a fixed 21 mM Mg^{2+} and linearized plot using double reciprocal linearization method, respectively. The enzyme exhibits Michealis-Menten kinetic behavior with respect to ATP.

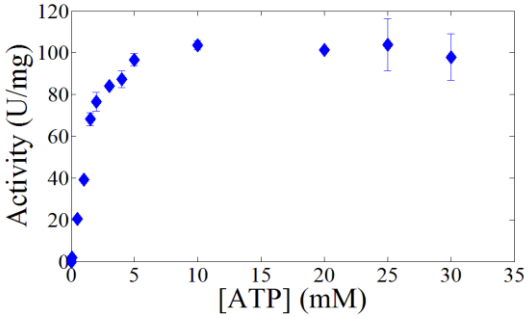

Figure 5.16: Activity of glycerol kinase from *Cellulomonas* sp. as a function of ATP concentration; reaction conditions: [0 -30 mM] ATP, 30 mM L-glyceraldehyde, 21 mM Mg^{2+}, various amounts of glycerol kinase from *Cellulomonas* sp. in 100 mM TEA buffer, pH 8, and 30°C

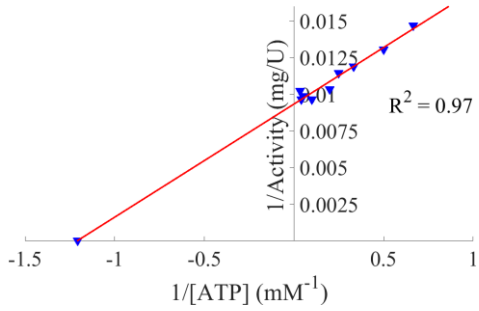

Figure 5.17: Linearization of hyperbolic activity response of glycerol kinase from *Cellulomonas* sp. as a function of ATP concentration; reaction conditions: [0 - 30 mM] ATP, 30 mM L-glyceraldehyde, 21 mM Mg^{2+}, various amounts of glycerol kinase from *Cellulomonas* sp. in 100 mM TEA buffer, pH 8, and 30°C

As expected at concentration of ATP higher than 30 mM, glycerol kinase exhibits a pseudo-substrate surplus inhibition by ATP due to the drop of Mg^{2+} to ATP molar ratio below the optimum value 0.7. This pseudo-ATP surplus inhibition can be circumvented by changing the concentration of Mg^{2+} that adjusts the Mg^{2+} to ATP molar ratio. Therefore, an attempt to determine the ATP surplus inhibition constant can lead to erroneous result. For instance, from the activity data shown in Figure 5.18 the ATP surplus inhibition constant was determined to be

22.6 mM using Dixon plot; however, validation of kinetics model that includes this inhibition constant generated non-fitting numerical data with experimental results. The activity of glycerol kinase was moreover assayed as a function of ATP concentration at 50 mM Mg^{2+} in order to investigate the effect of Mg^{2+} concentration on the enzyme activity profile. Figure 5.19 shows the activity of glycerol kinase as a function of ATP concentration at a fixed 50 mM Mg^{2+} that depicts the circumvention of pseudo-ATP surplus inhibition.

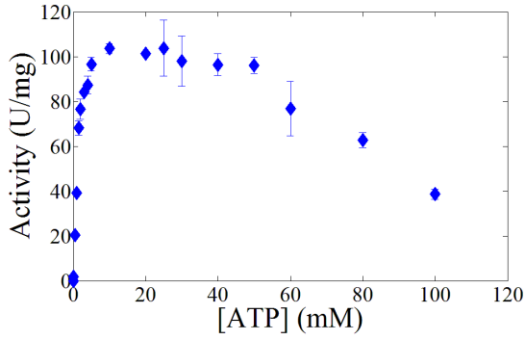

Figure 5.18: Activity of glycerol kinase as a function of ATP concentration at a fixed 21 mM Mg^{2+}; reaction conditions: 30 mM L-glyceraldehyde, 21 mM Mg^{2+}, various amounts of glycerol kinase from *Cellulomonas* sp. in 100 mM TEA buffer, pH 8, and 30°C

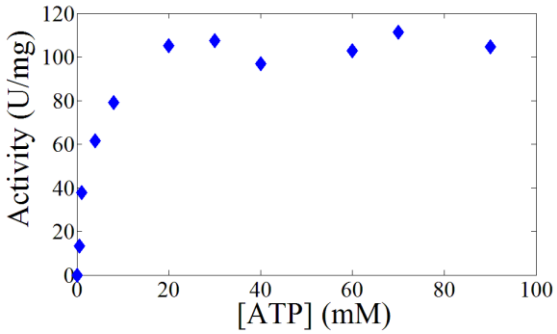

Figure 5.19: Activity of glycerol kinase as a function of ATP concentration at a fixed 50 mM Mg^{2+}; reaction conditions: 70 mM L-glyceraldehyde, 50 mM Mg^{2+}, various amounts of glycerol kinase from *Cellulomonas* sp. in 100 mM TEA buffer, pH 8, and 30°C

The enzyme exhibits competitive inhibition by the coproduct ADP that inhibition type and constants at 21 mM Mg^{2+} and 50 mM Mg^{2+} were determined and results are shown in Table 5.2. Additionally, inhibition of glycerol kinase from *Cellulomonas* sp. by AMP, PP_in, P_i and Ca^{2+} was examined for the synthesis of L-GAP. Results shown in Figure 5.20 depict that AMP and Ca^{2+} appear to be potent inhibitors while P_i is not. The enzyme may exhibit competitive inhibition of ATP by AMP and inhibition by Ca^{2+} can be explained due to the formation of enzymatically inactive Ca-ATP complex(s).

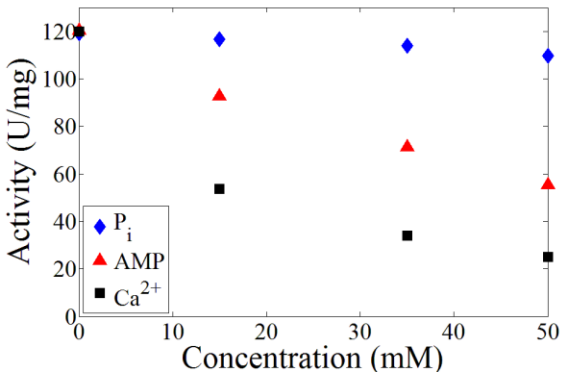

Figure 5.20: Inhibition of glycerol kinase from *Cellulomonas* sp. by inorganic orthophosphate (P_i), adenosine monophosphate (AMP), calcium ion (Ca^{2+}); reaction conditions: 45 mM ATP, 35 mM L-glyceraldehyde, 31.5 mM Mg^{2+} for activity assay as a function of AMP concentrations, 30 mM ATP, 30 mM L-glyceraldehyde, 21 mM Mg^{2+} for the activity assays as a function of P_i and Ca^{2+} concentrations, 0.08 mg/mL glycerol kinase from *Cellulomonas* sp. in 100 mM TEA buffer, pH 8, and 30°C

Furthermore, the extent of glycerol kinase inhibition by Ca^{2+} was assayed at different Mg^{2+} to ATP molar ratio. Activity assays were carried out as a function of Ca^{2+} concentration at the optimum Mg^{2+} to ATP molar ratio 0.7, less than the optimum Mg^{2+} to ATP molar ratio 0.12 and larger than the optimum Mg^{2+} to ATP molar ratio 2.1. The purpose of these assays was in order to study if Ca^{2+} can antagonize the inhibition of glycerol kinase by Mg^{2+}. As can be seen in Figure 5.21 in all activity measurements glycerol kinase displays inhibition by Ca^{2+}; however, the percent of inhibition exerted by the same concentration of Ca^{2+} depends on the Mg^{2+} to ATP molar ratio. The percent of inhibition due to the addition of Ca^{2+} is calculated using $Eqn(5.1)$.

$$\%\ of\ inhibtion = \frac{Activity\ with\ Ca^{2+} - Activity\ without\ Ca^{2+}}{Activity\ without\ Ca^{2+}} \times 100 \qquad Eqn(5.1)$$

Figure 5.22 shows the percent of inhibition as a function of Ca^{2+} concentration at different Mg^{2+} to ATP molar ratio. The complexation between Ca^{2+} and ATP has been mentioned to be similar as the complexation between Mg^{2+} and ATP except in case of Ca^{2+} complexes, the Ca^{2+}-phosphate exchange rate is faster than in cases of Mg^{2+} complexes [142, 167]. The different percent of glycerol kinase inhibition by the same concentration of Ca^{2+} at different Mg^{2+} to ATP molar ratio can be explained by mass action on the complexation equilibrium between Ca-ATP and Mg-ATP complexes. Addition of the same concentration of Ca^{2+} can yield different amounts of enzymatically inactive Ca-ATP complexes at different Mg^{2+} to ATP molar ratio; larger amount Ca-ATP complex at less Mg^{2+} to ATP molar ratio. Therefore, as it is shown in Figure

5.22, 15 mM Ca^{2+} impedes 76.0%, 55.3%, and 29.7% of glycerol kinase inhibition at Mg^{2+} to ATP molar ratio of 0.12, 0.7 and 2.1, respectively.

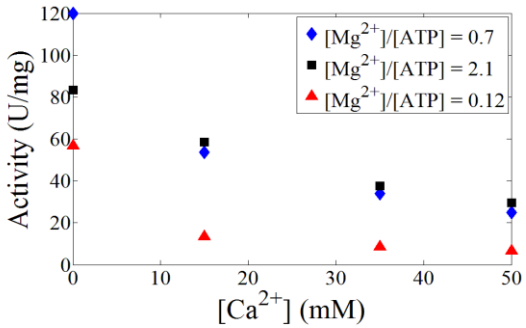

Figure 5.21: The effect of Ca^{2+} concentration on the activity of glycerol kinase from *Cellulomonas* sp. at different Mg^{2+} to ATP molar ratio; reaction conditions: 30 mM ATP, 30 mM L-glyceraldehyde, [3.5 mM, 21 mM, 63 mM] Mg^{2+}, 0.08 mg/mL glycerol kinase from *Cellulomonas* sp. in 100 mM TEA buffer, pH 8, and 30°C

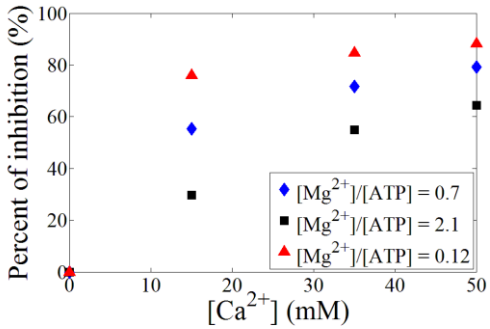

Figure 5.22: Percent of inhibition of glycerol kinase from *Cellulompnas* sp. as a function of Ca^{2+} concentration at different Mg^{2+} to ATP molar ratio; reaction conditions: 30 mM ATP, 30 mM L-glyceraldehyde, [3.5 mM, 21 mM, 63 mM] Mg^{2+}, 0.08 mg/mL glycerol kinase from *Cellulomonas* sp. in 100 mM TEA buffer, pH 8, and 30°C

The effect of PP_in on the activity of glycerol kinase depends on the magnitude of Mg^{2+} to ATP molar ratio. Results presented in Figure 5.23 depict that if the Mg^{2+} to ATP molar ratio is set to be at the optimum value or below, PP_in suppresses the enzyme activity; whereas, at larger Mg^{2+} to ATP molar ratio than the optimum value, PP_in enhances the enzyme. However, the addition of PP_in enhances the enzyme activity only until the excess amount of Mg^{2+} required to generate the optimum Mg^{2+} to ATP molar ratio is fully titrated by PP_in. Further addition of PP_in leads to suppress the enzyme activity. The inhibition and activation of glycerol kinase by PP_in at different Mg^{2+} to ATP molar ratio is due to the complexation of Mg^{2+} with PP_in.

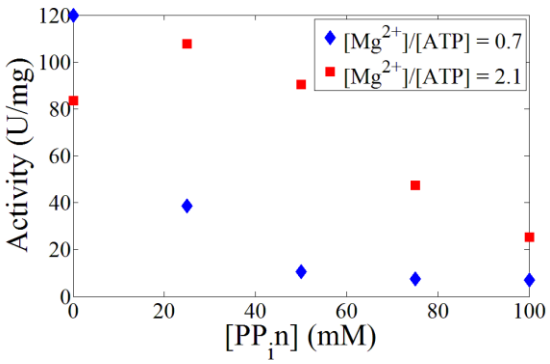

Figure 5.23: The effect of PP_in on the activity glycerol kinase from *Cellulomonas* sp. at the optimum Mg^{2+} to ATP molar ratio of 0.7 and at Mg^{2+} to ATP molar ratio of 2.1; reaction conditions: 30 mM ATP, 30 mM L-glyceraldehyde, [21 - 63 mM] Mg^{2+}, 0.08 mg/mL glycerol kinase from *Cellulomonas* sp. in 100 mM TEA buffer, pH 8, and 30°C

Table 5.2 shows relevant reaction kinetics parameters used for kinetic model development and reactor simulation. Hayashi, et al. (1967) and Janson, et al. (1974) have described the K_m of glycerol kinase from *E. coli* with respect to L-glyceraldehyde 3 mM and 3.7 mM, respectively, which are nearly similar values as determined in this study (i.e. 4 mM).

Table 5.2: Magnitude of reaction kinetics parameters for the phosphorylation of L-glyceraldehyde by ATP catalyzed by glycerol kinase from *Cellulomonas* sp.

Reaction components	K_m **(mM)**	K_i **(mM)**	v_{max} **(U/mg)**
ATP at 21 mM Mg^{2+}	0.8 ± 0.05	_____	110 ± 3.9
ATP at 50 mM Mg^{2+}	1.9	_____	110 ± 3.9
L-Glyceraldehyde	4 ± 0.058	_____	110 ± 3.9
ADP at 21 mM Mg^{2+}	_____	1.4 ± 0.18	_____
ADP at 50 mM Mg^{2+}	_____	3.3	_____

Eqn(5.2) shows the developed double substrate Michaelis-Menten reaction kinetics model for glycerol kinase catalyzed phosphorylation L-glyceraldehyde by ATP including competitive enzyme inhibition by coproduct ADP.

$$v_2 = v_{\max} \times \frac{[\mathrm{ATP}]}{K_{\mathrm{m,ATP}} \times \left(1 + \frac{[\mathrm{ADP}]}{K_{\mathrm{i,ADP}}}\right) + [\mathrm{ATP}]} \times \frac{[\mathrm{L-GA}]}{K_{\mathrm{m,L-GA}} + [\mathrm{L-GA}]} \qquad \mathrm{Eqn}(5.2)$$

The completeness and correctness of the reaction kinetics model was validated by simulating reaction time courses of several batch reactions at different starting substrate concentrations. Sets of numerical simulations were performed using the same kinetic model but kinetics parameters at 21 mM and 50 mM Mg^{2+}. Evaluations of the experimental data and numerically simulated data matrices generated 2-D correlation coefficients of 99.9% and 99.1% for kinetics parameters at 21 mM and 50 mM Mg^{2+}, respectively. Figure 5.24 shows graphical correlations between experimental conversions and numerically simulated conversions versus reaction time.

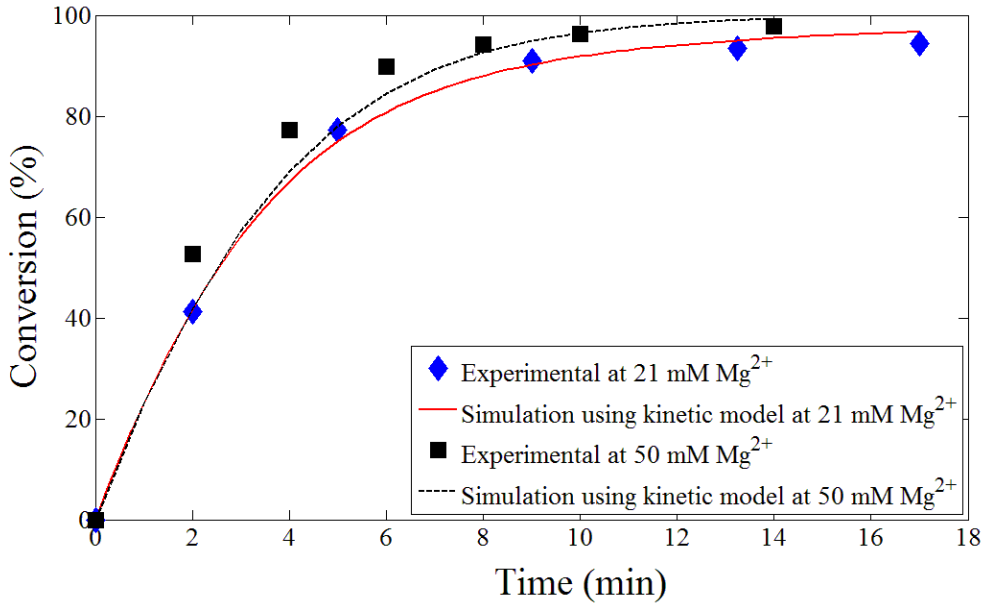

Figure 5.24: Comparison of experimental and numerically simulated conversion data using the reaction kinetics model for kinetics parameters at 21 mM and 50 mM Mg^{2+}; reaction conditions: 1) for kinetics parameters at 21 mM Mg^{2+}: 30 mM L-glyceraldehyde, 30 mM ATP, 21 mM Mg^{2+}, 0.08 mg/mL glycerol kinase from *Cellulomonas* sp. in 100 mM TEA buffer, pH 8, and 30°C and 2) for kinetics parameters at 50 mM Mg^{2+}: 70 mM L-glyceraldehyde, 40 mM ATP, 50 mM Mg^{2+}, 0.1 mg/mL glycerol kinase from *Cellulomonas* sp. in 100 mM TEA buffer, pH 8, and 30°C

5.4. Process Development and Evaluation

Development and evaluation of different processes were performed in order to choose the best performing reactor mode of operation. Evaluation of different reactor types such as stirred tank reactor (STR), continuously operated stirred tank reactor (CSTR) and 2- and 5-stages cascade continuously operated stirred tank reactors was performed. The performances of different reactor modes of operations were evaluated by simulation as well as experimentally, combining the developed reaction kinetics model, mass balances of each of the reactors and kinetics of the non-enzymatic decomposition of L-GAP. Experiments in a continuous mode of operation were carried out using an enzyme membrane reactor (EMR) set up shown in Figure 5.25.

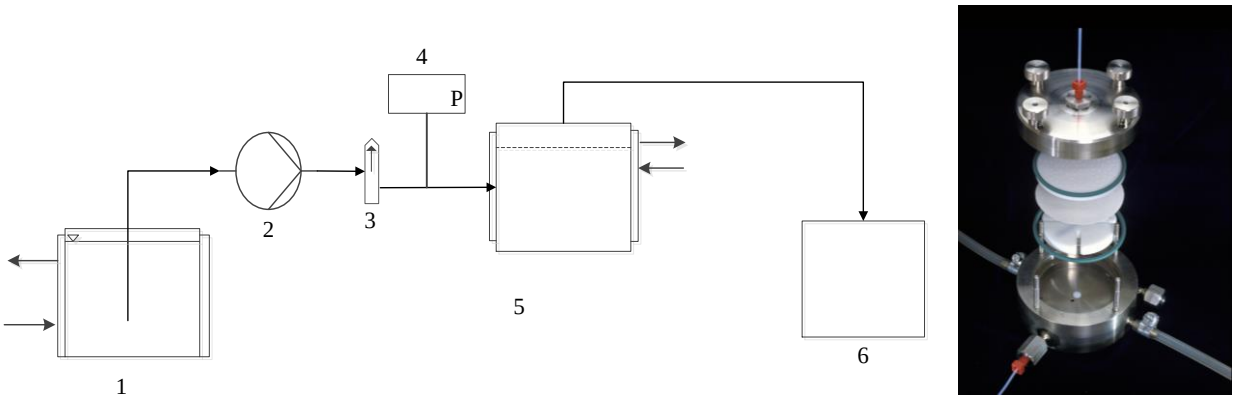

Figure 5.25: Flow diagram of an enzyme membrane reactor (EMR) set up (left) and photo of the EMR module (right, [197]), 1: thermostated substrate reservoir, 2: pump, 3: bubble trap, 4: pressure gauge, 5: ultrafiltration module and 6: product collector at pH < 4 for the stability of L-GAP

Reaction engineering parameters such as conversion, selectivity, space-time yield (volumetric productivity) and specific productivity were used as evaluation criteria as a function of time and enzyme concentration. The integration of the differential kinetics equation over time for the simulation was performed using ode45 solver of Matlab®2014b. Eqn(5.3) and Eqn(5.4) show differential equations for the simulation of substrate and product concentrations for a batch-wise mode of operation, respectively. Eqn(5.5) and Eqn(5.6) show steady state differential equations for the simulation of substrate and product concentrations for a continuous mode of operation, respectively, composed of convection and reaction terms. $[S]_0$ and $[S]$ represent influx and efflux substrate concentration, respectively. $[P]_0$ and $[P]$ are influx product concentration, which is negligible, and efflux product concentration, respectively. As can be seen, Eqn(5.4) and Eqn(5.6) include the decomposition kinetics of L-GAP at the reaction conditions assuming the unit of reaction time and residence time in hour.

$$\frac{\partial[ATP]}{\partial t} = \frac{\partial[L-GA]}{\partial t} = [Glycerol\ kinase](-v_2) \qquad \text{Eqn(5.3)}$$

$$\frac{\partial[L-GAP]}{\partial t} = [Glycerol\ kinase](v_2) \times \mathrm{e}^{-0.101\mathrm{t}} \qquad \text{Eqn(5.4)}$$

$$\frac{\partial[ATP]}{\partial t} = \frac{\partial[L-GA]}{\partial t} = \frac{([S]o-[S])}{\tau} - [Glycerol\ kinase]v_2 \qquad \text{Eqn(5.5)}$$

$$\frac{\partial[L-GAP]}{\partial t} = \left(\frac{([P]o-[P])}{\tau} + [Glycerol\ kinase]v_2\right) \times \mathrm{e}^{-0.101\tau} \qquad \text{Eqn(5.6)}$$

Conversion is defined as the number of phosphorylated L-GA molecules per starting L-GA molecules. An equal amount of enzyme was used for all the reactors to compare conversion. As can be seen in Figure 5.26, the best performance can be achieved via STR. The cascade configurations of CSTR show better performance than CSTR. The higher the number of stages, the better the performance approximates to STR. 42-fold larger for CSTR, 5-fold larger for 2-CSTRs and 2-fold larger for 5-CSTRs amounts of the enzyme are required to achieve the same 98.5% conversion as STR at the same time.

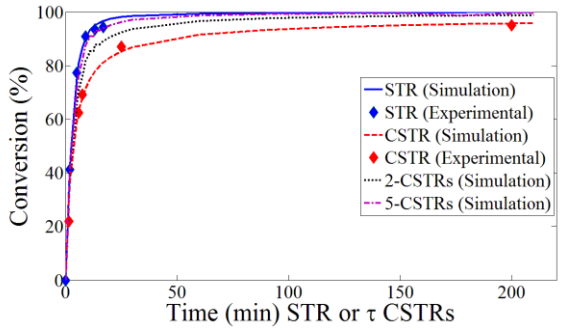

Figure 5.26: Comparison of stirred tank reactor (STR), continuously operated stirred reactor (CSTR) and 2- and 5-stages cascade CSTRs based on conversion as a function of reaction time for STR or residence time for the continuous operations for the synthesis of L-GAP; reaction conditions: 30 mM L-glyceraldehyde, 30 mM ATP, 21 mM Mg^{2+}, 0.08 mg/mL glycerol kinase from *Cellulomonas* sp. in 100 mM TEA buffer, pH 8, and 30°C

Selectivity is defined as the number of synthesized L-GAP molecules per numbers of converted L-GA molecules. For glycerol kinase catalyzed synthesis of L-GAP, selectivity decreases exponentially with time due to the first-order decay of L-GAP under the reaction conditions. The selectivity performance of the reactors was evaluated as a function of conversion applying equal amounts of enzyme. Figure 5.27 depicts that STR shows better selectivity performance than the continuous operations; moreover, the selectivity of CSTR can be enhanced by using a cascade configuration.

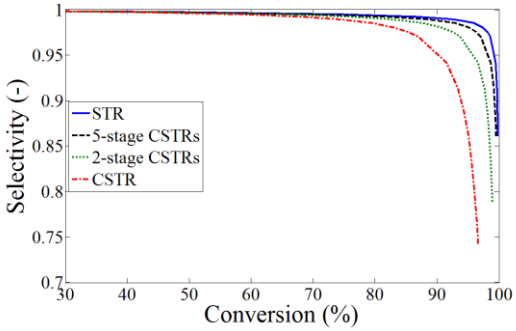

Figure 5.27: Comparison of stirred tank reactor (STR), continuously operated stirred reactor (CSTR) and 2- and 5-stages cascade CSTRs based on selectivity as a function conversion for the synthesis of L-GAP; reaction conditions: 30 mM L-glyceraldehyde, 30 mM ATP, 21 mM Mg^{2+}, 0.08 mg/mL glycerol kinase from *Cellulomonas* sp. in 100 mM TEA buffer, pH 8, and 30°C

STY is defined as the mass of synthesized L-GAP per unit reactor volume and residence time for CSTRs. The performance of the reactors with respect to STY was evaluated as a function of conversion. Figure 5.28 shows that cascade CSTR configurations offer better performance while CSTR exhibits the least performance. Moreover, the STY performance of the CSTR can be improved by using a large number of cascade CSTR configurations as shown for the case of 2- and 5-stage cascade CSTRs.

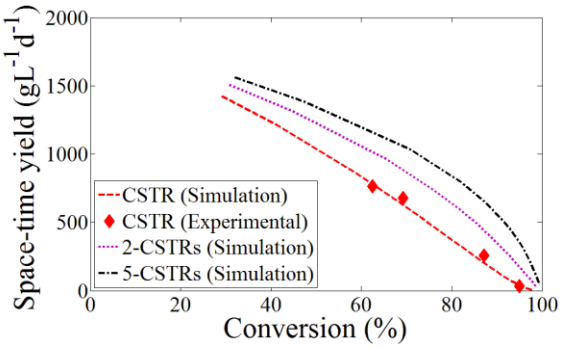

Figure 5.28: Comparison of continuously operated stirred reactor (CSTR) and 2- and 5-stages cascade CSTRs based on space-time yield (STY) as a function conversion for the synthesis of L-GAP; reaction conditions: 30 mM L-glyceraldehyde, 30 mM ATP, 21 mM Mg^{2+}, 0.08 mg/mL glycerol kinase from *Cellulomonas* sp. in 100 mM TEA buffer, pH 8, and 30°C

Specific productivity (SP) is defined as the mass of synthesized L-GAP per unit mass of enzyme and unit time. Evaluation of reactor performance based on specific productivity is of major importance; because it gives, a balanced weight to time that has a significant impact on process selectivity due to the decay of L-GAP and the amount of enzyme that influences process economy. A fixed conversion of 98.5% was considered in order to evaluate the performance of the reactors based on specific productivity. Figure 5.29 shows that STR offers the largest specific productivity, while CSTR performs least due to the low steady state reaction rate in CSTR that can be compensated either by large amount of enzyme loading or long residence time.

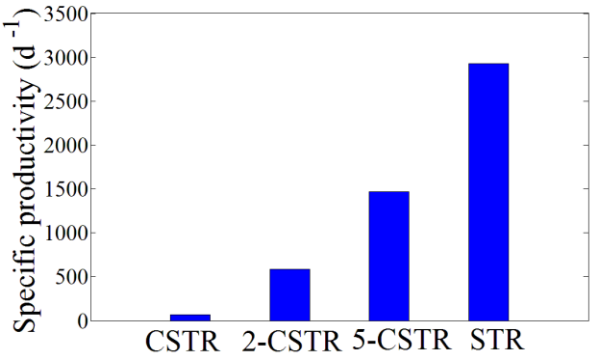

Figure 5.29: Comparison of stirred tank reactor (STR), continuously operated stirred reactor (CSTR) and 2- and 5-stages cascade CSTRs based on specific productivity by fixing conversion of 98.5% for the synthesis of L-GAP; reaction conditions: 30 mM L-glyceraldehyde, 30 mM ATP, 21 mM Mg^{2+}, 0.08 mg/mL glycerol kinase from *Cellulomonas* sp. in 100 mM TEA buffer, pH 8, and 30°C

Biocatalyst consumption is defined as the unit mass of glycerol kinase consumed per unit mass of L-GAP synthesized. As an early stage report of this study by collaboration partners, the synthesis of L-GAP via STR has been described with the biocatalyst consumption of 19.7 g kg^{-1} [41]. The biocatalyst consumption for the same reaction time and reactor type can be significantly reduced to 1.7 g kg^{-1} by applying reactor optimization criteria reported in this study. A DSP for the separation of target product (L-GAP) and coproduct (ADP) has been achieved based on the adsorption of the ADP using packed bed activated carbon. It was demonstrated in this study that the process of elution of reaction solution through packed bed activated carbon showed no effect on the concentration of L-GAP. The concentration of ADP at the inlet and outlet of the packed bed of 4 g activated carbon by elution 20 mL of 10 mM ADP solution and flow rate of 1 mL/min was analyzed by UV at 270 nm. Concentration of ADP at the outlet of the column was measured at different time point until all the volume of ADP solution was eluted. Results showed complete adsorption of ADP that no ADP was detected at the outlet of the column.

5.5. Interim Summary

Detailed reaction engineering aspects for the biocatalytic synthesis of L-GAP have been presented. Phosphorylation of enantiopure L-GA was selected instead of kinetic resolution of racemic DL-GA due to the enzymatic hydrolysis of ATP induced by D-GA. Results using a fixed 15 mM ATP and various concentrations up to 15 mM DL-glyceraldehyde have shown that nearly 10-fold stoichiometric excess of ATP with respect to L-glyceraldehyde in DL-glyceraldehyde was required in order to achieve full conversion of L-glyceraldehyde in DL-glyceraldehyde. The rate of DL-GAP depletion in 100 mM TEA buffer pH 8 and at different temperatures of 25°C, 30°C and 60°C were examined that rate constants of 2.3×10^{-5} s^{-1}, 2.8×10^{-5} s^{-1} and 1.2×10^{-3} s^{-1} with the corresponding half-lives of 8.35 h, 6.86 h and 0.15 h were determined, respectively. DL-GAP showed similar decomposition rates in different media including non-buffered aqueous medium pH 8, 100 mM TEA buffer pH 8, 50 mM TEA buffer pH 8 and 100 mM, PPB pH 8 while 100 mM Tris-HCl buffer pH 8 stabilizes DL-GAP.

The activity of glycerol kinase from *Cellulomonas* sp. depends on the Mg^{2+} to ATP molar ratio and exhibits maximum activity at the optimum molar ratio 0.7 for the phosphorylation of L-glyceraldehyde. Increasing the Mg^{2+} to ATP molar ratio suppresses the enzyme activity to the

non-zero asymptotic value but does not affect the equilibrium conversion. An appropriate reaction kinetics model has been developed following Michaelis-Menten kinetic behavior with respect to L-GA and ATP and taking into account a competitive inhibition by the coproduct ADP. Moreover, the enzyme kinetics with respect to ATP depends on Mg^{2+} concentration that exhibits pseudo-ATP surplus inhibition if Mg^{2+} to ATP molar ratio reaches below the optimum value. The enzyme shows different K_m values with respect to ATP at different fixed concentrations of Mg^{2+}. Validation of the model showed a 2-D correlation coefficients of 99.9% and 99.1% for kinetics parameters at 21 mM and 50 mM Mg^{2+}, respectively, between experimental data and numerical data matrices.

The enzyme shows inhibition by AMP, methylglyoxal and Ca^{2+}, but not by L-GAP and P_i. The same concentration of Ca^{2+} exerts different percent of inhibition at different Mg^{2+} to ATP molar ratio. This is due to mass action on the complexation equilibrium between Ca-ATP and Mg-ATP complexes. If the Mg^{2+} to ATP molar ratio is set to be at the optimum value or below, PP_in suppresses the enzyme activity; otherwise, PP_in enhances the enzyme activity. However, the activity enhancement by PP_in is only until the complete titration of the excess Mg^{2+} than the required amount to generate the optimum Mg^{2+} to ATP molar ratio. Different reactor types were simulated and evaluated based on reaction engineering parameters including conversion, selectivity, STY and specific productivity. STR offers the best performance in all of these parameters, while CSTR shows the least performance. The STR is therefore the most suitable reactor type for the biocatalytic synthesis of L-GAP, whereby the biocatalyst consumption could be significantly reduced from 19.7 g kg^{-1} to 1.7 g kg^{-1} by means of reaction engineering.

6. Mechanistic Elucidation of the Mg^{2+} to ATP Ratio Effect by NMR

As described in chapter 4 sub-chapter 4.3.1 and chapter 5 sub-chapter 5.3.1, the activity of glycerol kinase depends on the Mg^{2+} to ATP molar ratio in a reaction mixture. The mechanism by which Mg^{2+}, ATP and the interaction of Mg^{2+} and ATP influence the kinetics of glycerol kinase has not yet been elucidated. As a common practice, in most kinetic studies of glycerol kinase characterization, either stoichiometric or excess moles of Mg^{2+} relative to the moles of ATP have been applied [79, 144–148]. Few attempts have been made and all appear to assume the $[MgATP]^{2-}$ complex configuration as a "true" substrate for glycerol kinase [11, 57, 127, 149, 168]. Detailed kinetic characterization of glycerol kinase with respect to ATP at the fixed Mg^{2+} concentration and maintaining a constant Mg^{2+} to ATP molar ratio have already been described in the previous chapters 4 and 5. This chapter focuses on two main objectives starting with the elucidation of physical and chemical modifications of ATP by Mg^{2+} via ^{31}P and ^{1}H NMR. In addition, a mechanistic explanation of the glycerol kinase kinetics is presented as function of the Mg^{2+} to ATP molar ratio based on the role of Mg^{2+} in modifying the physical and chemical features of ATP.

ATP is a polydentate ligand with various electron donating sites including negatively charged oxygen atoms of the triphosphate chain at the reaction pH, hydroxyl groups of the ribose sugar and nitrogen atoms of the purine base. Despite the larger affinity of Mg^{2+} to the oxygen electron donating sites on the triphosphate chain of ATP in contrast to the nitrogen electron donating sites on the purine base moiety of ATP, Mg^{2+} can bind the purine base through inner- and outer-sphere coordination [169]. Structural elucidation of Mg-ATP complex formation is therefore a complex issue and needs to be investigated using different analytical methods. The binding of Mg^{2+} to ATP generates Mg-ATP complexes of various physical and chemical features. Such various physical and chemical features of Mg-ATP complexes affect the catalytic properties of glycerol kinase including the K_m and k_{cat} as demonstrated in the previous chapters.

Several, however inconsistent, results have described the chemical bond configuration of Mg-ATP complex products such as monodentate of β-phosphate group [170, 171], bidentate of β- and γ-phosphate groups [172–174], tridentate of α-, γ- and β-phosphate groups [142, 175, 176], a

mixture of bidentate of α- and β-phosphate groups, γ- and β-phosphate groups and α- and γ-phosphate groups [177] and a mixture of bidentate of β- and γ-phosphate groups and tridentate of α-, β-, γ-phosphate groups [178]. These equivocal interpretations of the chemical bond features of Mg-ATP complex products have as well extended to various possible stoichiometric configurations and dynamic exchange equilibria. The magnitude of the Mg^{2+} to ATP molar ratio is one among major factors that influence Mg-ATP complex formation chemistry. Other factors (e.g. pH and temperature) can be maintained in the glycerol kinase catalyzed phosphorylation reactions; however, the Mg^{2+} to ATP molar ratio increases with the course of reaction due to the depletion of ATP. The formation of $(Mg)_2ATP$ has been described at the Mg^{2+} to ATP molar ratio of 2 [142, 175] while at Mg^{2+} to ATP molar ratio of 0.5 the formation of a bis-nucleotide complex (i.e. $[Mg(ATP)_2]^{6-}$) has been reported [142, 179]. The formation of various complexes of different stoichiometric configurations including $[MgATP]^{2-}$, $(Mg)_2ATP$, $[Mg(ATP)_2]^{6-}$ and $[Mg_2(ATP)_2]^{4-}$ have been described in several studies [142, 143, 153, 169, 179, 180]. Figure 6.1 shows the reaction scheme of the interaction of Mg^{2+} to ATP yielding Mg-ATP complexes of various configurations. Figure 6.2 shows the chemical structure of ATP with labeled proton and phosphorus atoms.

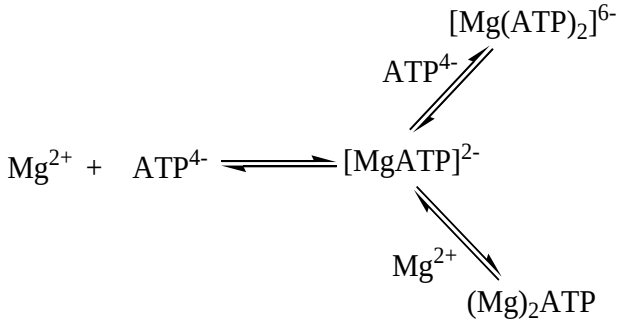

Figure 6.1: Reaction scheme illustrating the complex formation between ATP and Mg^{2+} yielding Mg-ATP complexes of various configurations

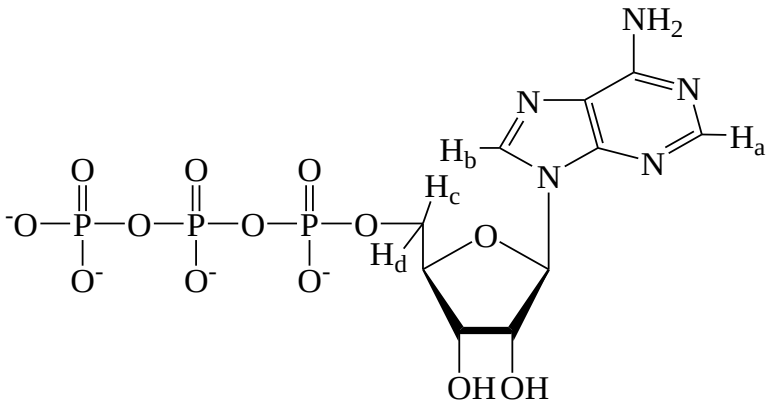

Figure 6.2: Chemical structure of ATP molecule

6.1. ^{31}P NMR Data Analysis

The ^{31}P resonance signals of ATP (i.e. α-, β- and γ-phosphate) shift to the lower magnetic field with the addition of the first molar equivalent Mg^{2+} compared to the chemical shifts of $[Na_2ATP]^2$. Figure 6.3 shows the ^{31}P NMR spectra of the $_\beta$P resonance of ATP for samples containing 20 mM $[(Na)_2ATP]^{2-}$ at different Mg^{2+} to ATP molar ratios.

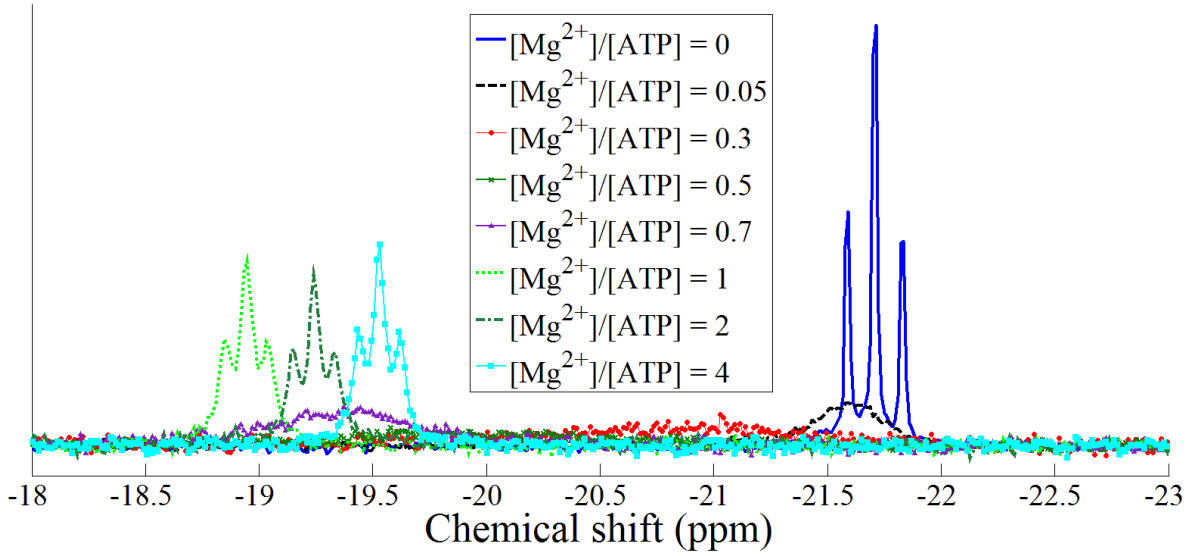

Figure 6.3: ^{31}P NMR spectra of β-phosphate resonance of ATP at different Mg^{2+} to ATP molar ratios; measurement conditions: 20 mM ATP, [0 - 80 mM] Mg^{2+} prepared in 100 mM Tris-HCl-D_2O buffer, pH 8, and 25°C

As shown in Figure 6.4, the ^{31}P resonances signals of ATP exhibit different gradients of ^{31}P chemical shifts as a function of the Mg^{2+} to ATP molar ratio. Up to the Mg^{2+} to ATP molar ratio

of 0.5 the gradients decrease in the order of $_{\beta}$P (4.05 ppm) > $_{\gamma}$P (1.03 ppm) > $_{\alpha}$P (0.54 ppm). The change in chemical shifts of all ^{31}P resonances of ATP indicates that all of them are involved in the interaction with Mg^{2+}. The chemical shifts change linearly as a function of Mg^{2+} to ATP molar ratio for the addition of nearly the first molar equivalent of Mg^{2+}. Subsequent addition of Mg^{2+} turns the chemical shifts to higher magnetic field, which has been interpreted due to binding difference between Mg^{2+} to the already generated $[MgATP]^{2-}$ and binding of Mg^{2+} to ATP [142]. The chemical shifts of the ^{31}P resonance signals of ATP after the addition of the first molar equivalent Mg^{2+} change linearly as a function of Mg^{2+} to ATP molar ratio with a break at the molar ratio of 2. This break indicates the saturation of $[MgATP]^{2-}$ and the formation of Mg_2ATP [142]. As shown in Figure 6.4, the change in chemical shifts after the addition of the second molar equivalent Mg^{2+} indicates the subsequent binding of Mg^{2+} per ATP molecule. The maximum loading of Mg^{2+} per ATP molecule has been described to be about 4:1 [175]. It has moreover been described that the change in chemical shifts in the region of large Mg^{2+} to ATP molar ratio becomes smaller and approaches to asymptotic values [142].

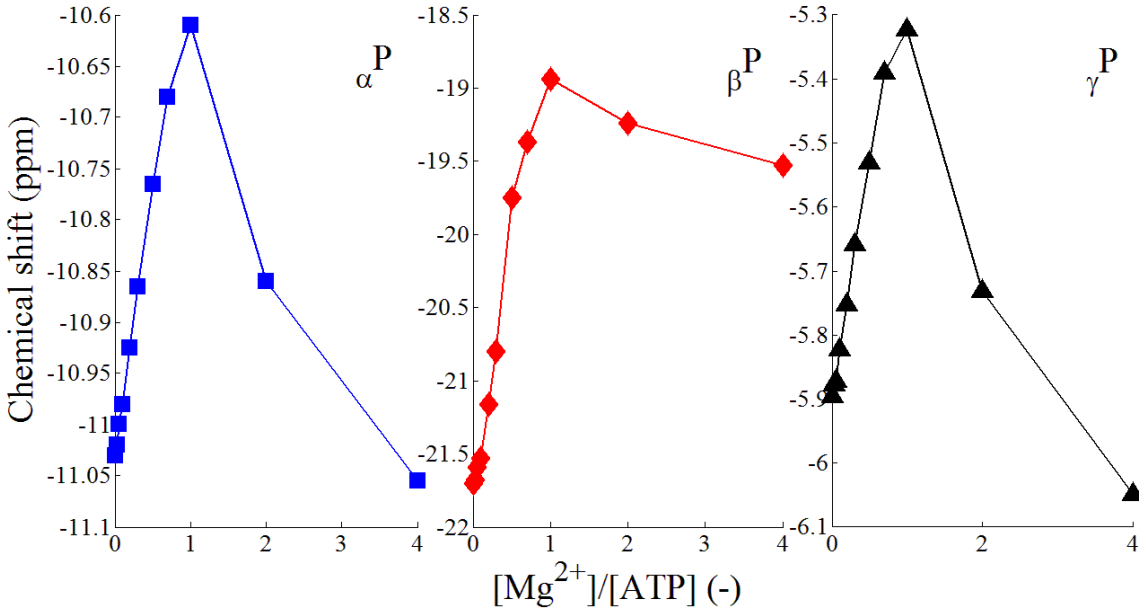

Figure 6.4: Change in chemical shifts of α-, β- and γ-phosphate ($_{\alpha}$P, $_{\beta}$P and $_{\gamma}$P) resonance ^{31}P NMR signals of ATP as a function of the Mg^{2+} to ATP molar ratio; measurement conditions: 20 mM ATP, [0 - 80 mM] Mg^{2+} prepared in 100 mM Tris-HCl-D_2O buffer, pH 8, and 25°C

Compare to line-width values of ^{31}P NMR signals of $[Na_2ATP]^{2-}$, the line-widths of all ^{31}P resonance signals of ATP are broadened by the addition of Mg^{2+}. Likewise, the change in

chemical shifts, the $_{\beta}$P resonance signal of ATP exhibits the largest broadening compare to $_{\alpha}$P and $_{\gamma}$P resonance signals. The ^{31}P resonances line-widths broadening indicates the existence of dynamic exchange processes operating among different physical and chemical states of Mg-ATP complexes [142, 181, 182]. Figure 6.5 and Figure 6.6 show the line-width of the ^{31}P NMR signal of $_{\beta}$P resonance of ATP and activity of glycerol kinase as a function of Mg^{2+} to ATP molar ratio, respectively, that both plots show similar pattern. As shown in Figure 6.3, in the region of Mg^{2+} to ATP molar ratio below one the line-width of $_{\beta}$P resonance becomes too broad that the presence of J-couplings have disappeared. The $_{\beta}$P resonance signals for Mg^{2+} to ATP molar ratio of less than one therefore represent the weighted average of chemical shifts, J-coupling constants and line-widths of all ATP species present in the sample solutions. For the $_{\beta}$P signals that the J-coupling are not observable due to signal broadening, line-width values were corrected dividing them by factor of 3. All the ^{31}P resonance signals of ATP exhibit maximum line-width broadening in the region of Mg^{2+} to ATP molar ratio of about 0.3.

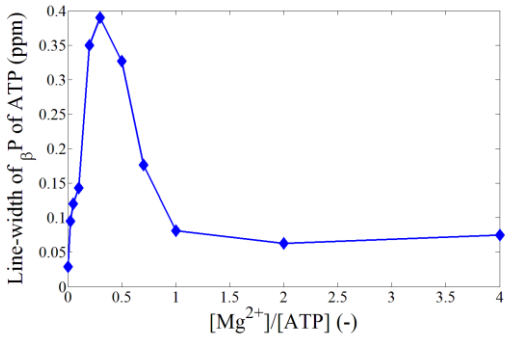

Figure 6.5: ^{31}P NMR line-width of $_{\beta}$P resonance of ATP as a function of Mg^{2+} to ATP molar ratio; measurement conditions: 20 mM ATP, [0 - 80 mM] Mg^{2+} prepared in 100 mM Tris-HCl-D_2O buffer, pH 8, and 25°C

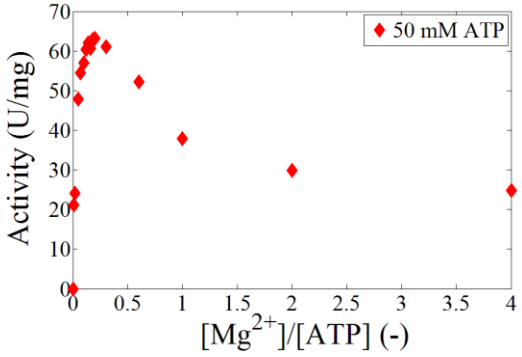

Figure 6.6: Activity of glycerol kinase as a function of Mg^{2+} to ATP molar ratio; reaction conditions: 50 mM ATP, 50 mM glycerol, [0 - 200 mM] Mg^{2+}, various amounts of glycerol kinase from *Cellulomonas* sp. in 100 mM Tris-HCl buffer, pH 8.5, and 25°C

It has been described that the ^{31}P NMR signals of $_{\beta}$P and $_{\gamma}$P resonances at Mg^{2+} to ATP molar ratio of 0.5 are single weighted average at ATP larger than 0.2 mM while resolved into two separate signals at ATP less than 0.2 mM [142]. At the same Mg^{2+} to ATP molar ratio of 0.5 and ATP larger than 0.2 mM, at 2°C the ^{31}P NMR signal of $_{\beta}$P resolved into two resonance signals while at 52°C the signals merge together and appear as a single resonance signal with an

averaged chemical-shift value [183]. These results of concentration and temperature effects therefore prove the co-existence of two ATP species in an exchange equilibrium that the rate of exchange slows down due to dilution and low temperature. The signals of $_{\beta}$P resonance resolved at low temperature have been interpreted as they originated from 2 entities of $[MgATP]^{2-}$ and $[Na_2ATP]^{2-}$; on the other hand, the splitting of $_{\beta}$P and $_{\gamma}$P resonance signals upon dilution has been interpreted as they originated from different conformations of 2 distinct ATP residues with in a single $[Mg(ATP)_2]^{6-}$ [142, 181]. The rate of exchange slows down by dilution due to the disaggregation of the complex; moreover, an asymmetric signal resolution excludes the origination of signals from 2 entities of $[MgATP]^{2-}$ and $[Na_2ATP]^{2}$ [142].

6.2. Mechanistic Interpretation of Enzyme Kinetics Based on ^{31}P NMR Results

Results of glycerol kinase activity assay (shown in Figure 6.6) have depicted that the enzyme shows maximum activity at Mg^{2+} to ATP molar ratio of [0.12 to 0.3]. Subsequent increase of Mg^{2+} to ATP molar ratio leads to suppress the enzyme activity; moreover, after the addition of the first molar equivalent Mg^{2+} the decrease of enzyme activity becomes smaller and approaches to a non-zero asymptotic value. The behavior of glycerol kinase activity and change in ^{31}P chemical shifts of ATP in the region of large Mg^{2+} to ATP molar ratio can be correlated that the changes in both cases become smaller and approach to asymptotic values. This may be due to formation of stable Mg-ATP complex and insignificant change of physical and chemical characteristics of ATP species. Moreover, the line-widths of the ^{31}P resonance signals of ATP, after reaching the optimum Mg^{2+} to ATP molar ratio of 0.3 in respect to the enzyme activity, drop and eventually become constant. This indicates the less operation of dynamic exchange process and the formation of stable complex configuration.

In the kinetics results of glycerol kinase with respect to ATP (presented in Table 4.3), the enzyme shows larger affinity (low K_m) at higher Mg^{2+} to ATP molar ratios than at the optimum Mg^{2+} to ATP molar ratio. Glycerol kinase therefore exhibits large affinity (low K_m) and less activity (low k_{cat}) for Mg-ATP complexes with a stoichiometric configuration or more saturated by Mg^{2+} like Mg_2ATP. The low k_{cat} at high Mg^{2+} to ATP molar ratios can be explained due to the requirement of large amount of energy for the dissociation of γ-phosphoryl group to be transferred to the phosphoryl acceptor substrate in the ternary complex at the enzyme active site [142]. On the other hand, glycerol kinase shows less affinity (large K_m) and high activity (large

k_{cat}) for unsaturated complexes like $[Mg(ATP)_2]^{6-}$ at the region of the optimum Mg^{2+} to ATP molar ratio. Figure 6.7 shows the effect of Mg^{2+} to ATP molar ratio and different Mg-ATP complex species on the catalytic properties (i.e K_m and k_{cat}) of glycerol kinase from *Cellulomonas* sp.

Glycerol kinase essentially requires Mg^{2+} for its activity. Using ^{25}Mg NMR [92] has described that Mg-ATP complex formation gets disrupted at pH below 4. Results in this study showed that glycerol kinase lost its activity at pH below 4; while the enzyme retained 43% of its activity after being incubated at pH 3 for 24 h. It may therefore be that at pH below 4 the enzyme shows no activity due to the disruption of Mg-ATP complex formation.

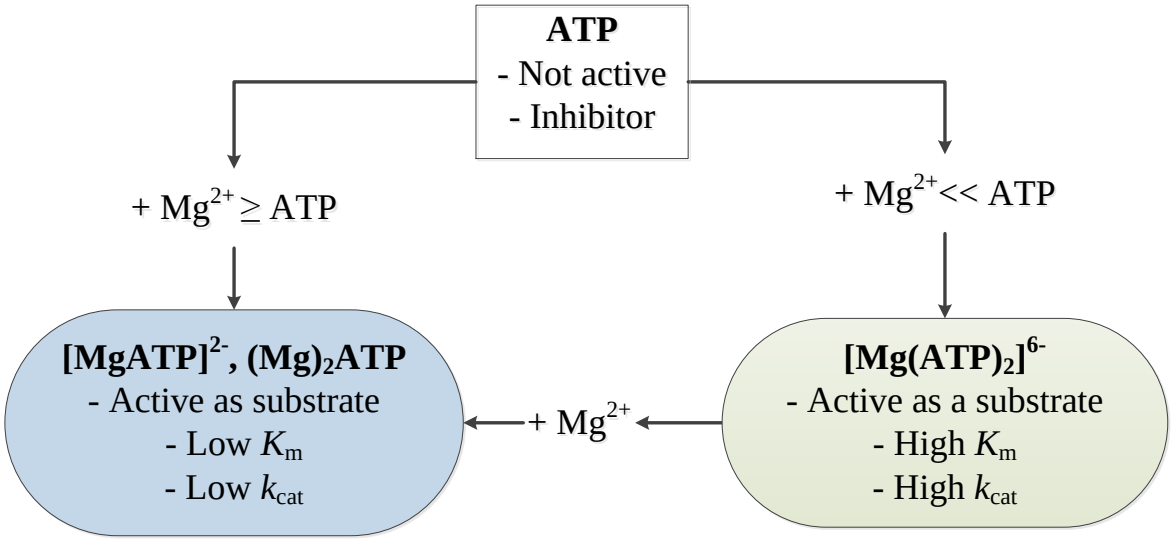

Figure 6.7: Schematic description illustrating the effect of Mg^{2+} to ATP molar ratios and different Mg-ATP complex species on the catalytic properties of glycerol kinase from *Cellulomonas* sp.

6.3. ^{1}H NMR Data Analysis and Correlation with Enzyme Kinetics

Besides ^{31}P NMR, the most widely used analytical method to study Mg-ATP complex formation is ^1H NMR spectroscopy. This was carried out for samples at different Mg^{2+} to ATP molar ratio. The interaction of Mg^{2+} and ATP can affect the protons on the adenine base and the protons on the ribose sugar moiety due to coordination and/or conformational modification of ATP. Since all parts of the ATP molecule (the adenine base, the ribose sugar, and the triphosphate chain) should contribute to binding to the active site of glycerol kinase, any conformational change of the ATP molecule induced by the addition of Mg^{2+} should be reflected in the K_m and k_{cat} values. Among the ^1H NMR signals of all the NMR active protons on the ribose sugar and purine ring

moieties of ATP only those that reflect the influence of Mg^{2+} will be discussed. The ^{1}H NMR spectra of the two protons on the purine ring (i.e. H_a and H_b) and their chemical shift values as a function of Mg^{2+} to ATP molar ratio are shown in Figure 6.8 left and right, respectively. The chemical shifts of ^{1}H NMR signals of the purine ring protons change linearly to higher magnetic field with the addition of the first molar equivalent Mg^{2+} compare to the chemical shifts of $[Na_2ATP]^{2-}$ for the same proton species. Subsequent addition of Mg^{2+} after the first molar equivalent leads to the less changes in chemical shifts and the more approach to asymptotic values likewise the ^{31}P chemical shifts of ATP as a function of Mg^{2+} to ATP molar ratio.

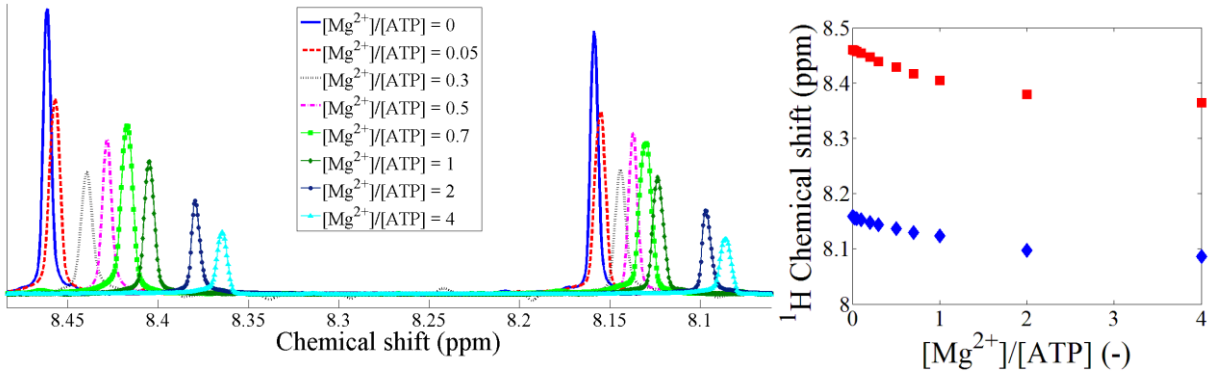

Figure 6.8: ^{1}H NMR spectra (left) of aromatic purine ring protons of ATP (H_a and H_b) and their chemical shift values as a function of Mg^{2+} to ATP molar ratios (right); measurement conditions: 20 mM ATP, [0 - 80 mM] Mg^{2+} prepared in 100 mM Tris-HCl-D_2O buffer, pH 8, and 25°C

An interesting observation was the response of the CH_2-protons on the ribose sugar moiety of ATP (i.e. H_c and H_d) in the titration by Mg^{2+}. Figure 6.9 shows the region of ^{1}H NMR spectra of the CH_2-protons at different Mg^{2+} to ATP molar ratio.

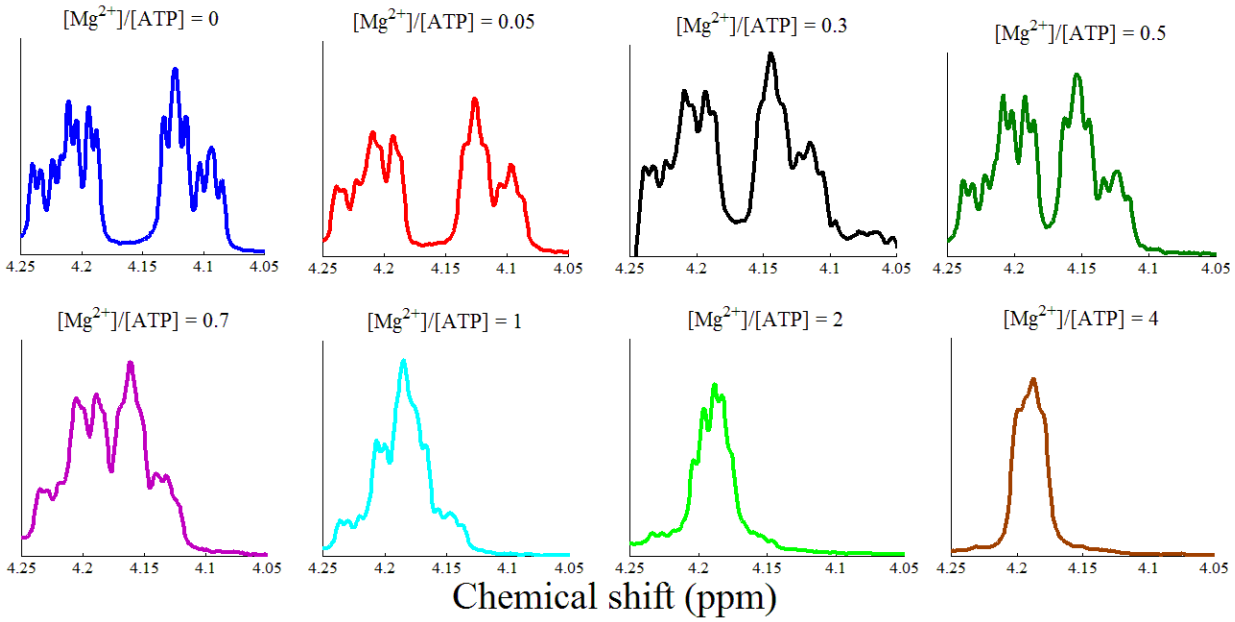

Figure 6.9: Chemical shift region of ^{1}H NMR spectra of the CH_2-protons on the ribose sugar moiety of ATP (H_c and H_d) at different Mg^{2+} to ATP molar ratios; measurement conditions: 20 mM ATP, [0 - 80 mM] Mg^{2+} prepared in 100 mM Tris-HCl-D_2O buffer pH 8 and 25°C

As expected, the signals for the diastereotopic protons of the CH_2-group in ribose sugar moiety of ATP are well separated by about 0.1 ppm. With the increase of Mg^{2+} to ATP molar ratio the signal difference of the diastereotopic protons has reduced by a non-significant value but until the Mg^{2+} to ATP molar ratio of 0.3 that reflects the availability of Mg^{2+}. The subsequent addition of Mg^{2+} after the Mg^{2+} to ATP molar ratio of 0.3 generates a new situation where the signals of CH_2-protons become nearly equivalent. This may happen when the phosphate chain residue of ATP folded back to the purine ring and intersects the H-C-H moiety. Glycerol kinase therefore appears to have high affinity for Mg-ATP complex with such conformation as it shows low K_m at Mg^{2+} to ATP molar ratio higher than one but low k_{cat} as the enzyme activity gets suppressed at Mg^{2+} to ATP molar ratio higher than 0.3 for the asymmetric phosphorylation of glycerol.

Moreover, the conformational change of ATP molecule by the addition of Mg^{2+} could be reflected on the change in ^{31}P-^{31}P NMR J-coupling constants since they indicate how the phosphorous nuclei in the phosphate chain see one another. As can be seen in Figure 6.10 the $J_{\alpha}P$-$_{\beta}P$ and $J_{\gamma}P$-$_{\beta}P$ coupling constants do not change with the addition of Mg^{2+} until the Mg^{2+} to ATP molar ratio of about 0.1 but decrease up to the addition of the first molar equivalent Mg^{2+}. Further increasing of Mg^{2+} to ATP molar ratio larger than one appears not to have much

influence on the $J_{\alpha}P$-$_{\beta}P$ and $J_{\gamma}P$-$_{\beta}P$ coupling constants. The change in $J_{\alpha}P$-$_{\beta}P$ and $J_{\gamma}P$-$_{\beta}P$ coupling constants at the region of Mg^{2+} to ATP molar ratio from 0.1 to 1 indicates conformational change of ATP while conformational stability after Mg^{2+} to ATP molar ratio of one. These J-coupling results moreover augment the conformational change of ATP observed in the ^{1}H NMR spectra of CH_2-protons of ribose ring moiety of ATP (as shown in Figure 6.9).

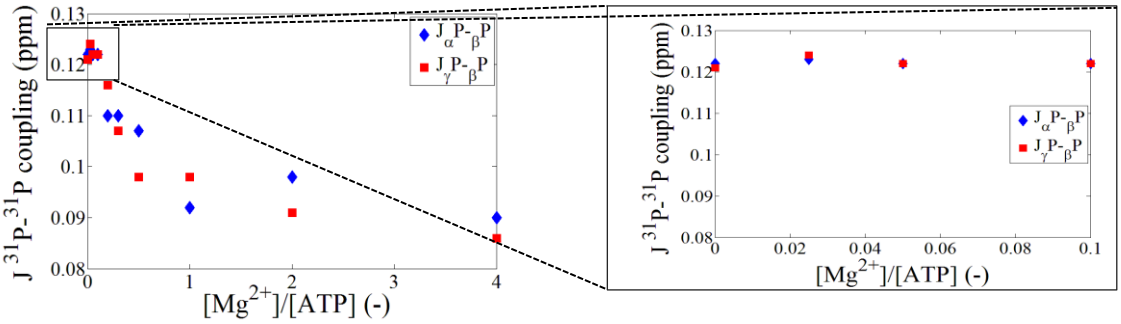

Figure 6.10: $J_{\alpha}P$-$_{\beta}P$ and $J_{\gamma}P$-$_{\beta}P$ coupling constants ATP as a function of Mg^{2+} to ATP molar ratio (left) and $J_{\alpha}P$-$_{\beta}P$ and $J_{\gamma}P$-$_{\beta}P$ coupling constants ATP as a function of Mg^{2+} to ATP molar ratio under magnification up to Mg^{2+} to ATP molar ratio of 0.1 (right); measurement conditions: 20 mM ATP, [0 - 80 mM] Mg^{2+} prepared in 100 mM Tris-HCl-D_2O buffer pH 8 and 25°C

6.4. Interim Summary

The change of ^{31}P resonance signals of ATP (i.e. α-, β- and γ-phosphate) by the addition of Mg^{2+} indicates that all of them are involved Mg-ATP complex formation. The $_{\beta}P$ signal of ATP exhibits the largest chemical shift and line-width broadening. Glycerol kinase exhibits high affinity (low K_m) and less activity (low k_{cat}) for complexes with a stoichiometric configuration or more saturated by Mg^{2+} like Mg_2ATP. On the other hand, the enzyme shows less affinity (high K_m) and high activity (high k_{cat}) for unsaturated complexes like $[Mg(ATP)_2]^{-6}$.

The CH_2-protons become nearly NMR equivalent after the Mg^{2+} to ATP molar ratio of 0.3 is reached. This may happen when the phosphate chain residue of ATP folded back to the purine ring and intersects the H-C-H moiety. Glycerol kinase therefore appears to have high affinity (low K_m) and less activity (low k_{cat}) for Mg-ATP complex with such conformation. The change in $J_{\alpha}P$-$_{\beta}P$ and $J_{\gamma}P$-$_{\beta}P$ coupling constants at the region of the Mg^{2+} to ATP molar ratio from 0.1 to 1 indicates conformational changes of ATP while conformational stability after surpassing a Mg^{2+} to ATP molar ratio of one.

7. Synthesis of D-Glyceraldehyde-3-Phosphate[1]

D-Glyceraldehyde-3-phosphate (D-GAP) is an essential phosphorylated metabolite occurring in various metabolic pathways such as glycolysis, thiamine biosynthesis [149] methylerythritol phosphate (MEP) pathway [144, 184] and photosynthesis [147, 185]. Several multi-step chemical synthetic routes have been described for the preparation of D-GAP including a 9 step sequence starting from a kilogram of D-mannitol to produce few grams of D-GAP using toxic reagents like $HgCl_2$ and HgO [8], a 10 step sequence starting from 2-*O*-benzyl-D-arabinose [9], oxidation of D-F6P by a highly toxic reagent $Pb(OAc)_4$ [10, 11], oxidative cleavage by H_5IO_6 of D-fructose-1,6-bisphosphate (D-F16BP) [186] or of D-F6P [41]. Beside to the safety issues, the lack of selectivity of all of these methods makes purification steps too laborious and drastically reduces product yields. The reported enzymatic synthesis of D-GAP applying aldolase to catalyze aldol cleavage of D-F16BP [188] has thermodynamics as a main drawback, being in favor of reverse aldol condensation with an equilibrium constant of 10^{-4} M [26]. As a strategy in order to overcome the reaction thermodynamics limitation and to shift the reaction equilibrium, the reaction was carried out in the presence of hydrazine yielding D-GAP hydrazone as a final product instead of the desired D-GAP [188].

In consequence, three main objectives of this chapter were defined, starting with the design of a one-pot enzymatic reaction sequence for the synthesis of D-GAP without protection and deprotection steps. The second objective was a comprehensive reaction engineering study like activity, stability and selectivity of all enzymes involved, stability of cofactors and products, reaction kinetics model development and simulation as well as performance evaluation of different reactor types. To develop a DSP method was the third objective.

7.1. Reaction Sequence Development

For the synthesis of D-GAP, fructose-1,6-bisphosphate aldolase from rabbit muscle (RAMA) (EC 4.1.2.13) catalyzed aldol cleavage of D-F16BP to D-GAP and dihydroxyacetone phosphate (DHAP) was used. *In situ* reduction of the coproduct DHAP to *sn*-glycerol-3-phosphate catalyzed by *sn*-glycerol-3-phosphate dehydrogenase from rabbit muscle (*sn*-G3PDH) (EC 1.1.1.8) was added as consecutive reaction step in order to shift the reaction equilibrium. The ΔG

[1] Parts of this chapter are published in [36].

for the reduction of DHAP is more favorable than for aldol cleavage of D-F16BP; however, cannot fully circumvent the thermodynamic barrier in order to achieve complete conversion of D-F16BP. Moreover, as the second reaction step requires the expensive cofactor NADH, it was coupled with formate dehydrogenase from *Candida boidinii* (FDH) (EC 1.2.1.2) catalyzing the *in situ* regeneration of NADH. FDH catalyzed reduction of NAD^+ was selected as the *in situ* NADH regeneration reaction system for the advantages including the utilization of inexpensive and stable substrate (formate), shifting of the entire reaction equilibrium to a complete conversion of D-F16BP as well as enabling easy removal of the byproduct CO_2. Figure 7.1 shows the entire reaction sequence designed for the synthesis of D-GAP.

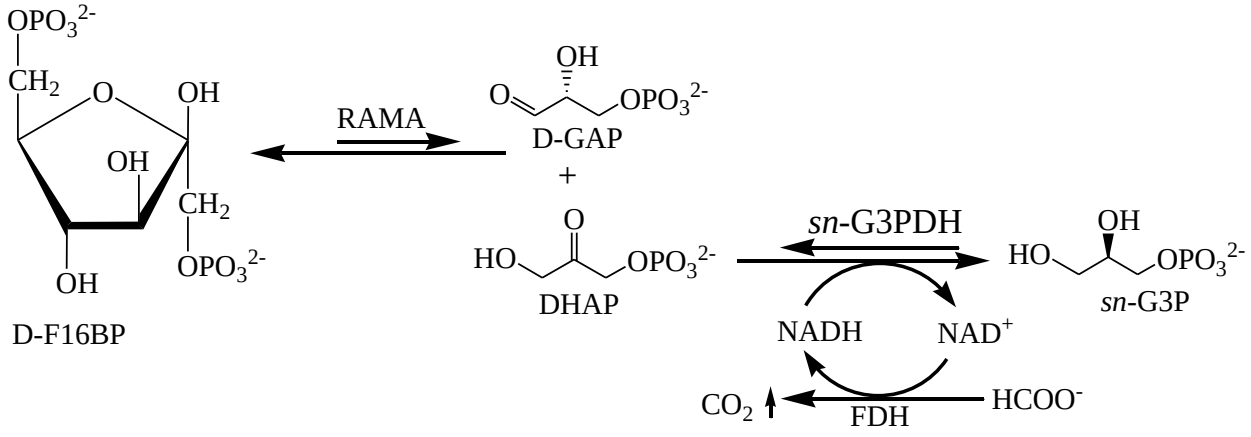

Figure 7.1: A one-pot cascade enzymatic reaction sequence designed for the synthesis of D-GAP; D-fructose-1,6-bisphosphate (D-F16BP), D-glyceraldehyde-3-phosphate (D-GAP), dihydroxyacetone phosphate (DHAP), rabbit muscle aldolase (RAMA), *sn*-glycerol-3-phosphate (*sn*-G3P), *sn*-glycerol-3-phosphate dehydrogenase (*sn*-G3PDH) and formate dehydrogenase (FDH)

7.2. Optimization of Reaction Conditions

The capability of the designed one-pot reaction sequence to shift the reaction equilibrium of RAMA catalyzed aldol cleavage of D-F16BP was examined by performing reactions using excess amount of NADH without coupling the cofactor regeneration system. Despite unfavorable change in Gibbs reaction free energy ($\Delta_r G$ = 20.2 kJ/mol at pH 8 and ionic strength of 100 mM) for aldol cleavage direction [138], Figure 7.2 shows the conversion plot of a batch reaction that demonstrates a complete conversions of D-F16BP. Conversion data were determined by

monitoring the stoichiometric depletion of NADH due to the formation of DHAP from the aldol cleavage D-F16BP; moreover, blank reaction without the addition of aldolase showed no depletion of NADH.

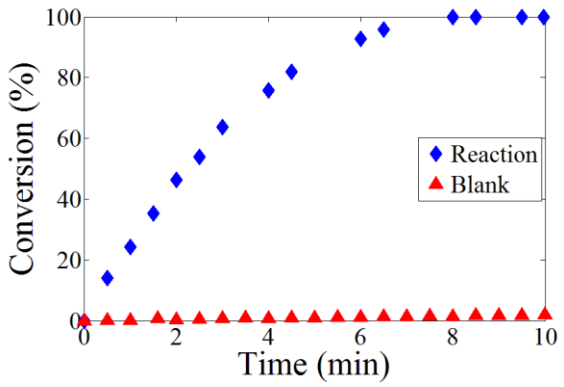

Figure 7.2: Conversion plots of aldol cleavage of D-fructose-1,6-bisphosphate catalyzed by rabbit muscle aldolase with the addition the consecutive reduction of dihydroxyacetone phosphate catalyzed by *sn*-glycerol-3-phosphate dehydrogenase; reaction conditions: 0.1 mM D-F16BP, 0.5 mM NADH, 0.0046 mg/mL RAMA, 0.044 mg/mL *sn*-G3PDH in 50 mM TEA buffer, pH 8, and 25°C for RAMA catalyzed aldol cleavage of D-F16BP and blank reaction contains all reaction components except RAMA

7.2.1. Stability of Cofactors and Product

Results shown in Figure 7.3 demonstrate that the reduced form of the nucleotide cofactor (NADH) is unstable at acidic pH while it is stable at alkaline pH region. On the other hand; the oxidized form of this nucleotide cofactor (NAD^+) is unstable at alkaline pH, while it is stable at acidic pH region [146]. The decrease of pH accelerates the decay of NADH; whereas, the increase of pH accelerates NAD^+ depletion. Determining the optimum pH value is crucial for the process development due to the reciprocal stability of NADH and NAD^+ as a function of pH. The stability of NADH can be improved by increasing the pH (half-life of 0.9 day at pH 5) to only 17% loss at pH 8 at the same temperature 25°C. Considering the half-lives of NADH and NAD^+ as a function of pH, pH 8 appears as an optimum pH value for the stability of NADH and NAD^+ under the same reaction mixture [189].

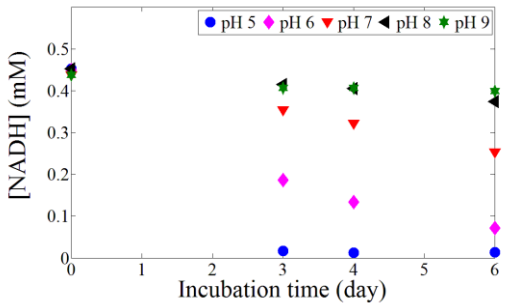

Figure 7.3: Stability of NADH at different pH; incubation conditions: 0.5 mM NADH in 50 mM TEA buffer at 25°C at the given pH levels

The kinetics of D-GAP decay in TEA buffer pH 8 is a critical parameter for the process development using the one-pot enzymatic reaction sequence. D-GAP is stable at pH below 4 while all the enzymes involved are not active nor NADH is stable at pH below 4. Figure 7.4 shows the decay of D-GAP in 50 mM TEA buffer pH 8 at 25°C with half-life of 8.35 h. Moreover, details of D-GAP stability in different buffer media and different temperature levels at pH 8 are described in chapter 5 sub-chapter 5.2.

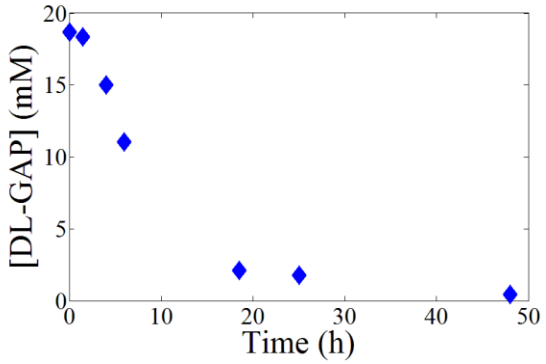

Figure 7.4: The decay of 20 mM DL-glyceraldehyde-3-phosphate incubated in 50 mM TEA buffer, pH 8, and 25°C

7.2.2. Selectivity, Activity and Stability of the Enzymes Involved in the Reaction

Due to the structural similarity of D-GAP and DHAP, the selectivity of *sn*-G3PDH was examined that no activity was detected when using D-GAP as a starting material. *sn*-G3PDH therefore exhibits 100% selectivity to DHAP. In the presence of all the three enzymes in the reaction mixture without the addition of D-F16BP no depletion of NADH by oxidation occurred. The selection of optimum reaction conditions like pH and temperature is indispensable for developing an efficient biocatalytic process. In order to define optimum reaction conditions, factors including the activity and stability of all the three enzymes involved as a function of pH and temperature need to be considered. Figure 7.5, Figure 7.6 and Figure 7.7 show the activity of

RAMA, *sn*-G3PDH and FDH as a function of pH, respectively. The activity of RAMA was monitored by UV at 340 nm by using the consecutive *sn*-G3PDH catalyzed reduction of DHAP that creates stoichiometric depletion of NADH. The RAMA to *sn*-G3PDH activity ratio in the reaction mixture was therefore adjusted so that the RAMA catalyzed aldol cleavage of D-F16BP was rate limiting.

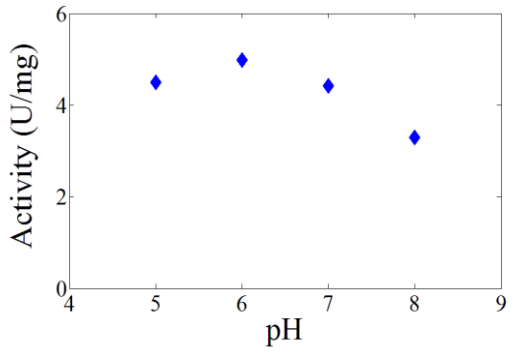

Figure 7.5: Activity of rabbit muscle aldolase (RAMA) as a function of pH; reaction conditions: 0.5 mM D-F16BP, 0.5 mM NADH, 0.012 mg/mL RAMA and 0.032 mg/mL *sn*-G3PDH in 50 mM TEA buffer at 25°C

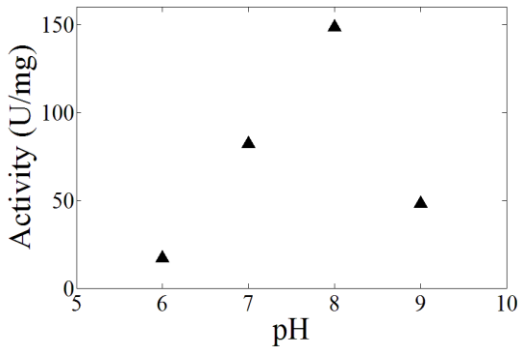

Figure 7.6: Activity of *sn*-glycerol-3-phosphate dehydrogenase (*sn*-G3PDH) as a function of pH; reaction conditions: 0.5 mM DHAP 0.5 mM NADH and 0.004 mg/mL *sn*-G3PDH in 50 mM TEA buffer at 25°C

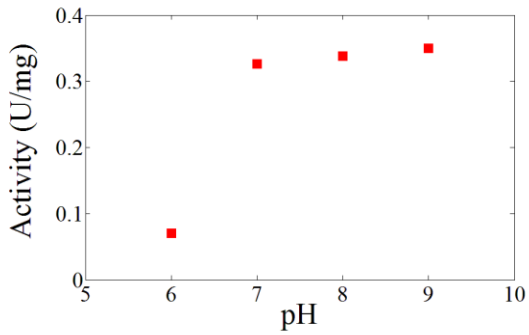

Figure 7.7: Activity of formate dehydrogenase (FDH) as a function of pH; reaction conditions: 50 mM NaHCOO, 0.5 mM NAD^+ and 0.5 mg/mL FDH in 50 mM TEA at 25°C

RAMA and *sn*-G3PDH show maximum activity at pH 6 and pH 8, respectively. FDH shows nearly constant activity from pH 7 to pH 9. In order to select an overall optimum reaction pH, the percentage loss of activity of RAMA and *sn*-G3PDH was determined at different pH values compare to their maximum activity at pH 6 and pH 8, respectively. Figure 7.8 shows the percentage of lost activity of RAMA and *sn*-G3PDH.

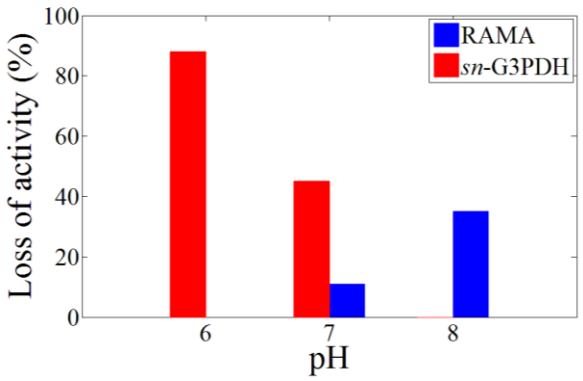

Figure 7.8: Percent loss of activity of RAMA and *sn*-G3PDH compare to their maximum activity at pH 6 and pH 8, respectively; the data in this plot were calculated using the data presented in Figure 7.5 and Figure 7.6

Figure B.13, Figure B.14 and Figure B. 15 in appendix B show the remaining activity of RAMA, *sn*-G3PDH and FDH plotted as a function of incubation period, respectively. RAMA, *sn*-G3PDH and FDH show no significant deactivation incubated in 50 mM TEA buffer pH 8 at 25°C for 6 days, 8 days and 12 days of incubation period, respectively. Table 7.1 shows the activities and stabilities of all the three enzymes involved in the reaction sequence as a function of pH. Considering that enzymes show maximum activity at different pH, the activity loss of one enzyme at a pH where another enzyme shows maximum activity and the different enzyme stabilities with respect to pH, pH 8 appears to represent an optimum pH value.

Table 7.1: Activity and stability of RAMA, *sn*-G3PDH and FDH as a function of pH; reaction conditions: 0.5 mM D-F16BP, 0.5 mM NADH, , 0.012 mg/mL RAMA and 0.032 mg/mL *sn*-G3PDH (for the activity assay of RAMA); 0.5 mM DHAP, 0.5 mM NADH and 0.004 mg/mL *sn*-G3PDH (for the activity assay of *sn*-G3PDH) and 50 mM NaHCOO, 0.5 mM NAD^+ and 0.5 mg/mL FDH (for the activity assay of FDH) in 50 mM TEA buffer at 25°C. Incubation conditions: RAMA (50 mM TEA buffer, 25°C and 400 rpm); *sn*-G3PDH (50 mM TEA buffer, 25°C and 400 rpm) and FDH (50 mM TEA buffer, 25°C and 400 rpm)

Enzyme	**Maximum activity**	**Most stable**
RAMA	At pH 6	At pH [7-8]
sn-G3PDH	At pH 8	At pH [6-9]
FDH	At pH [7-9]	At pH [6-8]

The effect of temperature on activity and stability of FDH was examined. As can be seen in Figure 7.9 the FDH activity increases steeply with increasing of temperature up to 45°C while

the enzyme shows in Figure 7.7 constant activity over a broad pH region. FDH shows maximum activity at 45°C; however, its half-life at 45°C drops to 1.8 day compare to no significant deactivation occurred at 25°C (as shown in Figure 7.10). Moreover, since temperature has large influence on the rate of D-GAP decay, that the increase of temperature from 25°C, 30°C to 60°C reduces its half-life 8.35 h, 6.86 h to 0.15 h, respectively, that the reaction temperature was maintained at 25°C for the synthesis of D-GAP.

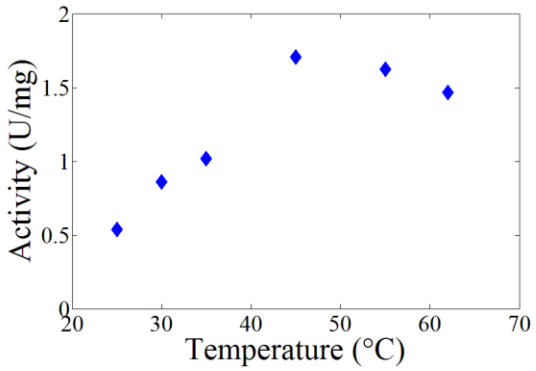

Figure 7.9: Activity of formate dehydrogenase (FDH) as a function of temperature; reaction conditions: 0.5 mM NAD^+, 300 mm NaHCOO, 0.5 mg/mL FDH in 50 mM TEA buffer, pH 8

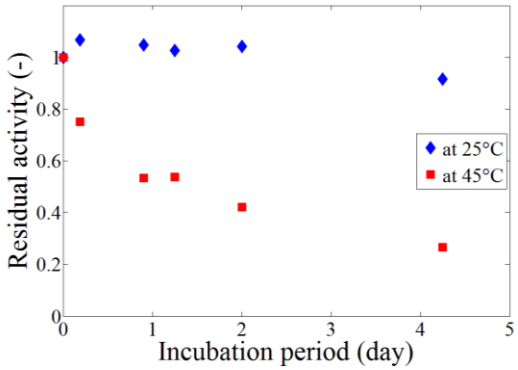

Figure 7.10: Residual activity of formate dehydrogenase (FDH) at 25°C and 45°C; incubation conditions: 50 mM TEA buffer, pH 8

7.3. Reaction Kinetics and Thermodynamics

7.3.1. Reaction Thermodynamics

One of the main limitations of implementing aldolase catalyzed aldol cleavage of D-F16BP for the synthesis of D-GAP is the unfavorable $\Delta_r G$ of the reaction beside to other challenge including the separation of D-GAP and the coproduct DHAP due to their structural similarity. Adding the consecutive reaction of the coproduct DHAP reduction to *sn*-glycerol-3-phosphate not only improves the thermodynamic barrier but also modifies the structure of DHAP that simplifies DSP. The reduction of DHAP has more favorable ΔrG than for aldol cleavage of D-F16BP; however, still cannot fully circumvent the thermodynamic barrier. Figure 7.11 and Figure 7.12 show the effect of pH on $\Delta_r G$ of aldolase catalyzed aldol cleavage of D-F16BP and *sn*-G3PDH catalyzed reduction of DHAP, respectively [138]. The thermodynamics of both reaction steps

favor forward decreasing the pH value. However, the effect of pH on the reaction thermodynamics was not considered in the selection of reaction pH due to its high significance and narrow range with respect to enzymes activity and cofactors stability. For instance, at pH 6 two of the enzymes involved in the reaction sequence (i.e. *sn*-G3PDH and FDH) nearly lost their activity. The FDH catalyzed reduction of NAD^+ coupled with the second reaction step has favorable $\Delta_r G$ (-24.6 ±3 kJ/mol) at the reaction pH 8 that shifts the entire reaction equilibrium to a complete conversion of D-F16BP.

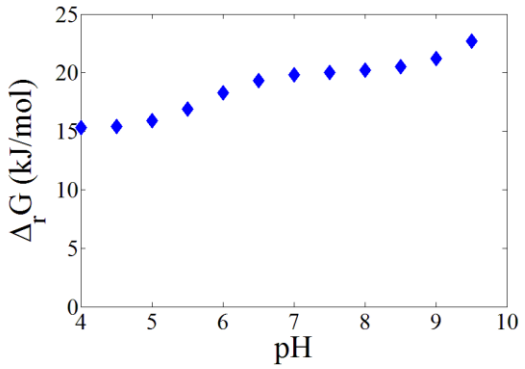

Figure 7.11: Change in reaction Gibbs free energy ($\Delta_r G$) of aldolase catalyzed aldol cleavage of D-F16BP as a function of pH; calculation conditions: 10 mM D-F16BP, 1 nM D-glyceraldehyde-3-phosphate, 1 nM dihydroxyacetone phosphate at ionic strength of 0.1 M and 25°C

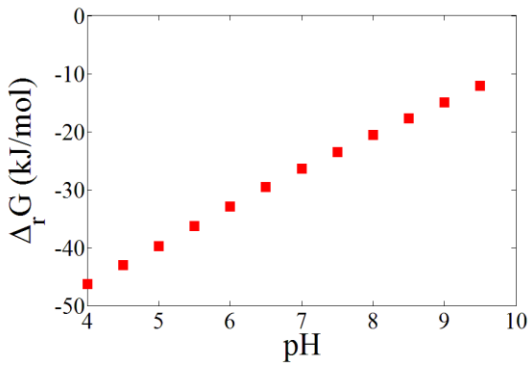

Figure 7.12: Change in reaction Gibbs free energy ($\Delta_r G$) of *sn*-glycerol-3-phosphate dehydrogenase catalyzed reduction of dihydroxyacetone phosphate as a function of pH; calculation conditions: 10 mM dihydroxyacetone phosphate, 10 mM NADH, 1 nM *sn*-glycerol-3-phosphate, 1 nM NAD^+ at ionic strength of 0.1 M and 25°C

7.3.2. Kinetics of Each of Enzymes

The investigation of biocatalytic reaction kinetics is essential for understanding the reaction mechanism, identifying relevant kinetics parameters and for process development, simulation as well as optimization. Since the designed reaction sequence for D-GAP synthesis contains, in addition to the native substrate and product of each of the enzymes, several other co-substances; therefore, examination of their influence on each of the enzyme activities was performed. These activity data can be included in the overall reaction kinetics model if necessary and are useful for selecting the concentration of each enzyme. Figure 7.13 and Figure 7.14 show the activity of FDH as a function of D-F16BP and *sn*-glycerol-1(3)-phosphate, respectively, that both reaction components do not influence the activity of FDH.

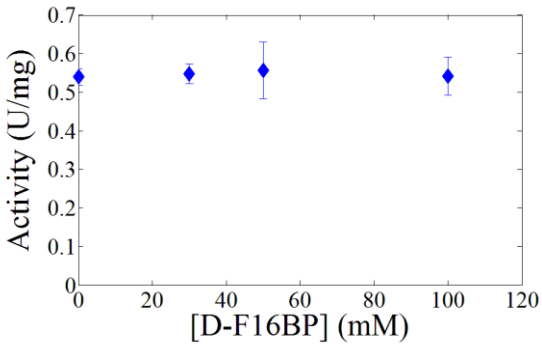

Figure 7.13: Activity of formate dehydrogenase (FDH) as a function of D-fructose-1,6-bisphosphate (D-F16BP) concentration; reaction conditions: 1 mM NAD^+, 300 mM NaHCOO, [0 mM 100 mM] D-F16BP, 0.5 mg/mL FDH in 50 mM TEA buffer, pH 8, and 25°C

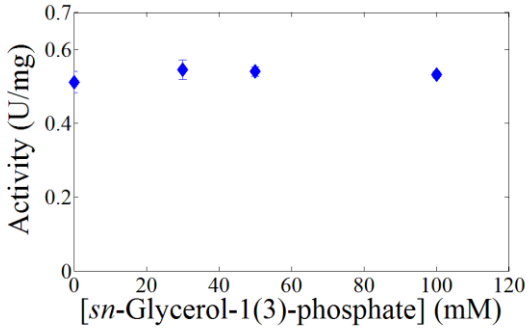

Figure 7.14: Activity of formate dehydrogenase (FDH) as a function of *sn*-glycerol-1(3)-phosphate concentration; reaction conditions: 1 mM NAD^+, 300 mM NaHCOO, [0 mM 100 mM] *sn*-glycerol-1(3)-phosphate, 0.5 mg/mL FDH in 50 mM TEA buffer, pH 8, and 25°C

Results of *sn*-G3PDH activity as a function of D-F16BP, NaHCOO and D-GAP concentration are shown in Figure 7.15, Figure 7.16 and Figure 7.17, respectively. The activity of *sn*-G3PDH shows not affected by D-F16BP while suppressed by D-GAP and NaHCOO.

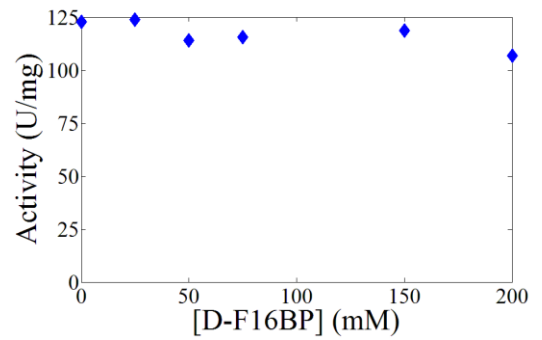

Figure 7.15: Activity of *sn*-glycerol-3-phosphate dehydrogenase (*sn*-G3PDH) as a function of D-Fructose-1,6-bisphosphate (D-F16BP) concentration; reaction conditions: 1.5 mM DHAP, 0.5 mM NADH, [0 - 200 mM] D-F16BP, 0.77 µg/mL *sn*-G3PDH in 50 mM TEA buffer, pH 8, and 25°C

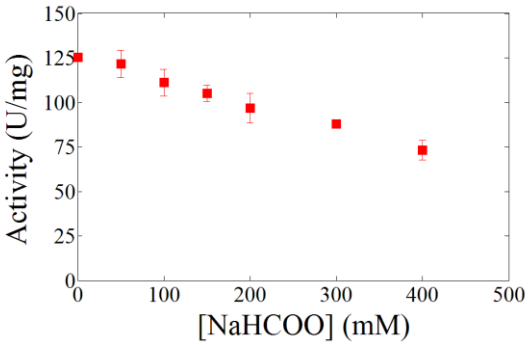

Figure 7.16: Activity of *sn*-glycerol-3-phosphate dehydrogenase (*sn*-G3PDH) as a function of sodium formate (NaHCOO) concentration; reaction conditions: 1.5 mM DHAP, 0.5 mM NADH, [0 - 400 mM] NaHCOO, 0.77 µg/mL *sn*-G3PDH in 50 mM TEA buffer, pH 8, and 25°C

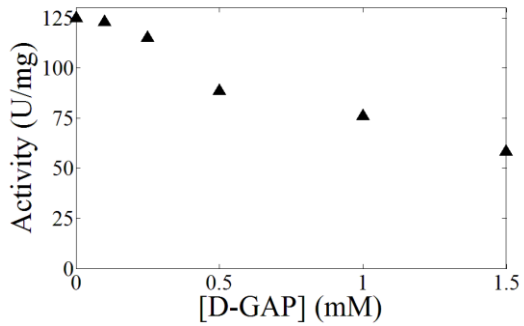

Figure 7.17: Activity of *sn*-glycerol-3-phosphate dehydrogenase (*sn*-G3PDH) as a function of D-glyceraldehyde-3-phosphate (D-GAP) concentration; reaction conditions: 1.5 mM DHAP, 0.5 mM NADH, [0 - 1.5 mM] D-GAP, 0.77 µg/mL *sn*-G3PDH in 50 mM TEA buffer, pH 8, and 25°C

As shown in Figure 7.18 and Figure 7.19 the activity of RAMA shows not affected by NaHCOO and sn-glycerol-1(3)-phosphate. Figure 7.20 shows that the native product D-GAP suppresses the activity of RAMA. In the activity assay of RAMA as a function of NaHCOO concentration, 2.25-fold excess amount of sn-G3PDH than the amount required to maintain RAMA to *sn*-G3PDH ratio so that RAMA catalyzed aldol cleavage of D-F16BP rate limiting was loaded in order to offset the inhibition of *sn*-G3PDH by NaHCOO.

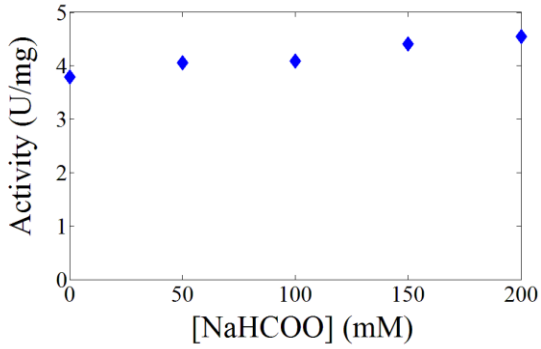

Figure 7.18: Activity of rabbit muscle aldolase (RAMA) as a function of sodium formate (NaHCOO) concentration; reaction conditions: 0.5 mM D-F16BP, 0.5 mM NADH, [0 - 200 mM] NaHCOO, 0.015 mg/mL RAMA, 0.09 mg/mL *sn*-G3PDH in 50 mM TEA buffer, pH 8, and 25°C

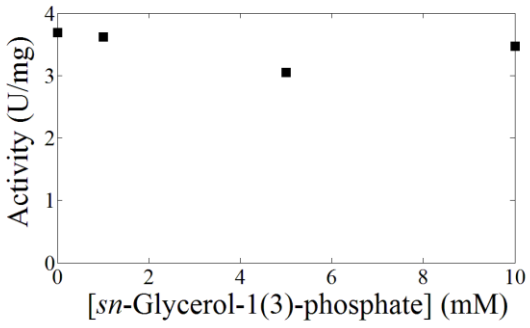

Figure 7.19: Activity of rabbit muscle aldolase (RAMA) as a function of *sn*-glycerol-1(3)-phosphate concentration; reaction conditions: 0.5 mM D-F16BP, 0.5 mM NADH, [0 mM 10 mM] *sn*-glycerol-1(3)-phosphate, 0.03 mg/mL RAMA, 0.18 mg/mL *sn*-G3PDH in 50 mM TEA buffer, pH 8, and 25°C

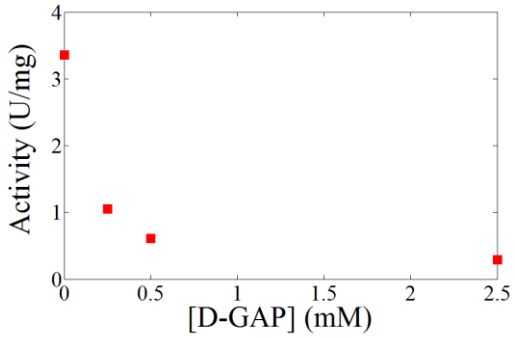

Figure 7.20: Activity of rabbit muscle aldolase (RAMA) as a function of D-glyceraldehyde-3-phosphate (D-GAP) concentration; reaction conditions: 0.5 mM D-F16BP, 0.5 mM NADH, [0 - 2.5 mM] D-GAP, 0.017 mg/mL RAMA, 0.06 mg/mL *sn*-G3PDH in 50 mM TEA buffer, pH 8, and 25°C

Table 7.2 shows activities of enzymes involved in the reaction sequence with respect to co-substances. The dependence of the enzyme activities on the concentrations of their native substrates and products was analyzed as well and taken into account in the development of reaction kinetics models.

Table 7.2: The influence of cosubstances present in the reaction mixture on the activity of rabbit muscle aldolase (RAMA), *sn*-glycerol-3-phosphate dehydrogenase (*sn*-G3PDH) and formate dehydrogenase (FDH) involved in the reaction sequence

Co-substance	**RAMA**	***sn*-G3PDH**	**FDH**
D-F16BP	Native	×	×
D-GAP	Native	✓	×
sn-G3P	×	Native	×
NaHCOO	×	✓	Native

✓ Indicates the cosubstance suppresses the enzyme activity

× Indicates the cosubstance does not influence the enzyme activity

The designed cascade reaction consists of three enzymes arranged in two reversible consecutive reactions and the last one coupled with the third irreversible cofactor regeneration (as shown in Figure 7.1). For the development of the overall reaction kinetics model, this simplifies the entire reaction sequence to a single substrate irreversible enzymatic reaction type. The kinetics behavior of each of the enzymes with respect to their native substrate and product must be known in order to choose the appropriate enzyme and substrate concentrations as well as enzyme

ratios. Identification and determination relevant kinetics parameters for all the three enzymes were therefore performed. Figure 7.21 and Figure 7.23 show the non-linear activity response of FDH as a function of NAD^+ and NaHCOO concentration, respectively. Kinetics constants were determined by rearranging the non-linear rate responses into a linear form using double reciprocal linearization method (as shown in Figure 7.22 and Figure 7.24). The effect of NADH on the kinetics of FDH was examined demonstrating that NADH competitively inhibits FDH with respect to NAD^+. The values of the kinetic parameters are shown in Table 7.3.

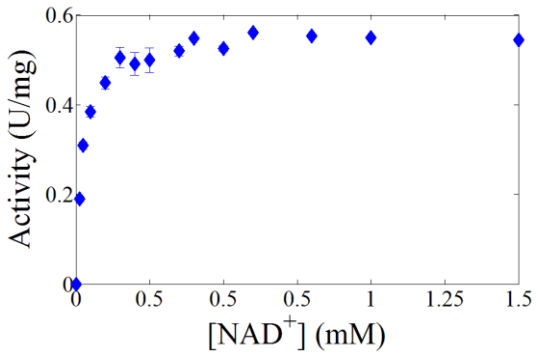

Figure 7.21: Activity of formate dehydrogenase (FDH) as a function of NAD^+ concentration; reaction conditions: 500 mM NaHCOO, 0.075 mg/mL FDH in 50 mM TEA buffer, pH 8, and 25°C

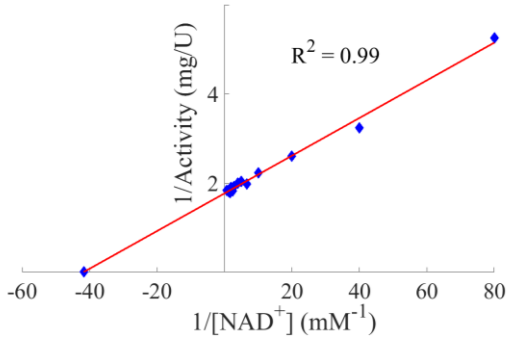

Figure 7.22: Linearization of hyperbolic activity response of FDH as a function of NAD^+ concentration using double reciprocal plot; reaction conditions: 500 mM NaHCOO, 0.075 mg/mL FDH in 50 mM TEA buffer, pH 8, and 25°C

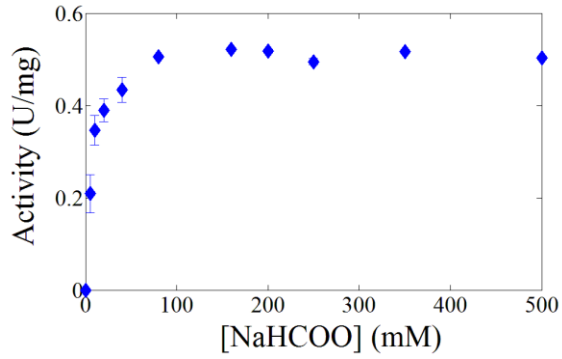

Figure 7.23: Activity of formate dehydrogenase (FDH) as a function of NaHCOO concentration; reaction conditions: 1.5 mM NAD^+, 0.075 mg/mL FDH in 50 mM TEA buffer, pH 8, and 25°C

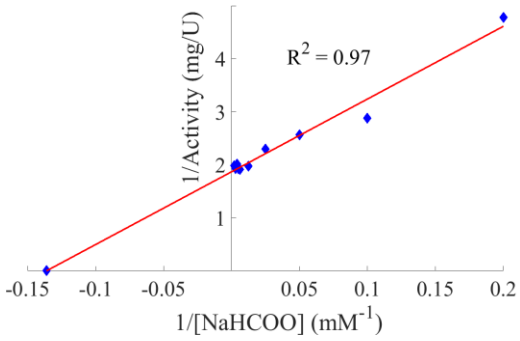

Figure 7.24: Linearization of hyperbolic activity response of FDH as a function of NaHCOO concentration using double reciprocal plot; reaction conditions1.5 mM NAD^+, 0.075 mg/mL FDH in 50 mM TEA buffer, pH 8, and 25°C

Figure 7.25 shows the activity response of RAMA as a function of D-F16BP concentration. Figure 7.26 shows the double reciprocal linear plot used to determine kinetic constants for the RAMA with respect to D-F16BP.

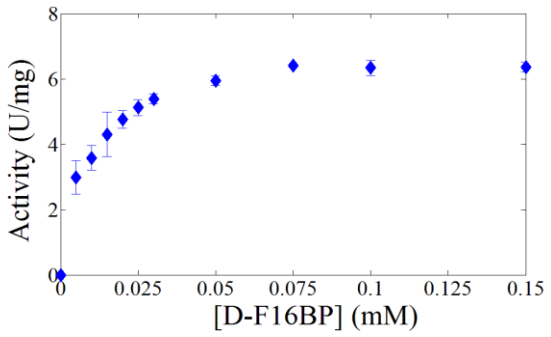

Figure 7.25: Activity of rabbit muscle aldolase (RAMA) as a function of D-fructose-1,6-bisphosphate (D-F16BP) concentration; reaction conditions: 0.5 mM NADH, 0.0043 mg/mL RAMA, 0.354 mg/mL *sn*-glycerol 3-phosphate dehydrogenase in 50 mM TEA buffer, pH 8, and 25°C

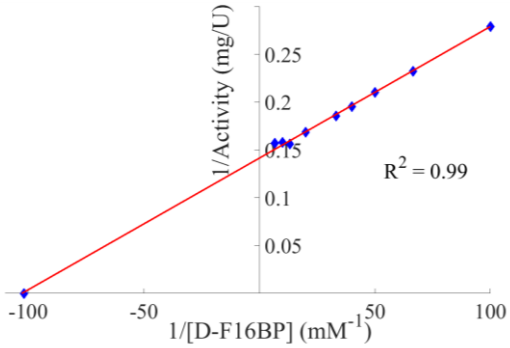

Figure 7.26: Linearization of hyperbolic activity response of RAMA as a function of D-F16BP concentration using double reciprocal plot; reaction conditions: 0.5 mM NADH, 0.0043 mg/mL RAMA, 0.354 mg/mL *sn*-glycerol 3-phosphate dehydrogenase in 50 mM TEA buffer, pH 8, and 25°C

Sets of activity measurements of RAMA as a function of D-F16BP concentration were carried out by adding different amounts of D-GAP in order to identify inhibition type and determine inhibition constants of RAMA by D-GAP. Results shown in Figure 7.27 depict that D-GAP affects both the K_m and v_{max} of RAMA with respect to D-F16BP; therefore, RAMA exhibits non-competitive inhibition by D-GAP. The competitive ($K_{ic,D\text{-}GAP}$) and un-competitive ($K_{iu,D\text{-}GAP}$) inhibition constants were determined using a secondary plot method.

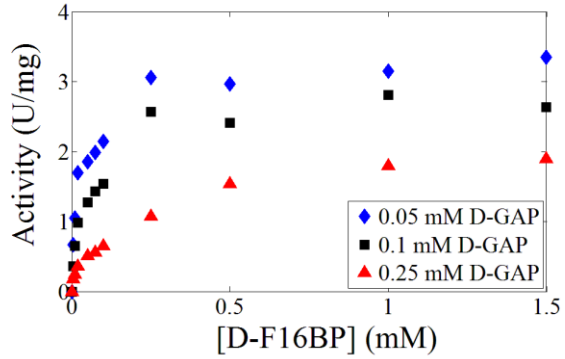

Figure 7.27: Activity of rabbit muscle aldolase (RAMA) as a function of D-fructose-1,6-bisphosphate (D-F16BP) concentration at different concentrations of D-glyceraldehyde-3-phosphate (D-GAP); reaction conditions: 0.5 mM NADH, [0 - 1.5 mM] D-F16BP, [0.05 mM 0.1 mM 0.25 mM] D-GAP, 0.0043 mg/mL RAMA, 0.354 mg/mL *sn*-glycerol-3-phosphate dehydrogenase in 50 mM TEA buffer, pH 8, and 25°C

The effect of DHAP on the activity of RAMA was not considered in kinetic examination of RAMA catalyzed aldol cleavage of D-F16BP, as it is *in-situ* reduced to *sn*-glycerol-3-phosphate. Table 7.3 shows the kinetics properties and magnitudes of the kinetics constants for RAMA, FDH and *sn*-G3PDH with respect to their native substrates and products.

Table 7.3: Kinetics properties and the magnitudes of kinetic constants for rabbit muscle aldolase (RAMA), formate dehydrogenase (FDH) and *sn*-glycerol-3-phosphate dehydrogenase (*sn*-G3PDH)

Kinetics parameters	**RAMA**	**FDH**	***sn*-G3PDH**
$K_{m,D\text{-}F16BP}$ (mM)	0.0065 ± 0.002	_____	_____
$K_{ic,D\text{-}GAP}$ (mM)	0.11	_____	_____
$K_{iu,D\text{-}GAP}$ (mM)	0.40	_____	_____
v_{max} (U/mg)	6.80 ± 0.2	_____	_____
$K_{m,HCOO^-}$ (mM)	_____	6.08 ± 2.2	_____
K_{m,NAD^+} (mM)	_____	0.02 ± 0.001	_____
$K_{ic,NADH}$ (mM)	_____	0.04 ± 0.01	_____
v_{max} (U/mg)	_____	0.55 ± 0.005	_____
$K_{m,DHAP}$ (mM)	0.049 [190]	_____	0.28
$K_{m,NADH}$ (mM)	_____	_____	0.0081 [191]
v_{max} (U/mg)	_____	_____	123

The smaller competitive inhibition constant ($K_{ic,D\text{-}GAP}$) compared to the un-competitive inhibition constant ($K_{iu,D\text{-}GAP}$) suggests that D-F16BP and D-GAP impede each other in binding with the active site of RAMA. Reaction kinetics models shown in Eqn(7.1) and Eqn(7.2) were developed for FDH catalyzed reduction of NAD^+ and RAMA catalyzed aldol cleavage of D-F16BP, respectively. The kinetics models were validated by simulating the time course conversions of several batch reactions at different starting substrate and enzyme concentrations.

Evaluations of the experimental data and the numerically simulated data matrices show for the models of FDH and RAMA 98.8% and 98.5% 2-D correlation, respectively. Figure 7.28 shows the comparison between experimental and simulated conversions versus reaction time for both models.

$$v_3 = v_{\max} \times \frac{[NAD^+]}{K_{\mathrm{m},NAD^+} \times \left(1 + \frac{[\mathrm{NADH}]}{K_{\mathrm{ic,NADH}}}\right) + [NAD^+]} \times \frac{[HCOO^-]}{K_{\mathrm{m},HCOO^-} + [HCOO^-]} \qquad \text{Eqn(7.1)}$$

$$v_4 = v_{\max} \times \frac{[\mathrm{D-F16BP}]}{K_{\mathrm{m,D-F16BP}} \times \left(1 + \frac{[\mathrm{D-GAP}]}{K_{\mathrm{ic,D-GAP}}}\right) + [\mathrm{D-F16BP}] \times \left(1 + \frac{[\mathrm{D-GAP}]}{K_{\mathrm{iu,D-GAP}}}\right)} \qquad \text{Eqn(7.2)}$$

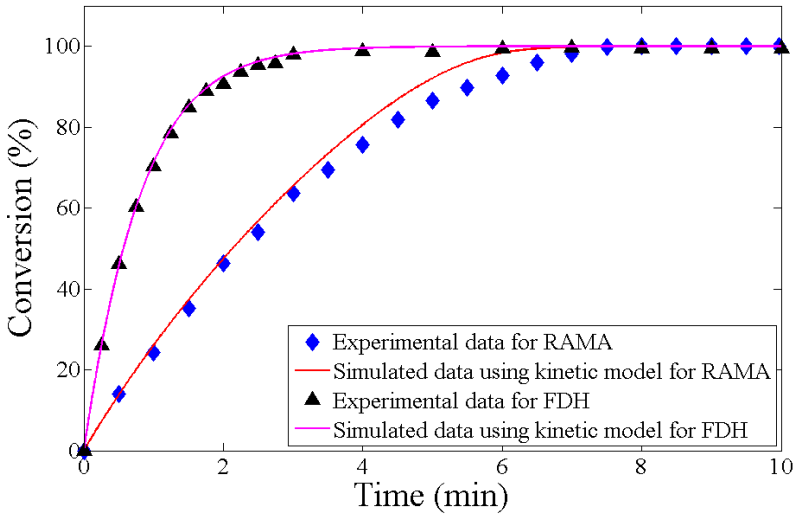

Figure 7.28: Comparison fitness of experimental data and numerically simulated data using the kinetics models for batch reactions of RAMA catalyzed aldol cleavage of D-F16BP and FDH catalyzed reduction of NAD^+; reaction conditions: 0.1 mM D-F16BP, 0.5 mM NADH, 0.0046 mg/mL RAMA, 0.044 mg/mL *sn*-G3PDH in 50 mM TEA buffer, pH 8, and 25°C for RAMA catalyzed aldol cleavage of D-F16BP and 0.0125 mM NAD^+, 500 mM NaHCOO, 0.075 mg/mL FDH in 50 mM TEA buffer, pH 8, and 25°C for FDH catalyzed reduction of NAD^+

7.3.3. Overall Reaction Kinetics Model

The overall model for the reaction kinetics can be developed by fixing one of the reaction steps as rate limiting. The rate limiting step can be adjusted using the knowledge of the kinetics behavior of each of the enzymes and choosing an appropriate enzyme ratio. In the case of the designed reaction sequence the RAMA catalyzed aldol cleavage of D-F16BP was set to be the rate limiting step for the purpose of simplification and to avoid the accumulation of D-GAP in the reaction solution. It is thus essential to maintain the *sn*-G3PDH catalyzed reduction of DHAP

at a larger rate than the RAMA catalyzed aldol cleavage of D-F16BP in order to suppress the reverse aldol condensation reaction and to prevent the effect of DHAP on the activity of RAMA. Additionally, the FDH catalyzed NADH regeneration must be adjusted to a larger rate than the *sn*-G3PDH catalyzed reduction of DHAP so that *sn*-G3PDH activity is not affected by NADH shortage. Therefore, the overall reaction kinetic is simplified to a *uni-uni* irreversible enzymatic reaction and can be defined using the reaction kinetics model developed for RAMA shown in Eqn(7.2).

7.4. Process Development and Evaluation

The performance of different reactor modes of operation for the synthesis of D-GAP was evaluated by combining the developed reaction kinetics model, mass balances of reactors and kinetics of the non-enzymatic decay of D-GAP. Eqn(7.3) and Eqn(7.4) show differential equations for the simulation of D-F16BP and D-GAP concentrations for batch-wise mode of operation, respectively. Eqn(7.5) and Eqn(7.6) show steady state differential equations for simulation of D-F16BP and D-GAP concentrations for a continuous mode of operation, respectively. $[D-F16BP]_0$ and $[D-F16BP]$ represent influx and efflux concentrations in CSTR respectively. $[D-GAP]_0$ and $[D-GAP]$ represent influx concentrations, which are negligible, and efflux, respectively. Eqn(7.4) and Eqn(7.6) include the kinetics of D-GAP decay at the reaction conditions assuming the unit of reaction time and residence time in hour.

$$\frac{\partial[D-F16BP]}{\partial t} = [RAMA](-v_4) \qquad \text{Eqn(7.3)}$$

$$\frac{\partial[D-GAP]}{\partial t} = [RAMA](v_4) \times \mathrm{e}^{-0.083\mathrm{t}} \qquad \text{Eqn(7.4)}$$

$$\frac{\partial[D-F16BP]}{\partial t} = \frac{([D-F16BP]o-[D-F16BP])}{\tau} - [RAMA]v_4 \qquad \text{Eqn(7.5)}$$

$$\frac{\partial[D-GAP]}{\partial t} = \left(\frac{([D-GAP]o-[D-GAP])}{\tau} + [RAMA]v_4\right) \times \mathrm{e}^{-0.083\tau} \qquad \text{Eqn(7.6)}$$

The performance of different reactor mode of operation was evaluated using the parameters conversion, selectivity and STY. Figure 7.29 shows a comparison of the batch-wise operation in a STR and the continuous operation in a CSTR based on conversion. Conversion is defined as the number of D-F16BP molecules transformed per starting D-F16BP molecules. Larger conversion in a short time can be achieved via STR, e.g. in order to achieve a comparable

conversion of 95% in the same reaction time for STR and residence time for CSTR, the CSTR requires a 20-fold larger amount of RAMA than the STR. Moreover, for the designed one-pot reaction sequence the requirement of 20-fold larger amount of RAMA means the requirement of nearly 20-fold larger amounts of *sn*-G3PDH and FDH.

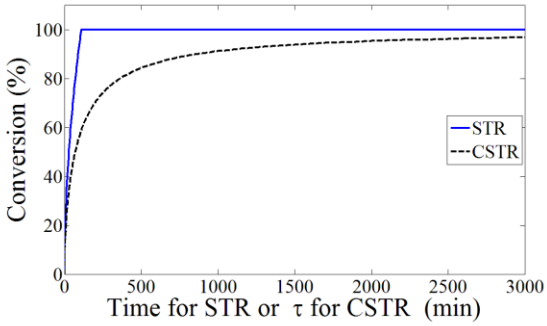

Figure 7.29: Comparison of stirred tank reactor (STR) and continuously operated stirred reactor (CSTR) based on conversion as a function of reaction time for STR or residence time for CSTR for the synthesis of D-GAP; simulation conditions. 5 mM D-F16BP, 0.5 mM NADH, 50 mM NaHCOO, 0.15 mg/mL RAMA, 1.43 mg/mL *sn*-G3PDH, 3.7 mg/mL FDH in 50 mM TEA buffer, pH 8, and 25°C

Selectivity is defined as the number of D-GAP molecules synthesized per number of D-F16BP molecules converted. As shown in Figure 7.30, STR shows a better selectivity performance as a function of conversion than CSTR. For the synthesis of D-GAP, selectivity is a critical parameter due to the exponential decay of D-GAP with time at pH 8. The selectivity performance of the reactors was evaluated as a function of conversion using the same amount of enzymes.

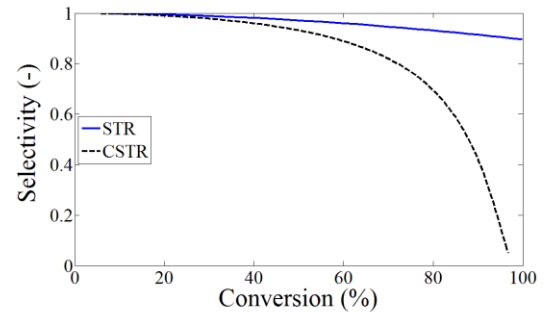

Figure 7.30: Comparison of stirred tank reactor (STR) and continuously operated stirred reactor (CSTR) based on selectivity as a function conversion for the synthesis of D-GAP, simulation conditions 5 mM D-F16BP, 0.5 mM NADH, 50 mM NaHCOO, 0.15 mg/mL RAMA, 1.43 mg/mL *sn*-G3PDH, 3.7 mg/mL FDH in 50 mM TEA buffer, pH 8, and 25°C

The inhibition of RAMA by D-GAP leads in the case of the CSTR to a low steady-state reaction rate. Using conditions given in Figure 7.29 and Figure 7.30 at the conversion of 95% the STY in the CSTR drops to 0.08 $gL^{-1}day^{-1}$ due to in selectivity difference. Thus, the most convenient reactor type for the one-pot cascade enzymatic synthesis of D-GAP is the STR, due to the gradual increase of product with reaction time.

7.5. Separation Method Development

The separation of the two final products of the one-pot reaction sequence, D-GAP and *sn*-glycerol-3-phosphate, has been achieved by using a TLC plate coated with the strong anion exchanger polyethylenimine (PEI)-cellulose. The developing solvent and pH were optimized considering the stability of D-GAP. A solution of 1 M KCl dissolved in 100 mM HCl, pH 2, was selected for high separation ability and stability of D-GAP. An excellent separation of D-GAP (R_f of 0.2) and *sn*-glycerol-3-phosphate (R_f of 0.9) has been achieved. The chromatogram shown in Figure 7.31 displays the separation of D-GAP and *sn*-glycerol-3-phosphate as well as the list of reagents that were analyzed in the TLC measurement according to their index # given in the TLC chromatogram.

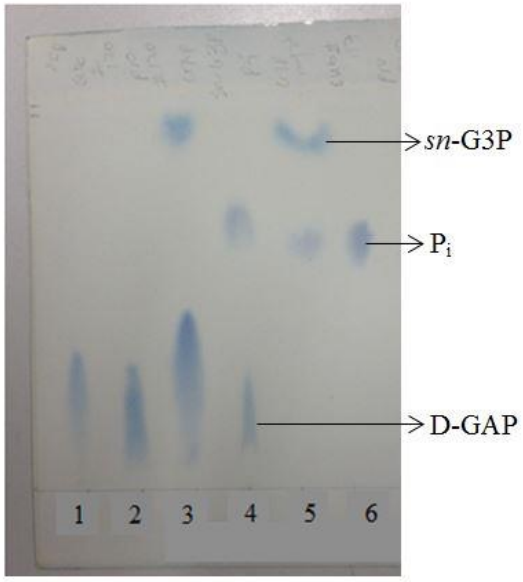

Figure 7.31: Separation of D-glyceraldehyde-3-phosphate (D-GAP) and *sn*-glycerol-3-phosphate (*sn*-G3P) by using PEI-cellulose coated anion exchange TLC plate and 1 M KCl in 100 mM HCl, pH 2, as a developing solvent; index #1 = ADP, index #2 = ATP, index #3 = a mixture of enzymatically synthesized *sn*-glycerol-3-phosphate and coproduct ADP, index #4 = D-GAP, index #5 = commercial *sn*-glycerol-3-phosphate and index #6 = inorganic orthophosphate (P_i)

7.6. Interim Summary

A one-pot enzymatic reaction sequence has been designed for preparing D-GAP. The reaction sequence shows a significant improvement of the RAMA catalyzed aldol cleavage of D-F16BP yielding 100% conversion of D-F16BP. Detailed characterization of the enzymatic reaction

sequence was performed. Considering the stability and activity of RAMA, *sn*-G3PDH and FDH as a function of pH at 25°C as well as stability of NADH and NAD^+ for the designed one-pot reaction sequence pH 8 appears as an optimum pH value. The kinetics of D-GAP decay at the reaction conditions of 50 mM TEA buffer pH 8 and 25°C can be defined by first order kinetics with a rate constant of 2.3×10^{-5} $s^{-1}$and a half-life of 8.35 h.

Each of the three enzymes involved in the reaction sequence was investigated in respect to kinetics in order to choose the appropriate enzyme and substrate concentrations as well as enzyme ratios. For the kinetics model development to the entire reaction sequence, the RAMA catalyzed aldol cleavage of D-F16BP was set to be the rate-limiting step for the purpose of simplification and to avoid the accumulation of D-GAP in the reaction solution. RAMA is non-competitively inhibited by D-GAP. The magnitudes of competitive and un-competitive inhibition constants suggest that D-F16BP and D-GAP impede each other for binding with the active site of RAMA. The developed reaction kinetics models for RAMA and FDH were validated by simulating the time course of several batch reactions. Validation results for FDH and RAMA kinetics models show 98.8% and 98.5% 2-D correlation between experimental data and the numerically simulated data matrices, respectively.

The performance of different reactor modes of operation for the designed one-pot enzymatic reaction sequence was evaluated by combining the developed reaction kinetics model, mass balances of reactors and kinetics of the non-enzymatic decomposition of D-GAP. Batchwise operation in a STR is the most convenient process for the one-pot enzymatic syntheses of D-GAP. Alternative to STR, continuous operation using packed bed reactor (PBR) can be applied due to the gradual increase of the inhibitory product across the length of the reactor. However, in this study, homogenous soluble enzymes were used and a strategy to use three immobilized enzymes often shows low efficiency due to mass transport limitations. The separation of D-GAP and the coproduct, *sn*-glycerol-3-phosphate, has been achieved using polyethylenimine (PEI)-cellulose coated TLC plate. The separation solvent and pH were optimized by considering D-GAP stability that a solution of 1 M KCl dissolved in 100 mM HCl pH 2 was selected for high separation ability and stability of D-GAP.

8. *In situ* ATP Regeneration

Few *in situ* ATP regeneration systems have been described. All of them utilize higher energy phosphoryl donors than ATP like phosphoenolpyruvate and acetyl phosphate [22, 41, 57–59, 192]. Most routinely pyruvate kinase catalyzed phosphorylation of ADP using phosphoenolpyruvate as a phosphoryl donor has been applied to regenerate ATP [41, 60, 192]. The stability of phosphoenolpyruvate in aqueous solution (half-life at pH 7.5 and 25°C of ~10^3 h) makes this system more attractive than others [59]; however, limited by the cost of phosphoenolpyruvate [266 €/g Sigma-Aldrich price catalog 2015] relative to the cost of ATP [6.52 €/g Sigma-Aldrich price catalog 2015]. The bulk scale chemical costs were considered for the purpose of comparison. The other commonly used ATP regeneration system is the use of acetyl phosphate as a phosphoryl donor catalyzed by acetate kinase [22, 57–59, 192]. This system is also limited by factors including the cost of acetyl phosphate [67.8 €/g Sigma-Aldrich price catalog 2015], inhibition of acetate kinase by acetate [22, 193], the instability of acetate kinase (half-life at pH 8.5 and 37°C of 90 min) [58] and acetyl phosphate (half-life at pH 7.5 and 25°C of 21 h) [59]. The applications of methoxycarbonyl phosphate and acetate kinase for ATP regeneration has been described [22, 59, 192]; however, very short life time of methoxycarbonyl phosphate (half-life at pH 7.5, 25°C of 0.3 h) [59]. The cost and stability of coenzymes as well as cosubstrates are critical factors as they determine the ttn of ATP regeneration. The ttn is defined as the number of moles of product formed per moles of ATP added for a complete course of reaction.

In most ATP dependent phosphorylation reactions, the main motivation of ATP regeneration is the cost of ATP; therefore, it is desirable to develop a system that utilizes a cheaper phosphoryl donor than ATP. Promising is the use of polyphosphate kinase (PPK) mediated regeneration of ATP using PP_in as a phosphoryl donor. Additionally, the high stability of PP_in makes the system attractive for synthetic applications [61, 62]. The utilization of PP_in as a co-substrate to regenerate ATP from AMP has been mentioned in a coupled system of PP_in-AMP phosphotransferase (PAP)/PPK [61, 62]. Purification and characterization of PPK have been described from microbial sources such as *E. coli* [62–66] and *Pseudomonas aeruginosa* [194].

8.1. Polyphosphate Kinase

8.1.1. Generating Expression Clones

Purified DNA samples from *Acinetobacter* sp. ADP1, *Mycobacterium smegmatis* str., *Neisseria flavescens* SK114 and *Vibrio cholerae O1 biovar El Tor* str. encoding PPK cloned in an entry vector of pDONRzeo were received from DSM ChemTech R&D Innovative Synthesis (Urmonderbaan 22, Geleen Netherlands). These clones were recombined with a destination vector of pDEST^{TM}14 using Gateway$^{®}$ LR clonase$^{®}$II enzyme mix and protocol in order to generate expression clones [195]. The cloned genes were transformed into competent *E. coli* DH5α^{TM} by heat shock for the purpose of selection and propagation of the expression clones. Positive clones were selected on LB medium containing 100 µg/mL ampicillin, as the wildtype *E. coli* DH5α^{TM} lacks this phenotype. Moreover, positive transformants were analyzed by restriction enzyme digestion. The restriction enzyme cut the plasmid once within the desired gene and once outside of it. This means that a successful clone should be cut into two pieces while an empty vector is cut only once that remains as a single DNA strand. With the chosen restriction enzyme, the plasmid for *Neisseria flavescens* SK114 should be cut into two fragments of about 450 and 5100 base pairs in length, while the plasmid for *Acinetobacter* sp. ADP1, *Mycobacterium smegmatis* str. and *Vibrio cholerae O1 biovar El Tor* str. should each be cut into two fragments of about 450 and 5500 base pairs in length. Figure 8.1 shows the agarose gel electrophoresis picture that demonstrates the success of the transformation.

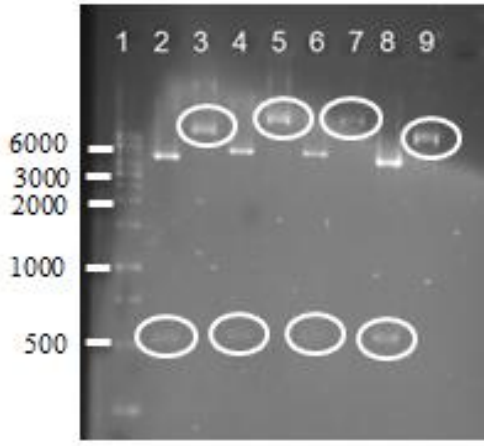

Figure 8.1: Photo of agarose gel electrophoresis results of restriction analysis; #1 = 1 kb DNA ladder, #2 = reaction of *Mycobacterium smegmatis* str., #3 = Blank of #2, #4 = reaction of *Acinetobacter* sp. ADP1, #5 = Blank of #4, #6 = Reaction of *Vibrio cholera O1 biovar El Tor* str., #7 = Blank of #6, #8 = reaction of *Neisseria flavescens* SK114 #9 = Blank of #8, Reaction samples are with the addition of restriction enzyme while blanks are samples undigested without the addition of restriction enzymes

8.1.2. Transformation and Protein Expression

Purified plasmid DNAs from positive clones were separately transformed into *E. coli* BL21 for protein expression. The success of plasmid transformation was confirmed by the growth of *E. coli* BL21 on ampicillin containing medium (as shown in appendix B, Figure B.16). Two sets of fermentations for the 4 clones were carried out overnight at room temperature and expression of the recombinant PPK were induced at the exponential growth phase (as shown in appendix B Figure B.17) using 0.5% L-arabinose for one set and 0.2 mM IPTG for the other. SDS-PAGE analysis results shown in Figure 8.2 depict that a distinct thick band between 35 to 55 kDa can be seen for the expression induced by 0.2 mM IPTG. Moreover, the formation of small amounts of this protein can also be seen for the expression induced by 0.5% L-arabinose. Furthermore, the fermentation of *E. coli* BL21 was carried out using a similar protocol except the addition of ampicillin in order to check the background activity of *E. coli* BL21 cell free extract (CFE).

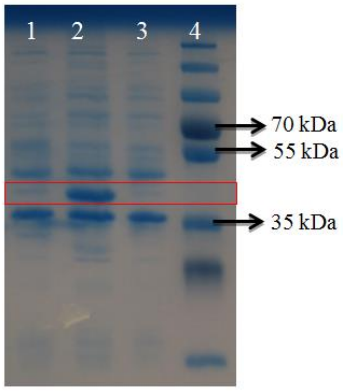

Figure 8.2: SDS-PAGE analysis of CFE for over-expression of PPK from *Neisseria flavescens* SK114 induced using; 1: 0.5% L-arabinose and 2: 0.2 mM IPTG, 3: *E. coli* BL21control and 4: protein ladder

8.1.3. Activity and Characteristics of Polyphosphate Kinase Cell Free Extracts

The two-step reaction sequence shown in Figure 8.3 was used for the activity assay of PPK crude CFE. The phosphorylation of ADP by PP_in catalyzed by PPK CFE should yield ATP in order for the phosphorylation of glycerol catalyzed by glycerol kinase from *Cellulomonas* sp. The activity was monitored by measuring the consumption of glycerol via HPLC.

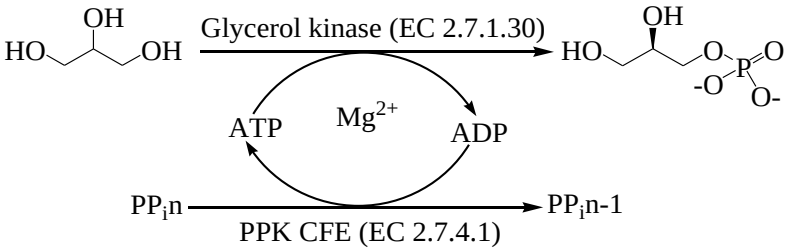

Figure 8.3: Reaction sequence used for the activity assay of polyphosphate kinase (PPK) crude cell free extract (CFE)

The activities of PPK CFE from *Acinetobacter* sp. ADP1, *Mycobacterium smegmatis* str., *Neisseria flavescens* SK114 and *Vibrio cholerae O1 biovar El Tor* str. gene clones were assayed. However, only activity results of PPK CFE from *Mycobacterium smegmatis* str. gene clone are presented as there was no activity pattern difference among all. Moreover, as shown in Table 8.1, the activity of the CFE was assayed by missing one of the reaction components at a time. Table 8.1 shows activity results of PPK CFE from *Mycobacterium smegmatis* str. gene clone.

Table 8.1: Activity of PPK crude cell free extract (CFE) from *Mycobacterium smegmatis* str. gene clone; reactions were carried out in 100 mM Tris-HCl buffer pH 8 and 30°C

Reactor #	**[Glycerol] (mM)**	**[ADP] (mM)**	**[PP_in] (mM)**	**[CFE] (v/v)**	**[Glycerol kinase] (mg/mL)**	**[Mg^{2+}] (mM)**	**Activity (U/ g of wet cell pellets)**
1	20	20	20	50%	0.07	40	4.77 ± 0.33
2	20	20	20	25%	0.07	40	3.00 ± 0.25
3	20	0	20	50%	0.07	40	0.43 ± 0.05
4	20	20	0	50%	0.07	40	2.00 ± 0.2
5	20	20	20	50%	0	40	0.94 ± 0.05
6	20	20	20	50%	0.07	0	0
7	20	0	0	50%	0.07	40	0
8	20	0	0	50%	0	40	0
9	20	0	0	50%	0	0	0

Results tabulated in Table 8.1 depict the PPK CFE dependent phosphorylation of glycerol. The detected small activities without the addition of glycerol kinase and ADP may be explained due to the endogenous glycerol kinase and ATP as well as ADP of the expression host *E. coli*. BL21.

Moreover, similar reactions were monitored by TLC and UV in order to confirm, if the depletion of glycerol ascribes to the formation of *sn*-glycerol-3-phosphate. Results of the TLC analysis using the procedure described in sub-chapter 7.5 indeed confirmed the formation of *sn*-glycerol-3-phosophate. For the purpose of online reaction monitoring by UV, a reaction sequence shown in Figure 8.4 was applied. In the reaction sequence, PPK catalyzes the first reaction step that would enable the other two consecutive reactions to take place and ultimately the formation of NADH was monitored online by UV spectrophotometer at 340 nm. Figure 8.5 shows the activity results monitored by UV that confirm the phosphorylation of glycerol to *sn*-glycerol-3-phosphate.

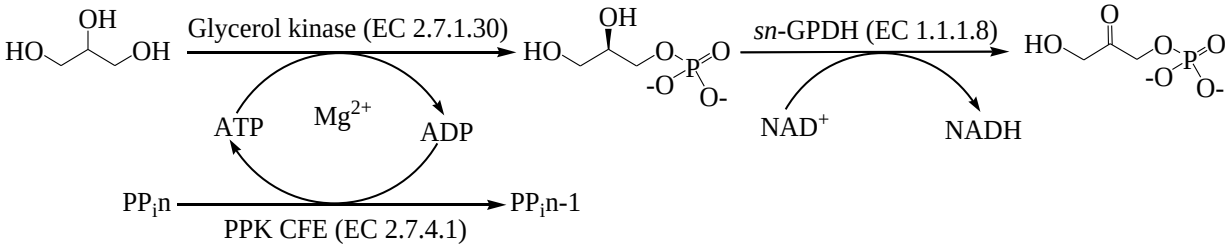

Figure 8.4: Reaction sequence for monitoring the polyphosphate kinase (PPK) CFE activity online via UV spectrophotometer at 340 nm, *sn*-G3PDH = *sn*-glycerol-3-phosphate dehydrogenase (EC 1.1.1.8)

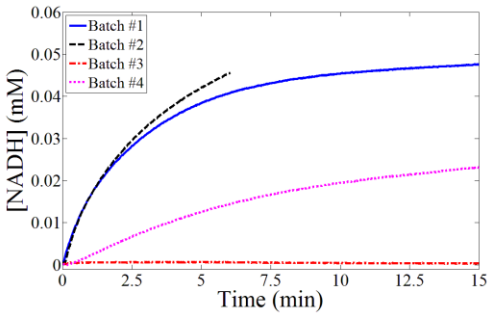

Figure 8.5: UV activity assay of PPK crude cell free extract (CFE) from *Mycobacterium smegmatis* str. gene clone; reaction conditions: Batch #1: 2 mM glycerol, 2 mM ADP, 2 mM PP_i6, 4 mM Mg^{2+}, 0.07 mg/mL glycerol kinase from *Cellulomonas* sp., 0.08 mg/mL *sn*-glycerol-3-phosphate dehydrogenase, 4%, v/v, PPK CFE; Batch #2: contains all components of Batch #1 except PP_i6; Batch #3: contains all components of Batch #1 except Mg^{2+}; Batch #4: contains all components of Batch #1 except glycerol kinase in 100 mM Tris-HCl buffer, pH 8, and 30°C

8.1.4. **Utilization of ADP as Phosphoryl Donor and Acceptor by PPK**

PPK CFE mediated phosphorylation of glycerol using ADP as a substrate was investigated in order to confirm the utility of ADP as a phosphoryl donor as well as acceptor. Figure 8.6 and Figure 8.7 show the reaction scheme and the PPK CFE activity as a function of ADP concentration, respectively.

Figure 8.6: Reaction scheme illustrating the utilization of ADP as a phosphoryl donor as well as acceptor for the PPK CFE mediated phosphorylation of glycerol; Gk = glycerol kinase

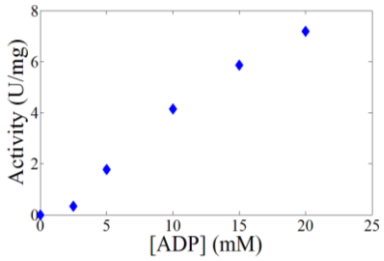

Figure 8.7: Activity of polyphosphate kinase (PPK) CFE from *Mycobacterium smegmatis* str. gene clone as a function of ADP concentration; reaction conditions: 20 mM glycerol, 40 mM Mg^{2+}, 0.07 mg/mL glycerol kinase from *Cellulomonas* sp. 50%, v/v, PPK CFE in 100 mM Tris-HCl buffer, pH 8, and 30°C

Not only the enzyme activity but also the final conversion depends on the concentration of ADP. Figure 8.8 shows reaction progress data of batch reactions at different starting ADP concentrations. Figure 8.9 shows reaction progress data of batch reactions with the addition of PP_in that depict PP_in enhances both the rate and final conversion of the reactions. The effect of pyrophosphate (PP_i) on the rate as well as final conversion of the similar reaction using ADP as a substrate was investigated and results (shown in appendix B Figure B.18) describe that PP_i does not influence the reaction rate nor the equilibrium conversion.

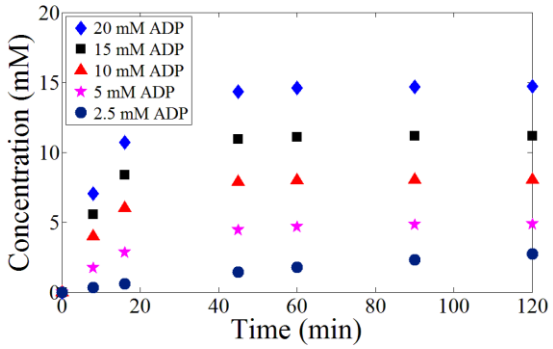

Figure 8.8: Increasing of final conversion of PPK CFE from *Mycobacterium smegmatis* str. gene clone mediated phosphorylation of glycerol by ADP with increasing starting ADP concentration; reaction conditions: 20 mM glycerol, 40 mM Mg^{2+}, 0.07 mg/mL glycerol kinase from *Cellulomonas* sp., 50% v/v PPK CFE in 100 mM Tris-HCl buffer, pH 8, and 30°C

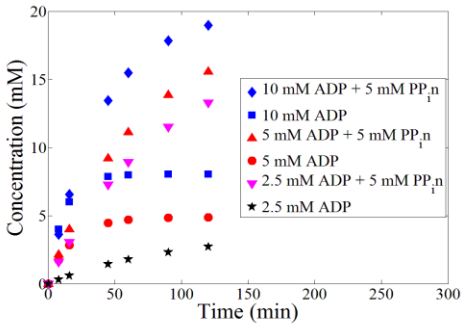

Figure 8.9: Effect of PP_in on reaction rate and final conversion of PPK CFE from *Mycobacterium smegmatis* str. gene clone mediated phosphorylation of glycerol by ADP; reaction conditions: 20 mM glycerol, 40 mM Mg^{2+}, 0.07 mg/mL, glycerol kinase from *Cellulomonas* sp. 50% v/v PPK CFE in 100 mM Tris-HCl buffer, pH 8, and 30°C

8.2. Interim Summary

Positive expression clones of PPK genes were generated and transformed into *E. coli* BL21 for a successful expression of PPK. SDS-PAGE analyses results showed the distinct thick band for expression induced by 0.2 mM IPTG as well as the formation of small amount PPK for expression induced by 0.5% L-arabinose. Results demonstrated that PPK CFE utilizes both ADP and PP_in as substrate for the phosphorylation of glycerol. Reactions monitored by UV and TLC confirmed the PPK/PP_in or ADP mediated phosphorylation of glycerol yielding *sn*-glycerol-3-phosphate.

Moreover, in order to check the background activity of endogenous enzymes of *E. coli* BL21, fermentation of wild type *E. coli* BL21 was carried out using the same conditions without the addition of ampicillin. Result of PPK activity assays showed that statistical significant activity was detected when CFE of *E. coli* BL21 without any of the PPK clones was used. Thus, the background activity obtained by using CFE of *E. coli* BL21 needs to be further investigated. Furthermore, issues such as purification and detailed characterization of PPK must be performed for practical scale application of PPK mediated *in situ* ATP regeneration.

9. Overall Discussion and Outlook

9.1. Overall Discussion

Detailed results concerning to the enzymatic syntheses of *sn*-glycerol-3-phosphate, L-GAP and D-GAP have been presented as well as discussed in chapters 4, 5 and 7, respectively. The ^{31}P and ^{1}H NMR results of Mg-ATP complex formation and kinetics as well as mechanistic explanation of glycerol kinase activity profile as a function of Mg^{2+} to ATP molar ratio have been discussed in chapter 6. Moreover, the feasibility and preliminary results of *in situ* ATP regeneration mediated by PPK utilizing PP_in as a phosphoryl donor have been discussed in chapter 8. The aim of this chapter is to provide overall discussion of results as well as future perspectives and remarks.

sn-Glycerol-3-phosphate has been described to be useful in various pharmaceutical, nutrition and synthetic applications. Glycerol kinase catalyzed asymmetric phosphorylation of glycerol utilizing ATP as a phosphoryl donor has been applied to synthesize *sn*-glycerol-3-phosphate. Even though this reaction system has been described as reversible [129–136], reaction thermodynamic properties analysis has proven that the reaction is practically irreversible. Enzyme screening and selection of optimum reaction conditions are crucial for bioprocess development. The influences of several factors including oxygen sensitivity, pH, buffer type, temperature and substrates concentration as well as the interactive effect of pH and temperature on the activity and stability of glycerol kinase from various microbial sources have been described in sub-chapter 4.2.1. Thus, the most convenient glycerol kinase from *Cellulomonas* sp. was selected among glycerol kinase *Bacillus stearothermophilus*, *E. coli* and *Streptomyces canus*.

Likewise, other most phosphotransferase/kinase, glycerol kinase requires Mg^{2+} as an essential enzyme activator. The activity of glycerol kinase depends on the Mg^{2+} to ATP molar ratio that shows maximum activity in the optimum Mg^{2+} to ATP molar ratio of [0.12 to 0.3]. Increasing the Mg^{2+} to ATP molar ratio larger than the 0.3 suppresses the enzyme activity to a final non-zero asymptotic value. Mg^{2+} binds ATP yielding complexes of different chemical and physical features depending on the Mg^{2+} to ATP molar ratio. The ^{31}P resonance signals of ATP by the addition of Mg^{2+} indicate all α-, β- and γ-phosphate groups involve in Mg-ATP complex

formation. The CH_2-protons of ribose sugar moiety of ATP become nearly NMR equivalent after reaching the Mg^{2+} to ATP molar ratio of 0.3. This may happen when the phosphate chain residue of ATP folded back to the purine ring and intersects the H-C-H moiety. Kinetics investigation and mechanistic elucidation using the ^{31}P and ^{1}H NMR data reveal that glycerol kinase exhibits high affinity (low K_m) and less activity (low k_{cat}) for complexes with a stoichiometric configuration or more saturated by Mg^{2+} such as Mg_2ATP. On the other hand, the enzyme shows less affinity (high K_m) and high activity (high k_{cat}) for unsaturated complexes such as $[Mg(ATP)_2]^{-6}$. Michaelis-Menten double substrate type including competitive enzyme inhibition by ADP kinetics model has been developed. Experimental and numerically simulated data matrices at different starting substrate concentrations using 10.5 mM Mg^{2+} and 21 mM Mg^{2+} show 2-D correlation of 96.8% and 98.8%, respectively. Simulation and performance evaluation of different reactor types lead to select STR as the most convenient reactor type for the synthesis of *sn*-glycerol-3-phosphate.

Enantiopure L-GAP is useful in various natural biological and synthetic processes. A process utilizing glycerol kinase from *Cellulomonas* sp. catalyzed phosphorylation of L-glyceraldehyde by ATP has been applied for the synthesis of L-GAP. The activity of glycerol kinase from *Cellulomonas* sp. depends on the Mg^{2+} to ATP molar ratio that shows maximum activity at the optimum ratio of 0.7. The reason that glycerol kinase from *Cellulomonas* sp. shows a different optimum Mg^{2+} to ATP molar ratio in the case of using glycerol or L-glyceraldehyde as a substrate may be due to unsymmetrical conformational modification of the enzyme upon binding these substrates. Therefore, it exhibits different catalytic properties upon binding glycerol or L-glyceraldehyde. Establishing a 23.7-fold higher Mg^{2+} to ATP molar ratio in contrast to the optimum Mg^{2+} to ATP molar ratio showed that a high concentration of Mg^{2+} does not affect the equilibrium conversion. However, the enzyme activity is suppressed by a factor of 22 relative to its activity at the optimum Mg^{2+} to ATP molar ratio.

Glycerol kinase from *Cellulomonas* sp. exhibits inhibition by ADP, AMP, methylglyoxal and Ca^{2+} but not by L-GAP and P_i. Equal concentration of Ca^{2+} exerts different percentage of inhibition on the enzyme at different Mg^{2+} to ATP molar ratio. This is due to mass action on the complexation equilibrium between Ca-ATP and Mg-ATP complexes. Equal concentration of Ca^{2+} generates different amounts of enzymatically inactive Ca-ATP complexes at different Mg^{2+}

to ATP molar ratio. An appropriate reaction kinetics model has been develop and validation of the model shows 2-D correlation of 99.9% between experimental and numerical data matrices. Based on reaction engineering parameters such as conversion, selectivity, STY and SP different reactor types were numerical and experimental evaluated. STR is therefore the most suitable reactor type for the synthesis of L-GAP, whereby the biocatalyst consumption significantly reduced from 19.7 g kg^{-1} to 1.7 g kg^{-1} by means of reaction engineering.

The utilization of expensive ATP as a phosphoryl donor for glycerol kinase based syntheses of *sn*-glycerol-3-phosphate and L-GAP reflects as one of factors on their price 227 €/g and 11.23 €/mg (Sigma-Aldrich price catalog 2016), respectively. The *in situ* ATP regeneration using a cheap high energy phosphoryl donor such as PP_in catalyzed by PPK is therefore an attractive system. In order to study reaction systems compatibility, the effect of cosubstrate (i.e PP_in) concentration on the activity of glycerol kinase was investigated. The glycerol kinase activity as a function of PP_in concentration depends on the Mg^{2+} to ATP molar ratio in the reaction mixture. If the Mg^{2+} to ATP molar ratio is less than the optimum molar ratio value, PP_in suppresses the glycerol kinase activity otherwise activates the enzyme. However, the enhancement of glycerol kinase activity is only true until the excess amount of Mg^{2+} than the amount required to establish optimum Mg^{2+} to ATP molar ratio is fully titrated by PP_in.

D-GAP is useful in various natural biological and synthetic applications as of its enantiomer. A one-pot enzymatic reaction sequence has been designed for the synthesis of D-GAP. The reaction sequence consists of D-fructose-1,6-bisphosphate aldolase from rabbit muscle (RAMA), *sn*-glycerol-3-phosphate dehydrogenase (*sn*-G3PDH) from rabbit muscle and formate dehydrogenase from *Candida boidinii* (FDH). The optimum pH 8 was selected considering stability and activity of RAMA, *sn*-G3PDH and FDH as well as the reciprocal stability relationship of NADH and NAD^+. The kinetics of RAMA catalyzed aldol cleavage of D-F16BP has been used to define the kinetics of the entire reaction sequence by setting RAMA catalyzed aldol cleavage of D-F16BP as the rate limiting step. RAMA exhibits non-competitive inhibition by D-GAP. The magnitudes of K_{ic} and K_{iu} suggest that D-F16BP and D-GAP impede each other for binding with the active site of RAMA. Validation of the kinetics model shows 98.5% 2-D correlation between experimental data and numerically simulated data matrices. The performance of STR and CSTR was evaluated by combining the reaction kinetics model, mass

balances of the individual reactors and the kinetics of non-enzymatic decomposition of D-GAP. Batchwise operation in a STR is the most convenient process for the one-pot enzymatic synthesis of D-GAP. The separation of the two final products of the one-pot reaction sequence, D-GAP and *sn*-glycerol-3-phosphate, has been achieved by using a TLC plate coated with the strong anion exchanger polyethylenimine (PEI)-cellulose. The separation solvent and pH were optimized by considering D-GAP stability and separation ability. A solution of 1 M KCl dissolved in 100 mM HCl, pH 2, was selected for high separation ability and stability of D-GAP.

9.2. Outlook and Remarks

The ^{31}P and ^{1}H NMR data of Mg-ATP complex formation at different Mg^{2+} to ATP molar ratio have given insights to explain the kinetics and mechanistic characteristics of glycerol kinase as a function of Mg^{2+} to ATP molar ratio. Detailed structural analysis of Mg-ATP complex is however required in order to identify the unequivocal Mg-ATP complex physical and chemical configurations as well as their composition at different Mg^{2+} to ATP molar ratio.

Developing a robust and economically attractive *in situ* ATP regeneration method is indispensable. The attempt to develop practical scale PPK mediated *in situ* ATP regeneration utilizing a cheap PP_in is in the early stage. Few basic remarks and outlooks concerning this reaction system are therefore listed below:

- In order to check the background activity of endogenous enzymes of *E. coli* BL21, fermentation of *E. coli* BL21 was carried out. Significant but quantitatively less activity than the activity of PPK CFE from *Mycobacterium smegmatis* str. gene clone was detected in the activity assay using CFE of *E. coli* BL21.
- It is therefore required to further investigate on the background activity obtained by using the CFE of *E. coli* BL21
- Purification and characterization of PPK including substrate spectrum (e.g. ttn of ATP regeneration with respect to the number of phosphoryl moieties in the phosphate chains of PP_in), activity of PPK as a function of concentrations of PP_in, ADP, Mg^{2+} as well as their ratio and, moreover, investigation of the kinetic behavior of PPK should be performed

Upscaling the TLC separation methodology developed to separate *sn*-glycerol-3-phosphate and D-GAP to preparative column chromatography scale is hindered by a current commercial none availability of the polyethylenimine (PEI)-cellulose material. This limitation also extends to the upscaling of the one-pot enzymatic reaction sequence designed to synthesize D-GAP. Therefore, preparing the polyethylenimine (PEI)-cellulose material is indispensable in order to overcome this limitation. Moreover, after scaleup is achieved; analysis and evaluation can be performed with the focus to synthesize *sn*-glycerol-3-phospahte either by the one-pot enzymatic reaction sequence designed to synthesize D-GAP or glycerol kinase catalyzed asymmetric phosphorylation of glycerol.

10. Summary

The aim of this chapter is to summarize milestone results achieved in this thesis discussed in each of the chapters.

- Reaction thermodynamic properties analysis for glycerol kinase catalyzed asymmetric phosphorylation of glycerol utilizing ATP, as a phosphoryl donor, has shown that the reaction is practically irreversible. Glycerol kinase requires Mg^{2+} as an essential enzyme activator.
- The activity of glycerol kinase depends on the Mg^{2+} to ATP molar ratio that shows maximum activity in the optimum Mg^{2+} to ATP molar ratio of [0.12 to 0.3] for the synthesis of *sn*-glycerol-3-phosphate. Increasing the Mg^{2+} to ATP molar ratio larger than the 0.3 suppresses the enzyme activity to a non-zero asymptotic value.
- The results of ^{31}P resonance signals of ATP by the addition of Mg^{2+} indicate all α-, β- and γ-phosphate groups involve in Mg-ATP complex formation. The results of ^{1}H resonance signals of ATP reveal that the CH_2-protons of ribose sugar moiety of ATP become nearly NMR equivalent after reaching a Mg^{2+} to ATP molar ratio of 0.3.
- Glycerol kinase exhibits Michaelis-Menten kinetics with respect to glycerol and ATP; however, with respect to ATP if only maintaining constant Mg^{2+} to ATP molar ratio. Glycerol kinase exhibits two-step kinetics behavior as a function of ATP concentration when assayed at a fixed Mg^{2+} concentration.
- Glycerol kinase exhibits high affinity (low K_m) and less activity (low k_{cat}) for complexes with a stoichiometric configuration or more saturated by Mg^{2+} such as Mg_2ATP. On the other hand, the enzyme shows less affinity (high K_m) and high activity (high k_{cat}) for unsaturated complexes such as $[Mg(ATP)_2]^{-6}$.
- The product, *sn*-glycerol-3-phoshate, synthesized using this process has been commercialized by the project partner, Sigma-Aldrich, referred with catalogue number (*G7886 SIGMA*) and 227 €/g (Sigma-Aldrich price catalog 2016).
- Glycerol kinase catalyzes kinetic resolution of DL-glyceraldehyde exhibits 100% selectivity towards to L-glyceraldehyde. However, the enzyme shows D-glyceraldehyde induced catalytic activity to the hydrolysis of ATP yielding ADP and P_i. The enzyme requires nearly a 10-fold stoichiometric excess of ATP with respect to L-glyceraldehyde

in DL-glyceraldehyde in order to achieve a full conversion of L-glyceraldehyde when DL-glyceraldehyde is used as a starting material.

- The product L-GAP demonstrates a half-life of 6.86 h under reaction conditions. The rate of DL-GAP depletion in 100 mM TEA buffer, pH 8, and at different temperatures of 25°C, 30°C and 60°C shows respective rate constants of 2.3×10^{-5} s^{-1}, 2.8×10^{-5} s^{-1} and 1.2×10^{-3} s^{-1}. Due to aldehyde condensation Tris-HCl buffer stabilizes DL-GAP.
- The enzyme shows Michaelis-Menten kinetics behavior with respect to L-glyceraldehyde and ATP. Moreover, it exhibits pseudo-ATP surplus inhibition if the Mg^{2+} to ATP ratio is less than 0.7.
- Glycerol kinase from *Cellulomonas* sp. exhibits inhibition by ADP, AMP, methylglyoxal and Ca^{2+} but not by L-GAP and P_i. Equal concentration of Ca^{2+} exerts different percentage of inhibition on the enzyme at different Mg^{2+} to ATP molar ratio.
- The effect of PP_in concentration on the activity of glycerol kinase depends on the Mg^{2+} to ATP molar ratio in the reaction mixture.
- The product, L-GAP, synthesized using this process has been commercialized by the project partner, Sigma-Aldrich, referred with catalogue number (*69312 SIGMA*) and 11.23 €/mg (Sigma-Aldrich price catalog 2016).
- Results of ADP phosphorylation indicate that PPK CFEs utilize both ADP and PP_in as phosphoryl donors for the *in situ* regeneration of ATP from ADP that ultimately used to phosphorylate glycerol.
- A one-pot enzymatic reaction sequence has been designed for the synthesis of D-GAP. The reaction sequence significantly improves the aldol cleavage of D-F16BP catalyzed by RAMA and yields 100% conversion of D-F16BP by overcoming thermodynamic limitation.
- RAMA exhibits non-competitive inhibition by D-GAP and the magnitudes of competitive and un-competitive inhibition constants suggest that D-F16BP and D-GAP impede each other for binding with the active site of RAMA.
- The separation of D-GAP and the coproduct *sn*-glycerol-3-phosphate has been achieved using polyethylenimine (PEI)-cellulose TLC.

A. Materials and Methods

A.1. Materials

Chemicals

Adenosine-5'-triphosphate (ATP) disodium salt, adenosine-5'-diphosphate (ADP) sodium salt, Adenosine-5'-monophosphate (AMP) disodium salt, ammonium molybdate, anthranilic acid, ascorbic acid, glycerol, calcium *sn*-glycerol-1(3)-phosphate, trichloroacetic acid (TCA), ammonium acetate, sodium hexametaphosphate (PP_i6), D-fructose-1,6-bisphosphate (D-F16BP), D-glyceraldehyde-3-phosphate (D-GAP), *sn*-glycerol-3-phosphate bis(cyclohexylammonium) salt, reduced form of β-nicotinamide adenine dinucleotide (NADH) disodium salt, oxidized form of β-nicotinamide adenine dinucleotide (NAD^+) disodium salt, DL-Glyceraldehyde, dithiothreitol (DTT), D-glyceraldehyde, L-glyceraldehyde, DL-glyceraldehyde-3-phosphate (DL-GAP), dihydroxyacetone (DHA), methylglyoxal, sodium formate, ampicillin, L-arabinose, isopropyl β-D-1-thiogalactopyranoside (IPTG), SOC medium, glycerol kinase from *Bacillus stearothermophilus*, glycerol kinase from *Cellulomonas* sp., glycerol kinase from *E. coli*, glycerol kinase from *Streptomyces canus*, *sn*-glycerol-3-phosphate dehydrogenase (*sn*-G3PDH) from rabbit muscle, fructose-1,6-bisphosphate aldolase from rabbit muscle (RAMA) and formate dehydrogenase from *Candida boidinii* (FDH) were purchased from Sigma-Aldrich (Buchs, Switzerland). Calcium chloride, magnesium chloride hexahydrate, phosphoric acid, potassium dihydrogen phosphate, sulfuric acid, tris(hydroxymethyl)aminomethane (Tris), triethanolamine (TEA), nitric acid (65%), potassium chloride, hydrochloric acid, methanol, LB medium and acetonitrile (HPLC-gradient grade) were purchased from Carl Roth GmbH (Karlsruhe, Germany). Deuterated water (D_2O) was purchased from Deutero (Kastellaun, Germany). Purified DNA strands from *Acinetobacter* sp. ADP1, *Mycobacterium smegmatis* str., *Neisseria flavescens* SK114 and *Vibrio cholerae O1 biovar El Tor* str. cloned in pDONRzeo entry vector were received from DSM ChemTech R&D (Geleen, Netherlands). SimplyBlue SafeStain, Gateway® LR clonase® II enzyme mix kit, proteinase K solution, TE buffer pH 8 (10 mM Tris-HCl, pH8, 1 mM EDTA), competent DH5α and BL21 *E. coli*, PageRuler^{TM} Plus pertained protein ladder 10 to 250 kDa, Hind III, "Red" buffer, 1kb DNA ladder were purchased from ThermoFisher Life Technologies (Carlsbad, USA). NucleoSpin® plasmid isolation kit, buffers A1, A2, A3, A4, AW, AE were purchased from Macherey-Nagel (Düren, Germany). Mini-

PROTEAN®TGX™ precast polyacrylamide gels, Biozym LE GP agarose, 1x Laemmli buffer and 1x TAE buffer were purchased from Bio-Rad Laboratories (München, Germany). LE GP agarose was purchased from Biozym Scientific (Oldendorf, Germany). All chemicals and solvents were analytical reagent grade and used without further purification.

Equipment

Equipment used in this thesis among other various commonly used labWare are listed as follows:

Agilent 1100 HPLC	Agilent Technologies, Waldbronn, Germany
Eurokat-H columns 300 mm × 8 mm	Knauer, Berlin, Germany
Nucleodur® HILIC column 250 mm × 4 mm	Macherey-Nagel, Düren, Germany
UviokoXL UV spectrophotometer	Bio-Tek Instruments, Bad Friedrichshall, Germany
Bruker AVANCE I 400 (400 MHz for 1H and 162 MHz for 31P	Bruker, Rheinstetten, Germany
Centrifuge 5415 D	Eppendorf AG., Hamburg, Germany
Thermos-mixer	Biometra, Göttingen, Germany
Balance Sartorius CP224S	Sartorius, Göttingen, Germany
pH-Meter	Carl Roth, Karlsruhe, Germany
Reaction vessels	Glasbläserei Brunswieg, Hamburg, Germany
Magnetic stirrer	IKA Werke, Staufen, Germany
E100 Ecoline Star Edition 003 thermostat	Lauda, Hamburg, Germany
Vortex MS2 Minishaker	IKA Werke, Staufen, Germany
Pharmacia LKB SuperFrac fraction collector	Pharmacia, Uppsala, Sweden

Pharmacia LKB HPLC pump	Pharmacia, Uppsala, Sweden
Stainless-steel enzyme membrane reactor (10 mL) and ultrafiltration membrane (cut-off, 30 kDa)	Millipore, Schwallbach, Germany
Polyethylenimine (PEI) cellulose strong anion exchange TLC plate	Merck KGaA, Darmstadt, Germany
Ultrasonic control unit Sonoplus HD 2200	Bandelin electronic, Berlin, Germany
SDS pellets	Carl Roth, Karlsruhe, Germany
NucleoSpin® plasmid (NoLid) column	Macherey-Nagel, Düren, Germany

Software

Matlab®2014b (MathWorks, Inc., Massachusetts, United States), eQuilibrator$^{2.0}$ [138] and MestReNova (Masterlab Research, Santiago de Compostela, Spain)

A.2. Methods

A.2.1. Synthesis of *sn*-Glycerol-3-Phosphate

The concentration of glycerol was analyzed by HPLC (Agilent 1100, Hewlett Packard) on a Eurokat-H columns (300 mm × 8 mm, Knauer) with 5 mM H_2SO_4 as eluent at a flow rate of 0.5 mL/min and 75°C, using a refractive index detector at 35°C. Typical retention time of glycerol was 17.56 min (shown in Figure B.1). All reactions which were analyzed by measuring the concentrations of glycerol were quenched by the addition of 10% (w/v) TCA stop reagent at a ratio of 1:1 (sample: stop reagent, v/v), followed by vigorous mixing. The concentrations of ATP, ADP and AMP were analyzed by HPLC (Agilent 1100, Hewlett Packard) on a Nucleodur® HILIC column (250 mm × 4 mm, Macherey-Nagel) with acetonitrile: 100 mM ammonium acetate in aqueous solution (70:30, v/v), pH 5.3, as eluent at a flow rate of 0.8 mL/min and 25°C, using a diode array detector (DAD) at 259 nm. Typical retention times for

AMP, ADP and ATP were 6.2 ± 0.1 min, 9 ± 0.1 min and 13 ± 0.3 min, respectively (shown in Figure B.7). All reactions which were analyzed by measuring the concentrations of ATP, ADP and AMP, were quenched by the addition of 111 mM phosphate solution, pH 1.8, stop reagent at a ratio of 1:1 (sample: stop buffer, v/v), followed by vigorous mixing that generated a final HPLC sample of pH 3. In the addition of the stop buffer, it was important to maintain the final pH of HPLC samples between 2.5 and 3.5, because ATP and APD are unstable at pH below 2 while at pH above 4 glycerol kinase retains its activity. The reaction kinetics of glycerol kinase with respect to glycerol was monitored by UviokoXL UV spectrophotometer at 340 nm measuring the formation of NADH.

A substrate solution of 50 mM ATP, 50 mM glycerol, 100 mM Mg^{2+} was prepared in 100 mM Tris-HCl buffer pH 8.5 and 25°C for the activity assays of glycerol kinases from *Bacillus stearothermophilus, Cellulomonas* sp., *E. coli* and *Streptomyces canus.* Reactions were started by the addition of pre-heated enzyme stock solutions prepared in 100 mM Tris-HCl buffer, pH 8.5, and 25°C. Substrate solutions containing 50 mM ATP, 50 mM glycerol, 100 mM Mg^{2+} were prepared in 200 mM Tris-HCl and TEA buffer for the purpose of reaction medium selection. Reactions were started by the addition of 0.24 mg/mL glycerol kinase from *Cellulomonas sp.* and 0.36 mg/mL glycerol kinase from *Streptomyces canus* at pH 8.5 and 30°C.

A substrate solution containing 50 mM ATP, 50 mM glycerol, 100 mM Mg^{2+} was prepared in 100 mM Tris-HCl buffer for the activity assay of glycerol kinases from *Cellulomonas* sp., *E. coli* and *Streptomyces canus* as a function of pH and temperature. Reactions were started by the additions of 0.046 mg/mL glycerol kinase from *Cellulomonas* sp. 0.0453mg/mL glycerol kinase from *E. coli* and 0.0453mg/mL glycerol kinase from *Streptomyces canus* into substrate solution pre-incubated at the required pH and temperature. The operational stabilities of the glycerol kinases from *Cellulomonas* sp., *E. coli* and *Streptomyces canus* were examined by incubation in 100 mM Tris-HCl buffer containing 100 mM ATP or 100 mM glycerol, and 100 mM Mg^{2+}, at pH 7.5, 8.5 and 9.5 and 25°C, 30°C and 45°C. Residual activities of the incubated enzymes were assayed every day for a month by applying the conditions used for the activity assays.

The reaction Gibbs free energy ($\Delta_r G$) and reaction equilibrium constant (K_{eq}) for the asymmetric phosphorylation of glycerol by ATP were computed using eQuilibrator$^{2.0}$ as a function of pH and ionic strength. Calculation conditions of 10 mM ATP, 10 mM glycerol, 1 nM ADP, 1 nM

sn-glycerol-3-phosphate at 25°C were employed as well as ionic strength of 0.1 M while varying pH and pH 8.5 while varying ionic strength. A reaction was performed using substrate solution containing 50 mM ATP, 50 mM glycerol, 10.5 mM Mg^{2+} and started by adding 0.06 mg/mL glycerol kinase from *Cellulomonas* sp. in 100 mM Tris-HCl buffer, pH 8.5, and 30°C in order to check the practical equilibrium conversion of the reaction.

Substrate solutions containing 50 mM ATP, 50 mM glycerol, 10 mM Mg^{2+}, 0 mM or 5 mM or 10 mM NAD^+ were prepared in 100 mM Tris-HCl buffer, pH 8.5, and 25°C in order to examine the activity of glycerol kinase from *Cellulomonas* sp as a function of NAD^+ concentration. The reactions were started by the addition of enzyme stock solution establishing 0.06 mg/mL enzyme in the reaction mixture. Once no effect of NAD^+ on the activity of glycerol kinase was demonstrated substrate solutions containing 30 mM ATP, 6 mM Mg^{2+}, 10 mM NAD^+ various amounts of glycerol were prepared in 100 mM Tris-HCl pH 8.5 in order to assay kinetics of glycerol kinase with respect to glycerol. The reactions were started by the addition of 0.1 µg/mL glycerol kinase from *Cellulomonas* sp. and 7 U/mL *sn*-glycerol-3-phosphate dehydrogenase at 25°C and online monitored by UV spectrophotometer at 340 nm. The inhibition of glycerol kinase from *Cellulomonas* sp. by *sn*-glycerol-1(3)-phosphate was assayed using the calcium salt of *sn*-glycerol-1(3)-phosphate by performing reactions at 50 mM ATP, 50 mM glycerol, 10.5 mM Mg^{2+} prepared in Tris-HCl buffer, pH 8.5. All reactions were started by the addition of 0.06 mg/mL glycerol kinase from *Cellulomonas* sp. at 30°C. Applying similar conditions, other set of reactions were performed using $CaCl_2$ instead of calcium salt of *sn*-glycerol-1(3)-phosphate in order to examine the effect of the counter cation (Ca^{2+}) on the enzyme activity.

Substrate solutions containing 50 mM glycerol and 5mM or 50 mM or 70 mM ATP were prepared in 100 mM Tris-HCl pH 8.5 in order to assay the activity of glycerol kinase from *Cellulomonas* sp. as a function of Mg^{2+} to ATP ratio. The reactions were started by adding different stock solutions of glycerol kinase from *Cellulomonas* sp. prepared in 100 mM Tris-HCl, pH 8.5, at 25°C. Moreover, other sets of reactions using similar substrates concentrations were performed in 100 mM Tris-HCl, pH 7.5, and in 100 mM TEA, pH 8, at 30°C in order to examine the effect of reaction buffer type and pH on the activity profile of glycerol kinase as a function of Mg^{2+} to ATP molar ratio. For the kinetics characterization of glycerol kinase with respect to ATP, initial rate measurements as a function of ATP concentrations were performed in

two approaches: 1) by varying ATP concentration while maintaining constant Mg^{2+} to ATP molar ratio of 0.3 and 2) fixing constant Mg^{2+} concentration. Substrate solutions containing 50 mM glycerol, [0 - 35 mM] ATP and [0 - 10.5 mM] Mg^{2+} were prepared in 100 mM Tris-HCl, pH 8.5. Reactions were started by the addition of glycerol kinase from *Cellulomonas* sp. at 30°C for the initial rate measurements maintaining constant Mg^{2+} to ATP molar ratio 0.3. Another sets of initial rate measurements as a function of ATP concentration were performed at 1.5 mM, 10.5 mM and 21 mM Mg^{2+} in order to characterize the kinetics of glycerol kinase with respect to ATP at a fixed Mg^{2+} concentration. For the purpose of mechanistic elucidation of glycerol kinase inhibition by ADP, the enzyme activity was assayed as a function of ADP concentration at different Mg^{2+} to ATP molar ratio. Substrate solutions containing 50 mM ATP, 50 mM glycerol, [3.5 mM or 6 mM, or 15 mM, or 50 mM] Mg^{2} and various amounts of ADP were prepared in 100 mM Tris-HCl buffer, pH 8.5. Reactions were started by the addition of glycerol kinase from *Cellulomonas* sp. at 30°C. Linear representations of Michaelis-Menten enzyme kinetics equation were applied in order to determine reaction kinetic constants.

The effect of sodium hexametaphosphate (PP_i6) concentration on the activity of glycerol kinase from *Cellulomonas* sp. was investigated by performing reactions at different Mg^{2+} to ATP molar ratio of 0.1, 0.3 and 2. Substrate solutions containing 50 mM glycerol, 50 mM ATP, 5 mM or 15 mM or 100 mM Mg^{+2} were prepare in 100 mM Tris-HCl buffer, pH 8.5. All reactions were started by the addition of 0.08 mg/mL glycerol kinase from *Cellulomonas* sp. at 30°C.

A.2.2. Synthesis of L-Glyceraldehyde-3-Phosphate

The concentrations of DL-glyceraldehyde, D-glyceraldehyde, L-glyceraldehyde, DHA and DL-GAP were analyzed by HPLC (Agilent 1100, Hewlett Packard) on a Eurokat-H column (300 mm × 8 mm, Knauer) with 5 mM H_2SO_4 as eluent at a flow rate of 0.5 mL/min and 75°C, using a refractive index detector at 35°C. Typical retention times were 15.3 ± 0.1 min for DL-GA and 9.8 ± 0.2 min for DL-GAP (shown in Figure B.3 and Figure B.5). All reactions analyzed by measuring the concentrations of DL-glyceraldehyde, D-glyceraldehyde, L-glyceraldehyde and DL-GAP were quenched by the addition of 10% (w/v) TCA stop reagent at a ratio of 1:1 (sample: stop reagent, v/v), followed by vigorous mixing. Reactions analyzed by measuring the concentrations of ATP, ADP and AMP, were quenched by the addition of 74 mM phosphate

buffer pH 1.8 stop reagent at a ratio of 1:1 (sample: stop buffer, v/v), followed by vigorous mixing that generated a final HPLC sample of pH 2.8.

For substrate screening the activity of glycerol kinase from *Cellulomonas* sp. was assayed with respect to racemic DL-GA, enantiopure D- and L-GA. Reactions for the activity assays were carried out using substrate solution of 25 mM D- or 25 mM L-GA or 25 mM DL-GA, 25 mM ATP and 30 mM Mg^{2+} prepared in 100 mM TEA buffer, pH 8, at 30°C. All reactions were started by the addition of 0.05 mL of glycerol kinase from *Cellulomonas* sp. (1.2 mg/mL) prepared in 100 mM TEA buffer, pH 8, into 1.45 mL of the substrate solutions pre-incubated at 30°C. In order to estimate the required excess amount of ATP to achieve full conversion of L-GA in DL-GA due to the side enzymatic hydrolysis of ATP in the presence of D-GA, reactions were carried out using substrate solutions of fixed 15 mM ATP and 15 mM Mg^{2+} at 3 mM, 7 mM and 15 mM of DL-GA prepared in 100 mM TEA buffer, pH 8, at 30°C. All reactions were started by using the same procedure as used for the activity assay.

The stability of DL-GAP was examined by incubating 40 mM of DL-GAP prepared in 100 mM TEA buffer, pH 8, at 30°C and 60°C. The stability of DL-GAP in different buffer media was examined by incubating 20 mM DL-GAP in 50 mM TEA buffer, pH 8, 100 mM Tris-HCl buffer, pH 8, and 100 mM PPB, pH 8, at 25°C.

To determine the optimum Mg^{2+} to ATP molar ratio, the activity of glycerol kinase from *Cellulomonas* sp. was assayed as a function of Mg^{2+} concentration, while maintaining fixed ATP concentrations. Two sets of enzyme activity assays were carried out as a function of Mg^{2+} concentrations [0 - 200 mM] at two different fixed concentrations (30 mM and70 mM) of ATP and 50 mM L-glyceraldehyde prepared in 100 mM TEA buffer, pH 8, and 30°C. All reactions were started by adding 0.05 mL of glycerol kinase from *Cellulomonas* sp. (1.2 mg/mL), prepared in 100 mM TEA buffer, pH 8, into 1.45 mL of the substrate solutions pre-incubated at 30°C. Additionally, the effect of Mg^{2+} concentration on the reaction thermodynamics was examined by performing a reaction using 30 mM L-glyceraldehyde, 30 mM ATP and 500 mM Mg^{2+}, prepared in 100 mM TEA buffer, pH 8, at 30°C. The activity of glycerol kinase from *Cellulomonas* sp. was assayed a function of Mg^{2+} to ATP molar ratio for the phosphorylation of dihydroxyacetone in order to elucidate the structural difference influence between glycerol and L-glyceraldehyde on the enzyme activity profile. For this purpose reactions containing substrate solutions of

40 mM ATP, 20 mM dihydroxyacetone, [0 - 200 mM] Mg^{2+} prepared in 100 mM TEA buffer, pH 8.5, were started by the addition of 0.05 mg/mL glycerol kinase from *Cellulomonas* sp. at 30°C.

In order to develop a reaction kinetics model, initial rate measurements as a function of concentrations of L-glyceraldehyde and ATP were carried out at a fixed 21 mM and 50 mM Mg^{2+} prepared in 100 mM TEA buffer, pH 8, at 30°C. Several sets of initial rate measurements as function of ATP concentration at fixed 50 mM L-GA, 21 mM and 50 mM Mg^{2+} and various concentrations [0 - 5 mM] of ADP were carried out in order to examine the inhibition type of glycerol kinase from *Cellulomonas* sp. by ADP and to determine the inhibition constant. Linear representations of Michaelis-Menten enzyme kinetics equation were applied in order to determine reaction kinetic parameters.

The inhibition of glycerol kinase from *Cellulomonas* sp. by AMP, methylglyoxal, DL-GAP, Ca^{2+}, PP_in and P_i was investigated by measuring enzyme activities as function of these species concentrations. Reactions were carried out using substrate solution containing 30 mM L-GA, 30 mM ATP and 21 mM Mg^{2+} prepared in 100 mM TEA buffer, pH 8, at 30°C. The enzyme activities were examined as a function of PP_in concentrations at different Mg^{2+} to ATP molar ratios in order to evaluate the effect of complexation between Mg^{2+} and PP_in. Furthermore, DSP to remove the coproduct ADP was developed by eluting the reaction solution through a packed bed activated carbon.

A.2.3. NMR Study of Mg-ATP Complexation

Samples of 20 mM $[Na_2ATP]^{2-}$ and [0 - 80 mM] Mg^{2+} were prepared in 100 mM Tris-HCl-D_2O buffer, pH 8. NMR measurements were carried out after 2 h of sample preparation in order to make sure that the complex formation reaches equilibrium though it has been described complex formation requires 1 to 2 min [142]. ^{31}P and ^{1}H NMR spectra were recorded using Bruker AVANCE I 400 (400 MHz for ^{1}H and 162 MH1 for ^{31}P) using manufacturer standard parameters (zg30 and zgpg30) at room temperature and referenced to the internal references. NMR spectral integration was performed MestReNova® (Masterlab Research) and spectral plots were generated by using Matlab®2014b.

A.2.4. The Synthesis of D-Glyceraldehyde-3-Phosphate

All activity measurements were performed using the UviokoXL UV spectrophotometer by measuring the concentration of NADH at 340 nm. A solution containing 0.5 mM D-F16BP and 0.5 mM NADH was prepared in 50 mM TEA buffer for the activity assays of RAMA as a function of pH. The reactions were started by the addition of 0.032 mg/mL *sn*-G3PDH followed by 0.012 mg/mL RAMA so that RAMA catalyzed aldol cleavage of D-F16BP is rate limiting at 25°C. A substrate solution of 0.5 mM DHAP and 0.5 mM NADH was prepared in 50 mM TEA buffer and used to assay the activity of *sn*-G3PDH as a function of pH. All reactions were started by the addition of 0.004 mg/mL *sn*-G3PDH at 25°C. For the activity assay of FDH as a function of pH, a substrate solution of 50 mM NaHCOO and 0.5 mM NAD^+ was prepared in 50 mM TEA buffer and all reactions were started by the addition of 0.5 mg/mL FDH at 25°C. Substrate solution containing 0.5 mM NAD^+ and 300 mM NaHCOO in 50 mM TEA buffer, pH 8, was used to assay the activity FHD as a function temperature and reactions were started by the addition of 0.5 mg/mL FDH. The long term operational stabilities of RAMA, *sn*-G3PDH and FDH were examined by incubating the enzymes in 50 mM TEA buffer at different pH from 5 to 9 and at 25°C. The residual activities were routinely analyzed with the assays described above for the activity measurements each of the enzymes as a function of pH.

The stability of NADH was monitored at different pH levels by incubating 0.5 mM NADH in 50 mM TEA at 25°C and routinely measuring the remaining concentration of NADH by UV at 340 nm. The stability of D-GAP was examined by incubating 20 mM of D-GAP prepared in 50 mM TEA buffer, pH 8, at 25°C. The degradation of D-GAP was monitored via HPLC.

The capability of the reaction sequence to shift the equilibrium was demonstrated by performing a batch reaction using a substrate solution of 0.1 mM D-F16BP and 0.5 mM NADH prepared in 50 mM TEA buffer, pH 8. The reaction was started by the addition of 0.044 mg/mL of *sn*-G3PDH and 0.0046 mg/mL of RAMA with the respective order. Blank control reaction contained all reaction components except RAMA was carried out. Two batch reactions using 0.25 mM and 0.5 mM D-GAP, both containing 0.5 mM NADH, were carried out for checking the selectivity of *sn*-G3PDH towards D-GAP and *sn*-glycerol-3-phosphate in 50 mM TEA buffer, pH 8, and 25°C. Reaction Gibbs free energy ($\Delta_r G$) of RAMA catalyzed aldol cleavage of D-F16BP was computed as a function of pH by eQuilibrator$^{2.0}$ employing calculation conditions

of 10 mM D-F16BP, 1 nM D-GAP, 1 nM DHAP at ionic strength of 0.1 M and 25°C. Reaction Gibbs free energy ($\Delta_r G$) of *sn*-G3DH catalyzed reduction of DHAP was computed as a function of pH by eQuilibrator$^{2.0}$ employing calculation conditions of 10 mM DHAP, 10 mM NADH, 1 nM *sn*-glycerol-3-phosphate, 1 nM NAD^+ at ionic strength of 0.1 M and 25°C

Activity assays of RAMA, *sn*-G3PDH and FDH as function of cosubstance concentrations were carried out in 50 mM TEA buffer, pH 8, and 25°C. The kinetics of FDH as a function of NAD^+ concentration was measured employing reaction conditions of 500 mM NaHCOO in 50 mM TEA buffer, pH 8, and reactions were started by the addition of 0.075 mg/mL FDH at 25°C. Reactions performed using 1.5 mM NAD^+ in 50 mM TEA buffer, pH 8, and started by the addition of 0.075 mg/mL FDH at 25°C were used to assay the kinetics of FDH with respect to NaHCOO. The kinetic of RAMA with respect to D-F16BP was investigated by performing reactions using 0.5 mM NADH in 50 mM TEA buffer, pH 8, and reactions were started by the addition of 0.354 mg/mL *sn*-G3PDH followed by 0.0043 mg/mL RAMA at 25°C. Another sets activity assays of RAMA as a function of D-F16BP were carried out at 0.05 mM, 0.1 mM and 0.25 mM D-GAP in order to examine inhibition type and determine inhibition constants. Linear representations of Michaelis-Menten enzyme kinetics equation were applied in order to determine the values of kinetics parameters.

Separation of D-GAP and *sn*-glycerol-3-phosphate by using polyethylenimine (PEI)-cellulose strong basic anion exchange TLC plate was performed using 1 M KCl dissolved in 100 mM HCl, pH 2, as a developing solvent. A staining solution containing 0.01 g/mL of ammonium molybdate, 0.01 g/mL of ascorbic acid and 0.01 g/mL of anthranilic acid was prepared in 65% nitric acid: methanol (1:9, v/v) using a method as described elsewhere [196].

A.2.5. PPK Mediated *in situ* ATP Regeneration

This section describes generic methods applied for all the purified DNA samples from *Acinetobacter* sp. ADP1, *Mycobacterium smegmatis* str., *Neisseria flavescens* SK114 and *Vibrio cholerae O1 biovar El Tor* str. cloned in pDONRzeo entry vector.

Generating expression clones: Since the genes were provided in Invitrogen Gateway® compatible entry clone, a high-throughput gateway protocol was applied for generating expression clones [195]. Among advantages of using the Gateway destination vectors is not only

their ampicillin resistance gene for selection in *E. coli* but also the presence of *ccd*B gene located at the recombination sites preventing F-negative bacteria strains from growing and can be exploited for negative selection. Therefore, every cell that grows in a medium containing the 0.1 mg/mL ampicillin, will be a successful clone, as neither bacteria containing the uncloned destination vector nor bacteria containing the entry clone will grow. About 1 ng of the entry vector containing the target gene was mixed with 1 µL of the destination vector pDEST^{TM}14 that was then filled to 8 µL by TE buffer pH 8. To this 2 µL of LR clonase® II enzyme mix was added and incubated at 25ºC for 1 h. The addition of 1 µL proteinase K solution and incubation at 37ºC for 10 min stopped the reaction. Subsequently, the LR recombination reaction mixture was used for transformation into competent *E. coli* DH5α as described below.

Transforming plasmids into *E. coli* DH5α: Transforming the plasmid into a competent *E. coli* DH5α was carried out by heat-shock. 1 µL of the LR recombination reaction mixture was added into 50 µL of *E. coli* DH5α followed by gentle mixing. The mixture was incubated on ice for 30 min. After the cells were heat-shocked at 42ºC for 30 sec, immediately transferred to ice. 450 µL of SOC medium were added into the mixture and incubated at 37ºC for 1 h. 20 µL and 100 µL of the cells were spread onto separate LB agar plates containing 100 µg/mL ampicillin. Two different volumes were chosen to guarantee at least one of the plates would yield well-spaced colonies for picking and further processing. The plates were incubated at 37ºC overnight and stored at 4ºC.

Plasmid isolation: The plasmid isolation was performed using NucleoSpin® plasmid isolation kit. In order to isolate plasmids, starter cultures were prepared by picking a colony and inoculated 10 mL LB medium containing 0.1 mg/mL ampicillin. The media were incubated overnight. About 8 mL of the culture were centrifuged for 5 min at 6000 rpm. After discarding the supernatant, the cell pellets were resuspended in 250 µL of the A1 buffer. 250 µL of the lysis buffer A2 were added and incubated for 5 min at room temperature. To this mixture 300 µL of A3 buffer was added to bind the cell debris. The mixture was centrifuged for 10 min at 13200 rpm so that the debris form a pallet and the supernatant containing the bacterial DNA was transferred to a NucleoSpin® plasmid (NoLid) column. It was centrifuged for 1 min at 13200 rpm and the permeate was discarded. In order to wash out the previously used buffers 500 µL preheated to 50ºC AW buffer were added and subsequently centrifuged for 1 min at 13200 rpm.

After the permeate was discarded 600 µL of A4 buffer were added and centrifuged for 1 min at 13200 rpm. The NucleoSpin® plasmid (NoLid) column placed on the top of 1.5 mL Eppendorf tube with subsequent addition of 50 µL of AE buffer and incubated for 1 min at room temperature to elute the plasmids. The plasmids were then stored in sterile tube at -20ºC for further restriction analysis and transforming into BL21 *E. coli*.

Analyzing transformants by restriction analysis: The success of cloning and transformation was analyzed by restriction analysis. A prechosen restriction enzyme was mixed with an appropriate buffer containing the required cofactors. For the desired gene containing pDEST^{TM}14 expression vector, Hind III buffer at 37ºC was used as a reaction medium. It cuts the strand after the first "A" at the nucleotide sequence "AAGCTT" site. Thereafter, the plasmids were added into the restriction enzyme containing buffer. As blank control samples, the same amount of plasmids were mixed with the buffer without the addition of the restriction enzyme. All the reaction samples as well as blank samples were incubated at 37ºC overnight. Subsequently, all the samples were analyzed by agarose gel electrophoresis.

Agarose gel electrophoresis: For agarose gel electrophoresis, 2% agarose gel consisting of Biozym LE GP agarose and 1x TAE buffer with 3 µL pockets was prepared. 3 µL of samples of the restriction analysis were transferred into each of the pockets of the gel. One pocket was filled with 3 µL of a 1 kb DNA ladder. In an electrophoresis chamber using 1x TAE buffer as a running buffer the gel was put under an electric tension of 100 V for 30 min. 1 mL of 1x TAE buffer containing 1 µL of sybr green DNA dye was spread onto the gel. Then the photo of the nucleotide bands on the gel was taken under black light.

PPK expression: For the expression of PPK the plasmids obtained from the plasmid isolation method were transformed into BL21 *E. coli* using the aforementioned plasmid transforming protocol. The bacteria containing the desired gene were cultivated. Two sets of starter cultures were prepared by picking a colony and inoculating in a sterile 10 mL LB medium containing 0.1 mg/mL ampicillin. The starter cultures were incubated at room temperature overnight. Using the 1% (v/v) of the starter cultures, bigger expression cultures were prepared in the same medium and concentration of antibiotic. The expression cultures were incubated at 37ºC until the OD values reach about 0.4 to 0.6. One set of the cultures were the induced by using either 0.5% L-arabinose and the other set of the cultures were induced by 0.2 mM IPTG. The induced cultures

were cultivated overnight at room temperature before cell harvesting. The expression and bacterial growth was stopped by centrifuging the cultures at 6000 rpm for 10 min. The cell pellets were washed and resuspended by the 100 mM Tris-HCl buffer, pH 8, that was used later for CFE preparation and activity assay medium. The cells were disrupted by ultra-sonication to prepare cell lysate. The disrupted cell containing solutions were centrifuged for 10 min at 6000 rpm and the cell debris were discarded. The supernatant containing the desired protein as well as other BL21 *E. coli* endogenous protein was used for activity assay. .

SDS-PAGE analysis: 500 µL of each expression cultures after 4 h of induction were collected and centrifuged for 1 min at 13200 rpm . The supernatant was discarded and the cell pellets were resuspended by 1x Laemmli buffer with subsequent heating to 95ºC for 5 min in order to destroy cells and denature the proteins. Samples were centrifuged for 1 min at 13200 rpm. 10 µL of each samples were loaded into a Mini-PROTEAN®TGX^{TM} precast polyacrylamide gel. One of the wells was filled with 10 µL of PageRuler^{TM} Plus pertained protein ladder 10 to 250 kDa. In an electrophoresis chamber using 1x SDS running buffer the gel was put under an electric tension of 200 V for about 35 min or until the colored band reached the lower mark of the precast gel. The gel was taken out of its plastic package and rinsed several times with distilled water. Subsequently, staining solution was added and the gel was incubated overnight. The solution was discarded and the gel was rinsed with distilled water until the protein bands in the gel are visible.

Activity assay: Substrate solutions containing substrates, cofactors and other enzymes required for the activity assay reaction sequences (shown in Figure 8.3, Figure 8.4 and Figure 8.6) were prepared in 100 mM Tris-HCl buffer, pH 8. Reactions were started the addition of PPK CFEs at 30°C. The utilization of ADP as a phosphoryl donor as well as acceptor for PPK CFE mediated *in situ* ATP regeneration was investigated without the addition of PP_in. The effect of ADP concentration on the reaction rate and equilibrium conversion was assayed by performing reactions using 20 mM glycerol, 40 mM Mg^{2+}, 0.07 mg/mL glycerol kinase from *Cellulomonas* sp. and [0 - 20 mM] ADP in 100 mM Tris-HCl buffer, pH 8. Reactions were started by the addition of 50% (v/v) PPK CFE at 30°C. Moreover, the reactions at different concentrations of ADP were carried out by the addition of 5 mM PP_in in order to study the effect of PP_in on the reaction rate as well as equilibrium conversion.

B. Supplementary Information

B.1. Analytical Methods and Calibration Plots

HPLC chromatograms and calibration plot for the analysis of reaction species

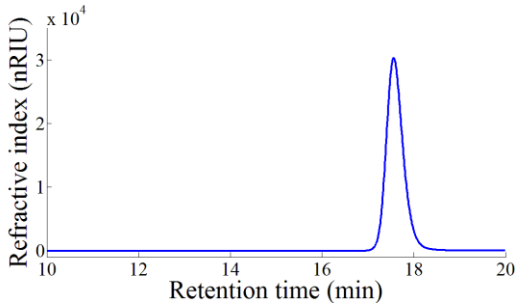

Figure B.1: Sample HPLC chromatogram for analysis of glycerol; measurement conditions are: HPLC (Agilent 1100, Hewlett Packard) using two Eurokat-H columns (300 mm × 8 mm, Knauer) connected in series with 5 mM H_2SO_4 as eluent at a flow rate of 0.5 mL/min and 75°C, using a refractive index detector at 35°C

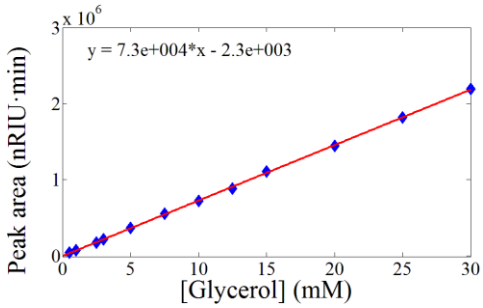

Figure B.2: HPLC calibration plot for the analysis of glycerol concentration; measurement conditions are: HPLC (Agilent 1100, Hewlett Packard) using two Eurokat-H columns (300 mm × 8 mm, Knauer) connected in series with 5 mM H_2SO_4 as eluent at a flow rate of 0.5 mL/min and 75°C, using a refractive index detector at 35°C

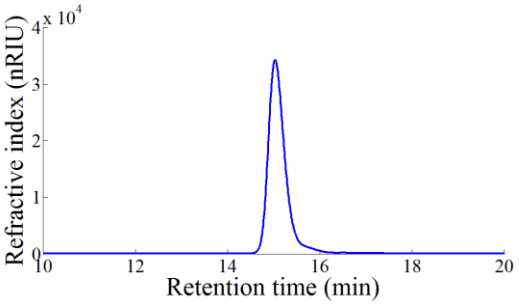

Figure B.3: Sample HPLC chromatogram for analysis of D-, L- and DL-glyceraldehyde; measurement conditions are: HPLC (Agilent 1100, Hewlett Packard) using a Eurokat-H column (300 mm × 8 mm, Knauer) with 5 mM H_2SO_4 as eluent at a flow rate of 0.5 mL/min and 75°C, using a refractive index detector at 35°C

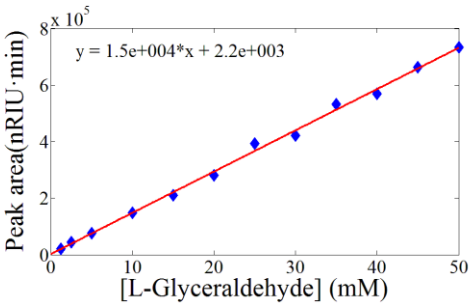

Figure B.4: HPLC calibration plot for the analysis of L-glyceraldehyde concentration; measurement conditions are: HPLC (Agilent 1100, Hewlett Packard) using a Eurokat-H column (300 mm × 8 mm, Knauer) with 5 mM H_2SO_4 as eluent at a flow rate of 0.5 mL/min and 75°C, using a refractive index detector at 35°C

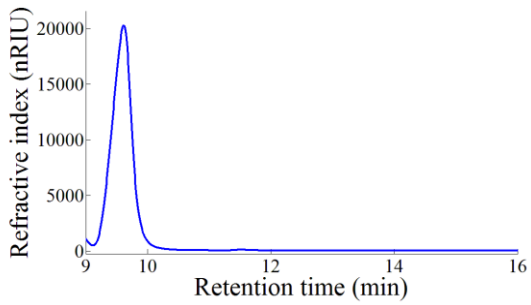

Figure B.5: Sample HPLC chromatogram for analysis of DL-glyceraldehyde 3-phosphate; measurement conditions are: HPLC (Agilent 1100, Hewlett Packard) using a Eurokat-H column (300 mm × 8 mm, Knauer) with 5 mM H_2SO_4 as eluent at a flow rate of 0.5 mL/min and 60°C, using a refractive index detector at 35°C

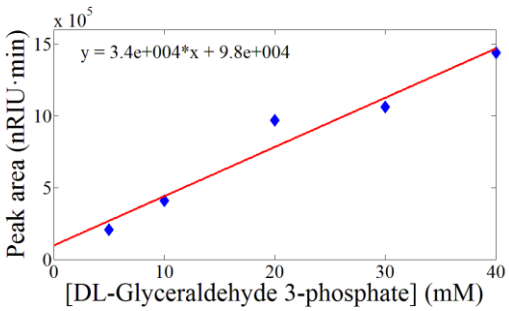

Figure B.6: Sample HPLC chromatogram for analysis of DL-glyceraldehyde 3-phosphate concentration; measurement conditions are: HPLC (Agilent 1100, Hewlett Packard) using a Eurokat-H column (300 mm × 8 mm, Knauer) with 5 mM H_2SO_4 as eluent at a flow rate of 0.5 mL/min and 60°C, using a refractive index detector at 35°C

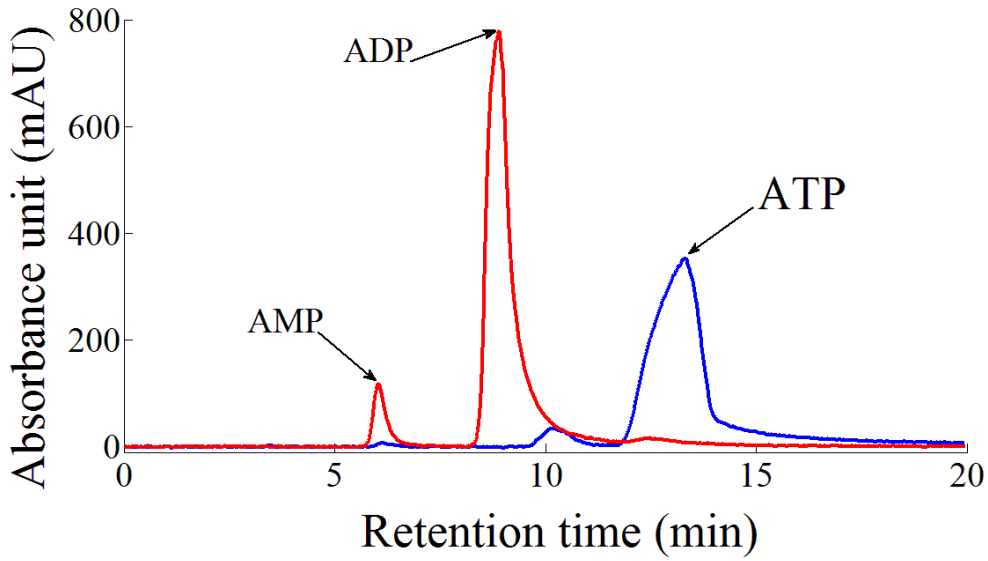

Figure B.7: Sample HPLC chromatogram for the separation and analysis of ATP, ADP and AMP; measurement conditions: HPLC (Agilent 1100, Hewlett Packard), equipped with a Nucleodur® HILIC column (250 mm × 4 mm, Macherey-Nagel) using acetonitrile: 100 mM ammonium acetate in aqueous solution (70:30, v/v) pH 5.3 as eluent at a flow rate of 0.8 mL/min and 25°C, using a diode array detector (DAD) at 259 nm

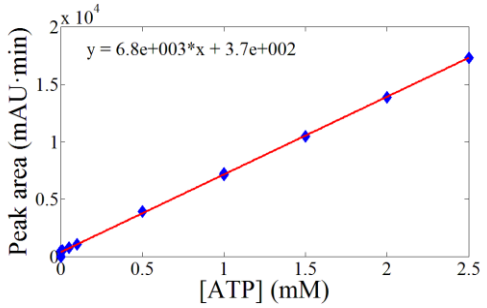

Figure B.8: HPLC calibration plot for the analysis of ATP concentration; measurement conditions: HPLC (Agilent 1100, Hewlett Packard), equipped with a Nucleodur® HILIC column (250 mm × 4 mm, Macherey-Nagel) using acetonitrile: 100 mM ammonium acetate in aqueous solution (70:30, v/v) pH 5.3 as eluent at a flow rate of 0.8 mL/min and 25°C, using a diode array detector (DAD) at 259 nm

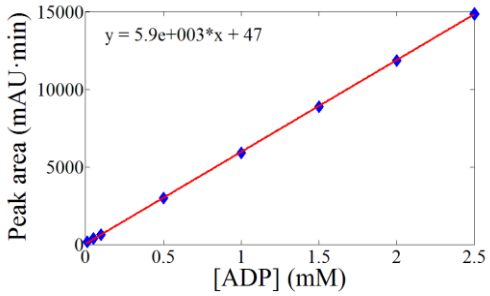

Figure B.9: HPLC calibration plot for the analysis of ATP concentration; measurement conditions: HPLC (Agilent 1100, Hewlett Packard), equipped with a Nucleodur® HILIC column (250 mm × 4 mm, Macherey-Nagel) using acetonitrile: 100 mM ammonium acetate in aqueous solution (70:30, v/v) pH 5.3 as eluent at a flow rate of 0.8 mL/min and 25°C, using a diode array detector (DAD) at 259 nm

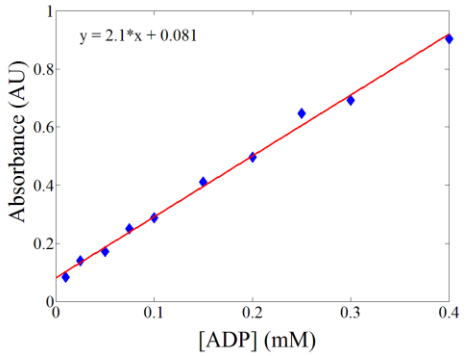

Figure B.10: UV calibration plot for the analysis of ADP concentration at 280 nm

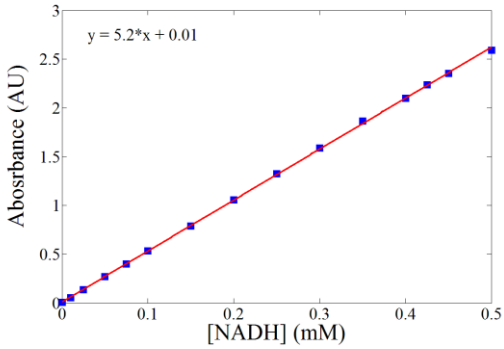

Figure B.11: UV calibration plot for the analysis of NADH concentration at 340 nm

B.2. Supplementary Data

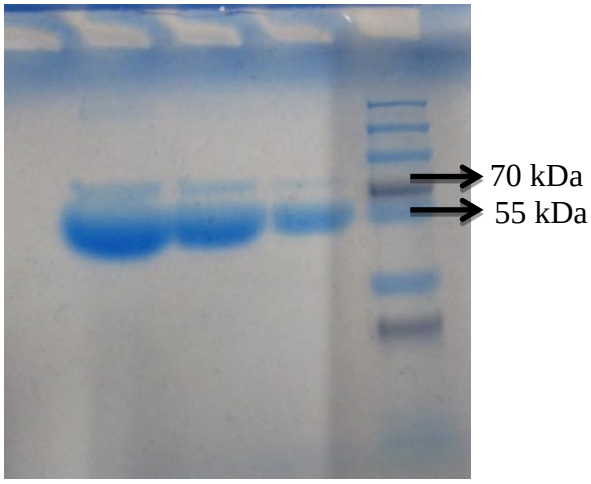

Figure B.12: SDS-PAGE picture of glycerol kinase from *Cellulomonas* sp.

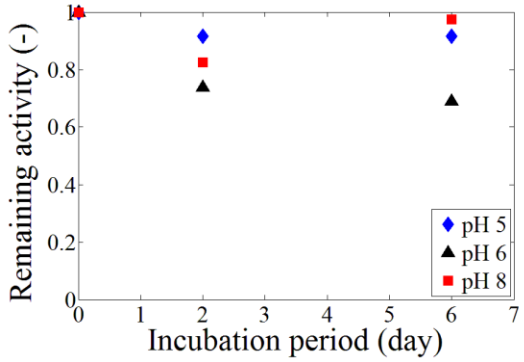

Figure B.13: Remaining activity of rabbit muscle aldolase (RAMA) incubated in 50 mM TEA buffer at 25°C; activity assay conditions: 0.5 mM D-F16BP, 0.5 mM NADH, 0.012 mg protein/mL RAMA and 0.032 mg protein/mL sn-G3PDH in 50 mM TEA buffer at 25°C

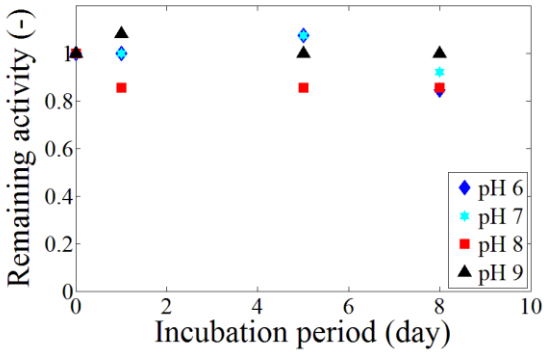

Figure B.14: Remaining activity of *sn*-glycerol-3-phosphate dehydrogenase (*sn*-G3PDH) incubated in 50 mM TEA buffer at 25°C; activity assay conditions: 0.5 mM DHAP 0.5 mM NADH and 0.004 mg protein/mL *sn*-G3PDH in 50 mM TEA buffer at 25°C

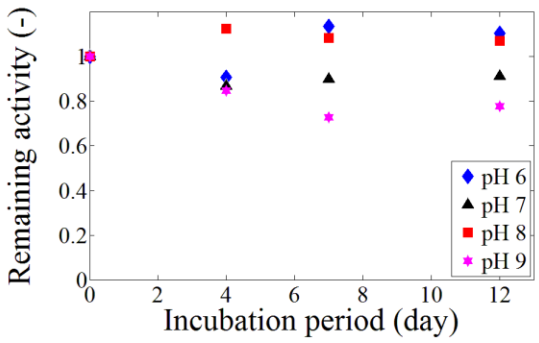

Figure B. 15: Remaining activity of formate dehydrogenase (FDH) incubated in 50 mM TEA buffer at 25°C; activity assay conditions: 50 mM NaHCOO, 0.5 mM NAD^+ and 0.5 mg/mL FDH in 50 mM TEA at 25°

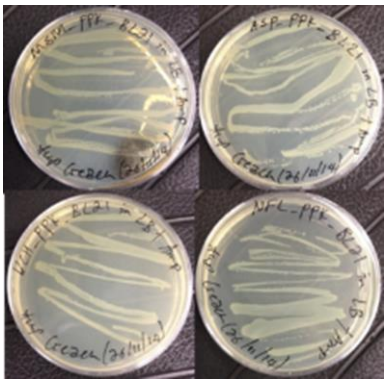

Figure B.16: Photos of agar plate showing the growth of ampicillin resistance plasmid DNA containing *E. coli* BL21 in 100 µg/mL ampicillin containing agar plate

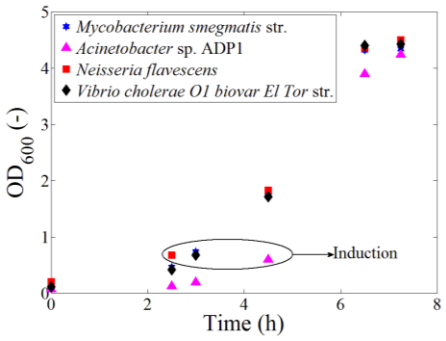

Figure B.17: Plot of OD values versus inoculation time that induction period marked on the plot during the growth phase

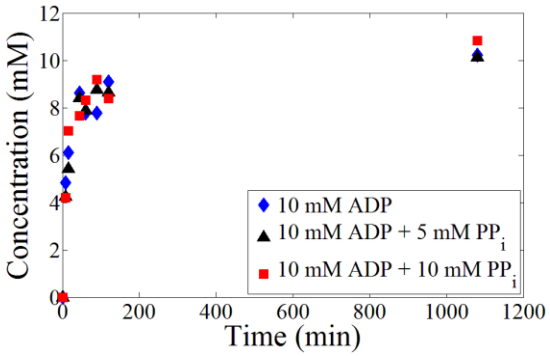

Figure B.18: Effect of PP_i on reaction rate and final conversion of PPK CFE mediated phosphorylation of glycerol by ADP; reaction conditions: 20 mM glycerol, 10 mM ADP, 40 mM Mg^{2+}, glycerol kinase from 0.07 mg/mL *Cellulomonas* sp., 50% v/v PPK CFE in 100 mM Tris-HCl buffer pH 8 and 30°C

Table B.1: A list of phosphotransferases/kinases grouped based on acceptor functional group type, transferred phosphoryl moiety and other type of acceptor group as provided in ExplorEnz the enzyme database [49]

Acceptor functional group type	**EC #**
Alcohol	EC 2.7.1.1 to EC 2.7.1.168
Carboxy	EC 2.7.2.1 to EC 2.7.2.15
Nitrogenous	EC 2.7.3.1 to EC 2.7.3.12
Phosphate	EC 2.7.4.1 to EC 2.7.4.24
Diphosphotransferases	EC 2.7.6.1 to EC 2.7.6.5
Nucleotidyltransferases	EC 2.7.7.1 to EC 2.7.7.68
Other substituted phosphate groups	EC 2.7.8.1 to EC 2.7.8.28
Paired acceptors	EC 2.7.9.1 to EC 2.7.9.5
Protein-tyrosine	EC 2.7.10.1 to EC 2.7.10.2
Protein-serine/threonine	EC 2.7.11.1 to EC 2.7.11.31
Dual-specificity kinases (those acting on Ser/Thr and Tyr residues)	EC 2.7.12.1 to EC 2.7.12.2
Protein-histidine kinases	EC 2.7.13.1 to EC 2.7.13.3
Other protein kinases	EC 2.7.99.1

B.3. Matlab® Scripts

B.3.1. Scripts for the simulation of *sn*-glycerol-3-phosphate synthesis:

```
function dy = sim_v1(t,y,par); % Function declaration
 % Assigning integration output concentration vector
c_ATP = y(1); % mM
c_ADP = y(2); % mM
c_Glycerol = y(3); % mM
c_Glycerol_3_phosphate = y(4); % mM
% Reading the par1ameters
vmax  =  par(1); % U/mg
Km_ATP  =  par(2); % mM
Km_Glycerol  =  par(3); % mM
Kic_ADP  =  par(4); % mM
[ATP]o = par(5); % Starting concentration in mM
[ADP]o = par(6); % Starting concentration in mM
[Glycerol]o = par(7); % Starting concentration in mM
[sn_Glycerol_3_phosphate] = par(8); % Starting concentration in mM
Gkconc = par(9); % Concentration of glycerol kinase from Cellulomonas sp. in mg/mL
τ = par (10) % residence time in min used for simulation of continuous mode of operation
% Reaction kinetic equation
v1 = Gkconc*vmax*c_ATP.*c_Glycerol./((Km_ATP*(1+(c_ADP./Kic_ADP))+c_ATP).*(Km_Glycerol+c_Glycerol));
% Rate of change in concentration of reaction components for a batch-wise mode of operation
dy(1) = -v1; % Decreasing
dy(2) = v1; % Increasing
dy(3) = -v1; % Decreasing
dy(4) = v1; % Increasing
dy=dy'; % Concentration vector
end
% Steady-state concentration of reaction components for a continuous mode of operation
dy(1) = (([ATP]o – c_ATP)/τ) - v1);
dy(2) = (([ADP]o  – c_ADP)/τ + v1);
dy(3) = (([Glycerol]o – c_Glycerol)/τ) - v1);
dy(4) = (([sn_Glycerol_3_phosphate]o  – c_sn_Glycerol_3_phosphate)/τ  + v1);
dy=dy';
end
```

%% Simulation using Runge-Kutta numerical initial value problem solving method

% Initial concentration vector

y_0 = [ATP;ADP;Glycerol; *sn*_Glycerol_3_phosphate];

[tn yn] = ode45(@sim_v_1, time, y_0, [], par);

end

B.3.2. Scripts for the simulation of L-glyceraldehyde-3-phosphate synthesis:

function dz = sim_v_2(t,z,par) % Function declaration

% Integeration output concentration vector:

ATP = z(1); % mM

ADP = z(2); % mM

L_Glyceraldehyde = z(3); % mM

L_Glyceraldehyde_3_phosphate = z(4); % mM

% Reading the parameters

v_{max} = par(1); % U/mg

$K_{m\_L\_Glyceraldehyde}$ = par(2); % mM

K_{m_ATP} = par(3); % mM

K_{ic_ADP} = par(4); % mM

$[ATP]_o$ = par(5); % Starting concentration in mM

$[ADP]_o$ = par(6); % Starting concentration in mM

$[L\_Glyceraldehyde]_o$ = par(7); % Starting concentration in mM

$[L\_Glyceraldehyde\_3\_phosphate]_o$ = par(8); % Starting concentration in mM

Gkconc = par(9);% Concentration of glycerol kinase from *Cellulomonas* sp. in mg/mL

τ = par (10) % residence time in min used for simulation of continuous mode of operation

% Reaction kinetic equation

v_2 = Gkconc*v_{max}*ATP.*L_Glyceraldehyde./((K_{m_ATP} *(1+(ADP./ K_{ic_ADP}))+ATP).*($K_{m\_L\_Glyceraldehyde}$ +L_Glyceraldehyde)); % Rate of change in concentration of reaction components for a batch-wise mode of operation

dz(1) = -v_2;

dz(2) = v_2;

dz(3) = -v_2;

dz(4) = v_2*$e^{-0.002t}$;

dz = dz';

% Steady-state concentration of reaction components for a continuous mode of operation

dz(1) = (($[ATP]_o$ – c_ATP)/τ)- v_2);

dz(2) = (($[ADP]_o$ – c_ADP)/τ + v_2);

dz(3) = (([L_Glyceraldehyde]$_o$ – c_L_Glyceraldehyde)/τ)- v_2);

dz(4) = ((([L_Glyceraldehyde_3_phosphate]$_o$ – c_L_Glyceraldehyde _3_phosphate)/τ + v_2))* $e^{-0.002\tau}$;

dz=dz';

end

%% Simulation using Runge-Kutta numerical initial value problem solving method

% Initial concentration vector

z_0 = [ATP;ADP;Glycealdehyde;L_Glyceraldehyde_3 _phosphate];

[tn yn] = ode45(@sim_v_2, time, z_0, [], par);

end

B.3.3. Scripts for the simulation of D-glyceraldehyde-3-phosphate synthesis:

function dw = sim_v_4(~,w,par) % Function declaration

global NADH; NaHCOO; *sn*_G3PDH; FDH

NADH = 0.5; % mM

NaHCOO = 50; % mM

*sn*_G3PDH = 1.43; % mg/mL

FDH = 3.7; % mg/mL

D_F16BP = w(1); % mM

D_GAP = w(2); % mM

% Reading the parameters

v_{max} = par(1); % U/mg

$K_{m\_D\_F16BP}$ = par(2); % mM

$K_{ic\_D\_GAP}$ = par(3); % mM

$K_{iu\_D\_GAP}$ = par(4); % mM

D_F16BP0 = par(5); % Starting concentration in mM

D_GAP0 = par(6); % Starting concentration in mM

RAMAconc = par(7); % mg/mL

τ = par (8) % residence time in minused for simulation of continuous mode of operation

% Reaction kinetic equation

v_4 = RAMAconc*v_{max}*D_F16BP./(($K_{m\_D\_F16BP}$*(1 +(D_GAP./$K_{ic\_D\_GAP}$))) + D_F16BP*(1 +(D_GAP./$K_{iu\_D\_GAP}$))); % Since the reaction was carried out in the presence of sn-G3PDH coupled with FDH mediated NADH regeneration the reverse reaction has not been considered

% Rate of change in concentration of reaction components for a batch-wise mode of operation

dw(1) = -v_4;

dw(2) = v_4*$e^{-0.001t}$;

dw = dw';

end

% Steady-state concentration of reaction components for a continuous mode of operation

dw(1) = (([D_F16BP]$_o$ – c_D_F16BP)/τ)- v_4);

dw(4) = ((([D_Glyceraldehyde_3_phosphate]$_o$ – c_D_Glyceraldehyde _3_phosphate)/τ + v_4))* $e^{-0.001\tau}$;

dw=dw';

%% Simulation using Runge-Kutta numerical initial value problem solving method

% Initial concentration vector

w_0 = [D_F16BP;D_Glyceraldehyde_3 _phosphate];

[tn yn] = ode45(@sim_v_4, time, w_0, [], par);

end

B.3.4. Scripts for the simulation to validate kinetic model for FDH

function dy = sim_v_3(t,x,par) % Function declaration

NAD = x(1); % mM

NADH = x(2); % mM

Formate = x(3); % mM

% Reading the parameters

v_{max} = par(1); % mg/mL

$K_{m\_Formate}$ = par(2); % mM

K_{m_NAD} = par(3); % mM

K_{ic_NADH} = par(4); % mM

NAD0 = par(5); % mM

NADH0 = par(6); % mM

Formate0 = par(7); % mM

FDHconc = par(8); % mg/mL

% Reaction kinetic equation

v_3 = FDHconc*v_{max}*NAD.*Formate./((K_{m_NAD}*(1+(NADH./K_{ic_NADH})+NAD).*($K_{m\_Formate}$+Formate));

% Rate of change in concentration of reaction components

dx(1) = -v_3;

dx(2) = v_3;

dx(3) = -v_3;

dx=dx';

end

%% Simulation using Runge-Kutta numerical initial value problem solving method

% Initial concentration vector

x_0 = [NAD;NADH;Formate];

[tn yn] = ode45(@sim_v_3, time, x_0, [], par);

end

C. List of Abbreviations and Symbols

Abbreviations

ATP	Adenosine-5’-triphosphate
ADP	Adenosine-5’-diphosphate
AMP	Adenosine-5’-monophosphate
CFE	Cell free extract
CSTR	Continuously operated stirred-tank reactor
D-GAP	D-Glyceraldehyde-3-phosphate
DHAP	Dihydroxyacetone phosphate
DL-GAP	DL-Glyceraldehyde-3-phosphate
D_2O	Deuterated water
DTT	Dithiothreitol
D-F16BP	D-fructose-1,6-bisphosphate
D-F6P	D-fructose-6-phosphate
DSP	Downstream process
EC	Enzyme Commission
FDH	Formate dehydrogenase
HPLC	High-performance liquid chromatography
IPTG	Isopropyl β-D-1-thiogalactopyranoside
L-GAP	L-Glyceraldehyde-3-phosphate
MW	Molecular weight
NAD^+	Nicotinamide adenine dinucleotide (oxidized)
NADH	Nicotinamide adenine dinucleotide (reduced)
n-CSTR	Multi-stage continuously operated stirred-tank reactor

NTPs	Nucleoside triphosphates
OD	Optical density
P_i	Orthophosphate
PBR	Packed bed reactor
PEI	Polyethylenimine
PFR	Plug flow reactor
PPB	Potassium phosphate buffer
PP_i	Pyrophosphate
PP_in	Polyphosphate
PPK	Polyphosphate kinase
RAMA	Rabbit muscle aldolase
RMSE	Root-mean-square error
SDS-PAGE	Sodium dodecyl sulfate polyacrylamide gel electrophoresis
sn-G3P	*sn*-Glycerol-3-phosphate
sn-G3PDH	*sn*-Glycerol-3-phosphate dehydrogenase
sn	Stereospecific numbering
STR	Stirred-tank reactor
TCA	Trichloroacetic acid
TLC	Thin-layer chromatography
TEA	Triethanolamine
Tris	Tris(hydroxymethyl)aminomethane
ttn	Total turnover number
UV	Ultraviolet
2-D	2-Dimensional

^{31}P NMR	^{31}P Nuclear magnetic resonance
^{1}H NMR	^{1}H Nuclear magnetic resonance

Symbols

k_{cat}	Catalytic constant (s^{-1})
K_m	Michaelis-Menten constant (mM)
K_{ic}	Competitive inhibition constant (mM)
K_{iu}	Uncompetitive inhibition constant (mM)
K_{eq}	Equilibrium constant (-)
∂	Partial derivative
SP	Specific productivity (d^{-1})
STY	Space-time yield ($gL^{-1}d^{-1}$)
t	Time (min or h)
τ	Residence time (min or h)
$\Delta_r G$	Change in reaction Gibbs free energy (KJ/mol)
$J_{\alpha P\text{-}\beta P}$	J-Coupling constant of α- and β-phosphate group of ATP (ppm)
$J_{\gamma P\text{-}\beta P}$	J-Coupling constant of γ- and β-phosphate group of ATP (ppm)
R_f	Retention factor (-)
v	Reaction velocity (U/mg)
v_{max}	Maximum reaction velocity (U/mg)
#	Number
~	Approximately

D. List of Tables

E. List of Figures

F. References

[1] Pelouze, J., Untersuchungen ber das Glycerin. *J. Prakt. Chem.* 1845, *36*, 257–261, DOI: 10.1002/prac.18450360157.

[2] Power, F. B., Tutin, F., The relation between natural and synthetical glycerylphosphoric acids. *J. Chem. Soc., Trans.* 1905, *87*, 249, DOI: 10.1039/ct9058700249.

[3] Abderhalden, E., Eichwald, E., Synthese von optisch-aktiver glyceryl-phosphorsäure. *Ber. Dtsch. Chem. Ges.* 1918, *51*, 1308–1312, DOI: 10.1002/cber.19180510218.

[4] Karrer, P., Salomon, H., ber die Glycerin-phosphorsuren aus Lecithin. *Helv. Chim. Acta* 1926, *9*, 3–23, DOI: 10.1002/hlca.19260090101.

[5] Baer, E., Fischer, Hermann O. L., Studies on acetone-glyceraldehyde: VI. synthesis of the biological l(-)-α-glycerophosphoric acid. *J. Biol. Chem.* 1939, *128*, 491–500.

[6] Fischer, Hermann O. L., Baer, E., Preparation and properties of optically active derivatives of glycerol. *Chem. Rev.* 1941, *29*, 287–316, DOI: 10.1021/cr60093a007.

[7] Baer, E., Kates, M., L-α-Glycerylphosphorylcholine. *J. Am. Chem. Soc.* 1948, *70*, 1394–1399, DOI: 10.1021/ja01184a031.

[8] Ballou, C. E., Fischer, Hermann O. L., The synthesis of D-glyceraldehyde-3-phosphate. *J. Am. Chem. Soc.* 1955, *77*, 3329–3331, DOI: 10.1021/ja01617a052.

[9] Gary R. Gray, Robert Barker, The synthesis of d-glyceraldehyde-3,3-d2 3-phosphate. *Carbohydr. Res.* 1971, *20*, 31–37, DOI: 10.1016/S0008-6215(00)84946-0.

[10] Li, H., Tian, J., Wang, H., Yang, S.-Q. *et al.*, An improved preparation of D-glyceraldehyde 3-phosphate and its use in the synthesis of 1-deoxy-D-xylulose 5-phosphate. *HCA* 2010, *93*, 1745–1750, DOI: 10.1002/hlca.200900441.

[11] Serianni, A. S., Pierce, J., Barker, R., Carbon-13-enriched carbohydrates: preparation of triose, tetrose, and pentose phosphates. *Biochemistry* 1979, *18*, 1192–1199.

[12] Uchiyama, M., Aso, Y., Noyori, R., Hayakawa, Y., O-selective phosphorylation of nucleosides without N-protection. *J. Org. Chem.* 1993, *58*, 373–379, DOI: 10.1021/jo00054a020.

[13] Gobley, N. T., *Recherches chimiques sur le jaune d'oeuf Rapport sur un mémoire ayant pour titre "Recherches chimiques sur le jaune d'oeuf*, impr. de Fain et Thunot, Paris, 1846.

[14] Thudichum, J. L. W., Kingzett, C. T., III. Communications from the pathological laboratory of Dr. Thudichum. No. I. On glycero-phosphoric acid and its salts, as obtained from the phosphorised constituents of the brain. *J. Chem. Soc.* 1876, *30*, 20, DOI: 10.1039/js8763000020.

[15] Folch, J., The nature of the glycerophosphoric acid present in phosphatides. *J. Biol. Chem.* 1942, *146*, 31–33.

[16] DuBois, G., The chemistry and properties of glycerophosphates (glycerinophosphates). *J. Ind. Eng. Chem.* 1914, *6*, 122–128, DOI: 10.1021/ie50062a008.

[17] King, H., Pyman, F. L., CXV. The constitution of the glycerylphosphates. the synthesis of and glycerylphosphates. *J. Chem. Soc., Trans.* 1914, *105*, 1238, DOI: 10.1039/ct9140501238.

[18] Baer, E., Kates, M., Migration during hydrolysis of esters of glycerophosphoric acid. II. The acid and alkaline hydrolysis of L-alpha-lecithins. *J Biol. Chem.* 1950, *185*, 615–623.

[19] Chargaff, E., Note on the mechanism of conversion of β-glycerophosphoric acid into the α form. *J. Biol. Chem.* 1942, *144*, 455–458.

[20] Wohlgemuth, R., Tools and ingredients for the biocatalytic synthesis of metabolites. *J. Biotechnol.* 2009, *4*, 1253–1265, DOI: 10.1002/biot.200900002.

[21] Buchholz, K., Kasche, V., Bornscheuer, U. T., *Biocatalysts and enzyme technology*, Wiley-VCH, Weinheim, 2005.

[22] Faber, K., *Biotransformations in organic chemistry: A textbook*, 6th edn., Springer-Verlag, Berlin, Heidelberg, 2011.

[23] Liese, A., Seelbach, K., Wandrey, C., *Industrial biotransformations*, 2nd edn., Wiley-VCH, Weinheim, 2006.

[24] Liese, A., Technical application of biological principles in asymmetric catalysis. *Adv. Biochem. Eng. Biotechnol.* 2005, *92*, 197–224.

[25] Tang, C. T., Engel, R., Tropp, B. E., L-Glyceraldehude 3-phosphate, a bactericidal agent. *Antimicrob. Agents. Chemother*. 1977, *11*, 147–153.

[26] Bednarski, M. D., Simon, E. S., Bischofberger, N., Fessner, W. D. *et al.*, Rabbit muscle aldolase as a catalyst in organic synthesis. *J. Am. Chem. Soc.* 1989, *111*, 627–635, DOI: 10.1021/ja00184a034.

[27] Fessner, W.-D., Sinerius, G., Synthesis of dihydroxyacetone phosphate (and isosteric analogues) by enzymatic oxidation; sugars from glycerol. *Angew. Chem. Int. Ed. Engl.* 1994, *33*, 209–212, DOI: 10.1002/anie.199402091.

[28] Sánchez-Moreno, I., Hélaine, V., Poupard, N., Charmantray, F. *et al.*, One-pot cascade reactions using fructose-6-phosphate aldolase: efficient synthesis of D-arabinose 5-phosphate, D-fructose 6-phosphate and analogues. *Adv. Synth. Catal.* 2012, *354*, 1725–1730, DOI: 10.1002/adsc.201200150.

[29] Schoevaart, R., van Rantwijk, F., Sheldon, R. A., A four-step enzymatic cascade for the one-pot synthesis of non-natural carbohydrates from glycerol. *J. Org. Chem.* 2000, *65*, 6940–6943.

[30] Roland Wohlgemuth, C2-Ketol elongation by transketolase-catalyzed asymmetric synthesis. *J. Mol. Catal. B: Enzym.* 2009, *61*, 23–29, DOI: 10.1016/j.molcatb.2009.04.001.

[31] Rosen, O. M., Hoffee, P., Horecker, B. L., The Mechanism of action of aldolases: VII. formation of a 2-methyl-2-deoxypentose catalyzed by deoxyribose 5-phosphate aldolase. *J. Biol. Chem.* 1965, *240*, 1517–1524.

[32] Racker, E., Enzymatic synthesis and breakdown of desoxyribose phosphate. *J. Biol. Chem.* 1952, *196*, 347–365.

[33] Lamb, R. G., Fallon, H. J., The formation of monoacylglycerophosphate from sn-glycerol 3-phosphate by a rat liver particulate preparation. *J. Biol. Chem.* 1970, *245*, 3075–3083.

[34] Ray, T. K., Cronan, J E Jr, Mavis, R. D., Vagelos, P. R., The specific acylation of glycerol 3-phosphate to monoacylglycerol 3-phosphate in Escherichia coli. Evidence for a single enzyme conferring this specificity. *J. Biol. Chem.* 1970, *245*, 6442–6448.

[35] Molla, G. S., Venkatesh, P. J., Liese, A., Single-pot enzymatic reaction sequence for the synthesis of D-glyceraldehyde-3-Phosphate. *Chem. Ing. Tech.* 2014, *86*, 1424, DOI: 10.1002/cite.201450599.

[36] Molla, G. S., Wohlgemuth, R., Liese, A., One-pot enzymatic reaction sequence for the syntheses of D-glyceraldehyde 3-phosphate and L-glycerol 3-phosphate. *J. Mol. Catal. B: Enzym.* 2016, *124*, 77–82, DOI: 10.1016/j.molcatb.2015.12.004.

[37] Meyer, H.-P., Eichhorn, E., Hanlon, S., Lütz, S. *et al.*, The use of enzymes in organic synthesis and the life sciences: perspectives from the Swiss Industrial Biocatalysis Consortium (SIBC). *Catal. Sci. Technol.* 2013, *3*, 29–40, DOI: 10.1039/C2CY20350B.

[38] Franssen, M. C. R., Kircher, M., Wohlgemuth, R., Industrial biotechnology in the chemical and pharmaceutical industries, in: Soetaert, W., Vandamme, E. J. (Ed.). *Industrial Biotechnology*, Wiley-VCH Verlag GmbH & Co. KGaA, Weinheim, Germany, pp. 323–350.

[39] Knowles, J. R., Enzyme-catalyzed phosphoryl transfer reactions. *Annu. Rev. Biochem.* 1980, *49*, 877–919, DOI: 10.1146/annurev.bi.49.070180.004305.

[40] Westheimer, F., Why nature chose phosphates. *Science* 1987, *235*, 1173–1178, DOI: 10.1126/science.2434996.

[41] Gauss, D., Schönenberger, B., Wohlgemuth, R., Chemical and enzymatic methodologies for the synthesis of enantiomerically pure glyceraldehyde 3-phosphates. *Carbohydr. Res.* 2014, DOI: 10.1016/j.carres.2013.12.023.

[42] Bonsignore, A., Leoncini, G., Siri, A., Ricci, D., Kinetic behavior of glyceraldehyde 3-phosphate conversion into methylglyoxal. *Ital. J. Biochem.* 1973, *22*, 131–140.

[43] Phillips, S. A., Thornalley, P. J., The formation of methylglyoxal from triose phosphates. Investigation using a specific assay for methylglyoxal. *Eur. J. Biochem.* 1993, *212*, 101–105, DOI: 10.1111/j.1432-1033.1993.tb17638.x.

[44] Pompliano, D. L., Peyman, A., Knowles, J. R., Stabilization of a reaction intermediate as a catalytic device: definition of the functional role of the flexible loop in triosephosphate isomerase. *Biochemistry* 1990, *29*, 3186–3194.

[45] Richard, J. P., Restoring a metabolic pathway. *ACS Chem. Biol.* 2008, *3*, 605–607, DOI: 10.1021/cb800238s.

[46] Richard, J. P., Mechanism for the formation of methylglyoxal from triosephosphates. *Biochem. Soc. Trans.* 1993, *21*, 549–553.

[47] Liese, A., Hilterhaus, L., Evaluation of immobilized enzymes for industrial applications. *Chem. Soc. Rev.* 2013, *42*, 6236–6249, DOI: 10.1039/c3cs35511j.

[48] Drauz, K., Waldmann, H. (Ed.), *Enzyme catalysis in organic synthesis*, Wiley-VCH Verlag GmbH, 2002.

[49] McDonald, A. G., Boyce, S., Tipton, K. F., ExplorEnz: the primary source of the IUBMB enzyme list. *Nucleic. Acids. Res.* 2009, *37*, D593-7, DOI: 10.1093/nar/gkn582.

[50] Martinez, R. J., Specificity of the phosphate donor in the hexokinase reaction. *Arch. Biochem. Biophys.* 1961, *93*, 508–513, DOI: 10.1016/S0003-9861(61)80044-1.

[51] Bublitz, C., Kennedy, E. P., Synthesis of phosphatides in isolated mitochondria. III. The enzymatic phosphorylation of glycerol. *J. Biol. Chem.* 1954, *211*, 951–961.

[52] Uyeda, K., Kurooka, S., Crystallization and properties of phosphofructokinase from Clostridium pasteurianum. *J. Biol. Chem.* 1970, *245*, 3315–3324.

[53] Sadava, D., Moore, K., Glycerol metabolism in higher plants: glycerol kinase. *Biochem. Biophys. Res. Commun.* 1987, *143*, 977–983.

[54] Stetten, M. R., Enzymatic synthesis of glycerol 1-phosphate. Elevation in diabetic and fasted animals, compared with glucose-6-phosphatase and related enzyme activities. *Biochim. Biophys. Acta* 1970, *208*, 394–403.

[55] Asano, Y., Mihara, Y., Yamada, H., A novel selective nucleoside phosphorylating enzyme from Morganella morganii. *J. Biosci. Bioeng.* 1999, *87*, 732–738.

[56] Krawiec, K., Kierdaszuk, B., Shugar, D., Inorganic tripolyphosphate (PPP_i) as a phosphate donor for human deoxyribonucleoside kinases. *Biochem. Biophy. Res. Commun.* 2003, *301*, 192–197, DOI: 10.1016/S0006-291X(02)03007-3.

[57] Whitesides, G. M., Siegel, M., Garrett, P., Large-scale synthesis of diammonium acetyl phosphate. *J. Org. Chem.* 1975, *40*, 2516–2519, DOI: 10.1021/jo00905a021.

[58] Li, T., Yeh, H., Kim, J. H., Ryu, D. D., Performance of batch membrane reactor: Glycerol-3-phosphate synthesis coupled with adenosine triphosphate regeneration. *Biotechnol. Bioeng.* 2001, *74*, 326–334.

[59] Crans, D. C., Whitesides, G. M., Glycerol kinase: synthesis of dihydroxyacetone phosphate, *sn*-glycerol-3-phosphate, and chiral analogs. *J. Am. Chem. Soc.* 1985, *107*, 7019–7027, DOI: 10.1021/ja00310a045.

[60] Bolte, J., Whitesides, G. M., Enzymatic synthesis of arginine phosphate with coupled ATP cofactor regeneration. *Bioorg. Chem.* 1984, *12*, 170–175, DOI: 10.1016/0045-2068(84)90026-9.

[61] Resnick, S. M., Zehnder, A. J., *In vitro* ATP regeneration from polyphosphate and AMP by polyphosphate:AMP phosphotransferase and adenylate kinase from *Acinetobacter johnsonii* 210A. *Appl. Environ. Microbiol.* 2000, *66*, 2045–2051.

[62] Kameda, A., Shiba, T., Kawazoe, Y., Satoh, Y. *et al.*, A novel ATP regeneration system using polyphosphate-AMP phosphotransferase and polyphosphate kinase. *J. Biosci. Bioeng.* 2001, *91*, 557–563.

[63] Murata, K., Uchida, T., Kato, J., Chibata, I., Polyphosphate kinase: distribution, some properties and its application as an ATP regeneration system. *Agric. Biol. Chem.* 1988, *52*, 1471–1477, DOI: 10.1271/bbb1961.52.1471.

[64] Noguchi, T., Shiba, T., Use of *Escherichia coli* polyphosphate kinase for oligosaccharide synthesis. *Biosci. Biotechnol. Biochem.* 1998, *62*, 1594–1596, DOI: 10.1271/bbb.62.1594.

[65] Shiba, T., Tsutsumi, K., Ishige, K., Noguchi, T., Inorganic polyphosphate and polyphosphate kinase: their novel biological functions and applications. *Biochemistry (Mosc)* 2000, *65*, 315–323.

[66] Trelstad, P. L., Purdhani, P., Geissdorfer, W., Hillen, W. *et al.*, Polyphosphate kinase of *Acinetobacter* sp. strain ADP1: purification and characterization of the enzyme and its role during changes in extracellular phosphate levels. *Appl. Environ. Microbiol.* 1999, *65*, 3780–3786.

[67] Nakamichi, Y., Yoshioka, A., Kawai, S., Murata, K., Conferring the ability to utilize inorganic polyphosphate on ATP-specific NAD kinase. *Scientific reports* 2013, *3*, 2632, DOI: 10.1038/srep02632.

[68] Smith, R. A., A new enzymatic synthesis of hexose phosphates 1. *J. Am. Chem. Soc.* 1959, *81*, 4758, DOI: 10.1021/ja01526a091.

[69] Fujimoto, A., Smith, R. A., Enzymatic phosphorylation of glucose by phosphoramidates. *J. Biol. Chem.* 1960, *235*, PC44-PC45.

[70] Crans, D. C., Whitesides, G. M., Glycerol kinase: substrate specificity. *J. Am. Chem. Soc.* 1985, *107*, 7008–7018, DOI: 10.1021/ja00310a044.

[71] Weinhouse, H., Benziman, M., Phosphorylation of glycerol and dihydroxyacetone in *Acetobacter xylinum* and its possible regulatory role. *J. Bacteriol.* 1976, *127*, 747–754.

[72] Boltralik, J. J., Noll, H., A specific, sensitive assay of glycerol and L-α-glycerophosphate. *Anal. Biochem.* 1960, *1*, 269–273, DOI: 10.1016/0003-2697(60)90054-3.

[73] Hayashi, S. I., Lin, E. C., Purification and properties of glycerol kinase from *Escherichia coli*. *J. Biol. Chem.* 1967, *242*, 1030–1035.

[74] Stetten, M. R., Rounbehler, D., Enzymatic synthesis of glycerol 1-phosphate (D-alpha-glycerophosphate). Inorganic pyrophosphate-glycerol phosphotransferase and inorganic pyrophosphate-glucose phosphotransferase compared. *J. Biol. Chem.* 1968, *243*, 1823–1832.

[75] Pradines, A., Klaebe, A., Perie, J., Paul, F. *et al.*, Large-scale enzymatic synthesis of glycerol 1-phosphate. *Enzyme. Microb. Technol.* 1991, *13*, 19–23, DOI: 10.1016/0141-0229(91)90183-B.

[76] Babich, L., Hartog, A. F., van der Horst, Michael A, Wever, R., Continuous-flow reactor-based enzymatic synthesis of phosphorylated compounds on a large scale. *Chemistry (Weinheim an der Bergstrasse, Germany)* 2012, *18*, 6604–6609, DOI: 10.1002/chem.201200101.

[77] Babich, L., Peralta, Joana L. V. M., Hartog, A. F., Wever, R., Phosphorylation by alkaline phosphatase: immobilization and synthetic potential. *I. J. C.* 2013, *5*, DOI: 10.5539/ijc.v5n3p87.

[78] Jenkins, B. T., Hajra, A. K., Glycerol kinase and dihydroxyacetone kinase in rat brain. *J. Neurochem.* 1976, *26*, 377–385.

[79] Rios-Mercadillo, V. M., Whitesides, G. M., Enzymatic synthesis of *sn*-glycerol 3-phosphate. *J. Am. Chem. Soc.* 1979, *101*, 5828–5829, DOI: 10.1021/ja00513a062.

[80] Thorner, J. W., Paulus, H., Composition and subunit structure of glycerol kinase from *Escherichia coli*. *J. Biol. Chem.* 1971, *246*, 3885–3894.

[81] Thorner, J. W., Paulus, H., Catalytic and allosteric properties of glycerol kinase from *Escherichia coli*. *J. Biol. Chem.* 1973, *248*, 3922–3932.

[82] Wong, C. H., Whitesides, G. M., Synthesis of sugars by aldolase-catalyzed condensation reactions. *J. Org. Chem.* 1983, *48*, 3199–3205, DOI: 10.1021/jo00167a012.

[83] Crans, D. C., Whitesides, G. M., A convenient synthesis of disodium acetyl phosphate for use in *in situ* ATP cofactor regeneration. *J. Org. Chem.* 1983, *48*, 3130–3132, DOI: 10.1021/jo00166a048.

[84] Voegele, R. T., Sweet, G. D., Boos, W., Glycerol kinase of *Escherichia coli* is activated by interaction with the glycerol facilitator. *J. Bacteriol.* 1993, *175*, 1087–1094.

[85] Butterworth, P. J., The pyrophosphatase activity of pig kidney alkaline phosphatase and its inhibition by magnesium ions and excess of pyrophosphate. *J. Biochem.* 1968, *110*, 671–675.

[86] Imamura, S., Matsumoto, T., Muto, N., Misaki, H., Glycerol kinase from *Streptomyces canus*, Google Patents, 1982. https://www.google.com/patents/US4347323.

[87] Grunnet, N., Lundquist, F., Kinetics of glycerol kinases from mammalian liver and *Candida mycoderma*. *Eur. J. Biochem.* 1967, *3*, 78–84, DOI: 10.1111/j.1432-1033.1967.tb19500.x.

[88] Fey, S., Elling, L., Kragl, U., The cofactor Mg^{2+}—a key switch for effective continuous enzymatic production of GDP-mannose using recombinant GDP-mannose pyrophosphorylase. *Carbohydr. Res.* 1997, *305*, 475–481, DOI: 10.1016/S0008-6215(97)10095-7.

[89] Penner, P. E., Cohen, L. H., Effects of adenosine triphosphate and magnesium ions on the fumarase reaction. *J. Biol. Chem.* 1969, *244*, 1070–1075.

[90] Denburg, J., DeLuca, M., Pseudo-allosteric behavior of firefly luciferase. *Biochem. Biophys. Res. Commun.* 1968, *31*, 453–460.

[91] Miles, R. D., Gorrell, A., Ferry, J. G., Evidence for a transition state analog, MgADP-aluminum fluoride-acetate, in acetate kinase from *Methanosarcina thermophila*. *J. Biol. Chem.* 2002, *277*, 22547–22552, DOI: 10.1074/jbc.M105921200.

[92] Shimizu, T., Hatano, M., ^{25}Mg NMR study of Mg^{2+}-ATP, ADP-creatine kinase complexes. *Biochem. Biophys. Res. Commun.* 1982, *104*, 720–726, DOI: 10.1016/0006-291X(82)90696-9.

[93] Datta, P., Calcium glycerophosphate preserves transepithelial integrity in the Caco-2 model of intestinal transport. *WJG* 2015, *21*, 9055, DOI: 10.3748/wjg.v21.i30.9055.

[94] Kligerman, A. E., Weis, M. T., Methods and compositions of treating and preventing intestinal injury and diseases related to tight junction dysfunction, Google Patents, 2014. http://www.google.com/patents/WO2014130678A2 cl=en.

[95] Greenberg, M. J., Chewing gum with dental health benefits employing calcium glycerophosphate, Google Patents, 1995. http://www.google.com/patents/US5378131.

[96] Kligerman, A. E., Rogers, S., Oral rinse methods and compositions, Google Patents, 2002. http://www.google.com/patents/US6447754.

[97] Paul, K., by, G. K., Sublingual aspirin tablet, Google Patents, 1980. http://www.google.com/patents/US4206209.

[98] Kligerman, A., Finnegan, S., Method for alleviating syndromes and conditions of discomfort of the mammalian intestinal and genito-urinary tracts, Google Patents, 2005. http://www.google.com/patents/US20050130938.

[99] Finnegan, S., Kligerman, A. E., Method for alleviating syndromes and conditions of discomfort of the mammalian intestinal and genito-urinary tracts, Google Patents, 2002. http://www.google.com/patents/WO2002056834A2?cl=en.

[100] Kligerman, A. E., Rogers, S., Acid neutralization of skin, Google Patents, 1999. http://www.google.com/patents/US5972321.

[101] Kligerman, A. E., Finnegan, S., Weis, M., Compositions and methods for treating skin conditions, Google Patents, 2008. http://www.google.com.ar/patents/US7402323.

[102] Kligerman, A. E., Hartzell, S., Method of reducing distress in mammals due to ingestion of acidic foods and beverages, Google Patents, 1999. http://www.google.com/patents/US5869119.

[103] McArdle, R. N., McGill, C. R., Letourneau, S. A., Green, N. R., Reduction of heartburn episodes after ingestion of orange juice, Google Patents, 2003. http://www.google.com/patents/US6565898.

[104] McArdle, R. N., Letourneau, S. A., McGill, C. R., Hart, C. L., Bolles, A. D., Reduction of heartburn episodes upon ingestion of orange juice, Google Patents, 2004. http://www.google.com/patents/US6682767.

[105] Kligerman, A., Finnegan, S., Edible candy compositions and methods of using same, Google Patents, 2002. http://www.google.com/patents/US20020064550.

[106] Melachouris, N., Lee, C. R., Calcium fortified acid beverages, Google Patents, 1988. http://www.google.com/patents/US4740380.

[107] Kligerman, A. E., Hartzell, S., Composition and method for increasing the pH of acid foods, Google Patents, 1997. http://www.google.com/patents/US5665415.

[108] Fallon, H. J., Lamb, R. G., Acylation of *sn*-glycerol 3-phosphate by cell fractions of rat liver. *J. Lipid. Res.* 1968, *9*, 652–660.

[109] Hill, E. E., Husbands, D. R., Lands, W. E., The selective incorporation of ^{14}C-glycerol into different species of phosphatidic acid, phosphatidylethanolamine, and phosphatidylcholine. *J. Biol. Chem*. 1968, *243*, 4440–4451.

[110] Martensson, E., Kanfer, J., The conversion of L-glycerol-^{14}C 3-phosphate into phosphatidic acid by a solubilized preparation from rat brain. *J. Biol. Chem.* 1968, *243*, 497–501.

[111] Zahler, W. L., Cleland, W. W., Studies on the microsomal acylation of L-glycerol-3-phosphate III. Time course of the reaction. *Biochim. Biophys. Acta* 1969, *176*, 699–703, DOI: 10.1016/0005-2760(69)90250-1.

[112] Abou-Issa, H. M., Cleland, W. W., Studies on the microsomal acylation of L-glycerol-3-phosphate II. The specificity and properties of the rat liver enzyme. *Biochim. Biophys. Acta* 1969, *176*, 692–698, DOI: 10.1016/0005-2760(69)90249-5.

[113] Hill, D. W., Pyman, F. L., The constitution of the glycerophosphates. *J. Chem. Soc.* 1929, 2236, DOI: 10.1039/jr9290002236.

[114] Pyman, F. L., Stevenson, H. A., 104. Constitution of glycerophosphates. Part III. *J. Chem. Soc.* 1934, 448, DOI: 10.1039/jr9340000448.

[115] Baer, E., Fischer, Hermann O. L., Synthesis of the D(+)-α-glycerophosphoric acid and the action of phosphatases on synthetic D(+)-, L(-)-, and DL-α-glycerophosphoric acids. *J. Biol. Chem.* 1940, *135*, 321–328.

[116] Meyerhof, O., Ueber die phosphorylierten zwischenprodukte und die letzten Phasen der alkoholischen Garung. *Biochem. Z.* 1933, *267*.

[117] Kalckar, H., Formation of a new phosphate ester in kidney extracts. *Nature.* 1938, *142*, 871, DOI: 10.1038/142871a0.

[118] Kalckar, H., The nature of phosphoric esters formed in kidney extracts. *Biochem. J.* 1939, *33*, 631–641.

[119] Schambye, P., Wood, H. G., Popjak, G., Biological asymmetry of glycerol and formation of asymmetrically labeled glucose. *J. Biol. Chem.* 1954, *206*, 875–882.

[120] Swick, R. W., Nakao, A., The biological asymmetry of glycerol. *J. Biol. Chem.* 1954, *206*, 883–886.

[121] Bublitz, C., Kennedy, E. P., A note of the asymmetrical metabolism of glycerol. *J. Biol. Chem.* 1954, *211*, 963–967.

[122] Eisenthal, R., Harrison, R., Lloyd, W. J., Specificity of glycerol kinase. *Biochem. J.* 1974, *141*, 305–307.

[123] Gancedo, C., Gancedo, J. M., Sols, A., Glycerol metabolism in yeasts. Pathways of utilization and production. *Eur. J. Biochem.* 1968, *5*, 165–172, DOI: 10.1111/j.1432-1033.1968.tb00353.x.

[124] Yeh, J. I., Kettering, R., Saxl, R., Bourand, A. *et al.*, Structural characterizations of glycerol kinase: unraveling phosphorylation-induced long-range activation. *Biochemistry* 2009, *48*, 346–356, DOI: 10.1021/bi8009407.

[125] Sogabe, A., Oka, M., Inagaki, K., Hatta, T., Nishise, H., Glycerol kinase, which has high resistance against preservative, Google Patents, 2009. http://www.google.com.ar/patents/US7618800.

[126] Seltzer, W. K., Bullen, W. W., McCabe, Edward R. B., Human glycerol kinase: comparison of properties from fibroblasts and liver. *Life. Sci.* 1983, *32*, 1721–1726, DOI: 10.1016/0024-3205(83)90834-2.

[127] Schneider, P. B., Activation of bovine liver glycerol kinase by ethanol. *Biochim. Biophys. Acta* 1975, *397*, 110–116.

[128] Pasteris, S. E., de Saad, A.M. Strasser, Characterization of glycerol kinase and NAD-independent glycerol-3-phosphate dehydrogenase from *Pediococcus pentosaceus* N5p. *Lett. Appl. Microbiol.* 1998, *27*, 93–97, DOI: 10.1046/j.1472-765X.1998.00391.x.

[129] Krakow, J. L., Wang, C. C., Purification and characterization of glycerol kinase from *Trypanosoma brucei*. *Mol. Biochem. Parasitol.* 1990, *43*, 17–25.

[130] Janson, C. A., Cleland, W. W., The kinetic mechanism of glycerol kinase. *J. Biol. Chem.* 1974, *249*, 2562–2566.

[131] Hammond, D. J., Bowman, I. B., Studies on glycerol kinase and its role in ATP synthesis in *Trypanosoma brucei*. *Mol. Biochem. Parasitol.* 1980, *2*, 77–91.

[132] Pettigrew, D. W., Yu, G. J., Liu, Y., Nucleotide regulation of *Escherichia coli* glycerol kinase: initial-velocity and substrate binding studies. *Biochemistry* 1990, *29*, 8620–8627, DOI: 10.1021/bi00489a018.

[133] Steinborn, K., Szallies, A., Mecke, D., Duszenko, M., Cloning, heterologous expression and kinetic analysis of glycerol kinase (TbGLK1) from *Trypanosoma brucei*. *Biol. Chem.* 2000, *381*, 1071–1077, DOI: 10.1515/BC.2000.132.

[134] Ohashi-Suzuki, M., Yabu, Y., Ohshima, S., Nakamura, K. *et al.*, Differential kinetic activities of glycerol kinase among African trypanosome species: phylogenetic and therapeutic implications. *J. Vet. Med. Sci.* 2011, *73*, 615–621.

[135] Balogun, E. O., Inaoka, D. K., Shiba, T., Kido, Y. *et al.*, Biochemical characterization of highly active *Trypanosoma brucei* gambiense glycerol kinase, a promising drug target. *J. Biochem.* 2013, *154*, 77–84, DOI: 10.1093/jb/mvt037.

[136] Faber, H. R., Pettigrew, D. W., Remington, S. J., Crystallization and preliminary X-ray studies of *Escherichia coli* glycerol kinase. *J. Mol. Biol.* 1989, *207*, 637–639, DOI: 10.1016/0022-2836(89)90473-7.

[137] Robinson, J., Newsholme, E. A., Some properties of hepatic glycerol kinase and their relation to the control of glycerol utilization. *Biochem. J.* 1969, *112*, 455–464.

[138] Flamholz, A., Noor, E., Bar-Even, A., Milo, R., eQuilibrator the biochemical thermodynamics calculator. *Nucleic. Acids. Res.* 2012, *40*, D770-5, DOI: 10.1093/nar/gkr874.

[139] Schnick, C., Polley, S. D., Fivelman, Q. L., Ranford-Cartwright, L. C. *et al.*, Structure and non-essential function of glycerol kinase in *Plasmodium falciparum* blood stages. *Mol. Microbiol.* 2009, *71*, 533–545, DOI: 10.1111/j.1365-2958.2008.06544.x.

[140] Robinson, J., Newsholme, E. A., Inhibition of liver glycerol kinase by adenosine monophosphate and L-alpha-glycerophosphate. *Biochem. J.* 1967, *104*, 70P.

[141] Newsholme, E. A., Taylor, K., Glycerol kinase activities in muscles from vertebrates and invertebrates. *Biochem. J.* 1969, *112*, 465–474.

[142] Glonek, T., ^{31}P NMR of Mg-ATP in dilute solutions: complexation and exchange. *Int. J. Biochem.* 1992, *24*, 1533–1559.

[143] Storer, A. C., Cornish-Bowden, A., Concentration of $MgATP_2$- and other ions in solution. calculation of the true concentrations of species present in mixtures of associating ions. *Biochem. J.* 1976, *159*, 1–5.

[144] Zhao, L., Chang, W.-c., Xiao, Y., Liu, H.-w. *et al.*, Methylerythritol phosphate pathway of isoprenoid biosynthesis. *Annu. Rev. Biochem.* 2013, *82*, 497–530, DOI: 10.1146/annurev-biochem-052010-100934.

[145] Begley, T. P., Ealick, S. E., McLafferty, F. W., Thiamin biosynthesis: still yielding fascinating biological chemistry. *Biochem. Soc. Trans.* 2012, *40*, 555–560, DOI: 10.1042/BST20120084.

[146] Lowry, O. H., Passonneau, J. V., Rock, M. K., The stability of pyridine nucleotides. *J. Biol. Chem.* 1961, *236*, 2756–2759.

[147] Hasunuma, T., Harada, K., Miyazawa, S.-I., Kondo, A. *et al.*, Metabolic turnover analysis by a combination of *in vivo* ^{13}C-labelling from $^{13}CO_2$ and metabolic profiling with CE-MS/MS reveals rate-limiting steps of the C3 photosynthetic pathway in *Nicotiana tabacum* leaves. *J. Exp. Bot.* 2010, *61*, 1041–1051, DOI: 10.1093/jxb/erp374.

[148] Herrmann, K. M., Weaver, L. M., The shikimate pathway. *Annu. Rev. Plant. Physiol. Plant. Mol. Biol.* 1999, *50*, 473–503, DOI: 10.1146/annurev.arplant.50.1.473.

[149] Jurgenson, C. T., Begley, T. P., Ealick, S. E., The structural and biochemical foundations of thiamin biosynthesis. *Annu. Rev. Biochem.* 2009, *78*, 569–603, DOI: 10.1146/annurev.biochem.78.072407.102340.

[150] Knight, W. B., Cleland, W. W., Thiol and amino analogues as alternate substrates for glycerokinase from *Candida mycoderma*. *Biochemistry* 1989, *28*, 5728–5734.

[151] Pawlyk, A. C., Pettigrew, D. W., Subcloning, expression, purification, and characterization of *Haemophilus influenzae* glycerol kinase. *Protein. Expr. Purif.* 2001, *22*, 52–59, DOI: 10.1006/prep.2001.1408.

[152] Rao, D. R., Kou, A. Y., Partial purification and characterization of glycerokinase from chicken liver. *Int. J. Biochem.* 1977, *8*, 295–298, DOI: 10.1016/0020-711X(77)90135-5.

[153] Burton, K., Formation constants for the complexes of adenosine di- or tri-phosphate with magnesium or calcium ions. *Biochem. J.* 1959, *71*, 388–395.

[154] Trentham, D. R., McMurray, C. H., Pogson, C. I., The active chemical state of D-glyceraldehyde 3-phosphate in its reactions with D-glyceraldehyde 3-phosphate dehydrogenase, aldolase and triose phosphate isomerase. *Biochem. J.* 1969, *114*, 19–24.

[155] Kalyananda, M. K., Engel, R., Tropp, B. E., Metabolism of L-glyceraldehyde 3-phosphate in *Escherichia coli*. *J. Bacteriol.* 1987, *169*, 2488–2493.

[156] Talukdar, D., Chaudhuri, B. S., Ray, M., Ray, S., Critical evaluation of toxic versus beneficial effects of methylglyoxal. *Biochemistry* 2009, *74*, 1059–1069.

[157] Thornalley, P. J., The glyoxalase system: new developments towards functional characterization of a metabolic pathway fundamental to biological life. *Biochem. J.* 1990, *269*, 1–11.

[158] Kalapos, M. P., Methylglyoxal in living organisms: chemistry, biochemistry, toxicology and biological implications. *Toxicol. Lett.* 1999, *110*, 145–175.

[159] Ko, J., Kim, I., Yoo, S., Min, B. *et al.*, Conversion of methylglyoxal to acetol by *Escherichia coli* aldo-keto reductases. *J. Bacteriol.* 2005, *187*, 5782–5789, DOI: 10.1128/JB.187.16.5782-5789.2005.

[160] Desai, K. K., Miller, B. G., A metabolic bypass of the triosephosphate isomerase reaction. *Biochemistry* 2008, *47*, 7983–7985, DOI: 10.1021/bi801054v.

[161] Adelman, R. C., Brox, L., Krulwich, T. A., Preparation of radioactive L-glyceraldehyde 3-phosphate. *Anal. Biochem.* 1969, *32*, 258–262.

[162] Bell, R. P., The Reversible hydration of carbonyl compounds, in: V. Gold (Ed.). *Adv. Phys. Org. Chem.*, Academic Press, pp. 1–29.

[163] Trigalo, F., Jachymczyk, W., Young, J. C., Szab, L., Phosphorylated sugars. Part XV. syntheses of 3-deoxy-D-erythro- and 3-deoxy-D-threo-hexulosonic acid 6-(dihydrogen phosphates). *J. Chem. Soc., Perkin. Trans. 1* 1975, 593, DOI: 10.1039/p19750000593.

[164] Bubb, W. A., Berthon, H. A., Kuchel, P. W., Tris buffer reactivity with low-molecular-weight aldehydes: NMR characterization of the reactions of glyceraldehyde-3-phosphate. *Bioorg. Chem.* 1995, *23*, 119–130, DOI: 10.1006/bioo.1995.1010.

[165] Mao, C., Ozer, Z., Zhou, M., Uckun, F. M., X-ray structure of glycerol kinase complexed with an ATP analog implies a novel mechanism for the ATP-dependent glycerol phosphorylation by glycerol kinase. *Biochem. Biophys. Res. Commun.* 1999, *259*, 640–644, DOI: 10.1006/bbrc.1999.0816.

[166] Yeh, J. I., Charrier, V., Paulo, J., Hou, L. *et al.*, Structures of enterococcal glycerol kinase in the absence and presence of glycerol: correlation of conformation to substrate binding and a mechanism of activation by phosphorylation. *Biochemistry* 2004, *43*, 362–373, DOI: 10.1021/bi034258o.

[167] Vasavada, K. V., Ray, B. D., Nageswara Rao, B. D., ^{31P} NMR lineshapes of β-P (ATP) in the presence of Mg^{2+} and $Ca^{2+:}$ estimate of exchange rates. *J. Inorg. Biochemi.* 1984, *21*, 323–335, DOI: 10.1016/0162-0134(84)85054-0.

[168] Ormo, M., Bystrom, C. E., Remington, S. J., Crystal structure of a complex of *Escherichia coli* glycerol kinase and an allosteric effector fructose 1,6-bisphosphate. *Biochemistry* 1998, *37*, 16565–16572, DOI: 10.1021/bi981616s.

[169] Szabó, Z., Multinuclear NMR studies of the interaction of metal ions with adenine-nucleotides. *Coord. Chem. Rev.* 2008, *252*, 2362–2380, DOI: 10.1016/j.ccr.2008.03.002.

[170] Son, T.-D., Roux, M., Ellenberger, M., Interaction of Mg^{2+} ions with nucleoside triphosphates by phosphorus magnetic resonance spectroscopy. *Nucl. Acids. Res.* 1975, *2*, 1101–1110, DOI: 10.1093/nar/2.7.1101.

[171] Tran-dinh, S., Roux, M., A Phosphorus-magnetic-resonance study of the interaction of Mg^{2+} with adenyl-5'-yl imidodiphosphate. binding sites of Mg^{2+} ion on the phosphate chain. *Eur. J. Biochem.* 1977, *76*, 245–249, DOI: 10.1111/j.1432-1033.1977.tb11589.x.

[172] Cohn, M., Hughes, T R Jr, Nuclear magnetic resonance spectra of adenosine di- and triphosphate. II. Effect of complexing with divalent metal ions. *J. Biol. Chem.* 1962, *237*, 176–181.

[173] Cowan, J. A., Transition metals as probes of metal cofactors in nucleic acid biochemistry. *Comments Inorg. Chem.* 1992, *13*, 293–312, DOI: 10.1080/02603599208048465.

[174] Jiang, L., Mao, X. A., NMR evidence for Mg(II) binding to N1 of ATP. *Spectrochim. Acta. A Mol. Biomol. Spectrosc.* 2001, *57*, 1711–1716.

[175] Bishop, E. O., Kimber, S. J., Orchard, D., Smith, B. E., A ^{31}P-NMR study of mono- and dimagnesium complexes of adenosine 5′-triphosphate and model systems. *Biochim. Biophys. Acta* 1981, *635*, 63–72, DOI: 10.1016/0005-2728(81)90007-4.

[176] Huang, S. L., Tsai, M. D., Does the magnesium(II) ion interact with the alpha-phosphate of adenosine triphosphate? An investigation by oxygen-17 nuclear magnetic resonance. *Biochemistry* 1982, *21*, 951–959.

[177] Ramirez, F., Marecek, J. F., Coordination of magnesium with adenosine 5'-diphosphate and triphosphate. *Biochim. Biophys. Acta* 1980, *589*, 21–29.

[178] Takeuchi, H., Murata, H., Harada, I., Interaction of adenosine 5'-triphosphate with Mg^{2+}: vibrational study of coordination sites by use of 18O-labeled triphosphates. *J. Am. Chem. Soc.* 1988, *110*, 392–397, DOI: 10.1021/ja00210a013.

[179] Bock, J. L., Crull, G. B., Wishnia, A., Springer, C S Jr, ^{25}Mg NMR studies of magnesium binding to erythrocyte constituents. *J. Inorg. Biochem.* 1991, *44*, 79–87.

[180] Sari, J. C., Hadida, M., Chauvet-Monges, A. M., Crevat, A., Microcalorimetric study of magnesium-adenosine triphosphate ternary complex. *J. Bioenerg. Biomembr.* 1982, *14*, 171–179.

[181] Klaus, W., Schlichting, I., Goody, R. S., Wittinghofer, A. *et al.*, ^{31}P-NMR studies on ATP·Mg^{2+} p21·nucleotide, and adenylate kinase·nucleotide complexes. chemical shifts, rate and equilibrium constants. *Biol. Chem. Hoppe-Seyler* 1986, *367*, 781–786, DOI: 10.1515/bchm3.1986.367.2.781.

[182] Bishop, E. O., Miles, R., Smith, B. E., A ^{31}P-NMR study of the mechanism of and salt effect on Mg^{2+}-ATP exchange. *Biochim. Biophys. Acta* 1990, *1019*, 276–282.

[183] Jiang, L., Mao, X. A., NMR evidence for Mg(II) binding to N1 of ATP. *Spectrochim. Acta. A Mol. Biomol. Spectrosc.* 2001, *57*, 1711–1716.

[184] Rohmer, M., Diversity in isoprene unit biosynthesis: The methylerythritol phosphate pathway in bacteria and plastids. *Pure Appl. Chem.* 2007, *79*, DOI: 10.1351/pac200779040739.

[185] Dijkhuizen, L., Harder, W., Current views on the regulation of autotrophic carbon dioxide fixation via the Calvin cycle in bacteria. *Antonie Van Leeuwenhoek* 1984, *50*, 473–487.

[186] Szewczuk, A., Wolny, E., Wolny, M., Baranowski, T., A new method for obtaining d-glyceraldehyde-3-phosphate. *Acta. Biochimica. Polonica.* 1961, *8*, 201–207.

[187] Lima-Ramos, J., Neto, W., Woodley, J. M., Engineering of Biocatalysts and Biocatalytic Processes. *Top. Catal.* 2013, *57*, 301–320, DOI: 10.1007/s11244-013-0185-0.

[188] Leo M. Hall, Preparation of D-glyceraldehyde-3-phosphate and dihydroxyacetone phosphate hydrazones. *Biochem. Biophys. Res. Commun.* 1960, *3*, 239–243, DOI: 10.1016/0006-291X(60)90231-X.

[189] Andreas Liese, Lecture Notes of *Biocatalysis and Enzyme Technology*, 2013.

[190] Callens, M., Kuntz, D. A., Opperdoes, F. R., Kinetic properties of fructose bisphosphate aldolase from *Trypanosoma brucei* compared to aldolase from rabbit muscle and *Staphylococcus aureus*. *Mol. Biochem. Parasitol*. 1991, *47*, 1–9.

[191] Bentley, P., Dickinson, F. M., Jones, I. G., Purification and properties of rabbit muscle L-glycerol 3-phosphate dehydrogenase. *Biochem. J.* 1973, *135*, 853–859.

[192] Crans, D. C., Kazlauskas, R. J., Hirschbein, B. L., Wong, C. H. *et al.*, Enzymatic regeneration of adenosine 5'-triphosphate: acetyl phosphate, phosphoenolpyruvate, methoxycarbonyl phosphate, dihydroxyacetone phosphate, 5-phospho-alpha-D-ribosyl pyrophosphate, uridine-5'-diphosphoglucose. *Methods Enzymol.* 1987, *136*, 263–280.

[193] Miles, R. D., Gorrell, A., Ferry, J. G., Evidence for a transition state analog, MgADP-aluminum fluoride-acetate, in acetate kinase from *Methanosarcina thermophila*. *J. Biol. Chem.* 2002, *277*, 22547–22552, DOI: 10.1074/jbc.M105921200.

[194] Kuroda, A., Kornberg, A., Polyphosphate kinase as a nucleoside diphosphate kinase in *Escherichia coli* and *Pseudomonas aeruginosa*. *Proc. Natl. Acad. Sci. USA* 1996, *94*, 439–442.

[195] Life Technologies Corporation, *E. coli* expression system with gateway technology, 2012(25-0517).

[196] Bochner, B. R., Maron, D. M., Ames, B. N., Detection of phosphate esters on chromatograms: an improved reagent. *Anal. Biochem.* 1981, *117*, 81–83, DOI: 10.1016/0003-2697(81)90695-3.

Curriculum Vitae

Name	Getachew Shibabaw
Surname	Molla
Date of birth	10 Jan 1986
16 Sep 2004 - 20 Jul 2007	B.Sc. in Applied Chemistry, Arba Minch University, 21 Arba Minch (Ethiopia)
1 Jul 2006 - 1 Sep 2006	Product quality control, MOHA Soft Drink Factory, Gondar (Ethiopia)
1 Sep 2007 - 1 Sep 2009	Graduate and research assistant, Applied chemistry department, Hawassa University, 05 Hawassa (Ethiopia)
9 Sep 2009 - 30 Sep 2011	M.Sc. in Environmental Technology, University of Aveiro (Portugal), Aalborg University (Denmark), University of Barcelona (Spain) and Technical University of Hamburg-Harburg (Germany)
16 Nov 2011 - 30 April 2015	PhD candidate, Institute of Technical Biocatalysis, Technical University of Hamburg-Harburg, Denickestrasse. 15, 21071 Hamburg (Germany)
01 Sep 2015 - 29 Feb 2016	Research assistant, Department of Chemical and Biochemical Engineering, Technical University of Denmark, Søltofts Plads, 2800 Kgs. Lyngby, Denmark
01 Nov 2016 – up to date	Postdoc, Department of Chemical and Biochemical Engineering, Technical University of Denmark, Søltofts Plads, 2800 Kgs. Lyngby, Denmark